ZEOLITE Ω:

ITS

SYNTHESIS AND PROPERTIES

by

ARUNA VARMA, BSc(Dunelm)

Thesis submitted for the Degree of

Master of Philosophy

University of Edinburgh

October 1985

To

Dr. Barrie M. Lowe

Abstract

Previous work on the Mobil and Union Carbide zeolites ZSM-4 and Ω is reviewed in detail and it is concluded that the materials are essentially identical. The crystallisation of zeolite Ω from the optimum reaction composition is investigated with regard to the order of mixing of the reactants, partial replacement of tetramethylammonium bromide (TMABr) by hexanediol and the temperature at which the reactants are mixed. The crystallisation was monitored by pH measurements, X-ray powder diffraction (XRD), differential thermal analysis (DTA) and thermal gravimetric analysis (TG). TG was shown to detect microcrystalline structure which is amorphous to X-rays. The order in which the reactants are mixed in the presence of hexanediol was found to have a significant effect on the gel pH and the crystallinity of the product, though little effect on crystallisation rate was detected. X-ray fluorescence analysis (XRF) suggests that there may be a relationship between the order of mixing and the framework composition of the product. Mixing the reactants at 95°C rather than at room temperature changed the nature of the gel (from a thick paste to a thin clear solution), the mechanism of the reaction, the crystallisation rate and the products. The change in the mechanism was initially detected by pH measurements and subsequently confirmed by XRD. The reaction proceeded via sodalite with an increased induction period for zeolite Ω. Mixed products resulted even after reaction for 672 hours. A mechanism for the formation of faulted Ω is proposed. The DTA of zeolite Ω in admixture with sodalite suggests the presence of TMA-sodalite. The pure zeolite Ω products give rise to four new types of DTA pattern. Type IV exhibits an exotherm at ∿1000°C. A detailed investigation of the effect of water on the as made pure zeolite Ω was made. It showed that the exotherm at ∿1000°C in the type IV DTA pattern was removed after the zeolite had

been contacted with water at room temperature for 20 minutes and after a similar treatment for 1 hour the DTA curve was completely transformed. Thorough washing of the as made zeolite gave rise to one characteristic DTA curve. The origin of the exotherms in this curve were identified by simple experiments. Sorption/ion exchange of TMA from aqueous solution by (Na,TMA)-Ω at room temperature and at 95°C examined by DTA and TG allowed external surface and main channel sorption to be differentiated. Room temperature TMA sorption isotherms for (Na,TMA)-Ω which distinguished external surface, main channel and total sorption capacity were determined.

Acknowledgement

I would like to thank Professors Donovan, Ebsworth and Kemball for provision of laboratory facilities. I thank my supervisor Dr. B.M. Lowe for his initiation and help with such an interestingarea of research. I thank Dr. C.A. Beevers and Dr. A. Blake for many helpful discussions on the crystallographic side of this work; Dr. J.G. Fitton and Dr. A. Livingstone for valuable discussions and references on the geological side of this work. Thanks go to Mrs. Hazel Hirst and Mrs. Thea Grieve for many references they have obtained for me.

I thank Mrs. Margaret Betty May Kahn for the painstaking task she has endured over the past eight weeks typing, correcting and recorrecting her errors. And a final thanks to Mrs. Glass for the final corrections.

CONTENTS

Page

Chapter Three Some Techniques of Zeolite Characterisation

Chapter Four The Crystallisation of Zeolite Ω

CHAPTER ONE

An Introduction to Zeolites

Nature has provided man with a wondrous class of minerals: Zeolites. Their beauty has placed them as gem stones in jewellery and as prized crystals that adorn every mineralogical collection [1]. Their versatile structural chemistry has placed them not only in industry and agriculture, but virtually in every day use. They are used in: the petroleum industry for catalytic cracking and the conversion of methanol to petrol [2], in energy conservation using solar energy for refrigeration, in detergents as water softeners, in agriculture to help fatten pigs (in Japan), in pollution control e.g. radioactive waste disposal, in fluoride-containing toothpastes as a polishing agent, and many other areas [3-7].

1.1 Historical Developments

The history of zeolites began with the discovery of stilbite in 1756 by the Swedish mineralogist Crønsted [8]. The name zeolite is derived from the Greek zein and lithos, condensed to the Swedish zeolith, which means 'boiling stones'. It refers to the manner in which they lose water when heated. Zeolite minerals were first recognised as crystals in cavities of volcanic rocks. Synthesis of these species was commenced by mineralogists interested to imitate the natural processes and define the conditions for their occurrence and stability [9-12]. The first zeolite to be synthesised was levynite in 1862 by Ste Claire Deville [9]. The useful exchange properties of zeolites were demonstrated by Eichorn (1858) and Damour (1857), but they were not considered of technological importance [6, 9, 10].

It was work by Grandjean (1910), Weigel and McBain that demonstrated the notable selective sorption capacity of chabazite that spurred interest in zeolites [9, 10, 13]. McBain introduced the term molecular sieve to describe the steric control for the sorption of molecules in chabazite. This stimulated the interest of Barrer in Britain and Sameshima in Japan and work commenced on sorption and ion exchange of zeolite minerals. Sources of suitable zeolites were unknown and so this prompted chemists to turn to synthesis. The first success by the chemists was synthetic zeolite P, and from then onwards a steady supply of zeolites for commercial application emerged.

The possible use of zeolites for gas separations interested Linde Air Products (Union Carbide) and they began work on synthesis. Soon synthetic zeolites A, X and Y of commercial value were prepared. In order to determine the impact of naturally occurring zeolites on the new synthetic zeolite business and specifically to ascertain whether or not the new zeolites A, X and Y occurred naturally, the Linde division initiated a programme of geological exploration for zeolites. Vast quantities of zeolites were discovered and bought by Union Carbide [9, 10]. The natural mineral counterpart of zeolites X and Y, faujasite was found, but so far there is no natural equivalent for zeolite A.

New techniques of synthesis were developed by the chemists, the introduction of nitrogenous templates [14] into the reaction mixture led to many novel structures, notably Mobil's petrol producing zeolite catalyst ZSM-5 [15]. As this research progressed, silica rich frameworks were synthesised, which culminated in the aluminium free i.e. microporous silica polymorphs Silicalite I and Silicalite II, the analogues of ZSM-5 and ZSM-11 [16].

Silicalites preserve the molecular sieve properties of zeolites, but lose the ion exchange capabilities as aluminium is removed from the framework. At the other end, the latest class of molecular sieves to be discovered are the aluminophosphates ($AlPO_4$) [17, 18]. They represent the first class of molecular sieves with framework oxide composition free of silica. Thus the description of molecular sieves requires amendments. At present it stands as the version by J. V. Smith [19] based on structural properties of zeolites:

> An aluminosilicate framework structure enclosing cavities occupied by large ions and water molecules, both of which have considerable freedom of movement, permitting ion exchange and reversible dehydration with formula $M_{x/n}\,[(AlO_2)_x\,(SiO_2)_y]_m\,H_2O$.

Crønsted's discovery of this new class of minerals, and Barrer's work in Britain and Breck's work at Union Carbide certainly opened the door to a whole new arena of science and technology.

1.2 Occurrence

1.2.1 Geological Aspects of Synthesis

Zeolites are one of the earth's most abundant mineral classes [10, 12]. World wide deposits are found in volcanic environments in Rome, Oregon, Nevada, Loire Valley, France, Japan, Arizona, Lake Warakei in New Zealand, Turkey, the Rocky Mountains of the USA, Yellow Stone National Park (USA) and many other locations, even in Arthur's Seat in Edinburgh [20].

Zeolites often occur as fine crystals lining cavities and cracks in basaltic rocks of volcanic origin [10, 11, 12, 21]. The cavities are considered to be formed by bubbles of fluids in the parent magma and the zeolite crystals grow as a result of the chemical action on the magma of these fluids or of fluids which have subsequently displaced

them. The bulk composition of the zeolites tends to correlate with those of the parent rock; the more aluminous zeolites are associated with rocks deficient in silica and more siliceous zeolites with rocks high in silica. More than one zeolite species may be present and evidence suggestive of slow replacement of one zeolite by another, rather than co-crystallisation is sometimes found. Zeolites of this type are usually dispersed in occurrence and are not suitable for industrial purposes.

More massive deposits occur as very small crystal grains in certain sediments and low grade metamorphic rocks. Aqueous and alkaline solutions which act upon volcanic ash deposited in lakes account for much of the zeolitization. They are occasionally found in arid alkaline soils rich in salts. Zeolite rich beds, hundreds of metres thick with some deposits primarily of one zeolite species and others of only one zeolite have been found. Such deposits are ideal for commercial exploitation.

Other zeolite rich deposits have been the result of low grade metamorphism and metasomatism of deep-seated rocks. The extent to which these zeolites are metastable is unknown, but once formed they often resist subsequent transformation for long periods of time.

1.2.2 Zeolite Exploration

It was the Linde Division of Union Carbide that embarked on the geological exploration of zeolites in 1957 to investigate the commercial availability of these minerals [9, 10]. This investigation was primarily to determine the impact of naturally occurring zeolites on Union Carbide's new zeolite business and specifically to see whether Zeolite A was found naturally.

In the five year period, January 1958 to December 1962, more than 3,000 samples were collected and approximately 200 new locations of zeolite minerals in volcanic sedimentary rocks were discovered. Nearly 100 other occurrences of these species in the United States became known at the time due to the efforts of university geologists. Union Carbide's exploration effort was guided by newly developed knowledge that zeolites were abundant in flat lying light coloured tuffaceous beds (and light coloured altered ash-flow tuff) in Tertiary pyroclastic rocks. Until 1957 zeolites were thought to exist as late stage hydrothermal products, by 1962 they were recognised as common constituents of altered material in wide varieties of volcanic environments. During this period the useful and until then rare zeolite, erionite, was found in large mineable deposits and the widespread distribution of clinoptilolite was established.

1.3 Aspects of Synthesis

1.3.1 Principles

Once it was demonstrated that pure zeolites could be synthesised under relatively simple reproducible alkaline mild hydrothermal conditions (80-300°C), the scientific interest coupled with industrial potential yielded a rich supply of crystalline materials. These were the porous zeolite crystals, crystalline silicas, expanded layer silicates and the latest addition to this field, the alumino-phosphates [9, 17, 18]. Zeolite synthesis may be considered in the stages given below:

Stages in Zeolite Synthesis

Reactants
↓
Reaction Mixture
↓
Precursor Species
↓
Crystal Growth

The zeolites which crystallise may be partially dependent on the nature of the reactants used rather than the overall chemical composition, temperature and pressure [9, 22, 23]. The variety of materials used as sources of alumina, silica and base has been considerable. Some sources of silica and alumina are considered 'inactive', and much work on the activity of reactants has been carried out by Whittam [24, 25, 26].

The reaction mixture composition in a crystallisation experiment is defined by the mole ratios in Table 1.1 which also gives the primary function of each ratio.

Table 1.1

Reaction Mixture Composition and Primary Function of Each Ratio

MOLE RATIO	PRIMARY INFLUENCE
SiO_2/Al_2O_3	Framework composition
H_2O/SiO_2	Rate, crystallisation mechanism
OH^-/SiO_2	Silicates molecular weight, OH^- concentration
Na^+/SiO_2	Structure, cation distribution
R_4N^+/SiO_2	Framework alumina content

The SiO_2/Al_2O_3 ratio places constraints on the framework composition of the zeolite produced and it may define the structural competitors in a nucleation controlled experiment. With the exception of aluminium rich NaA, zeolites normally incorporate all of the aluminium present in a reaction mixture into the framework structure, leaving varying amounts of silica (silicates) in solution according to the hydroxide concentration and reaction conditions.

The H_2O/SiO_2 and OH^-/SiO_2 strongly influence the 'molecular' or 'polymeric' species present in a reaction mixture composition and the rate at which these species interconvert, by hydrolysis, to form the ordered 3-dimensional network of the zeolite product. Control of hydrolysis rate and polysilicate (or polyaluminosilicate) distribution significantly influences the product formed among competing, possibly metastable structures in a crystallisation experiment.

The cations present are often the dominant factor which determines the zeolite structure formed. The cations are required to balance the negative charge generated by the aluminate species ($Al(OH)_4^-$). Table 1.2 below shows how variation of the nature of cation in the reaction mixture influences the product formed. The reaction conditions were: SiO_2/Al_2O_3 16-20, H_2O/SiO_2 14 to 25, $^-OH/SiO_2$ 0.7 to 0.9, static conditions at 100°C.

Table 1.2

Product Dependence on Cation [22]

ZEOLITE	Na/SiO_2	TMA/SiO_2	K/SiO_2
Y	0.8	0.0	0.0
Ω	0.6	0.1	0.0
L	0.0	0.0	0.8
TMA-O	0.0	0.1	0.8

Mixing of the aqueous alkaline aluminate and silicate or silica sol usually produces a precipitation and gel formation. However when a large volume of strong alkali solution is mixed with small amounts of SiO_2 and Al_2O_3 gel formation is avoided and zeolite crystallisation may eventually occur from a seemingly clear solution. The usual behaviour is initial gel formation, due to strong interaction between aluminate and silicate.

The initial gel is metastable in that under appropriate conditions and time it is consumed by dissolution and precipitation as a zeolite or crystalline product. This illustrates Ostwald's rule of successive transformation. The first phase which appears is always thermodynamically less stable than that which subsequently follows. The first crystals to nucleate and grow from the gel may be replaced by another crystalline species and so sequences of growth and replacement are possible, the sequence is always in the direction of increasing thermodynamic stability, e.g.

Amorphous $\rightarrow$ Faujasite $\rightarrow$ ZSM-4 [27, 28]

The above illustrates that the thermodynamic ladder is descended in steps rather than one jump.

The composition of a zeolite is variable for any given framework structure. In patents it is usually cited as a range. A specific framework structure does not have a unique composition. It can be controlled by the type of cation or the SiO_2/Al_2O_3 in the reaction mixture. An example of the cation type is illustrated by sodalite. This zeolite may be synthesised with Na or TMA (tetramethylammonium) as the cation. When Na is the cation, the composition is $Na_3\ Al_3\ Si_3O_{12}$, however, when TMA replaces the Na, the composition is $(CH_3)_4NAlSi_5O_{12}$ i.e. the SiO_2/Al_2O_3 ratio is

changed from 2 to 10, but the framework structure remains unchanged.

1.3.2 Templates

The type of molecular sieve which forms may be influenced or directed by the specific addition of particular cations or salts to the reaction mixture. The introduction of organic cations, quaternary ammonium ions and amines into the reaction mixture resulted in many known zeolites with higher SiO_2/Al_2O_3 ratios and also novel structures [9, 29, 17, 22, 30]. Those species which seem to exert a unique structure directing influence during crystallisation of the molecular sieve are templates. Their action appears to depend on both electronic and steric effects.

The example of sodalite synthesis in which Na is replaced by TMA is representative of template action. The sodalite contains one TMA per sodalite cavity and since TMA is too large to enter the cavity once it is formed, it must be incorporated during crystal growth. The anionic cage must grow around the TMA which acts as both template and charge balancing agent [31, 32].

In the crystallisation of zeolite Ω/ZSM-4, there is a powerful structure directing role by the TMA ion which generates the gmelinite cage around itself.

A striking example of template action is that exerted by cationic polyelectrolytes [33]. The polyelectrolyte Dab-4-Br is produced by the reaction of 1, 4 diazobicyclo [2.2.2] octane with $Br(CH_2)_4Br$. This species when incorporated in the reaction mixture directs the crystallisation to pure gmelinite from Y and Y + P. This represents the first synthesis of pure gmelinite, free from chabazite intergrowths which have been observed to block the 12 ring channel in all previous

synthetic and natural samples. The Dab-4-Br is incorporated into the 12 ring channel and thus prevents the chabazite intergrowth. The reaction is sensitive to changes in concentration of the electrolyte and is specific for Dab-4-Br, any other polymer repeat unit generates the faulted material or Y and Y + P.

The use of the other quaternary ammonium ions and amines led to the formation of ZSM-5, other novel structures and extremely high SiO_2/Al_2O_3 zeolites, culminating in the aluminium free molecular sieves. The pure silica molecular sieves [16], Silicalite I and Silicalite II, are the analogues of zeolites ZSM-5 and ZSM-11. The silicalite analogues are synthesised with TPA (tetrapropylammonium) and TBA (tetrabutylammonium) respectively. The latest addition to this class of pure silica molecular sieves is the analogue of zeolite ZSM-48 and EU-2 named EU-11 [34]. These materials preserve the molecular sieve properties but lose the ion exchange capabilities as all the aluminium is removed from the framework.

A new addition to the family of molecular sieves is the crystalline microporous aluminophosphates [17, 18]. They represent the first class of molecular sieves with framework oxide composition free of silica. Some of their frameworks are analogues of zeolites. The novel phases are synthesised hydrothermally in the presence of organic amines and quaternary ammonium templates. The steric component of the template appears to be the dominant feature. One aluminophosphate, $AlPO_4$-5, may be synthesised using 23 different organic templates. It is claimed that the structure of $AlPO_4$-5 is novel with no zeolite analogue. $AlPO_4$-20 is only made with TMA and is the TMA-sodalite analogue.

Recently, the successful use of other organic molecules [29] such as alcohols, ketones and glycerol have been claimed in zeolite synthesis, e.g. for ZSM-5 and ferrierite. The exact role of these

organics is not fully understood.

There is overwhelming evidence that the presence of organic quaternary ammonium ions and organic amines in zeolite and aluminophosphate synthesis helps the formation of a particular structure. The role of the organic demonstrates structure directing influence and supports the template theory. However the fact that so many templates may be used to synthesise one species and that multiple structures are formed with one template indicates that the template fit is not the only factor in structure determination.

Several researchers have found that the classic example normally given for the template theory, ZSM-5 using TPA, can be synthesised in the absence of organic templates [35]. Similarly, pure gmelinite synthesis, with an XRD pattern identical to that published for pure gmelinite by Daniels, Kerr and Rollmann [33] and hence free from chabazite faults has been achieved in a simple sodium system without organic or polymer templates [36]. It was found that in the presence of selected organic cations there was no change in the product, and the organic was not incorporated into the zeolite.

Thus the hydrogel composition appears to be the primary factor in zeolite synthesis and the need for organic templates certainly raises questions.

1.4 Structure

Knowledge of the structure of a zeolite is important as it governs the catalytic and sorptive properties. Consequently the impact of zeolite technology on the petroleum and chemical industries, and the advances in X-ray analysis resulted in a surge of increased activity in structure determination [37-41]. To date there are

about 40 known zeolite structures, which include natural and synthetic zeolites, and most of these have been solved since 1960. The lack of synthetic crystals large enough for single crystal X-ray diffraction determination has hindered the progress in structure elucidation of numerous synthetic zeolites. In most cases only the topology of the anionic aluminosilicate framework is known. Complete structure determination i.e. precise information on the Si/Al distribution, the positions of the cations, organic and water molecules is only available for a few zeolites. Zeolite species with the same topology are called isotypic, they represent the same framework structure type irrespective of composition distribution of different Si and Al tetrahedral (T) atoms, cell dimensions and symmetry.

The most appropriate description of a zeolite is that in terms of its structural composition. A zeolite is an ordered, porous, crystalline aluminosilicate composed of rigid 3-dimensional networks of SiO_4 and AlO_4 tetrahedra, crosslinked by the sharing of oxygen atoms whereby the ratio of the total aluminium and silicon atoms to oxygen is 1:2 i.e. (Al + Si)/O = 1:2. The negative charge of the tetrahedra containing aluminium is balanced by the inclusion in the crystal of a cation e.g. an alkali or alkaline earth metal cation although more recently the cation has included organic nitrogen cations notably quaternary ammonium ions. The crystal structure of zeolites comprise open spaces of uniform molecular dimensions which are filled with water of hydration. Within a specific zeolite material, some of these open spaces are interconnected by smaller channels or pores of precisely uniform size. Zeolite frameworks with their linked tetrahedra can be represented by line diagrams. The straight connections in these diagrams

representative of T-O-T bridges are schematic in nature since T-O-T angles are ideally around 140-150° and rarely 180° [39-44].

Prior to 1963 zeolites were classified according to their morphological and molecular sieve properties. In 1963 Smith [19] drew up the first structural classification of zeolites based primarily on the common structural units of the framework. Meier classified zeolites according to their secondary building units (SBU) or polyhedral building blocks. These SBUs have been derived under the condition that a zeolite network is composed entirely of only one type of unit. The 9 SBUs are illustrated in Fig. 1.1. These SBUs are sufficient to describe the zeolite framework and build hypothetical structures. However Kokotailo [38] has suggested that 3 rings and 9 rings should be added. Based on the SBUs, Meier has classified zeolites into 7 groups. Kokotailo has extended this to 9 in order to accommodate the 3 and 9 ring structures. The main groups and their SBUs are summarised in Table 1.3.

Table 1.3

Classification of Zeolites

ZEOLITE GROUP	SBU
Analcime	4 and 6 rings
Natrolite	Linked 4 rings
Chabazite	Parallel 6 rings
Phillipsite	4 rings lying at least approximately parallel
Heulandite	Four 5 rings and two 4 rings linked into chains
Mordenite	Four 5 rings forming complex chains
Faujasite	Based on sodalite cages
Melanophologite*	3 and 5 rings
Lovdarite*	9 rings

* These were added by Kokotailo

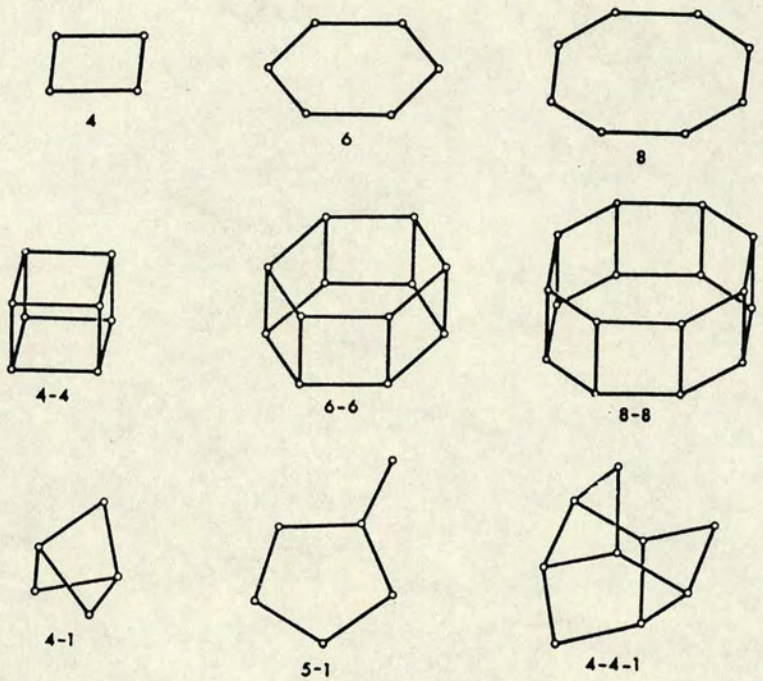

Fig. 1.1 Secondary Building Units of zeolite frameworks described by Meier

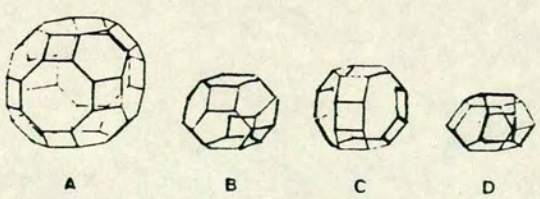

Fig. 1.2 Larger polyhedral building units and frequently occurring cages (α cage, A; sodalite cage, B; gmelinite cage, C; cancrinite cage, D)

Meier has since proposed a simplification of this grouping system, again based on SBU. This is given in Table 1.4 [41].

Table 1.4 illustrates that many of the zeolite networks can be generated from several different SBUs. For this reason, conventional classification systems of zeolite structure types based on SBUs are not completely unambiguous. This table shows that on this basis there are only three distinct families of zeolite networks. These are designated a, b, and c. Type a consists of parallel single and/or double six ring units and the stacking of these 12 valent SBUs may be described like polytypic sequences of hexagonal layers or sphere packings (e.g. cubic sodalite net A B C). The natrolite family, designated b, is made up of 4-1 rings and the mordenite family, designated c, is made up of 5-1 rings. Only 5 out of the 9 SBUs in Fig. 1.1 are strictly necessary to generate all the known zeolite framework types. The essential SBUs are 4, 6, 4-1, 4-4-1 and 5-1 units.

Five rings are observed in many zeolite networks, but none of these can be built of 5 ring units only.

Polyhedral cage type units have been proposed by Breck. These are shown in Fig. 1.2. The cage type building units should be supplemented with 6-6 and 8-8 ring units. The cage units are often used to describe zeolite structures since the building blocks are easily recognisable, but less than half the known zeolite structures are based on cage type units. Frameworks composed of cage units generally have low density whereas those composed of 5-1 units have high density.

The remaining type of building unit is the one dimensional infinite cage or tubular unit - see Fig. 1.3. These units are only of chemical interest.

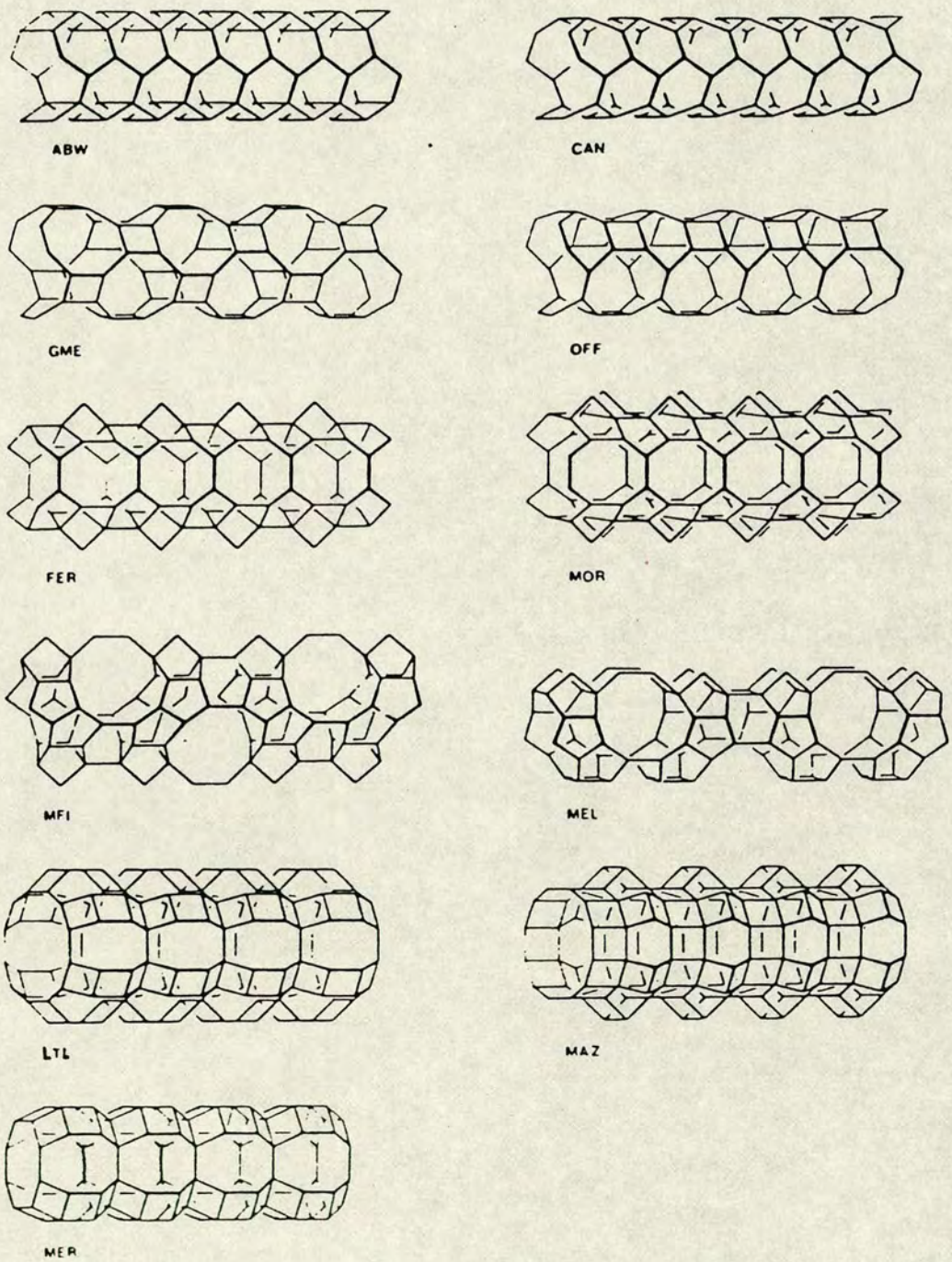

Fig. 1.3 Tubular building units (having at least 8-ring apertures)

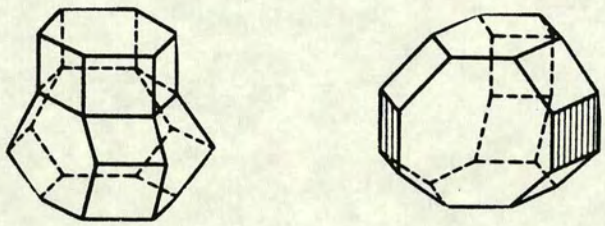

Fig. 1.4 Transformation of cancrinite cage (A) to gmelinite cage (B) by outward rotation of 6 ring tetrahedra

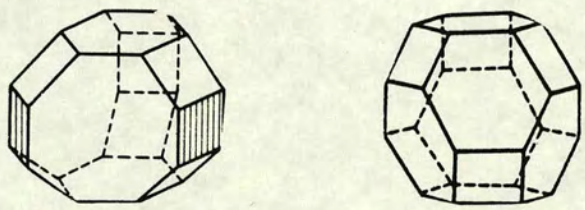

Fig. 1.5 Transformation of gmelinite cage (B) to sodalite cage (C) by breakage of bonds in plane through 4-ring and rotation of top half through 60°

Table 1.4

Constituent Units of Zeolite Structure Types

STRUCTURE TYPE DESIGNATION		SECONDARY BUILDING UNITS [a]	CAGE UNITS [b]	TUBULAR UNITS [c]	DISTINCT FAMILIES	FRAMEWORK DENSITY [d]
CODE	FULL NAME					
FAU	Faujasite	4 6 6-6	B			12.7
LTA	Linde type A	4 6 8 4-4	A B			12.9
RHO	Rho	4 6 8 8-8	A			14.3
GME	Gmelinite	4 6 8 6-6	C	•	a	14.6
CHA	Chabazite	4 6 6-6			a	14.6
KFI	ZK-5	4 6 8 6-6	A			14.7
LEV	Levyne	6			a	15.2
GIS	Gismondine	4 8				15.4
EAB	TMA-E (AB)	4 6			a	15.4
OFF	Offretite	6	D	•	a	15.5
PAU	Paulingite	4				15.5
ERI	Erionite	4 6	D		a	15.6
LIO	Liottite	6			a	15.7
LOS	Losod	6			a	15.8
PHI	Phillipsite	4 8				15.8
AFG	Afghanite	4 6			a	15.9
MER	Merlinoite	4 8 8-8		•		16.0
MAZ	Mazzite	4	5-1	•		16.1
LTL	Linde type L	6	D	•		16.4
CAN	Cancrinite	6	D	•	a	16.7
EDI	Edingtonite		4-1		b	16.7
THO	Thomsonite		4-1		b	17.7
NAT	Natrolite		4-1		b	17.8
STI	Stilbite		4-4-1			16.9
HEU	Heulandite		4-4-1			17.0
SOD	Sodalite	4 6	B		a	17.2
MOR	Mordenite		5-1	•	c	17.2
DAC	Dachiardite		5-1		c	17.3
BRE	Brewsterite	4				17.5
LAU	Laumontite	6				17.7
FER	Ferrierite		5-1	•	c	17.7
MEL	ZSM-11		5-1	•	c	17.7
MFI	ZSM-5		5-1		c	17.9
EPI	Epistilbite		5-1		c	18.0
YUG	Yugawaralite	4 8				18.3
ANA	Analcime	4 6				18.6
ABW	Li-A (BW)	4 6 8		•		19.0
BIK	Bikitaite		5-1		c	20.2

[a] Shown in Fig. 1.1

[b] Shown in Fig. 1.2

[c] Shown in Fig. 1.3

[d] Number of T-atoms nm^3

The sigma transformation developed by Shoemaker et al [39] generates new building blocks by the removal of tetrahedral T-atoms in a plane and subsequent replacement with a pair of T-atoms with oxygen bridges. These may be used to generate new structures and transform structures into others. For example, inverse transformation may be used to reduce a double 6 ring to a single one in the framework; the cancrinite cage wih double 6 ring may be transformed to a gmelinite cage by rotating the tetrahedra of the interior 6 ring outwards; transformation of a gmelinite cage to a sodalite cage is performed by breakage of the bonds in a plane through the 4 ring and rotation of the top half through 60°. The latter two are illustrated in Fig. 1.4 and 1.5.

Comparison of the many hypothetical structures with the observed ones shows that high symmetry structures are favoured; this is especially evident for the 6 ring family. Stereochemical requirements i.e. energetically favoured conformations play a significant role in determination of the chemical feasibility.

The first zeolite to have its structure predicted prior to its synthesis is zeolite Rho [45].

With increased knowledge of zeolite chemistry and synthesis, it should one day be possible to design and produce zeolites with chosen structures and hence make catalysts for specific reactions [39].

1.5 Properties

The properties of a zeolite are dictated by its structure. The three main properties that have commercial applications are cation exchange, sorption and catalysis. Catalysis is the most outstanding application in the petroleum industry.

1.5.1 Cation Exchange Properties [6, 46]

As mentioned earlier, zeolites are ordered, porous, crystalline, three dimensional aluminosilicates composed of three dimensional networks of SiO_4 and AlO_4 tetrahedra which are connected by the sharing of oxygen atoms such that (Al + Si)/O = 1:2. The aluminium tetrahedra gives rise to a negative charge which is balanced by the inclusion of cations in the structure. The crystal structure comprises cavities of uniform molecular dimensions filled with cations and water of hydration. The water of hydration in the cavities gives the cations mobility and thus cation exchange capabilities. Removal of the water of hydration produces a drastic decrease in the rate of exchange. Ion exchange may be expressed by the stoichiometric reaction:

$$Z_A\overline{M}_B + Z_BM_A \rightarrow Z_AM_B + Z_B\overline{M}_A$$

where M_A and M_B are the two cations involved in the exchange reaction Z_A and Z_B are the valencies of these cations. $\overline{M}_A$ and $\overline{M}_B$ represent the cations in the zeolite phase.

The ion exchange capacity is basically a function of the degree of substitution of aluminium for silicon in the framework structure; the greater the substitution, the greater the charge deficiency and correspondingly the greater the number of alkali or alkaline earth cations required for electrical neutrality. In practice the cation exchange behaviour is dependent on a number of other factors which include [47, 48]:

(1) nature of cation species, i.e. size, charge

(2) temperature

(3) concentration of the cation species in the solution

(4) the structural characterisation of the particular zeolite under investigation.

In certain zeolites, cations may be trapped in structural positions that are relatively inaccessible e.g. cavities or channels, thereby the effective exchange capacity of that species for that ion is reduced, thus giving rise to partial exchange.

Cation sieving may take place if the size of the cations in solution is too large for them to pass through the entry ports into the central cavities of the structure. The framework of a crystalline zeolite dictates its selectivity towards competing ions, and different structures offer different sites for the same cation.

Cation exchange enables the pore sizes to be varied by suitable selection of particular cations e.g. two univalent cations may be replaced by one bivalent cation and so an increase in the space in the pore occurs; alternatively bivalent cations may be replaced by univalent cations.

When a zeolite is immersed in an electrolyte solution, sorption of non- or weak electrolytes and/or salt imbibition may take place in addition to ion exchange [6]. Salt imbibition is small under the usual operating conditions, however sorption of electrolytes may have a marked effect on exchange behaviour in zeolites under some conditions. Least salt imbibition occurs in hydrophobic zeolites with low exchange capacities i.e. high SiO_2/Al_2O_3 and when the external electrolyte solution is dilute. These processes are non-stoichiometric in contrast to the stoichiometric cation exchange reaction.

1.5.2 Adsorption Properties [6, 46-48]

The negative charge generated by the AlO_4^- tetrahedra is partially delocalised over the whole of the framework and pockets of localised

charge are still found in the lattice. The pockets of charge may be effective as adsorption centres. Also the zeolite framework exhibits interstices of molecular dimensions occupied by water of hydration. When efficiently dehydrated, usually by heating to 350°C or 400°C for a few hours or overnight, these zeolites may be utilised as efficient adsorbents whereby the adsorbate molecules which have effective cross sectional diameters small enough to pass through the entry channels are readily adsorbed into the dehydrated channels and central cavities. Molecules too large to pass through the entry channels are excluded. It is this characteristic property which has led to their designation as molecular sieves. In addition to molecular size and shape, other factors may also influence the selective adsorption of certain foreign molecules by the molecular sieves. Among these factors are:

(1) Shape, size and polarity of the absorbate molecules
(2) Cation distribution, size, charge and number
(3) Concentration of sorbate within the crystals
(4) Temperature
(5) Lattice defects such as stacking faults
(6) Presence of impurities in the diffusion pathways
(7) Structural changes brought about by penetrants
(8) Structural changes associated with physical and chemical treatments

The surface area available for adsorption ranges up to several hundred square metres per gram, and some zeolites are capable of adsorbing up to 30% of their dry weight. Most of the surface area is found within the zeolite structure and represents the inner surface of dehydrated channels and cavities. Only about 1% sorption occurs on the external surface of the zeolite. The adsorption is usually characterised by Langmuir type isotherms.

1.5.3 Catalytic Properties [49]

The catalytic activity of a zeolite is usually associated with its acid sites. Zeolites are thus catalysts for cracking, isomerisation, dehydration, and polymerisation.

The acid sites, Lewis or Brønsted, may be generated from the as synthesised material by ion exchange. This is normally accomplished by ammonium ion exchange, followed by calcination to give the hydrogen form of zeolite H-Z. Direct conversion to the H-Z form is rarely carried out with acid as it attacks the zeolite and dealumination of the framework occurs. The exact nature of Lewis acid sites is still a matter of dispute.

Conversion to the hydrogen form may be represented by:

$$Na\ Z + NH_4^+\ (aq) \rightleftharpoons NH_4\ Z + Na^+\ (aq)$$

$$NH_4\ Z \rightleftharpoons NH_3\ (g) + HZ$$

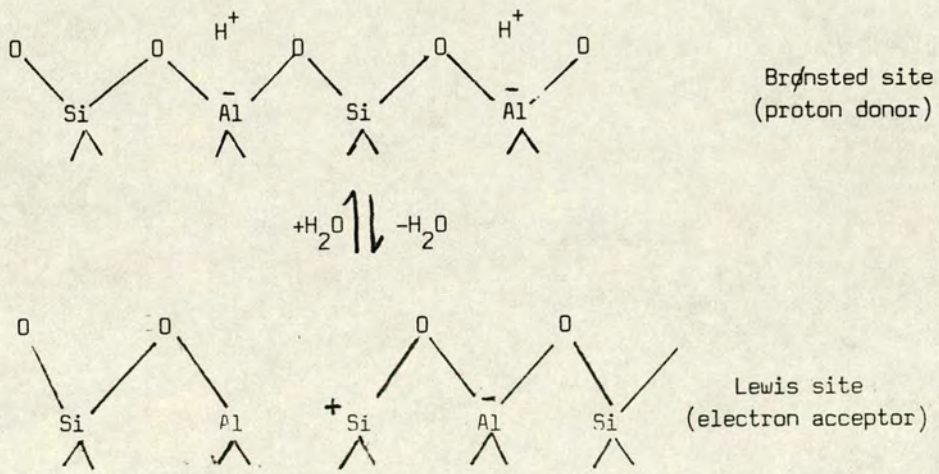

Superacid sites are found to exist in the structure and are a result of the inductive effects associated with neighbouring Lewis sites enhancing the acidity of the Brønsted sites.

The acid strengths can be measured by a variety of methods which include base titration, ammonia temperature programmed desorption,

NMR and IR. The catalytic properties of acid zeolites depend on the number of active sites as well as their strength. Zeolites become more acidic with increase in SiO_2/Al_2O_3 ratio of the framework composition. Hence methods for dealumination are often employed to modify the surface and increase the acidic properties for catalytic work.

Heterogeneous catalysis occurs with zeolites. In order for this type of catalysis to proceed, the reactant species must be transported to and transformed at the reactive surface sites. The products are transported from these sites in the fluid phase. A typical zeolite crystal (around 1μm in size) has an external surface to internal surface ratio of approximately 0.5%. Consequently, although some reactions can be catalysed by external surface sites, a requirement for practical zeolite catalysis is that the reactants can invade the crystals and products can exit. Thus the shape and size of the channels of the zeolite control which molecules may enter, undergo catalysis and leave the zeolite. Other factors which determine which molecules may enter are basically the same as for sorption.

Some zeolites are excellent catalysts in hydrocarbon conversion processes such as reforming, cracking, isomerisation, and dehydrogen -ation. The mechanisms involved in catalysis are quite complex and consequently the precise chemical properties of the zeolite which contribute to a particular catalytic activity are not fully under-stood.

1.6 Commercial Applications [3, 4]

Historically zeolite tuffs have been used by man for more than 2000

years as light weight dimension stone; however, it is only within the last 35 years that the zeolite content of many of these building materials were recognised. The discovery of hundreds of high grade zeolite deposits in rocks of volcanic origin since 1950 and their relative ease of synthesis, with attractive physical and chemical properties has led to the development of a host of applications. Several hundred million pounds' worth of synthetic molecular sieves are sold each year throughout the world. The current use of natural zeolites is relatively small, and restricted to small tonnages in the US, Japan and several other countries.

Zeolites find their main applications as ion exchangers, sorbents and catalysts in the detergent industry, agriculture and petroleum industry. The zeolites in commercial application are: mordenite, chabazite, erionite, clinoptilolite, A, X, Y, L, Ω, Zeolon (synthetic mordenite) and ZSM-5. Their prime application is as catalysts in the petroleum industry. They are used for cracking of heavy oil, selective reactions of n-alkanes and xylene isomerisation. Probably their most outstanding potential application arises from the Mobil discovery that gasoline can be produced from methanol using ZSM-5 [2]. The reaction may be represented by the equation:

$$XCH_3OH \xrightarrow{ZSM-5} (CH_2)_x + YH_2O$$

Zeolites are used as ion exchangers where resins are unsuitable [6]. Where resins and zeolites are interchangeable, the resin remains the preferred material. Most of the applications are based on the ability of certain zeolites to exchange large cations selectively from aqueous solution.

As ion exchangers their most important application is in the detergent industry where zeolite A is used as a water softener and for the partial replacement of tripolyphosphate builders.

As pollution control agents in the nuclear industry, their high resistance to thermal and radiation damage makes them an attractive option. They have been used to remove radioisotopes from spent pile effluent and to store radioisotopes since 1960. They were used in the clean up of 'hot' water which resulted from the Three Mile Island accident in USA.

Natural zeolites, especially clinoptilolite, are used in the removal of ammonia, and ammonium ions from fresh water and in sewage effluent treatment [5, 6]. The spent zeolites may be biologically regenerated. It is likely that synthetic zeolites F and W will supersede the use of clinoptilolite. They have also been used in oil spill clean up and oxygen production.

The energy conservation applications include natural gas purification and solar energy use; solar refrigeration makes use of their hydration-dehydration properties.

In agriculture [5] they act as slow release fertilisers to provide K and N in agriculture soils (they are reported to increase yields of spinach and strawberries), as carriers of herbicides, fungicides and insecticides and as possible traps for heavy metal contaminants in soil amended with municipal sewage sludge. Their addition to the normal diets of swine (in Japan), poultry and ruminants has resulted in increased body weight and feed efficiencies, with simultaneous decrease in intestinal disease. They have been shown to deodorise and increase nutrient content of animal excrement,

improving the fertiliser value of the manure and reducing the energy required for ventilation of buildings for confined livestock.

In aquaculture [50], zeolite filtration is employed to remove toxic concentrations of ammonia and produce oxygen enriched air which allows more fish to be raised in the same volume of water.

Zeolites have been used as flame extinguishers by the release of absorbed material (CO_2 blankets the flame and H_2O produces cooling effects) and as flame resistant finishes on various materials. As electrical conductors by the mobile cations imparting ionic electrical conductivity, this is utilised in developments of improved surface coatings of special papers. They are used as sorbents in double glazing, drying, purification, where the separation is based on sieving and selectivity.

These are just some of the myriad applications for which zeolites have been adopted. There are more than 15,000 scientific papers and over 10,000 patents on zeolites. Hopefully, in the future it will be possible to design synthetic zeolites to meet the application intended. Initially industrial applications of zeolites involved separations; these were followed by catalytic uses. Now they are used to solve environmental problems and are entering into everyday use.

1.7 Natural Fibrous Zeolites as Potential Health Hazards

These wondrous materials that are finding applications in virtually every sphere of life may not be entirely without hazard. It has been found that deposits of fibrous erionite in the small villages of the province of Cappadocia, Turkey, may be responsible for the high rates of pleural mesothelioma [51-53]. One village, Karain, which is a famous tourist attraction because of volcanic rock

formations has houses with walls shaped from the ancient soft volcanic rock. Many cases of, and deaths from, mesothelioma have been reported in this area, but because of the low concentration of erionite Mumpton has suggested that it may be genetic in origin or related to other materials [51]. In other villages where there are high concentrations of erionite, mesothelioma is not endemic.

However, animal studies [52] have shown that fibrous erionite from Eastgate, Nevada, which was injected into mice, caused fibrinoid reactions in 1 day and after 1 week there were several small nodules and after 2 weeks they were larger and more numerous.

Stanton et al [52] suggested that the carcinogenity is related to the physical characteristics of the fibres, such that fibres which are less than 1.5 μm in diameter and greater than 8 μm in length are carcinogenic and this size range has the highest correlation coefficient with mesothelioma induction in rats. Smaller particles, less than 5 μm in length and greater than 3 μm in diameter are processed by phagocytes and are essentially non-carcinogenic. Turkish and Nevada erionite samples have 10-15% of the fibre sizes that correlate with mesothelioma.

Further work is required to clarify this issue, but no published work to date infers any harm from any zeolite (natural or synthetic) other than fibrous erionite. Maltoni et al [52] have reported that other natural and synthetic zeolites failed to create pleural tumours in rats. The morphology of the zeolites in commercial application is rarely, if ever, fibrous. Despite the hazards of fibrous erionite, no doubt zeolites will soon be part of our everyday lives and of benefit to mankind.

1.8 Aims of this Study

One of the zeolites discovered by Mobil and Union Carbide which emerged from the introduction of organic cations, namely TMA, as templates in the reaction mixture is that designated as ZSM-4 or Ω [54, 55]. It is commonly referred to as zeolite Ω. Its natural counterpart, mazzite, was discovered 6 years later [56-58]. The structure determination of the mineral, carried out by Galli [59], showed it to be a 12 ring channel zeolite. X-ray powder diffraction illustrated that ZSM-4, Ω and mazzite were the same material. Although Rinaldi [60], Cole [61] and other workers stated that the introduction of stacking faults into this structure was not possible, Kokotailo et al [62] observed stacking faults, by transmission electron microscopy, in ZSM-4. Thus it was shown that the 12 ring channel of zeolite Ω was blocked by stacking faults which caused a reduction in the channel size from 7.4Å to ~4Å. This blockage was confirmed by reduced sorption capacity for a 12 ring channel zeolite.

The present investigation is concerned with the study of zeolite Ω. It may be divided into three parts:

(1) Synthesis of Ω from the optimum composition

(2) Effect of contact with water

(3) Sorption of molecules from aqueous solution

(1) Synthesis of Ω from the optimum composition

The optimum composition for the crystallisation of zeolite Ω was found by Lowe et al [63] to be:

$$6Na_2O \quad Al_2O_3 \quad 15SiO_2 \quad 300H_2O \quad 3TMABr$$

under stirred conditions at 95°C, for 6 days.

However, it was not established how many of the other variables known to affect zeolite crystallisation influenced the formation of zeolite Ω . It was therefore decided to investigate the effects of order of mixing of the reactants, temperature of mixing the reactants and partial replacement of TMABr by the neutral molecule hexanediol. This molecule was introduced into the reaction mixture in an attempt to occlude it in the main channel during crystal growth and hence synthesise a fault free Ω.

(2) Effect of contact with water

Zeolites are formed in aqueous solution and freed from soluble contaminants by frequent washing with water. The aim of this part of the project was to examine the effect of this washing process on zeolite Ω. It was an essential pre-requisite to studies of sorption by zeolite Ω from aqueous solution.

(3) Sorption of Molecules from Aqueous Solutions

In view of the manner in which zeolite Ω is formed by templating about the TMA cation, it seemed likely that it might sorb other organic molecules from aqueous solution. Only preliminary experiments designed to establish whether this does indeed occur were carried out.

REFERENCES

1. A. Dyer, Chemistry and Industry, 1984, 241

2. W. O. Haag, R. M. Lago, P. G. Rodewald, J. Mol. Cat. 1982, 17, 161

3. D. W. Breck, "The Properties and Applications of Zeolites". p.391.
R. P. Townsend, Chemical Society.

4. F. A. Mumpton, Short Course Notes, Mineral. Soc. Am., 1977, 4, 177

5. F. A. Mumpton, "Zeo-Agriculture, Use of Natural Zeolites in Agriculture and Aquaculture", edited by W. G. Pond and F. A. Mumpton, Westview Press, Boulder Colorado 1984, p. 3.

6. R. P. Townsend, Chemistry and Industry 1984, 246.

7. I. Izod, European Patent 0 013 451, 1980

8. D. W. Breck, "Zeolite Molecular Sieves", John Wiley and Sons, New York, 1974

9. R. M. Barrer, 'Proceeds of 6th International Conf. on Zeolites', Reno, Nevada, Butterworths, Guildford, 1983.

10. F. A. Mumpton, 'Proceeds of 6th International Conf. on Zeolites', Reno, Nevada, Butterworths, Guildford, 1983.

11. R. M. Barrer, 'Zeolites and Clay Minerals as Sorbents and Molecular Sieves', Academic Press, London, 1978. p.1-5.

12. R. M. Barrer, "Hydrothermal Chemistry of Zeolites", Academic Press, New York, 1982, p.2, 43.

13. M. Grandjean, Bull. Soc. Fr. Mineral., 1910, 33, 5.

14. R. M. Barrer and P. J. Denny, J. Chem. Soc., 1961, 983.

15. R. J. Argauer and G. R. Landolt, United States Patent 3 702 886, 1972.

16. D. M. Bibby, N. B. Milestone and L. P. Aldridge, Nature, 1979, 280, 664.

17. S. T. Wilson, B. M. Lok, C. A. Messina, T. R. Cannan and E. M. Flanigen. Intrazeolite Chemistry, edited by F. G. Dwyer, G. D. Stucky, Am. Chem. Soc., 1983, p.79.

18. S. T. Wilson, B. M. Lok, E. M. Flanigen, United States Patent 4 310 440, 1982.

19. J. V. Smith, Min. Soc. Am. Spec. Pap. 1963, 1, 281.

20. M. F. Heddle, "Mineralogy of Scotland", D. Douglas, Edinburgh, 1901.

21. W. A. Deer, R. A. Howie, J. Zussman, "Minerals and Rocks", Longman, London.

22. L. D. Rollmann, NATO ASI Ser., Ser. E 1984, 80, (Zeolites: Sci. Technol.) 109.

23. R. M. Barrer, "Hydrothermal Chemistry of Zeolites", Academic Press, New York, 1982, p.133.

24. T. V. Whittam, British Patent 1 171 463, 1969.

25. T. V. Whittam and K. Pickard, British Patent 1 171 462, 1969.

26. T. V. Whittam and S. Sunderland, British Patent 1 300 946, 1972.

27. F. G. Dwyer and P. Chu. J. Cat., 1970, 59, 263.

28. F. G. Dwyer, United States Patent 3 642 434, 1972.

29. B. M. Lok, T. R. Cannan and C. A. Messina, Zeolites, 1983, 3, 283.

30. L. D. Rollmann, Amer. Chem. Soc. Adv. in Chem. Series 1979, No. 173, 387.

31. C. Baerlocher and W. M. Meier, Helv. Chim. Acta. 1969, 52, 1953.

32. R. Aiello and R. M. Barrer, J. Chem. Soc. (A), 1970, 1470.

33. R. H. Daniels, G. T. Kerr, and L. D. Rollmann, J. Am. Chem. Soc., 1978, 100, 3097.

34. A. Araya and B. M. Lowe, J. Cat., 1984, 85, 135.

35. R. W.Grose and E. M. Flanigen, United States Patent 4 257 885, 1981.

36. A. Varma, Unpublished work.

37. W. M. Meier and D. H. Olson, "Atlas of Zeolite Structure Types", International Zeolite Association, Special publication 1978.

38. G. T. Kokotailo, NATO ASI Ser., Ser. E. 1984, 80, (Zeolites:Sci. Technol.) 83.

39. G. T. Kokotailo, "Proceeds 6th International Conf. on Zeolites", Reno, Nevada, Butterworths, Guildford, 1983.

40. W. M. Meier, "Molecular Sieves", Society of Chem. Indust., London, 1968, p.10.

41. R. W. Gramlich-Meier and W. M. Meier, J. Solid State Chem. 1982, 44, 41.

42. J. Ciric, United States Patent 3 923 639, 1975

43. H. W. Kouwenhoven and J. F. Cole, British Patent 1 345 363, 1974

44. E. M. Flanigen, British Patent 1 178 186, 1970

45. R. M. Barrer, S. Barri and J. Klinoski, 5th International Conf. on Zeolites, Naples 1980, Recent Progress Reports and Discussion, 1981, p.261

46. F. A. Mumpton, Short Course Notes, Mineral Soc. Am., 1977, 4, 165.

47. E. M. Flanigen. Union Carbide, British Patent 1 178 186, 1970

48. E. M. Flanigen. Union Carbide, United States Patent 4 241 036, 1980

49. J. Dwyer, Chemistry and Industry, 1984, 258.

50. R. G. Piper and C. E. Smith, "Zeo-Agriculture. Use of Natural Zeolites in Agriculture and Aquaculture" edited by W. G. Pond and F. A. Mumpton, Westview Press, Boulder, Colorado, 1984, p.223.

51. F. A. Mumpton, 5th International Conf. on Zeolites, Naples, 1980, Recent Progress Reports and Discussion, 1981, p.261.

52. W. N. Rom, W. E. Wright, F. Moatamed, Arch. Environ. Health, 1983, 38 (2), 99. and references therein.

53. K. R. Spurny, Sci. Total Environ. 1983, 30, 147

54. Mobil, British Patent 1 117 568, 1968

55. Union Carbide, Netherlands Patent 6 710 729, 1968.

56. E. Galli and G. Gottardi, Natural Zeolites, Springer-Verlag, Berlin, Heidelberg, New York, Tokyo, 1985.

57. E. Galli, E. Passaglia, D. Pongiluppi and R. Rinaldi, Contr. Min. and Petrol., 1974, 45, 99

58. E. Galli, Soc. Italian a di Mineralogia e Petroligia-Rendiconti, 1975, 3 (2), 599.

59. E. Galli, Cryst. Struct. Comm., 1974, 3, 399.

60. R. Rinaldi, J. J. Pluth and J. V. Smith, Acta Cryst., 1975, B31, 1603

61. J. F. Cole and H. W. Kouwenhoven, Adv. Chem. Series, 1973, 121, 583

62. S. Sawruk, A. C. Rohrmann and G. T. Kokotailo, 5th International Conf. on Zeolites, Naples, 1980, Recent Progress Reports and Discussion 1981.

63. B. M. Lowe, A. Araya, T. J. Barber, D. S. Sinclair, A. Varma, Zeolites, 1984, 4, 263.

CHAPTER TWO

Zeolite Ω:

its Natural Counterpart, Synthesis, Structure and Physical Properties

2.1 Introduction

The discovery of the molecular sieving properties of naturally occurring zeolites [1] promoted interest in the laboratory preparation of their synthetic counterparts. New methods of preparation, especially with the use of nitrogenous organic bases in the reaction mixture [2] revolutionised the zeolite field. Many high silica products with unusual structures and highly improved sorption and catalytic properties emerged. One such material was zeolite Ω [3]/ZSM-4 [4].

2.2 Discovery of Natural Counterpart of Synthetic Zeolite Ω

Mazzite [5, 6] is the first mineral to be discovered(six years) after the preparation of its synthetic counterpart. Named in honour of Professor Mazzi of Pavia University, Italy, it was located at the site of the famous, only known, offretite occurrence: Mont Semiol, Loire, France. Mazzite occurred as bundles of needle-like crystals,long thin hexagonal prisms terminated by basal pinacoids, which were up to 1.5 mm long and 20 μm in diameter. Twins of phillipsite and rhombohedra of chabazite, both fine transparent crystals, were found with mazzite. The crystallisation order, based on superposition of the crystals is phillipsite and chabazite, with offretite probably at the same time as mazzite and also later, Mazzite being superseded by calcite and siderite.

2.3 Organic Nitrogenous Bases in Zeolite Synthesis

Barrer and Denny [2] pioneered the synthesis of nitrogenous crystalline aluminosilicates in the absence of metal cations. Crystallisation of several zeolites, TMA-V, TMA-faujasite, N-L (harmotome), N-A and TMA-sodalite in admixture with TMA-V, using only alkyl ammonium or methyl ammonium ions as the source of cations, was achieved. However, product analysis showed the presence of substantial amounts of sodium which was due to the dissolution of the glass reactor [7]. The latter ion was not intentionally added to the reaction composition, but this is the first record of the usage of mixed inorganic and organic bases in zeolite synthesis. Prior to this, the literature contained little reference to the possibility of use of nitrogenous bases, although Merril and Spencer [2] had reported quaternary silicate formation.

It was argued [2, 8] that the introduction of a large univalent organic cation into the synthesis mixture, to effect partial or complete replacement of the alkali metal cation in the zeolite cavity, would for the retention of electrical neutrality, imply an increase in SiO_2/Al_2O_3 ratio of the zeolite framework. This would enhance the properties of the zeolite towards higher thermal and hydrothermal stability. The application of this concept led to the use of various quaternary alkyl ammonium ions and the successful preparation of silica rich forms of a variety of known zeolites. Direct use of organic cations in the reaction mixture can significantly alter the crystallisation process [7, 8, 9, 10] such that: unusual structures and hence novel zeolites result; crystallisation rate may be strongly

enhanced or inhibited; the framework remains unchanged but with a significantly new composition and alteration in microscopic texture e.g. crystal size, occur. When a different structure results and the crystallisation rate is enhanced by the presence of the organic cations the latter are said to act as templates and the phenomena is called a "templating effect". Zeolite Ω was one of the first materials to be crystallised by this technique.

2.4 Zeolite Ω or ZSM-4?

Both zeolite Ω and ZSM-4 appeared in the patent literature as two new zeolites in 1968. However, in 1978, it was shown that they were in fact the same material [11].

ZSM-4 was first synthesised by Mobil Oil Corporation. A British patent application was filed in 1966 and was granted in June 1968 [4]. Meanwhile, at Union Carbide, Flanigen and Kellberg applied for a Dutch patent in 1967 [3] for a material designated zeolite Ω This patent was granted in February 1968. It was discovered at a later date that these two materials bore a striking resemblance with virtually identical X-ray powder diffraction patterns.

Since the first published data appeared [4, 3] in table I of the respective patents, both Mobil and Union Carbide have amended the original XRD data which characterised these zeolites. In Table I of the Dutch patent, a m-ms line at d = 3.51 Å was present; however, in subsequent patents on Ω, namely British patent 1970 [12] and US patent 1980 [13] this line was replaced by a m-ms line at d = 3.15 Å. Comparison of ZSM-4 data shows that Mobil inadvertently patented a non-existent line (100%) at interplanar spacing d = 5.37 Å

in Table I of the 1966 patent [4] which is absent from both the data for Ω [3, 12, 13] and future patents on ZSM-4 [13-21]. Subsequent Mobil patents also show the absence, from Table I, of the first line w at d = 16.07 Å and the addition of the w line at d = 5.5 Å, although both these lines are reported in tabulated powder diffraction patterns for examples of ZSM-4 and Ω.

It is perhaps on the basis of the absence of the major line supposedly characterising ZSM-4 that zeolite Ω was recognised as an independent species in 1968 and with the corrected data published at a later date [12], Mobil, in order to identify them as separate entities continue to omit the first line from Table I. The zeolite is generally recognised as zeolite Ω, since Union Carbide were the first to patent the correct XRD data in 1970 [12]. In 1982 Mobil finally acknowledged that Ω is a ZSM-4 analogue [21].

2.5 ZSM-4 and Zeolite Ω Synthesis

Although zeolite Ω is readily synthesised at temperatures below 100°C, there has been little published work on its crystallisation and much of this is to be found in the patent literature [3, 4, 12-21]. Several improvements in the preparation techniques have been developed. These are: inexpensive routes using clays as sources of alumina and silica, and the in situ formation of TMA from CH_3-X and $(CH_3)_3N$; incorporation of Li and K ions in addition to Na and TMA during synthesis; and advantages in the replacement of TMA by pyrrolidine, choline chloride and diazobicyclo [2, 2, 2] octane (Dabco).

The first published crystallisation of Ω [3] was by the more or less standard hydrogel preparation. This required the reactants sodium hydroxide and alumina trihydrate to be dissolved in water, combined with TMAOH (aq) and blended with aqueous colloidal silica. The reaction mixture was placed in teflon lined glass jars, under quiescent conditions and allowed to crystallise for 64 h at 100°C. However, the ZSM-4 preparation [4] used a crystallisation directing agent (CDA) which increased yields, reproducibility and provided the alumina and silica in reactive forms. In the CDA procedure sodium aluminate and sodium hydroxide are dissolved in water and sodium silicate solution is then added, the mixture is heated for 0.5 h at 60°C to give a clear solution. This CDA is added to sodium silicate solution in a Waring Blender, mixed for five to ten minutes followed by aluminium chloride addition. The resulting slurry is heated at 100°C for 0.5 h and filtered; TMAOH (10% aqueous solution) is then thoroughly mixed with the filter cake and the mixture heated at 100°C for 3 to 7 days under static conditions. Less TMA_2O is required by use of the wet filter cake preparation [14] provided the sodium hydroxide is included in the TMA solution to balance the electronegative charge of the aluminosilicate tetrahedra. However, this results in an increase in crystallisation time.

Crystallisation of ZSM-4 via metastable faujasite, using TMA to shift the equilibrium from zeolite P to ZSM-4 has been achieved [15, 22]. Faujasite (zeolites X or Y) crystallised from aluminosilicate gels is metastable and if allowed to remain in its mother liquor, it recrystallises to the more thermodynamically stable zeolite P. However, in the presence of TMA, faujasite is converted to ZSM-4.

This may be effected under both quiescent and agitated conditions at 100°C, although the latter [15] is preferred. A faujasite crystallisation directing agent (FCD) prepared from a mixture of silica, alumina, sodium hydroxide and water, aged for 0.5 h at 60°C is employed. The FCD is then combined with the remainder of the required reactants and placed in polypropylene jars for 14 days. In the agitated system crystallisation time is reduced to 3 days. The FCD technique directs the mechanistic path to faujasite and then ZSM-4. After 12 h all the products are faujasite, but the presence of TMACl in the reaction mixture results in ZSM-4 within 13 days, whereas in the absence of organic zeolite P is formed.

Crystalline zeolite Y has been employed as seed in an Ω synthesis [23]. In this case the incorporation of 50% zeolite Y into the alumino-silicate gel resulted in zeolite Y after 10 h at 140°C but after 12 h, conversion to Ω had occurred and in 24 h the process attained completion. The XRD pattern illustrated [23] showed good crystalline samples of zeolite Y, Ω (12 h) and Ω(24 h). The product yield was increased by 50%, indicative of the seeding effect by zeolite Y.

Clays have been used as the major source of alumina and/or silica [16, 20] in the preparation of hard aggregates of highly crystalline ZSM-4. The latter permits subsequent chemical processing with the elimination of pelletization which is normally necessary prior to the use of zeolites as adsorbents or catalysts. A reaction mixture contains at least sodium and TMA (the quaternary may be synthesised in situ in the reaction mixture), silica, alumina of which 80% is provided by the clay, and less than 50 weight per

cent water. The clay may be selected from kaolin, halloysite or montmorillonite and it is preferable that it is heated at 1700°F for 6 h before use. Crystallisation of ZSM-4 is achieved within 42 h at 100°C.

Zeolite Ω with Na, K, and TMA incorporated during synthesis has been achieved by Barrer and Aiello [24]. The procedure required aluminium hydroxide, obtained by the action of water on amalgamated aluminium foil, to be dissolved in the mixed aqueous bases, and the resulting solution mixed with silica (from silica gel and Syton 2X) in polythene bottles. The bottles were sealed and during crystallisation rotated in an air oven at 80°C for 7 days. In addition to these alkali cations, Li may also be incorporated during synthesis [8, 25]. This crystallisation was carried out under reflux for 72 h with stirring to prevent erionite formation. The system tolerates Li, but little K. The sodium can be completely removed from the uncalcined product by exhaustive ion-exchange with 2M NH_4NO_3 (six times). However, calcination followed by ion exchange facilitates the removal of Na, since the TMA is no longer blocking the exits.

Crystallisation of ZSM-4 using precursors to the organic cation TMA [16, 17] was carried out by Schwartz. The precursors, trimethylamine and TMA-halide are mixed together in situ in the reaction mixture. The in situ reaction which occurred in the presence of alkali, water, silica and alumina was unexpected. This route results in substantial economic savings.
Prior to 1977, TMA was thought to be the only organic template to effect ZSM-4 crystallisation. However, in that year Mobil announced the use of pyrrolidine and choline chloride salts [19]

in the preparation of ZSM-4. Both organics, used independently, in the presence of alkali metal cations, such as sodium, result in a ZSM-4 product with very low nitrogen level. The sodium content from this ZSM-4 preparation is readily removed by one exchange with an ammonium salt. Thus a more stable product may be produced, prior to the removal of the organic species by calcination.

In 1977, the Gulf Research and Development Company [11] carried out an investigation into the synthesis of both ZSM-4 and Ω, from their respective methods of synthesis according to patent specification [14, 3], to determine the difference, if any between the two materials. The results of their investigation were certainly enlightening.

The following compositions were used in the synthesis as specified in Table 2.1 below.

Table 2.1

Mole ratios of oxides in Ω and ZSM-4 synthesis

ZEOLITE	$\frac{Na_2O}{Na_2O + TMA_2O}$	$\frac{TMA_2O + Na_2O}{SiO_2}$	$\frac{SiO_2}{Al_2O_3}$	$\frac{H_2O}{TMA_2O + Na_2O}$
ZSM-4 [a]	0.96	0.55	27.2	34.9
Ω [a]	0.8	0.4	10.0	40.0
ZSM-4 [b] (Pref.)	0.75-0.99	0.15-0.75	6-30	20-150
(Gen.)	0.31-1.0	0.05-0.9	3-60	15-600
Ω [c] (Pref.)	0.68-0.99	0.2-0.4	6-10	15-60
(Gen.)	0.33-1.0	0.1-0.6	5-30	10-125

a Work by Gulf Research & Development Co. b Mobil US patent 3578 723 (1971)
c Union Carbide US patent 6710 729 (1968)

It is apparent that there is overlap in the compositions claimed to produce zeolite Ω and ZSM-4: a much higher SiO_2/Al_2O_3 ratio [11] is suggested for ZSM-4 than for Ω. Despite this the TMA_2O/Na_2O ratio is higher in Ω formulation. The reagents used as sources of silica and TMA_2O are different in each preparation

Ω : Ludox AS SiO_2 and TMAOH

ZSM-4: N brand sodium silicate (28.7 wt % SiO_2 8.9 wt % Na_2O) and TMACl.

In spite of the differences in the reaction mixtures, the Gulf workers [11] found that the XRD patterns for Ω and ZSM-4 showed a striking resemblance, although it was apparent that the pattern for Ω had sharper peaks. Hence on the basis of XRD pattern, the aluminosilicate frameworks are quite similar, although the aluminium concentration in the tetrahedral framework site may be different in these two isomorphous zeolites. Chemical analysis of a typical Ω and ZSM-4 preparation gave the respective final product compositions:

Ω : 0.75 Na_2O 0.25 TMA_2O Al_2O_3 6.01 SiO_2 4 H_2O

ZSM-4: 0.92 Na_2O 0.28 TMA_2O Al_2O_3 6.43 SiO_2 6.5 H_2O

The excess alkali, in ZSM-4, may be due to incomplete washing of the sample. ZSM-4 had a slightly higher SiO_2 content compared with that of Ω. The cell constants and differences in port size are given in Table 2.2 below. Comparison is also made with its natural counterpart Mazzite.

Table 2.2

Unit Cell characteristic of Ω , ZSM-4 and Mazzite

ZEOLITE	CELL TYPE	CELL CONSTANTS/Å		SORPTION
ZSM-4	Cubic	a = 22.4	(1)	Absorbs cyclohexane
Ω	Hexagonal	a = 18.1 c = 7.59	(2)	Large port Size ~11 Å absorbs $[(C_4F_9)_3N]$
Mazzite	Hexagonal	a = 18.392 c = 7.646	(3)	

(1))
) Gulf Research and Development Co. [11]
(2))

(3) [5, 6]

Comparison of the mechanism of crystallisation of Ω and ZSM-4 from Flanigen's and Bowes' respective synthesis [3, 14] illustrates that there is a difference. Samples taken during synthesis of zeolite Ω (which crystallised over a 10 day period) contained detectable amounts of faujasite crystals which separated from the gel and slowly transformed into zeolite Ω over a few days. Bowes' route to ZSM-4 did not proceed via any intermediate phase. However, a significant relationship in the mechanism of ZSM-4 and Ω synthesis is apparent in Dwyer's route to ZSM-4 [15, 22]. Dwyer's route proceeds via the metamorphosis of faujasite in the presence of TMA. Also, as previously mentioned, the use of zeolite Y as seed by Xu Qinhua et al [23] produces Ω .

Thus: Faujasite → Ω Union Carbide [3] (Gulf workers 1978)

Faujasite → Ω Xu Qinhua et al [23] 1980
seed

Faujasite → ZSM-4 Dwyer 1972. [15, 22]

No intermediate phase → ZSM-4 Bowes 1971. [14]

It is therefore apparent that both Ω and ZSM-4 may be obtained via a faujasite intermediate. The mechanism of ZSM-4 formation from faujasite [22] appears to be by nucleation on the surface or edges of the faujasite crystal, rather than from the mother liquor.

In 1982, Rubin and Rosinski described the use of diazobicyclo [2, 2, 2] octane, Dabco, substituted for TMA in the basic ZSM-4 composition [21]. According to C:N analysis, the Dabco is encapsulated in the zeolite. The crystallisation was carried out in sealed plastic jars under static conditions at 100°C for 125 days and 146 days and produced pure ZSM-4. In this patent, Mobil finally acknowledged that Ω is the ZSM-4 analogue.

Union Carbide have only patented one route of synthesis for Ω [3, 12, 13] whereas Mobil continue to find new routes to their ZSM-4. Chao Hui and Xu Ruren [26] and Xu Qinhua et al [23] have contributed much to the kinetics and mechanism of crystallisation. However the details of the kinetics of the reaction at 140°C cannot be given here as the publication is in Chinese and no translation is available.

2.6 Morphology of Ω , ZSM-4 and Mazzite

The morphologies of Ω and ZSM-4 from the various synthesis routes are summarised in Table 2.3; the mineral mazzite is also included. Comparison of the morphology of Ω and ZSM-4 [11] by SEM showed that Ω consisted of spherulites with poorly resolved crystal faces, small fissures and rough texture, whereas ZSM-4 was composed of smooth faced spherulites. Union Carbide [3], and Cole [8] disclosed that their material consisted of extremely small

Table 2.3

Comparison of Morphology of Ω , ZSM-4 and Mazzite

REFERENCE	ZEOLITE	MORPHOLOGY	PARTICLE SIZE/μ	COMMENTS
Flanigen & Kellberg (Union Carbide) [3]	Ω	Anhedral to spherical	0.2	Line broadening in XRD
Aiello & Barrer [24]	Ω	Very small spherulites, some hexagonal		
Xu Qinhua et al [23]	Ω	Rough texture spherical aggregates		Sharp peaks in XRD pattern
Chao Hui et al [26]	Ω	Very small crystals spherical aggregates		
Cole & Kouwenhoven [8]	Ω	Very small crystallites	1.5	Size of aggregates line broadening in XRD
Lowe et al [27]	Ω	2 types: spherulites and rods		Dependent on reaction mixture composition - not a mixture of morphological types
Perrotta et al [11]	Ω	Fissured spherulites rough texture		Sharp XRD pattern, mechanism via faujasite
Mobil [4]	ZSM-4	Cube	1.2	
Bowes [14]	ZSM-4	Rod-like		
Dwyer & Chu [22]	ZSM-4	Hexagonal prismatic rods		Mechanism proceeds via Faujasite
Perrotta et al [11]	ZSM-4	Smooth spherulites		
Ciric [28]		Fine fibres	500-1000 Å x 3-8 μm	
Mazzite [5, 6]		Hexagonal prismatic rods	1.5 mm x 20 μm	

aggregates of small particles 0.2μm [3] with rough texture, the small particles presence was confirmed by line broadening in XRD. Similarly, reports on Ω synthesis by Chao Hui et al and Xu Qinhua et al [26, 23] have shown the presence of the rough texture. Barrer [24] reported samples of Ω consisting of both very small aggregates with rough texture and rod type structures; and from different compositions, Lowe et al [27] have found that both types may be synthesised independently. ZSM-4 synthesised via faujasite, by Dwyer and Chu [15, 22], and the CDA technique by Bowes [14], was found to consist of rods, whereas Mobil claimed [4] ZSM-4 to be cubes of 1-2 μm in size. It is apparent that the ZSM-4 rod type morphology is analogous to that of mazzite. The rough texture of spherulites has been used to differentiate Ω from ZSM-4 by Xu Qinhua et al and Chao Hui et al [23, 26].

2.7 Structure of Mazzite and Ω

2.7.1 Framework Structure

Comparison of the XRD patterns of mazzite and Ω [5] illustrated that they both have the same aluminosilicate framework. The pattern of zeolite L is similar to, but distinct from, that of mazzite and zeolite Ω. The lattice constants have similar values in all 3 cases, but the structure of mazzite is not in accordance with that proposed for the synthetic zeolite Ω by Barrer and Villiger [29]. The data are given in Table 2.4 below:

Table 2.4

ZEOLITE	MAZZITE	Ω	L
Space group	$P6_3/mmc$ (a) (or $P\bar{6}2c$ or $P6_3mc$)	P6/mmm (b)	P6/mmm (c)
a/Å	18.392	18.15	18.40
c/Å	7.646	7.59	7.52

(a) Galli et al [5]

(b) Barrer & Villiger 1969 [29]

(c) Barrer & Villiger 1969 Structure of Zeolite L

The chemical formulae of mazzite and related synthetic phases [5] are:

Mazzite : $Na_{0.03}\ K_{1.91}\ Mg_{1.99}\ Ca_{1.35}\ [Al_{9.77}Si_{26.53}O_{72}]\ 28.06H_2O$

Zeolite Ω: $Na_{6.8}\ (TMA)_{1.6}\ [Al_8Si_{28}O_{72}]\ 17.9\ H_2O$
Barrer & Villiger 1969

Zeolite L : $Na_{0.8}\ K_{8.2}\ [Al_9Si_{27}O_{72}]\ 17.9\ H_2O$
Original paper

Zeolite Ω has a similar Si/(Si + Al) ratio (0.75) to mazzite, but its cation content (TMA, Na) is impossible for a natural phase. Neither magnesium nor calcium are present in Ω. Mazzite has a markedly higher water content than Ω, probably because the channels of the latter are partly filled by the huge TMA ion. The structure determination of Ω, by X-ray powder diffraction [29] was carried out prior to the discovery of the mineral. Single crystal determination work on mazzite [30, 31] resulted in a slightly different structure to that proposed for Ω.

Structure elucidation of hydrated mazzite showed it to be built up

of a 3 -dimensional framework of tetrahedra $(Si, Al)O_4$ with all verticies in common. The characteristic feature of the framework is the presence of the gmelinite cages. The unit cell has two such cages shifted by c/2 (see Fig. 2.1). The framework contains isolated large, near cylindrical, channels parallel to c; these have an average free diameter of ~ 7.5 Å and are surrounded by rings of 12 tetrahedra. There are two types of smaller channels parallel to c; the first consists of gmelinite cages stacked one on top of the other and is surrounded by rings of 6 tetrahedra; the second is between 2 cross-linked rows of cages surrounded by distorted 8 membered rings. The exchangeable cations are distributed into three positions, (I) inside the cages, (II) in the channels between the cages, and (III) in the middle of the large 12 ring channel. The structure of mazzite is illustrated in Fig. 2.2.

The topological difference between mazzite's structure and that proposed by Barrer and Villiger [29] for Ω lies in the interconnection of the columns of gmelinite cages and results in a different space group from that obtained using single crystal data for mazzite. The difference between the two arises because, in X-ray powder diffraction many reflections are superimposed and weaker ones cannot be observed, whereas in single crystal work all the reflections may be observed. The X-ray powder diffraction pattern of mazzite was found to be the same as Ω and ZSM-4 [31, 28]. Hence they could have the same space group and framework. The loss of resolution of reflections may account for Barrer's proposed structure with the gmelinite cages at the same level. The structure of Ω viewed down the c axis is illustrated in Fig. 2.3.

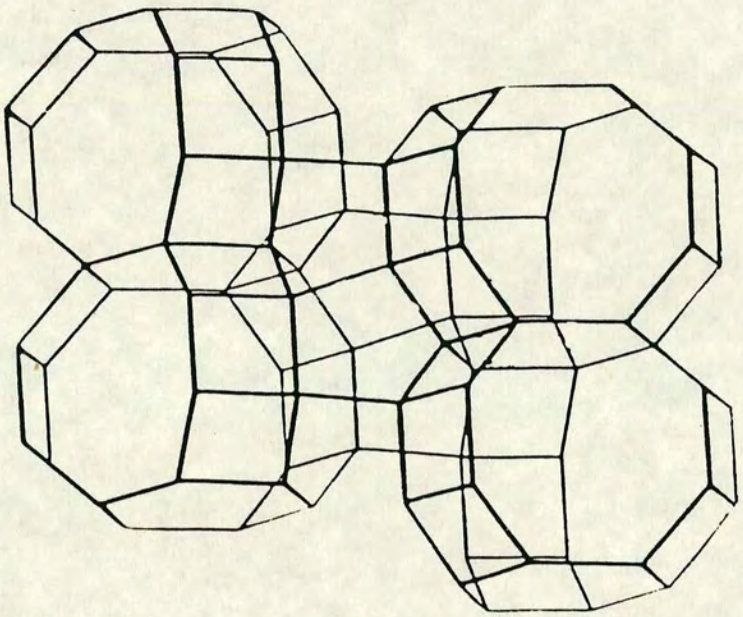

Fig. 2.1 The superimposition and cross linking of gmelinite type cages in the mazzite structure [31]

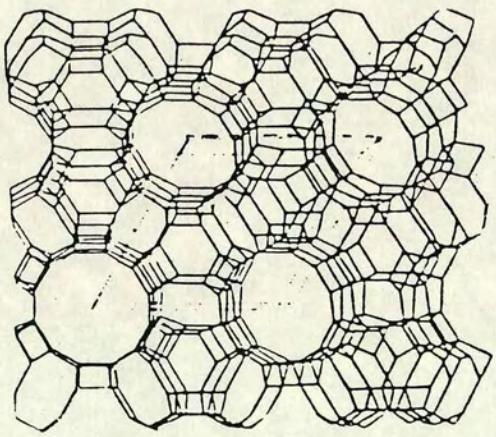

Fig. 2.2 Structure of Mazzite [40]

2.7.2 Cation Sites

2.7.2.1 Cation sites in mazzite

The distribution of the cation sites in mazzite is illustrated in Fig. 2.4 [31]. One of the characteristic features of mazzite, as a zeolite, is its high Mg content. Mg ions occur in site I at the centre of all the gmelinite cages. Each magnesium ion has two water molecules above and below at any instance, tetrahedrally coordinated, though there are a total of nine positions for water. The magnesium water complex may act as a template in gmelinite cage formation in much the same way as the large organic TMA ions template the gmelinite cage in Ω crystallisation.

Site II is 50% occupied by a mixture of ions, in order of abundance K~42%, Na~5%, Ca~3% and 50% empty. These cations co-ordinate mainly to framework oxygens and water molecules.

Site III is occupied by calcium ions and water molecules. The cations are located at regular intervals in the middle of this wide channel lined with water molecules. This is the most plausible configuration, although the distribution of cations and water molecules in these wide channels is not as well defined as it may be in smaller cavites due to the considerable thermal motion.

2.7.2.2 Cation sites in Ω

In Ω cationic sites were determined by ion exchange and pyrolysis studies [24, 8]. A typical sample contains 8 cations per unit cell with about 6 sodium and two TMA ions. Exhaustive ion exchange of Na with NH_4NO_3 proceeded to completion albeit with some difficulty, with the TMA ions firmly encapsulated in the framework. Similarly,

removal of TMA by ion exchange was found impossible by Flanigen [3] and Barrer [24]. Accordingly two TMA ions occupy the two gmelinite cages per unit cell, showing that TMA is incorporated into the zeolite framework during crystallisation. These ions are too large to escape through the 8 ring windows of the cages and are thus not exchangeable. Location of TMA in the main channel is improbable as a single ion exchange at reflux temperature would be capable of removing them [24]. However, according to Cole and Kouwenhoven [8], freshly prepared Ω contains some TMAOH or silicate imbibed in the main channel which may be readily removed during preliminary ion exchange.

The sodium ions are expected to be sited in the two small cavities per unit cell which link the gmelinite cages and in the 12 ring channels.

2.7.3 Structure at 600°C

The structure of dehydrated mazzite was studied by Rinaldi et al [32, 6]. Upon dehydration at 600°C the aluminosilicate framework undergoes only minor distortion, whereas the cations migrate in order to maintain a stable configuration. All the water present in the channels formed by the 12 rings was removed and between 1 and 5 potassium ions moved to the walls of the channel in square co-ordination with four framework oxygens. Magnesium jumps from the centre of the gmelinite cage to the centre of the 6 ring at the top or bottom of the cage, where it co-ordinates with 3 oxygens plus some residual water which lies on the same inversion hexad. Calcium lies in the channels between cages and is octahedrally co-ordinated to four oxygens and two water molecules. The water

molecules lie near the centre of the boat shaped 8 ring at the sides of the gmelinite cages. This site is also occupied by the remaining one potassium ion and ~ $2H_2O$ unbound to calcium. Potassium and calcium interchange their sites upon dehydration; this is an example of "internal ion exchange". In all 9 molecules of water remain after dehydration at 600°C with slight shrinkage of the unit cell.

2.7.4 Stacking Faults

2.7.4.1 Evidence for stacking faults

According to Rinaldi et al [32], there is no simple manner in which stacking faults may be introduced into the mazzite structure. Similarly, it was stated by Cole and Kouwenhoven [8], that an important property of the Ω structure, proposed by Barrer and Villiger, is that the main channel system cannot be blocked by stacking faults. However, since Barrer's structure was determined by powder work, the displacement of the gmelinite cages by c/2 was not detected. Now, having established that Ω and mazzite are isostructural, then Ω too should be free from stacking faults. However, it has been reported [28] by Sawruk, Rohrman and Kokotailo, that stacking faults are present in ZSM-4. The introduction of random stacking faults changes the channel system in ZSM-4 and also the adsorption properties. This has also been observed in gmelinite. Random stacking when superimposed on a structure with ordered stacking sequence results in slight changes in the XRD pattern (such as the appearance of weak odd l lines in offretite). A direct method of observation of random stacking faults is provided by transmission electron microscopy (TEM).

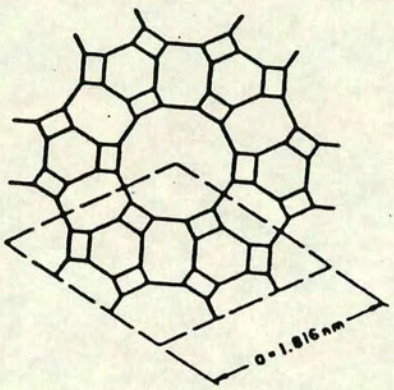

Fig. 2.3 Structure of Zeolite Ω [8]

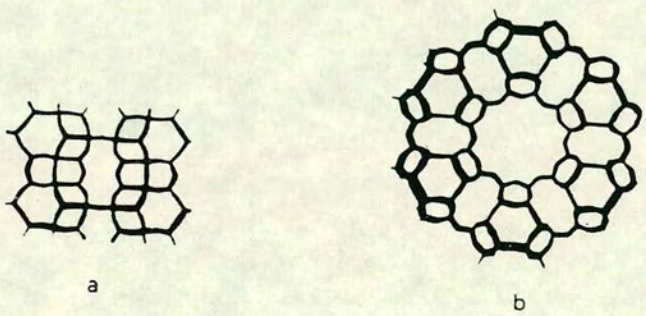

Fig. 2.5 Framework Structure of Zeolite L

(a) linked columns of cancrinite and sodalite cages

(b) view along c axis

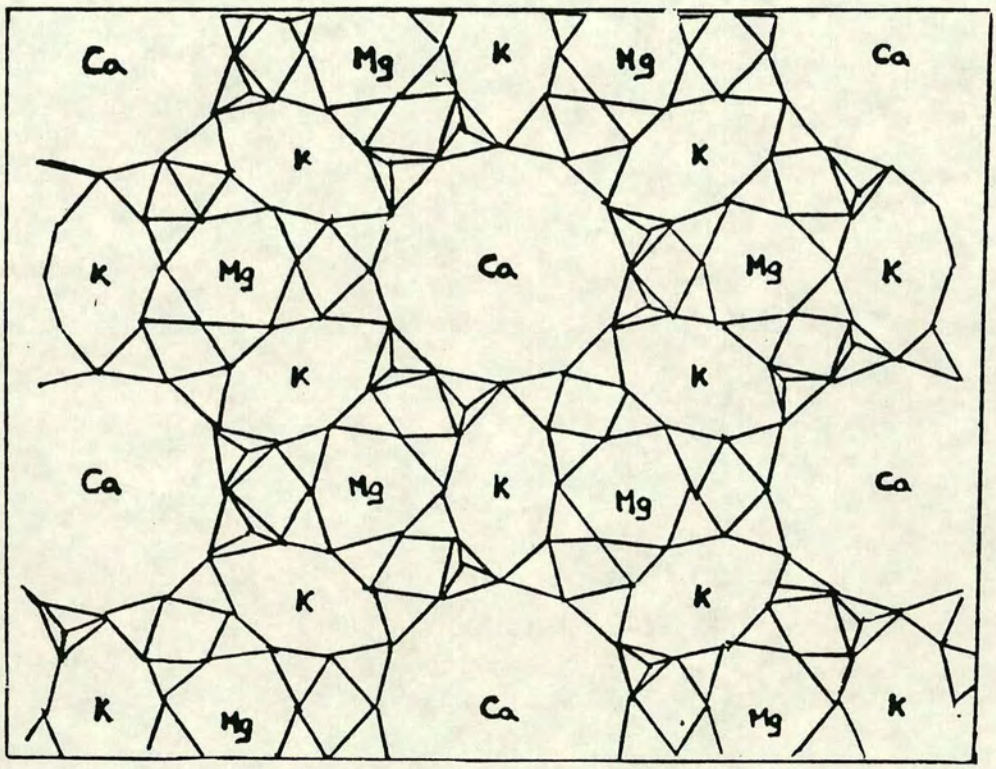

Fig. 2.4 Structure of mazzite projected along c axis, illustrating cation sites

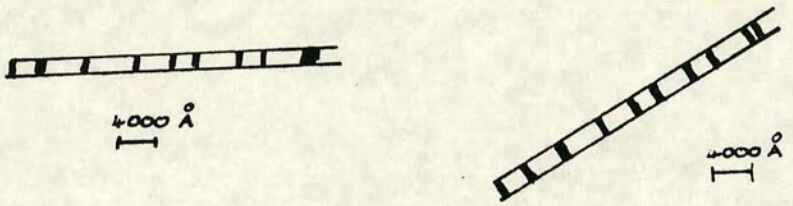

Fig. 2.6 TEM of Ω, illustrating faults

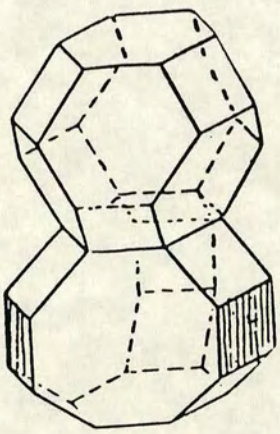

Fig. 2.7 Column of gmelinite and sodalite cages

Fig. 2.8 Framework of stacked ZSM-4

(a) linked columns (b) viewed along c axis

The stacking faults are characterised in TEM by contrast lines due to a phase difference between the electrons scattered on either side of a fault.

The presence of stacking faults in ZSM-4 was indicated by the difference in adsorptive properties of the latter and Linde L which has essentially the same channel system. The proposed alteration of the stacking sequence, which is thought to occur, results in the blockage of the 12 ring channel. The Linde L structure consists of stacks of cancrinite cages, linked through double six-membered rings; these columns are linked through 8 membered rings to form a hexagonal structure with 12 ring channels parallel to the c direction. The framework structure of zeolite L is illustrated in Fig. 2.5. The adsorption of molecules larger than those admitted by 8 ring systems is much greater in zeolite L than in ZSM-4/Ω. Consequently this suggested that ZSM-4 channels may be blocked.

Synthesis of ZSM-4 in a mixed base TMA and sodium system, by Ciric [28], produced fine fibres 500-1000 Å in diameter and 3-8 μm long. Examination of these fibres by TEM [28], resulted in the observation of contrast lines similar to those in erionite (which has stacking faults) indicative of the presence of stacking faults. This is illustrated in Fig. 2.6. These rather broad contrast lines, extended over a distance of more than 25 Å; the distance between stacking faults is as small as 300 Å i.e. about 40 unit cells.

2.7.4.2 Mechanism proposed for Production of Stacking Faults

A suggested mechanism for the production of stacking faults, and blockage of the 12 ring channel, is based on the relationship between the sodalite and gmelinite cages. The gmelinite cage may be converted into the sodalite cage by rotation of the upper half through 60° with respect to the lower half. Rotation of a layer of gmelinite cages in ZSM-4 results in columns of gmelinite cages terminated by sodalite cages. The linkage of these alternate columns terminated by sodalite cages, viewed along the c axis of the three dimensional structure with a stacking fault is illustrated in Fig. 2.7 and 2.8. Blockage of the large channel is clearly evident.

The same mechanism may be applied in stacking Linde L; however this is complicated by the substitution of a layer of gmelinite cages for cancrinite, followed by rotation to give a sodalite cage. Stacking faults in Linde L have not been observed, probably due to the two step process in the stacking sequence.

2.7.5 Transformation of Offretite to Mazzite

Mazzite, discovered in the famous offretite site at Mont Semiol, has an interesting structural relationship with offretite [33]. The presence of hydrated magnesium ions in the gmelinite cage, superimposition of these column forming cages and the large 12 ring channel system are all common to both zeolites. A rotation of 60° and translation of c/2 of the columns is all that is necessary to transform one structure into the other. Geological conditions may have changed in favour of this process and hence the occurrence of mazzite.

2.8 Sorption Properties of Zeolite Ω /ZSM-4

At the time of discovery of the new zeolite Ω [3], Flanigen published sorption data which showed that this novel zeolite is capable of sorbing perflurotributylamine and thus implied that Ω had an aperture size of at least 11 Å. Hence with such a pore size, heavier feedstocks which contained molecules too large to enter the faujasite framework could be processed. Thus interest in the synthesis of this material for its properties was aroused and the investigation to distinguish ZSM-4 from Ω , which are isostructural with the mineral mazzite, commenced. A summary of the molecules sorbed by Ω and ZSM-4 appears in Table 2.5 and a comparison with a nother 12 ring system, devoid of faults, Linde L is given in Table 2.6

The sorption data in Table 2.6 illustrates that the 12 ring channel of ZSM-4/Ω is afflicted by stacking faults and thus sorption capacity is considerably reduced. In order to find a feasible explanation for Flanigen's claim to $(C_4F_9)_3N$ adsorption by Ω [3], thus implying a pore size of 11.5 Å the morphology and structure must be considered. On the basis of structural evidence, Ω has a channel diameter of 7.5 Å and therefore it is highly unlikely that $(C_4F_9)_3N$ is adsorbed into the large main channel. However it may be adsorbed onto the rough textured surface, and to give the impression of $(C_4F_9)_3N$ actually adsorbing into a channel, the spaces between the crystallites (0.2 μm in size) probably gives rise to a secondary pore system. Xu Qinhua et al [23] observed this with sorption of Et_3N and benzene, i.e. condensation and not sorption occurred, and although a small amount of sorption was apparent, the rapid increase was suggestive of condensation in the secondary pore system.

Table 2.5

Sorption Properties of ZSM-4 and Ω

REF.	ZEOLITE	MOLECULES SORBED	COMMENTS
[3]	Ω	Perflurotributyl amine $(C_4F_9)_3N$	Critical diameter 11.5 Å aperture 11 Å
		C_6H_6, $C_8F_{16}O$, cyclic compounds	activated at 200°C
		21% H_2O @ 25°C	Morphology: rough texture very small spherulites
[24]	Ω	17.0% H_2O	Mixture of spherulites and rods
[23]	Ω	Water, MeOH, C_6H_6 Et_3N	Condensation in secondary pore structure of aggregate of Ω Morphology: rough textured spherulites
[11]	Ω ZSM-4	hexane, C_6H_{12} $(C_4F_9)_3N$ cyclooctatetrene	$(C_4F_9)_3N$ not rapid. Sorption at 80°C
[14]	ZSM-4	3.9% C_6H_{12} at 20°C 20 mm Hg 12.3% H_2O at 20°C 12 mm Hg	Rod type crystals
[4]	ZSM-4	C_6H_{12} 4-7% 13-14% H_2O	Activated and at least partially dehydrated 200-600°C
[8]	Ω	n hexane 2, 3 dimethylbutane	5 Å Very small crystallites

Table 2.6

Adsorptive Data for Zeolite L, ZSM-4 and Ω at 298 K suggestive of stacking faults [28]

MOLECULE	PRESSURE/TOR	ZEOLITE L g/100g	Ω g/100g	ZSM-4 g/100g
Isobutane	10	5.3	1.7	
	100	6.7	2.2	
neopentane	10	5.2	2.5	
	100	6.6		
benzene	100	6.6	3.3	
	1	6.0		1.11

The most recent synthesis of ZSM-4, by Rubin and Rosinski [21] in 1982 may have achieved the successful synthesis of a fault free Ω using diazobicyclo [2.2.2.] octane (Dabco). This molecule, on the basis of C:N analysis was encapsulated into the zeolite. It is probably trapped in the main channel, and so removal of Dabco, by calcination, will probably provide a fault free Ω. However sorption data is not given.

2.9 Thermal Properties

2.9.1 Introduction

The thermochemical properties of a zeolite are an important aspect of its characterisation, as prior to application as a catalyst or sorbent the zeolite is usually converted into its activated form, H-zeolite, by heat treatment. Many zeolites are synthesised with the aid of organic templates and so prior to application it is important to know the temperature at which complete organic removal is effected and also the structural collapse temperature. This information is readily obtainable from DTA of the zeolite. However, only limited information is available on the thermal behaviour of zeolites Na-TMA-Ω and NH_4-TMA-Ω ; the latter is of interest as it is the intermediate stage to catalyst preparation.

2.9.2 Na-TMA- Ω

The thermal analysis data of zeolite Ω, especially in relation to the removal of TMA is somewhat contradictory. The oxidation of TMA from Na-TMA-Ω and NH_4-TMA-Ω is referred to as giving rise to rather complex DTA/TG curves in the region of 400-700°C. The thermal data for zeolite Ω is summarised in Table 2.7. This table

Table 2.7

Thermal Behaviour of Zeolite Na-TMA- Ω

REFERENCE	ENDO /°C	ENDO /°C	EXO /°C	EXO /°C	EXO /°C	EXO /°C High Temp	COLLAPSE TEMP /°C
Union Carbide [3]				> 400* Removal of TMA by thermal decomposition of TMA in cages			800
Barrer & Aiello [24]		Up to 400* water loss - dehydration			~ 580* TG 650 oxidative breakdown of TMA in gmelinite cage.	Not observed	700
Cole et al [8]			DTG 350** TMA decomposition in main channel		DTG 500-600** decomposition of TMA in gmelinite cage.		
Sidamondize et al [34]	25 ** at $p = 10^{-4}$ torr Slight decomposition of TMA and removal of main part of water adsorbed in zeolite			480 ** heated in oxygen jet, effected decationised form	500-600 ** intensive decomposition of TMA completed by 600		
Xu Qinhua et al [23]	150 dehydration	350 decomposition of TMA in main channel 570 decomposition of more stable TMA in gmelinite cage		480 perhaps oxidation of part TMA	720 structural collapse		720 exo collapse
Penchev et al [35]	127-177 dehydration		375 * sharp	460 * sharp	~ 525	960	960 exo collapse
Lowe et al [27]	100 sharp dehydration	100-300 gradual very slight endo due to water	300-475 gradual organic (TMA) loss	475-575 Sharp TMA decomposition	~ 500 (n) ~ 515 (s) centred at these temps		810-900 endotherm

** Mode of thermal decomposition not specified, i.e. whether exothermic or endothermic
* Temp determined from published thermal analysis curves
(n) Needle-like crystals
(s) Spherulitic crystals

Table 2.8

Thermal Behaviour of NH_4-TMA- Ω and NH_4- Ω

REFERENCE	ENDO /°C	ENDO /°C	EXO /°C	EXO /°C	EXO /°C	EXO /°C High Temp	COLLAPSE TEMP /°C
Weeks et al [36]	150 water loss			460 and 500 oxidation of NH_3	500 broad peak TMA oxidation		600
Deep bed calcination NH_4-TMA- Ω					520-720 (TMA is removed in deep bed calcination)	980 and 1040 double EXO due to crystal structure collapse	980 and 1040
Penchev et al NH_4- Ω [35]			300*		Very weak exo TG ⇒ NH_4 decomposition 310-780 (organic lost before NH_4+)	900 *	

clearly illustrates that there is no unique thermal behaviour for zeolite Ω ; the interpretation of the thermal processes involved are somewhat diverse, the observed temperature of TMA removal is varied and similarly the structural collapse temperature fluctuates. The differences in observed thermal behaviour may be partly attributed to the different apparatus used, conditions of operation and sample size.

There are two distinct types of weight loss which occur:

(1) due to organic removal

(2) the endothermic dehydration

Only Sidamonidze et al [34] report the loss of TMA at 25°C at pressure of 10^{-4} torr. Apart from this, it is unanimously agreed that evolution of organic occurs at temperatures of $\gtrsim$ 350°C, and the TMA is encapsulated in the gmelinite cage. However, removal of the TMA from the cage is at various temperatures and is described as an endothermic [23], exothermic [3, 24, 27] or complex exothermic process from 350° to 1000°C. Exothermic collapse near 1000°C (960°C) [35] is reported in only one instance by Penchev et al; other workers claim it is not observed in the samples examined.

Flanigen and Kellberg [3], Cole and Kouwenhoven [8] and Barrer and Aiello [24] employed ion exchange as a technique of cation site determination and concluded that the inability to remove TMA in this manner implied it is located in cages. Cole [8] with the aid of pyrolysis experiments identified the weight loss peak centred at 350°C in DTG as TMA decomposition in the main channel, as this is the only site large enough to allow the reaction:

$$(CH_3)_4N^+ + OH^- \longrightarrow (CH_3)_3N + CH_3OH$$

to proceed.

The higher temperature pyrolysis products were smaller molecules. At 560°C evolution of hydrogen, methane and carbon monoxide occurred and at 650°C hydrogen, methane, ammonia, acetylene, ethylene and carbon dioxide were formed. The latter necessitates escape from the tight ring structure i.e. the gmelinite cage, since molecules firmly encaged in the zeolite cavities are thermally more stable than in the bulk.

Cole et al [8] identified the process at 350°C as oxidative degradation of TMA in the main 12 ring channel, based on the structure proposed by Barrer and Villiger [29] which is said to be fault free i.e. no blocking of the 12 ring channel, now known to be incorrect. TMA hydroxide, or silicate is located at this site and may be readily removed by ion exchange. Barrer [24] also states that TMA may be located in the main channel but it appears to avoid it. Barrer's DTA showed only one exotherm at ~580°C.

Perhaps the incorrect axis labelling of endothermic and exothermic process on the DTA curve by Barrer [24] and Cole's statement [8] of TMA decomposition in the main channel at 350°C, has led Xu Qinhua et al [23] to identify this site in the same way (Cole and Kouwenhoven and Barrer are cited as references) but as an endothermic process (Cole does not define the mode of thermal process). Penchev et al [35] observe an exotherm at 375°C and Lowe et al [27] obtained a similar result of a gradual exotherm at 300-475°C. Sidamonidze et al [34] state that the decationised form of Ω is obtained at 480°C if heated in a jet of oxygen, the thermal process is not specified; however, it is recorded as an exothermic process in references [23, 35] which occurs at 480°C and 460°C respectively.

Removal of TMA from the gmelinite cage is said to occur at >400°C [3], ~580°C [24], 500 to 600°C from DTG [8], 500 to 600°C [34], 500°C and 515°C [27] dependent on morphology (the lower temperature is due to the fibrous form) and 570°C [23], the latter is recorded as endothermic process and also 525°C which is referred to as TMA breakdown.

Structural collapse is reported to occur between 700 to 800°C [3, 24] 810 to 907°C [27] by endothermic process, but exothermic collapse is reported at 720°C [23] and 960°C [35].

Comparison of the thermal analysis curves in Figs. 2.9 and 2.10 illustrates that there is no unique pattern which characterises the oxidative decomposition of TMA in zeolite Ω. Comparison of the DTG of Cole [8] and DTA, TG of Barrer [24] shows similarity in that two distinct regions of weight losses, which are exhibited at ~500°C before commencement of the sharp peak centred at 585°C [8] and 570°C [24]. However, the first weight loss is attributed to water [24] by Barrer, and TMA hydroxide or silicate oxidation in the main channel [8] by Cole. Adjustment of the base line in Fig. 2.9 (c) [23] such that the apparent endotherm at 570°C is now on the base line shows slight similarity with Fig. 2.9 (f) [35]. There are similar features in Fig. 2.9 (a) [24] and Fig. 2.9 (d) [27].

The two morphological types of Ω [27], fibrous and spherulitic, were observed to differ in their water and organic content. The fibrous Na-TMA-Ω [27] contained 11.2% water and 7.9% organic, compared with 12.9% water and 7.3% organic for the spherulitic form, after equilibration at 25°C over saturated NaCl solution. The increase in water content for the latter is accounted for by the probable larger surface area and hence partial surface water which causes an initial sharp weight loss. Increase in calcination temperature resulted in a corresponding

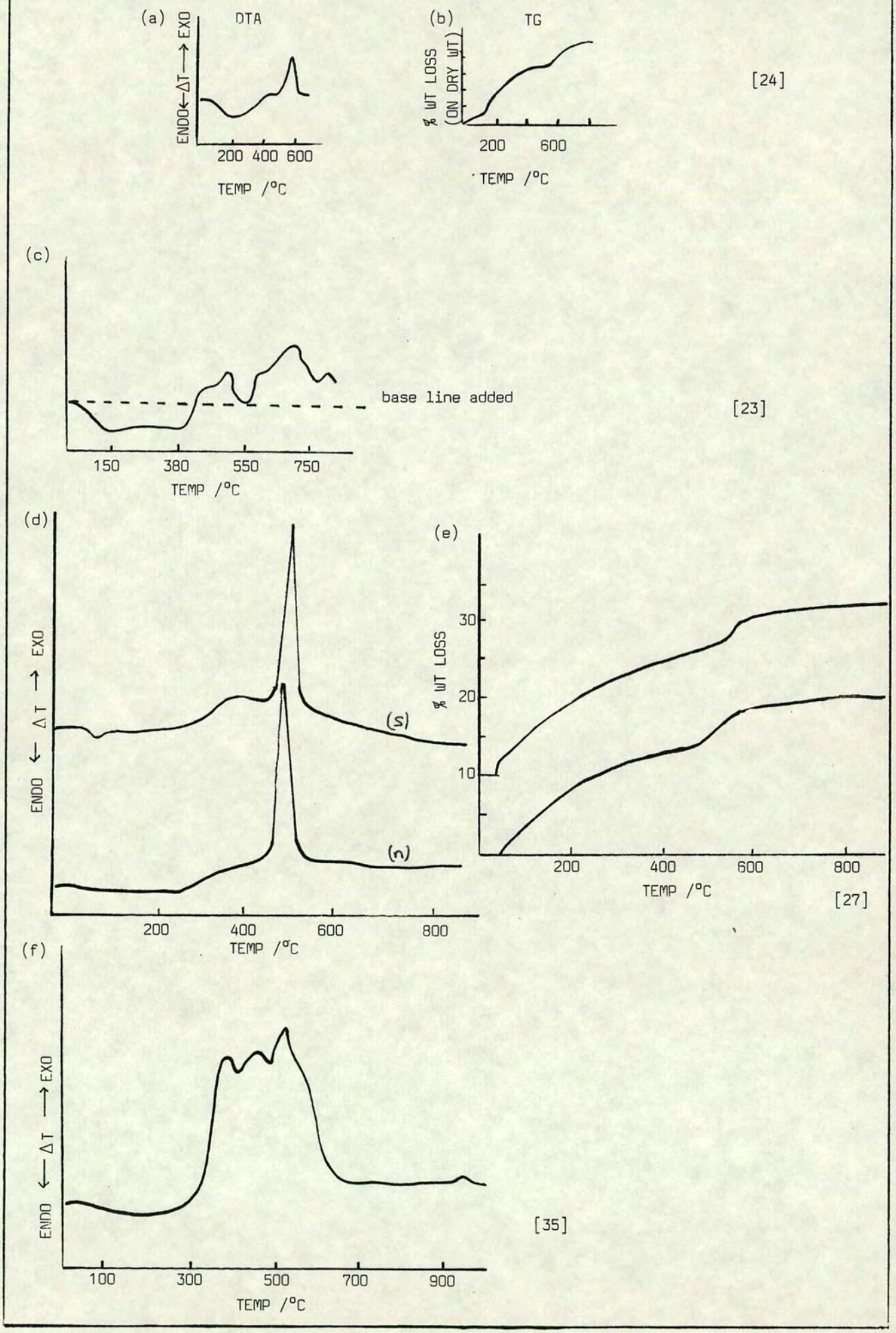

Fig. 2.9 Thermal Analysis curves for Zeolite (Na, TMA)-Ω in air

(n) needle type crystals (s) spherulitic type crystals

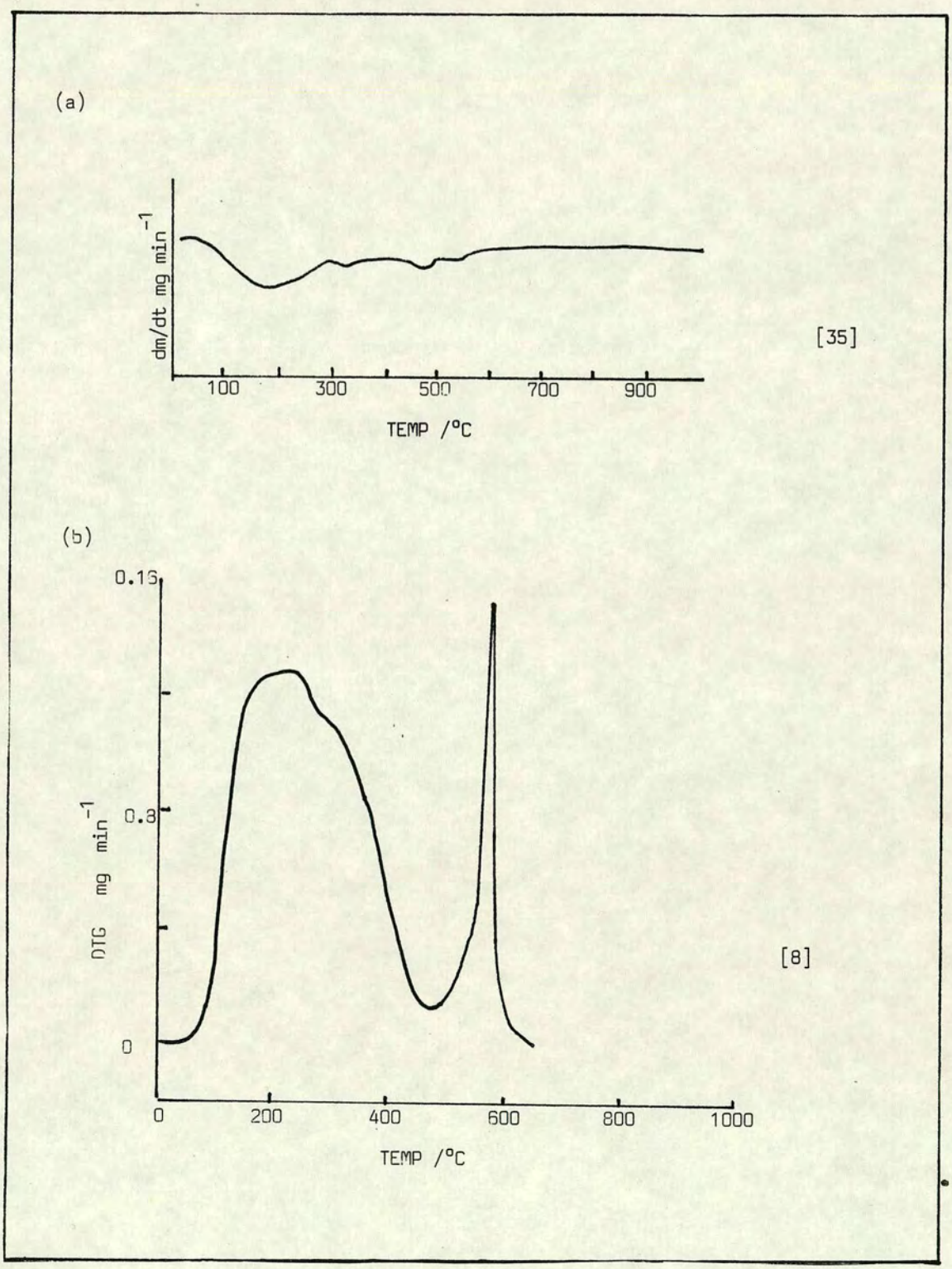

Fig. 2.10 Illustration of DTG curves of (Na, TMA)- Ω

decrease in XRD intensities and water content. The spherulitic material is more susceptible to thermal degradation than the fibrous form. Water loss is observed to occur in two stages: the sharp loss at <100°C is due to water loosely bound to the zeolite surface, the remainder is a gradual loss up to 300°C from the zeolite cavities. Increase in calcination temperatures showed a decrease in both types of water, with lower intracrystalline water capacity for the spherulitic type and higher capacity for low temperature water. Intracrystalline water correlated with the X-ray diffraction intensities, and implied that the fibrous type is more crystalline and thermally stable. The fibrous and spherulitic samples used for this comparison were recycled such that the sample was calcined in air for 2 h at 607°C, a portion removed, reheated to 707°C for a further 2 h period and the process repeated at 810°C, and 907°C. This may have contributed to loss of crystallinity as was mentioned by Weeks et al [36].

2.9.3 Na-H-Ω

The Na-H-Ω was obtained by the action of heat on Na-TMA-Ω, in air, at temperatures up to 650°C [24]. The Na-H-Ω showed a water loss of 18.2% compared with 17.0% for Na-TMA-Ω, after rehydration for 1 week in a dessicator over calcium nitrate solution. The number of water molecules per unit cell increased from 22.8 to 23.4 in Na-H-Ω.

2.9.4 Li-H-Ω

The Li-H-Ω [2] was prepared by ion exchange of Na-H-Ω with 5N lithium nitrate solution at 80°C in two runs of 12 h duration. The weight loss from Li-H-Ω corresponded to 27.9 water molecules per unit cell. The loss of water and TMA at 600°C was accompanied by a change in unit cell dimensions. There was a decrease in a from 18.95 Å to 18.05 Å and an increase in c from 7.595 Å to 7.62 Å. These results were obtained from X-ray powder diffraction programmed heating camera.

2.9.5 The Effect of TMA Removal on Sorption Capacity

Cole and Kouwenhoven [8] have reported that thermal TMA removal resulted in considerable loss in sorption capacity. When thermally activated a further reduction in sorption capacity with significantly reduced crystallinity at 700°C is observed.

2.9.6 Ammonium Ion Exchanged Ω

2.9.6.1 NH_4-TMA- Ω

Only two reports in the literature have provided information on the thermochemical properties of NH_4-TMA- Ω [35, 36]. This species is of interest as it is the intermediate phase to catalyst preparation (H-Ω). The Ω is synthesised by Shell's route [8] i.e. mixed alkali metal cations are incorporated during synthesis and complete removal of sodium is possible by exhaustive ion exchange with 2M NH_4NO_3. Weeks et al [36] ion exchanged Ω with 4M NH_4Cl (aq), refluxed for 1 h and repeated this 5 times with washing between each step. The thermally stable form of NH_4- Ω was prepared by placement of the hydrated zeolite in a premuffle furnace at 600°C for 1.5 h. Calcination resulted in decomposition of TMA and NH_4 ions. It was then ion exchanged with 4M NH_4Cl (aq). The species formed was termed ammonium deep bed calcined Ω.

Ion exchange failed to remove the TMA intercalated during synthesis and thus the material contained two volatile cations. The thermal analysis curves are described as rather complex [36] (see Fig. 2.11). The DTA in air showed an endotherm at 150°C due to water loss, and exotherms at 460°C and 500°C. On the basis of IR evidence, the exotherms may be assigned to oxidation of ammonia; the broad exotherm

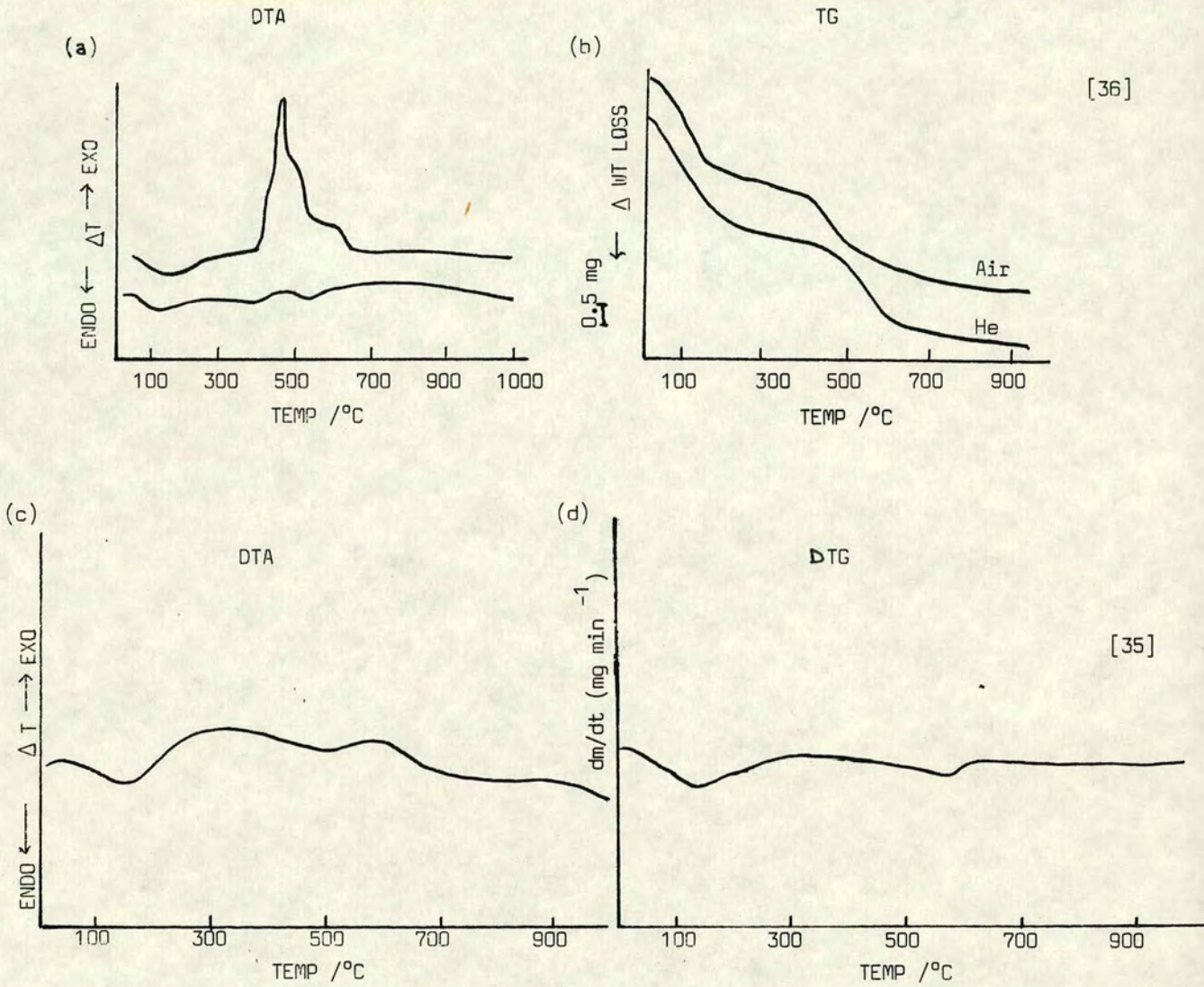

Fig. 2.11 Thermal Analysis curves for NH_4-TMA-Ω (a) and (b); NH_4-Ω, (c) and (d)

at 590°C is due to oxidation of TMA, and no decomposition peak near 1000°C is observed. The DTA in He, with double sensitivity gave a nondescript pattern. The TG illustrated that the weight loss is not uniform in air or He. In air, the weight loss is slow from 222 to 440°C, rapid from 440 to 500°C and gradual from 500 to 750°C. The differing rates of weight loss may be attributed to the overlapping effects of loss of NH_4 and TMA cations and dehydroxylation. In He atmosphere, the major weight loss occurred at 500°C, a higher temperature than in air. Chemical analysis of the TG samples showed adsorbed water of 11% and as the TG analysis indicated that, exclusive of water loss, 10.4% weight loss occurred in air and 8.8% weight loss in He - the latter implying a residue remained on the zeolite in an He purge.

Samples removed from TG (heating rate 10°C min^{-1}) at various temperatures and subsequently subjected to X-ray analysis showed significant loss in crystallinity at 500°C and substantial loss at 625°C. The decomposition temperatures are ~100°C higher than those in isothermal studies, illustrative of the difference between dynamic and static heating.

IR studies illustrated that physically adsorbed water is removed after evacuation for 1 h at room temperature. The ammonium ion is lost at a lower temperature than TMA. IR studies indicated that water removed by room temperature evacuation results in the appearance of amorphous material. At 600°C, a 'zeolitic' hydroxy band attained its maximum intensity; however, X-ray diffraction showed that the zeolite is amorphous, thus implying that the presence of a zeolitic hydroxy group band is not evidence for crystallinity. Loss of TMA results in crystal collapse prior to dehydroxylation raising the possibility that the zeolitic hydroxy group is not part of the zeolite framework, but due to the hydroxy-aluminium species.

X-ray diffraction of NH_4-TMA- Ω at various temperatures on a singly thermally cycled sample showed, in contrast to the IR spectra, increase in intensity of the low angle peaks, substantial loss of crystallinity at 500°C and by 600°C the zeolite was amorphous. Prior to the onset of deammonation (400°C) there is little change in the cell constants, at this temperature a slight decrease in a_o resulted with a further decrease just before crystal collapse at 500°C. Poor thermal stability is surprising for such a high silica/alumina zeolite; however, cycling of the single sample used may be a contributing factor. A fresh sample, when rapidly heated to 600°C became amorphous in 2 h. Thus indicative of extensive crystal degradation occurring during TMA loss. Poor thermal stability and diffuse X-ray diffraction pattern may be attributed to small particle size. The thermal stability may be enhanced by exchange with rare earth cations.

2.9.6.2 Deep bed calcination of NH_4-TMA- Ω [36]

This technique resulted in a substantial increase in thermal stability at 600°C and higher silica/alumina ratio. IR studies on the ammonium exchanged deep bed calcined material shows loss of ammonium ion near 500°C and deep bed calcination decomposed the TMA cations. The DTA in air of this material which, although free from TMA is still grey, shows a single broad exotherm between 520 and 720°C and a double exotherm at 980 and 1040°C, the latter indicative of crystal collapse. There is overlap due to cation loss and dehydroxylation. Crystal collapse can be prevented by both multivalent cation exchange and/or deep bed calcination.

2.9.6.3 NH_4- Ω

The decationised zeolite form was obtained [35] by heating Na-TMA- Ω

in air for 6 h to 640°C to effect the decomposition of organic cations. Conversion to the NH_4 form was obtained by ion exchange with 1M NH_4Cl at 80°C, and by thermal treatment in air for 6 h at 640°C: 98% decationised H-Ω resulted. The thermal decomposition of NH_4 form illustrated by DTA/DTG (Fig. 2.11 (c) (d)) showed dehydration and a very weak exotherm at 600°C which corresponds to decomposition of NH_4 ion and according to TG occurs from 310-780°C.

Comparison of the DTA curves for Na-TMA-Ω and NH_4-Ω shows that the temperature of decomposition of ammonia lies above the temperature of TMA oxidation.

2.10 Hydronium ion exchanged ZSM-4

Hydronium ion exchange [37] may be carried out by use of aqueous acid ion exchange resin. This method permits direct hydronium exchange via an infinitely dilute acidic medium with elimination of the possibility of attack of the zeolite structure by excess acid and subsequent degradation. The Na-TMA-ZSM-4 prefers hydronium ion to Na with two thirds of the sodium content exchanged by the hydronium ion. The remaining one third sodium are located in the smaller cages next to the gmelinite cages which are inaccessible to the hydronium ion. Removal of the one third sodium is achieved by use of ammonium exchange resin.

2.11 Acidity of Ω

The ammonia decomposition temperature is found to be related to the acidity of the zeolite [35]. This is in agreement with the results of Whyte [35]. The acidity is increased with the strength of the ammonia bond which usually increases with silica/alumina ratio. Thermal desorption studies of ammonia show Ω to have a broad distribution of sites with different binding energy of the ammonia molecule, suggestive

of various sites with different acidities. On the basis of ammonia adsorption data, the H-Ω is more acidic than ZSM-5, but as the zeolites have different structures and pore sizes, it is difficult to predict whether this will be reflected on the catalytic properties.

In accordance with the classic Brønsted acid definition, the acid strength of a zeolite increases with decrease of selectivity for hydronium ion. ZSM-4 is classified as intermediate strength with ZSM-5 and ZSM-11, zeolite Y is the weakest and mordenite the strongest acid [37].

2.12 Surface Modification

Modification of the hydrophobic/hydrophilic [38] nature of the surface and catalytic activity of zeolites may be achieved by fluorine gas treatment. The mechanism involves framework dealumination. Dealumination usually results in increased stabilisation of the structure at high temperatures. However, subsequent high temperature calcination in air at 600°C did not achieve structure stabilisation and surface hydrophobicity in the case of Ω, but in other zeolites, e.g. mordenite and erionite, the technique was successful. Dealumination may also be effected by steaming at high temperatures, and reaction with cation complexing agents such as EDTA. ^{29}Si MASNMR and ^{27}Al MASNMR have been used to investigate the effect of dealumination reactions on a variety of zeolites which gives further insight into the structures of these systems [39]. ^{27}Al spectra of Ω shows clearly that there is not a random distribution in the lattice. The spectra are complex and unambiguous quantitative interpretation is difficult.

2.13 Catalytic Activity of ZSM-4

Zeolites have catalytic properties, the mechanisms involved are quite complex [3] and the precise chemical properties of zeolites which contribute to a particular catalytic activity are not fully understood. Zeolites are usually converted to the hydrogen form i.e. H- Ω/H-ZSM-4 prior to use as catalysts. ZSM-4 is a useful cracking and hydrocracking catalyst, as are other zeolites, but the catalytic property which distinguishes ZSM-4 from all previously known zeolites is its high selectivity factor [14, 18-21]. Selectivity is measured by the ratio of o-xylene isomerised to that disproportionated. o-xylene is isomerised to meta xylene and then para xylene and disproportionated to a mixture of methylbenzenes, primarily toluene and trimethylbenzene. All previously known crystalline aluminosilicates, even when rare earth exchanged, have a maximum selectivity factor of approximately 3.7, but it is generally much lower, whereas ZSM-4 has a unique selectivity factor in excess of 4 and generally at least 6. It is ideally suited for carrying out isomerisation (and disproportionation) of alkyl aromatic hydrocarbons in low temperature liquid phase operations. With the use of pyrrolidine and choline chloride salts, the H-ZSM-4 produced is an even more stable catalyst [19] than other routes of synthesis. However Ω /ZSM-4 has an unidimensional channel system and so readily 'cokes up' and thus its suitability as a catalyst leaves a lot to be desired.

2.14 Summary

Zeolites Ω and ZSM-4, discovered within months of each other by Union Carbide and Mobil Oil Corporation respectively, were proved to be the same material in 1977 by Perrotta et al. Since its discovery, in 1966, Mobil have developed improved syntheses routes which use

inexpensive clays, in situ formation of TMA and substitution of TMA by pyrrolidine, choline chloride and Dabco. Cole and Kouwenhoven, and Barrer et al have incorporated Li and K ions in addition to TMA and Na into the reaction composition. Qinhua et al and Chao Hui et al have contributed studies on the synthesis and kinetics of crystallisation.

Barrer and Villiger's structure determintion of Ω from X-ray powder diffraction was proved incorrect when the natural counterpart, mazzite, was discovered by Galli in 1972 and single crystal structure determination carried out. Mazzite, Ω and ZSM-4 have the same X-ray powder diffraction pattern and hence are probably isostructural. The sorption capacity for Ω is considerably less than that for zeolite L, another 12 ring channel system. This provided evidence suggestive of stacking faults in Ω which were confirmed by TEM. Kokotailo proposed a mechanism for the introduction of stacking faults into the structure by the conversion of the gmelinite cages to sodalite cages.

Zeolite Ω has two morphological forms - spherulitic and fibrous with its mineral mazzite occurring as the latter. The thermal stability of Ω is less than that expected of an intermediate SiO_2/Al_2O_3 ratio zeolite. The fibrous form is thermally more stable than the spherulitic form. TMA is removed above 350°C from the main channel, > 400°C from the gmelinite cages and endothermic structural collapse occurs between 700 to 900°C. Exothermic structural collapse at 960°C has only been reported by Penchev et al. Deep bed calcination of NH_4-TMA- Ω increases thermal stability such that structural collapse is recorded by a double exotherm at 980°C and 1040°C. Ammonia adsorption studies illustrates that H- Ω is more acidic than H-ZSM-5 and has a random distribution of acid sites. Catalytically Ω is distinguished from all known zeolites by its high selectivity factor

for xylene isomerisation.

REFERENCES

1. R. M. Barrer, Proc. of 6th International Conf. on Zeolites, Reno, Nevada Butterworths, Guildford, 1983, p 17

2. R. M. Barrer and P. J. Denny, J.Chem. Soc., 1961, 971

3. E. M. Flanigen and E. R. Kellberg, Union Carbide, Netherlands Patent 6 710 729, 1968

4. Mobil, British Patent 1 117 568, 1968

5. E. Galli, E. Passaglia, D. Pongiluppi and R. Rinaldi, Contr. Min. and Petrol., 1974, 45, 99

6. E. Galli and G. Gottardi, Natural Zeolites, Springer-Verlag, Berlin, Heidelberg, New York, Tokyo, 1985

7. B. M. Lok, T. R. Cannan and C. A. Messina, Zeolites, 1983, 3, 283

8. J. F. Cole and H. W. Kouwenhoven, Adv. Chem. Series, 1973, 121, 583

9. L. D. Rollmann, Adv. Chem. Series, 1979, 173, 387

10. L. D. Rollmann, NATO ASI Ser., Ser. E. 1984, 80 (Zeolites: Sci. Technol.), 109

11. A. J. Perrotta, C. Kibby, B. R. Mitchell and E. R. Tucci, J. Cat. 1978, 55, 240

12. Union Carbide, British Patent 1178 186, 1970

13. Union Carbide, United States Patent 4 241 036, 1980

14. Mobil, United States Patent 3 578 723, 1971

15. Mobil, United States Patent 3 642 434, 1972

16. Mobil, British Patent 1 321 460, 1973

17. Mobil, British Patent 1 365 318, 1974

18. Mobil, United States Patent 3 923 639, 1975

19. Mobil, United States Patent 4 021 447, 1977

20. Mobil, United States Patent 4 091 007, 1978

21. Mobil, United States Patent 4 331 643, 1982

22. F. G. Dwyer and P. Chu, J.Cat. 1979, 59, 263

23. Xu Qinhua, Zhang Huizhu, Dong Jialu and Wang Rui, Kexue Tongbao, 1980, 25(10), 833

24. R. Aiello and R. M. Barrer, J. Chem. Soc (A), 1970, 1470

25. Shell, British Patent 1 345 363, 1974

26. Chao Hui and Xu Ruren, Huaxue Xuebao, 1983, 41 (10) 916

27. B. M. Lowe, A. Araya, D. S. Sinclair, T. J. Barber and A. Varma, Zeolites, 1984, 4, 263

28. S. Sawruk, A. C. Rohrman and G. T. Kokotailo, 5th International Conf. on Zeolites, Naples, 1980, Recent Progress Reports and Discussion, 1981, p 261

29. R. M. Barrer and H. Villiger, J. Chem Comm., 1969, 659

30. E. Galli, Cryst. Struct. Comm., 1974, 3, 399

31. E. Galli, Soc. Italiana di Mineralogia & Petroligia - Rendiconti, 1975, 3(2), 599

32. R. Rinaldi, J. J. Pluth and J. V. Smith, Acta. Cryst., 1975, B31, 1603

33. J. A. Gard, J. M. Tait, Acta Cryst., 1972, B28, 825

34. Sh. I. Sidamondize, G. V. Tsitsishvili, D. M. Shavladze, I. I. Iashvili and M. M. Gvilana, Soobstrich. Akad Nauk Gruz SSR, 1978, 90(3), 597

35. V. Penchev, Ch. Minchev, V. Kanazirev, O. Pencheva, N. Borisova, L. Kosova, H. Lechert and H. Kacirek, Zeolites, 1983, 3, 249, and references therein.

36. T. J. Weeks, Jr., R. L. Bujalski, A. P. Bolton and D. G. Kimak, J. Chem. Soc. Faraday Trans. 1976, 72, 572

37. P. Chu and F. G. Dwyer, Zeolites, 1983, 3, 72

38. B. M. Lok and T. P. J. Izod, Zeolites, 1982, 2, 66

39. C. A. Fyfe, Personal Communication 1984

40. W. M. Meier and D. H. Olson, "Atlas of Zeolite Structure Types", International Zeolite Association, Special Publication 1978

CHAPTER THREE

Some Techniques of Zeolite Characterisation

3.1 Introduction

Advances in scientific technology have provided myriads of analytical techniques for the characterisation of materials. Many of these techniques are now applied to zeolite chemistry. The major methods of physical characterisation of zeolites are microscopy, diffraction, spectroscopy and thermal analysis. Each one of these methods is sub-divided to provide more specific information.

Microscopy, using an ordinary optical microscope, in many instances provides quick information on particle size and shape; for smaller crystals, electron microscopy or scanning electron microscopy allows observation of these features. A branch of this technique is the relatively new method (1973) - high resolution electron microscopy .(HREM) [1]. This provides a superior technique to X-ray diffraction for elucidation of crystal structures by the production of a direct image (direct magnification) of the crystal at near atomic resolution. Intergrowths among closely related structures which lead to stacking faults may thus be readily detected [2]. However HREM is limited to materials which have a reasonable degree of thermal stability as destruction in the electron beam has been known to occur in some instances.

The established technique of X-ray powder diffraction (XRD) is of prime importance for structural identification of the sample. XRD may be supplemented by neutron diffraction [3] experiments for localisation of light atoms and study of the mobility of water molecules inside the zeolite cavities. For small crystals electron diffraction is available.

Among the spectroscopic techniques ^{29}Si and ^{27}Al Magic Angle Spinning Nuclear Magnetic Resonance (MASNMR) are new and provide a method for determination of the distribution of silicon and aluminium atoms in the zeolite framework. The other spectroscopic techniques, of which IR is the most widely used, give information on the strength and accessibility of acid sites in the zeolite and the sorption of molecules. X-ray fluorescence spectroscopy (XRF) allows elemental analysis of the sample.

Thermal analysis, of which differential thermal analysis and thermogravimetry are the two major techniques, permits strength of interaction and the amount of sorbed material to be studied. Information on the stability of zeolites and structural collapse temperature are obtained. Investigations of this kind are important for the description of the limits of stability of zeolite catalysts in technical processes.

These techniques are all applicable to the solid state and do not allow analysis of a reaction mixture during crystallisation. A new, rapid, reliable and simple procedure, developed in Edinburgh, which gives information about the solid/liquid phase equilibria is pH measurements [4].

Naturally there are limitations to the techniques which may be applied to this work, mainly imposed by availability. But given a choice of facilities for this work, SEM, HREM, XRD, XRF (modern ED instrument which allows rapid analysis of milligram samples) thermal analysis and pH would have been ideal for work on zeolite Ω . SEM for crystal shape and size, HREM would have provided information on the presence/absence of stacking faults and imbibed material in the channels either as a result of poor washing or sorption. XRF for SiO_2/Al_2O_3 of a kinetic series of samples from crystallisation would have shed some light on the mechanism of the reaction. Unfortunately, SEM, HREM

and EDXRF were not available and hence this work employs XRD, XRF (time consuming glass disc technique) thermal analysis and pH measurements.

3.2 Microscopy

The physical characterisation of a material such as a zeolite begins in principle by the visual inspection. In the case of synthetic zeolites, the crystals are very small and necessitate observation under a microscope, or scanning electron microscope. This method readily gives information on the shape of the crystal, the type of zeolite, crystalline impurities and any amorphous material which may be present in the sample. Kinetics of crystallisation may be monitored, using the dependency of the particle size distribution with time. Knowledge of the crystal shape is important for sample preparation in XRD and thermal analysis.

3.3 X-Ray Powder Diffraction

3.3.1 Introduction

Laue's [5] discovery of the diffraction of X-rays by matter which possess a regular internal arrangement of atoms gave scientists a very powerful tool. The primary use of X-ray diffraction (XRD) in analytical work, zeolite chemistry in particular, is the identification and characterisation of the crystalline material. From the XRD pattern the lines may be indexed, cell constants determined and in very special cases complete structure elucidation achieved.

Some of the first XRD studies were carried out on minerals [6]. Prior to this, zeolites were characterised by their crystal morphology, optical behaviour and other physical properties. The advent of XRD

made the recognition of new materials and identification and distribution of known phases much easier than was possible with earlier technology.

X-rays are generated by bombardment of a target with high speed electrons, and are emitted as continuous white radiation on which are superimposed lines characteristic of the target material. By suitable choice of the target material (copper in this work), filters, monochromators and slit size for the diffractometer in use, X-rays in the required wavelength region may be generated.

X-rays are diffracted by crystalline materials such as zeolites. The fundamental process which occurs when X-rays strike a crystal is scatter or diffraction, conveniently regarded as reflection. The incident X-rays penetrate the surface of the crystal, and the emergent reflected rays from the successive atomic planes are either in phase or out of phase. When in phase contribution from successive planes occur i.e. constructive interference, a maximum reflected intensity is observed. The condition is expressed by the Bragg equation:

$$n\lambda = 2d\sin\theta$$

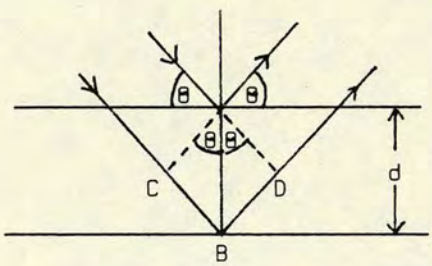

Where d is interplanar spacing

θ is Bragg angle

λ is wavelength of radiation

(in this work $\lambda_{CuK_\alpha} = 1.54179$ Å)

n is an integer

Fig. 3.1 Path difference $n\lambda = 2d\sin\theta$

The equation is normally given as $\lambda = 2d\sin\theta$

Since for a given set of planes with spacing d, the reflection is regarded as occurring with phase difference $n\lambda$ or phase difference λ from planes with one nth of spacing, and so second order reflection from (111) may be regarded as first order from (222).

3.3.2 Instrument Specification

A diffraction pattern may be recorded using either a camera or a diffractometer. In the present work a Philips automatic X-ray powder diffractometer was used. The machine was fitted with a fine focus copper X-ray tube with K_α radiation and an AMR graphite focusing monochromator, channel control PW 1390, automatic sample changer PW 1170/02, PW 1394 motor control, PW 1965/60 goniometer and PW 8203 single pen recorder.

3.3.3 The Diffraction Pattern

The sample preparation is very important [5, 6, 7, 8] as it determines the quality of the resultant data and the degree of success of a diffraction experiment [7]. The diffraction pattern yields 3 types of information:

(1) Position of diffraction maxima i.e. 2θ values

(2) Intensities of diffraction maxima

(3) Intensity distribution as a function of diffraction angle

The optimisation of any one of these parameters rarely leads to optimisation of the others. A standard reference pattern, verification of a known phase or identification of an unknown phase requires the accuracy of the d-values to be determined within the limits of the instrument and the intensities to be representative of a truly random orientation of crystallites. However attainment of both these qualities in the same sample is difficult. Consequently, the samples are prepared to maximise the quality of each parameter individually and the pattern is subsequently generated. Two types of sample mount are used for diffractometers; they are the cavity mount and the microslide surface. Neither of these achieves the desired optimum conditions, since both have flat surfaces and so there is a slight shift of the 2θ

values. Consequently to compensate for these common and systematic errors in d-spacing, an internal standard of known d-spacing is mixed with the sample and hence accurate values obtained. The peak position is determined by the X-ray beam penetration at half depth of the sample and is not influenced by the surface. The d-spacings are independent of orientation effects, the latter may affect the peak intensity.

3.3.4 Factors Affecting Peak Intensity

The main factors that affect the peak intensity are the particle size which arises from grinding of the sample, crystal size, orientation of the crystallites, and sensitivity of the sample to the atmosphere.

3.3.4.1 Grinding

Samples must be reduced to finely ground powders with particle size of the order of 1-10 μm [6] before they are mounted in the cavity holder. Insufficiently ground samples will result in the persistence of large particles which give rise to misleading intensities in the diffraction pattern which are not easily recognisable, but are observed as uneven or spottiness on film. Excessively ground samples show structure deterioration. However, in some cases grinding under acetone may prevent decomposition.

3.3.4.2 Orientation Effects

Materials consisting of crystallographically related shapes such as rhombohedra, cubes, plates and fibres, align themselves in such a way, i.e. preferred orientation, that when X-rayed the resulting intensities are due to reflections from only one particular set of planes.

Preferred orientation is desirable in the cases of platy clay minerals where reflections from planes other than (001) is rare and thus enhancement of reflections from this plane occurs. Such a sample is prepared by tightly pressing the powder into a cavity mount with an aluminium backing plate producing a flat surface which is smoothed over with a glass microslide [6, 8].

For quantitative work, the peak intensities of a diffraction pattern must normally be a representation of the average of all the possible orientations of the crystals. Therefore reflections from every set of planes are required and this may be achieved from samples with a high degree of randomness. Samples of spherical habit are randomised and do not align themselves in any particular manner and so the problem of preferred orientation does not arise. Consequently, to overcome orientation effects, the techniques employed basically change the shape of crystal aggregate to spherulitic type. The techniques employed are extremely varied. Some use back loading and side loading of cavity holders; mixing of samples with fillers, viscous binders; dusting onto greased or adhesive surface, mixing with starch or silica gel, and the industrial technique of spray drying [9].

Samples in which preferred orientation exists may be used for quantitative work provided the sample is prepared such that there is reproducibility of intensities [7, 8].

Fortunately, the work described in this thesis is predominantly concerned with samples of the spherulitic type of zeolite Ω and so orientation effects are not a problem.

3.3.4.3 Air Sensitive Samples

Many samples are reactive towards the oxygen, water or carbon dioxide

of the atmosphere. Zeolites with low SiO_2/Al_2O_3 ratios are hydrophilic compared with silicalite and ZSM-5 which have extremely high SiO_2/Al_2O_3 ratios and hence are hydrophobic. Thus zeolites with low and intermediate SiO_2/Al_2O_3 ratios are sensitive to the water content of the atmosphere [10]. Although it is possible to protect samples from atmospheric moisture, the normal practice is to equilibrate them with water vapour before analysis by XRD.

3.3.4.4 Line Broadening in Powder Diffraction

The main causes of line broadening in XRD powder patterns are due to small crystallite size, powders with zoned crystals, structural stacking faults e.g. intergrowths, mechanical strain and chemical inhomogenity. The most important of these in zeolite chemistry is crystal size.

The scattered intensity falls off very rapidly away from the Bragg position [6, 11, 12], but the spread of reflection bears an inverse relationship with the crystallite size.

Thus $\delta(2\theta) \sim \lambda / t\cos\theta$

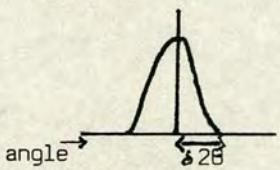

δ 2θ is as shown

t = thickness of crystal

Intensity profile of powder reflection

The half breadth $\delta(2\theta)$ is influenced by crystallite size

Fig. 3.2

The broadening of a reflection is appreciable if the crystallite size is less than ~2000Å For example, for a crystal of thickness 1 mm and $\theta = 60°$, gives $\delta(2\theta) \sim 0.001'$, but for crystal of thickness 1000Å, $\delta(2\theta) \sim 0.2°$. However for thick crystals, instrumental

broadening is more important. Synthetic zeolite crystals may be very small and so line broadening is observed.

Mechanical strain and chemical inhomogenity cause line broadening by the existence of a range of d-values for a given set of crystal planes. Structural stacking faults e.g. chabazite intergrowths in gmelinite are exhibited as broadened reflections in the XRD pattern with sharp lines corresponding to the pure gmelinite phase. In single crystal photographs it is detected as streaking of the spots.

3.3.5 Quantitative Use of Intensities

The peak intensities are proportional to the amount of material present and hence under certain circumstances peak areas can be used to determine the percentage crystallinity. Peak heights can be used if the peaks are uniform in width. In this work peak heights were used as a quantitative measurement of the percentage of zeolite present.

The intensities of the emitted X-rays decrease with the age of the tube. This is corrected for by the regular calibration with a micro-crystalline quartz stone which allows both the peak positions and heights to be checked.

3.3.6 Application of XRD Data

Once the sample is prepared such that the most accurate d and I values may be obtained from the diffractometer, then a unique pattern characteristic of the sample may be obtained and used for identification purposes. The 2θ values are converted to d-spacings by use of the Bragg equation, the relative intensities (RI) calculated in relation to the most intense peak height, and hence a set of d and RI values obtained. Comparison of this data with that in the ASTM Powder Diffraction File

(PDF) usually leads to identification of several materials with diffractions close to that of the unknown. This is followed by detailed comparison of the powder data on the ASTM cards for these materials and generally results in identification of the unknown material, provided it has been previously reported. In Edinburgh, the data for the XRD patterns for most known zeolites are stored on EMAS computer files and comparisons of the patterns for unidentified materials with this data are readily achieved using computer programs.

For some new materials, powder patterns may be indexed and cell constants obtained. However, determination of crystal structure from powder data is rarely possible as many reflections are superimposed and weaker ones cannot be observed. Structures determined in this manner may often be incorrect e.g. zeolite Ω by Barrer and Villiger [13]. Single crystal work is much better than powder diffraction for structure determination, as all reflections are observed. However it is not always possible to obtain a synthetic zeolite crystal large enough (20-50 μm) [10] for a single crystal study.

3.3.7 Limitations of XRD

If the crystals are exceedingly small, the powder diffraction lines become so broad that the material appears to be X-ray amorphous. Evidence for X-ray amorphous zeolite samples is given in two publications on ZSM-5 [14, 15]. In 1981, ZSM-5 crystals of less than 8nm were prepared which exhibited an infrared (IR) spectrum and catalytic properties typical of ZSM-5 in an amorphous matrix. X-ray amorphous particles of ZSM-5 were characterised quantitatively by the detection of the presence of strongly bound structure directing organic guest molecule tetrapropylammonium ion (TPA) occluded within the zeolite framework, but absent from the amorphous gel. The amount of TPA

was proportional to the percentage crystallinity which could thus be determined by weight loss (TG) or by the DTA peak area. HRMAS ^{13}C NMR could be used to characterise the position and configuration of the TPA molecule in 100% crystalline ZSM-5 and amorphous ZSM-5.

Thus it should be recognised that some materials, that are X-ray amorphous, may well contain very small crystallites ($\lesssim$ 8 nm).

3.3.8 Experimental

3.3.8.1 Procedure

The technique of sample preparation for XRD analysis must be carefully selected if orientation effects are to be avoided. However, the work described in this thesis is predominantly concerned with samples of zeolite Ω, which on the basis of bulk density measurements or texture, were considered to have spherulitic morphology. Consequently sample preparation was relatively simple and the intensities could be used for quantitative analysis.

The samples were ground using a mortar and pestle until a powder resulted, in most instances only very light pressure was required. The samples were front mounted in an aluminium backed cavity holder, smoothed over with a glass microslide and equilibrated with the atmosphere overnight in the room in which they were to be X-rayed. They were loaded into the sample changer cassette and X-rayed. The operating conditions were: scan speed $1° 2\theta\,min^{-1}$, range 4×10^3, time constant 2, chart recorder speed 1 cm min^{-1}, 2θ range 4° to 40°. A complete series of samples, e.g. from a kinetic experiment were, as far as possible X-rayed in the same run or in consecutive runs. Deterioration of the X-ray tube causes a decrease in the intensities, if samples are examined at different times; although allowance could

be made for this by regular calibration with microcrystalline quartz stone, it was preferable to run a series of samples in a single batch. When all the zeolite syntheses had been completed, the final products were re-X-rayed to determine the most crystalline sample i.e. the sample with the most intense peak occurring at $2\theta = 23.45°$. This was taken as 100% crystalline Ω and percentage crystallinities of the rest were calculated on this basis. The kinetic series were similarly calibrated and percentage crystallinity of Ω determined.

For most of the work in this thesis it was not necessary to determine d-spacings. However in a few cases 2θ values and peak heights were determined, and with the use of a computer program converted to d and RI values. These were then compared with the literature results for ZSM-4, Ω and mazzite.

3.3.8.2 Investigation of the Effect of Prolonged Grinding

3.3.8.2.1 Procedure

A simple examination of excessive grinding on an Ω related material, zeolite S, was carried out. During grinding high temperatures are reached and thus zeolite S was selected since it is said to convert to the dehydrated form with structural change at ~250°C. The specimen was ground in a mortar and pestle, by hand, for successive five minute periods and X-rayed between each grinding. This by no means represents an accurate study, as the degree of grinding in the 5 minute period is naturally subjected to variations in pressure, but is used to illustrate the effects.

3.3.8.2.2 Results

The grinding experiment illustrated in Fig. 3.3 shows that gradual structural damage is incurred and detected by XRD. Perhaps a more

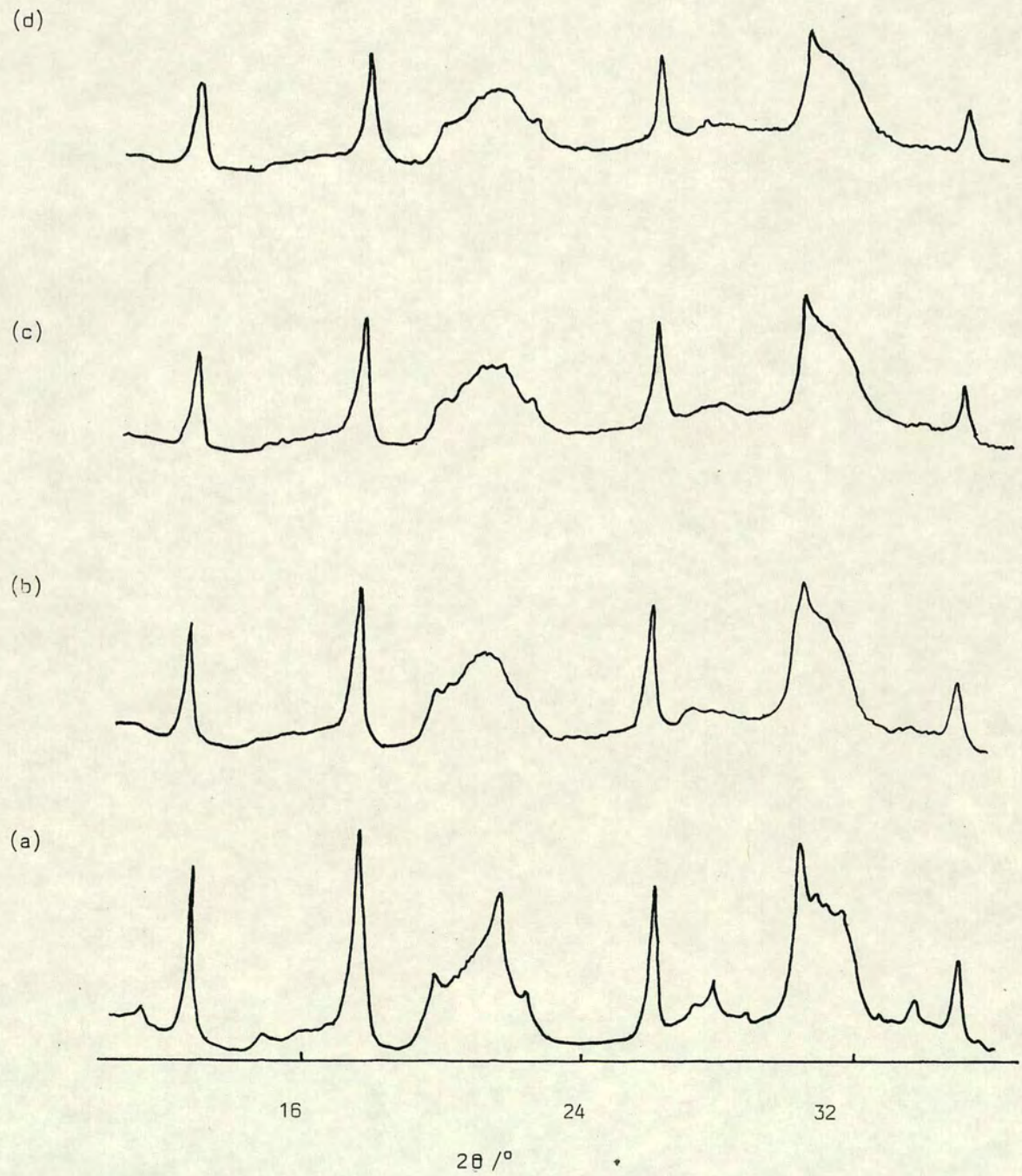

Fig. 3.3 Effect of Prolonged Grinding on Zeolite S

(a) before grinding
(b) 5 minutes grinding
(c) 2x5 minutes grinding
(d) 3 x 5 minutes grinding

dramatic change may have been observed in morphology, but facilities for SEM were not available at the time. Although high temperatures are attained during grinding they were not sufficiently high to effect the transformation to the dehydrated phase.

3.3.8.3 Investigation of Line Broadening

Examples of line broadening observed for two different materials are given here as an illustration. The first example illustrates how for hydroxysodalite the peak width decreases as the crystallisation proceeds, and the small crystals increase in size (Fig. 3.4). The second example (Figs. 3.5, 3.6, 3.7) illustrates how for zeolite S a structural fault i.e. chabazite intergrowth, can lead to line broadening. For this sample small crystal size may also be a contributing factor, but as SEM facilities were not available, this remains uncertain.

3.3.8.4 Calibration with Internal Standard

Accurate d-spacings were obtained for TMA-sodalite by use of a silicon internal standard. The silicon (10% by weight) was ground and thoroughly mixed with the zeolite, and then mounted in the afore-mentioned manner. This zeolite had a very high degree of crystallinity. The operating conditions were: range 2×10^4, scan speed $0.5° \text{ min}^{-1}$, time constant 4, 2θ range 4° to 90°. It was necessary to run out beyond 40° in order to have sufficient Si lines present for calibration purposes. The XRD pattern of Si/TMA-sodalite is given in Fig. 3.8. The 2θ values were measured as accurately as possible, by eye, and used to calculate the cell constants using computer programs. TMA-sodalite was indexed to cubic cell I and the cell constant determined was in good agreement with the value obtained by Barrer and Denny but slightly less than that of Meier and Baerlocher (Table 3.1).

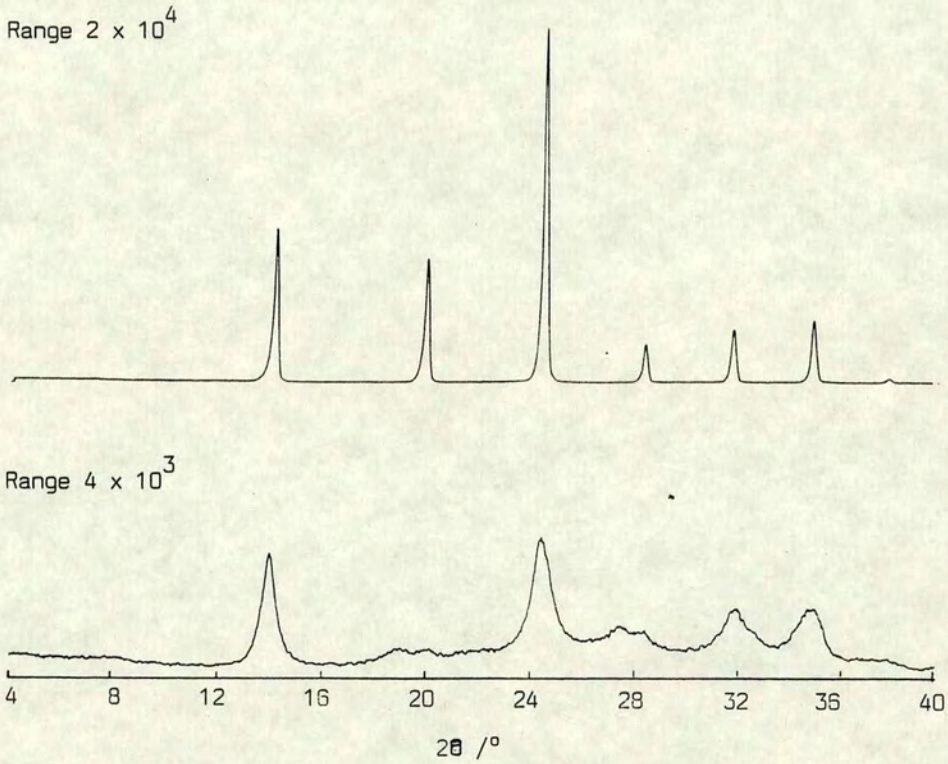

Fig. 3.4 X-Ray Diffraction Patterns of Sodalite

Lower pattern shows broad peaks of a sample taken early in the crystallisation.

Upper pattern shows sharp peaks for the final product.

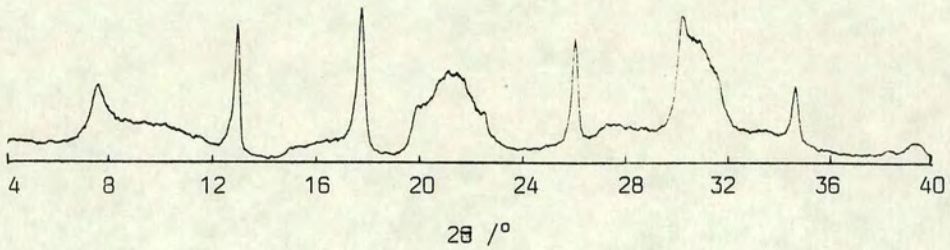

Fig. 3.5 X-Ray Diffraction Pattern of Synthetic Zeolite S

Broad peaks indicative of structural fault caused by chabazite intergrowth

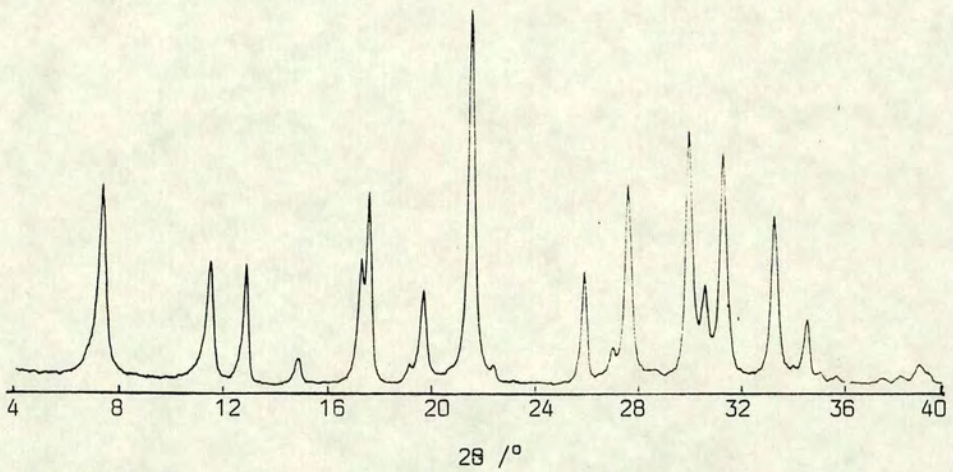

Fig. 3.6 X-Ray Diffraction Pattern of Pure Synthetic Gmelinite

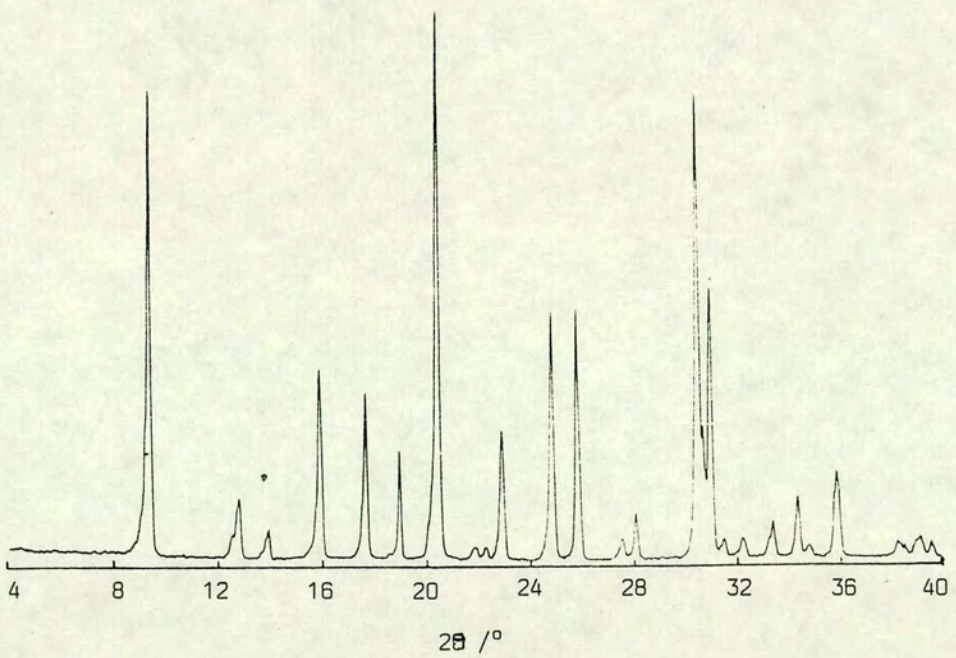

Fig. 3.7 X-Ray Diffraction Pattern of Chabazite (mineral)

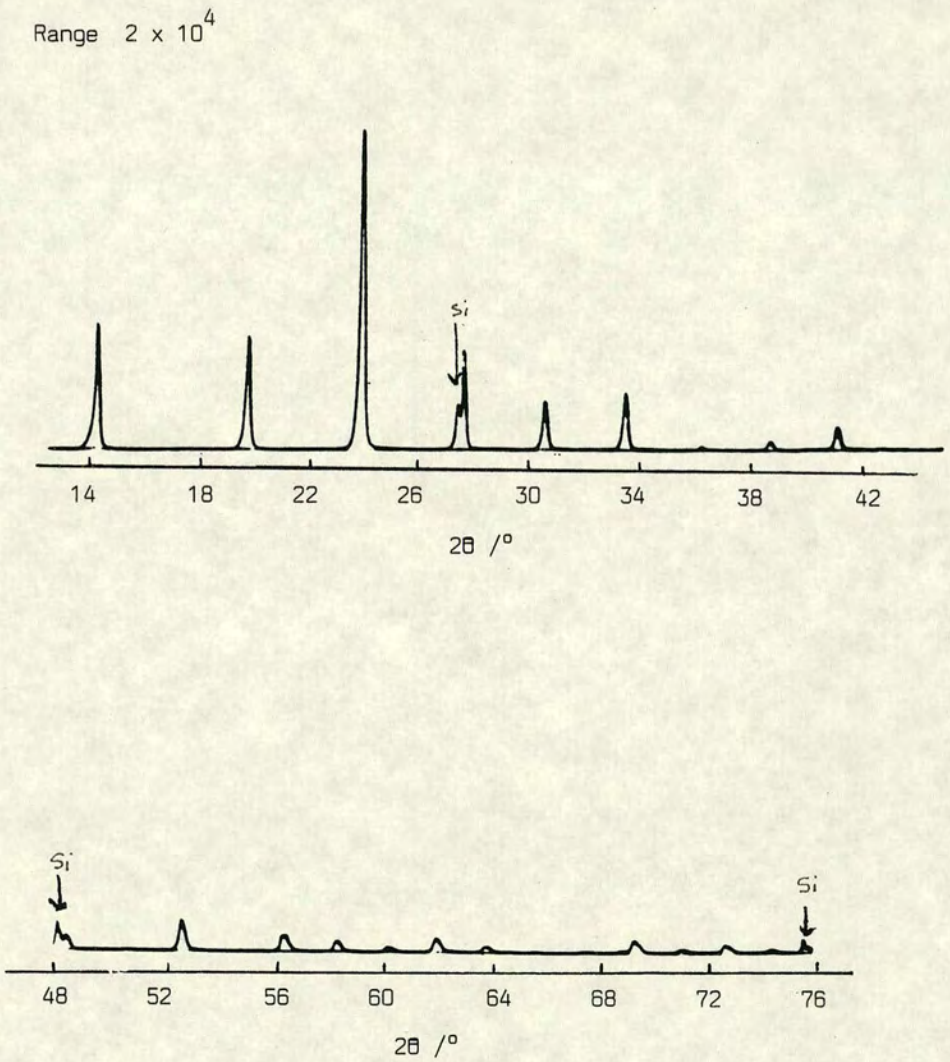

Fig. 3.8 Calibration of TMA-Sodalite
with Silicon Internal Standard

Table 3.1

Comparison of Cell Constant a for TMA-sodalite with previous work

TMA-SODALITE	a./Å
This work	8.9 4 11 ± 0.0006
Meier & Baerlocher	8.9 75 ± 0.001
Barrer & Denny	8.9 3 ± not given

3.3.8.5 Accuracy

The errors in sample preparation are expected to be the same throughout as the samples were mounted by the same procedure each time. Zeolite Ω with SiO_2/Al_2O_3 ratio of ~6 is hydrophilic and so humidity conditions will affect the intensities.

3.4 X-ray Fluorescence Spectrometry

3.4.1 Introduction

Quantitative and qualitative determination of the elemental composition of aluminosilicates may be determined by X-ray fluorescence spectrometry (XRF). It is a fast, precise and non-destructive method for detection of elements from B to F and Na to U [16]. In XRF a beam of X-rays is directed onto the surface of the specimen and a secondary target, the latter causes secondary X-rays or fluorescent radiation to be emitted. This is illustrated in Fig. 3.9. This radiation contains wavelengths which are characteristic of the elements present in the sample. The methods employed for separation of the characteristic X-rays defines two types of instrument: energy dispersive (ED) and wavelength dispersive (WD).

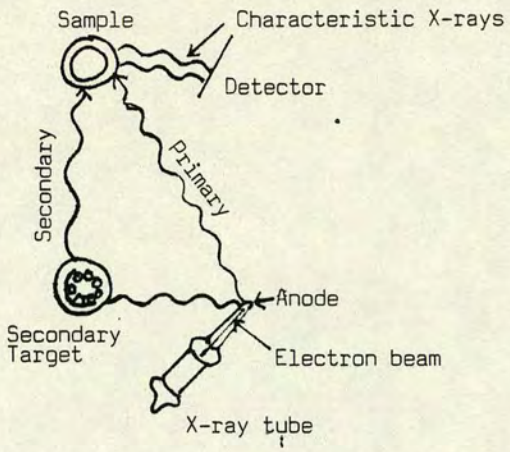

Production of Fluorescent Radiation

Fig. 3.9

In this work, a WD instrument was used. Quantitative analysis of the light elements required the samples to be cast into glass discs. The zeolite samples were dissolved into lithium tetraborate glass [17]; the latter readily dissolves silicates, overcomes particle size problems and does not emit characteristic X-rays in the wavelength region used. The molten glass is then cast into discs directly inserted into the diffractometer, and analysis carried out.

3.4.2 Experimental

3.4.2.1 Introduction

The facilities for routine analysis of silicate rock, mineral and zeolite samples by XRF methods for major elements Si, Al and Na available in the Department of Geology, Edinburgh University, were used in the present work. The technique employs a Cr X-ray tube and fused glass discs (45 mm diameter), the Norrish and Hutton method 1969. The analysis is corrected for both interference and mass absorption effects by use of the tables of Theisen and Vollach, 1967. Calibration is constructed by use of standards chosen to cover a range of compositions. The results are data processed by a computer program by Thirlwall (1979).

3.4.2.2 Preparation of Fused Glass Disc [18]

The powdered zeolite samples, initially dried at 110°C, were ignited at 1100°C in porcelain crucibles in a furnace overnight (16 h) to ensure complete removal of volatile organic material. (Free carbon or organic material attacks the Pt-Au crucibles.) The dried sample (1 to 1.2 g) was accurately weighed into a Pt-Au crucible. To this was added flux (Johnson Matthey Spectroflux 105) in quantity five times the weight of sample used. As the flux contains volatile material (0.5%) it is advisable to take slightly more flux ca 0.03 g than required. The samples were prepared in batches of four. Pt-Au crucibles were placed on a silica tray, covered with Pt lids, and placed into the furnace at 1100°C for 0.5 h. The tray of samples was then removed from the furnace. The fused molten material in the crucible was swirled to ensure mixing, covered with lids and placed on a stainless steel cooling block. Samples which were not completely dissolved in the flux were returned to the furnace until completely molten.

When the crucible was completely cold, the weight of flux added to the samples was accurately made up (no more than 0.05 g was required). The crucible was then placed over a Meker burner, covered with a lid, and allowed to fuse completely. The molten mixture was swirled to ensure thorough mixing and heated for a few minutes.

A stainless steel cylinder was placed over a disc shaped graphite mould on a hot plate at 220°C, and an aluminium plunger allowed to attain equilibrium temperature. The crucible, when at bright red heat, was removed from the Meker burner, the lid removed, mixture swirled again and poured onto the graphite mould. The plunger was carefully inserted into the steel cylinder and gently lowered onto the molten globule. Gentle pressure was applied for ~10 seconds to ensure contact between the plunger and graphite mould, and removed after a further 5 seconds.

The resulting disc had a uniform "orange peel" surface texture. The disc remained in the graphite mould for ~0.5 h, and was then moved to the front of the hot plate to cool. The cold disc was removed from the mould, any excess glass trimmed with pliers, labelled with a self adhesive sticker attached to the back of the disc (i.e. side in contact with graphite) and stored in a self sealing polythene packet. The disc was then analysed on an automatic XRF Spectrometer. The total of the elemental compositions expressed as percent oxide was between 97 and 100.

3.4.2.3 Precision and Accuracy

The analytical precision is essentially a measure of reproducibility which may be measured by analysis of several glass discs of the same sample and mean and standard deviation calculated from the results. However, in this work the latter was not carried out.

The accuracy is a measure of the absolute quality of the analysis and is more difficult to estimate.

3.5 Thermal Analysis

3.5.1 Introduction

Since the discovery of fire, early man has observed the effect of heat on rocks and minerals [19]. Theophrastus used this as a means of identification of rocks and minerals from as early as 300 B.C. After this, an increase in technological application of heat to numerous processes followed. The basic principles for thermogravimetry (TG) and differential thermal analysis (DTA) were established by Lovejoy (1886) and Le Chatlier (1887) respectively. Mass-loss data of clays at the melting points of different metals was the basis of

TG; while the identification of clays by their heating curves which manifested absorption and evolution of heat was the beginnings of the technique of DTA.

Thermal analysis is a general term covering a group of related techniques whereby the dependence of any physical property of a substance on temperature is measured [19-23]. The majority follow changes in some property of the system (e.g. mass, energy, gas volume or pressure changes) as a dynamic function of temperature. The principal thermal analysis techniques are (a) differential thermal analysis (DTA), and (b) thermogravimetry (TG).

In DTA the temperature of a sample compared to the temperature of a thermally inert material, is recorded as the sample is heated or cooled at a uniform rate [19, 20]. It is a differential method in that the temperature of the sample, compared to the temperature of an inert reference material is recorded as a function of the sample, reference or furnace temperature. The name of the technique has been a source of confusion for many years and attempts have been made to change it.

TG is the technique in which the change in sample mass is recorded as a function of temperature [19, 20]. Three modes of thermogravimetry may be described: (a) isothermal or static thermogravimetry, in which the sample mass is recorded as a function of time at constant temperature; (b) quasistatic thermogravimetry in which the sample is heated to constant mass at each of a series of increasing temperatures; (c) dynamic thermogravimetry in which the sample is heated in an environment for which the temperature is changed in a predetermined manner, preferably at a linear rate. The present work is predominantly concerned with dynamic thermogravimetry designated as TG, and with DTA.

DTA and TG are complementary techniques which provide information relating to the physical and chemical phenomenon listed below in Table 3.4.

Table 3.4

Information obtainable from DTA and TG curves

PHYSICAL PHENOMENA	CHEMICAL PHENOMENA
Crystalline transition	Chemisorption
Second order transition	Desolvation (esp. dehydration)
Fusion	Decomposition
Vaporisation	Oxidative degradation
Sublimation	Solid-state reactions
Absorption	Solid-gas reactions (e.g. oxidation and reduction)
Adsorption	
Desorption	

Thermogravimetry can provide information on all the above phenomena except crystalline transition, fusions, and solid state reactions which occur without change in weight.

3.5.2 Thermogravimetry

3.5.2.1 Instrument Specification

Thermogravimetry is carried out on an instrument called a thermobalance. The apparatus used in this work was a Stanton Redcroft TG-770 thermobalance. It gives a direct plot of percentage weight change versus sample temperature over the temperature range of room temperature to 1500°C. The thermobalance consists of the following parts [24]:

(1) Electronic-microbalance and Balance Control module. The thermobalance is fitted with a CI Mark 2c electronic microbalance with aluminium and beryllium column beam and 5 ranges which enable sample weights of 0-100 mg to be used. In this work range 3 was selected for 0-10 mg weight samples. Repeatability of the balance is ± 0.5 µg.

(2) Microfurnace. The high temperature microfurnace is made from chromium-plated brass and is water cooled. The sample is contained in a 5% Rh-Pt pan 6 mm diameter. Sample temperature is measured by plate-type Pt v 0.3% Rh Pt thermocouple carried in twin bore ceramic rod. The plate is accurately positioned at a distance of ~ 1.5 mm from the sample pan and suspension. The programmed heating and cooling rates are 1, 2, 3, 5, 10, 15, 20, 30 and 50°C min^{-1} with 10°C min^{-1} selected for this work.

(3) A Kipp and Zonen two channel recorder. Channel 1 records temperature, it is attached to a digital temperature indicator and so readout is in °C. Channel 2 records the signal from the balance output which is proportional to weight, 50% f.s.d. was used for most measurements. A chart speed of 2 mm min^{-1} was selected.

The DTG unit was not available for use.

An illustration of the thermobalance is given in Fig. 3.10.

3.5.2.2 The TG and DTG Curves

Automatic continuous recording of the weight and temperature is usual; this ensures that no features of the weight loss temperature curve are overlooked [22]. The results from a TG run may be presented as:

(i) weight versus temperature (or time) curve, referred to as thermogravimetric (TG) curve.

(ii) rate of loss of weight versus temperature curve, referred to as the differential thermogravimetric (DTG) curve.

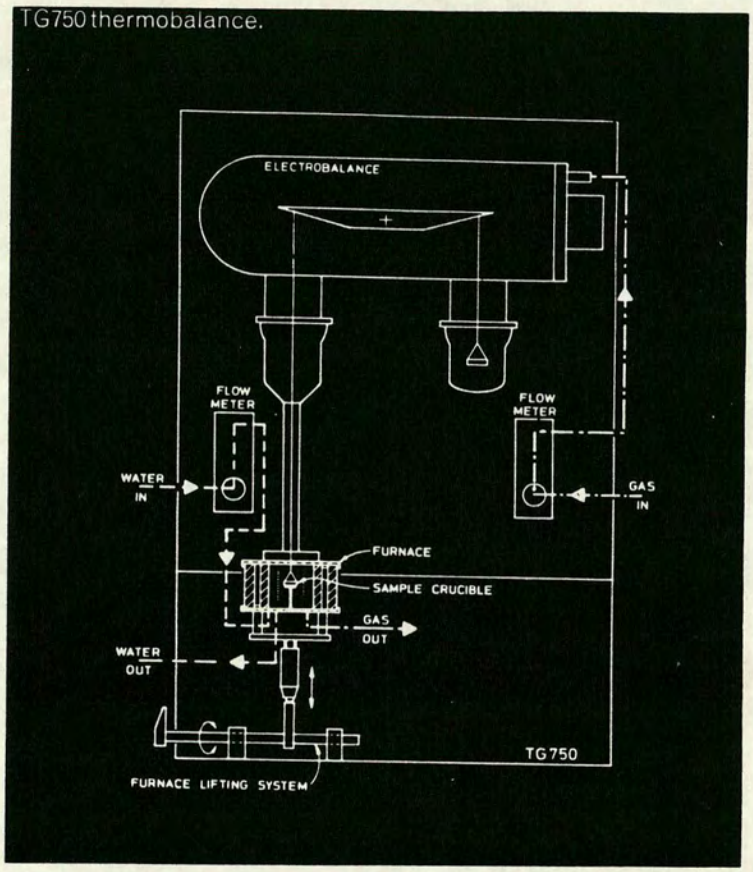

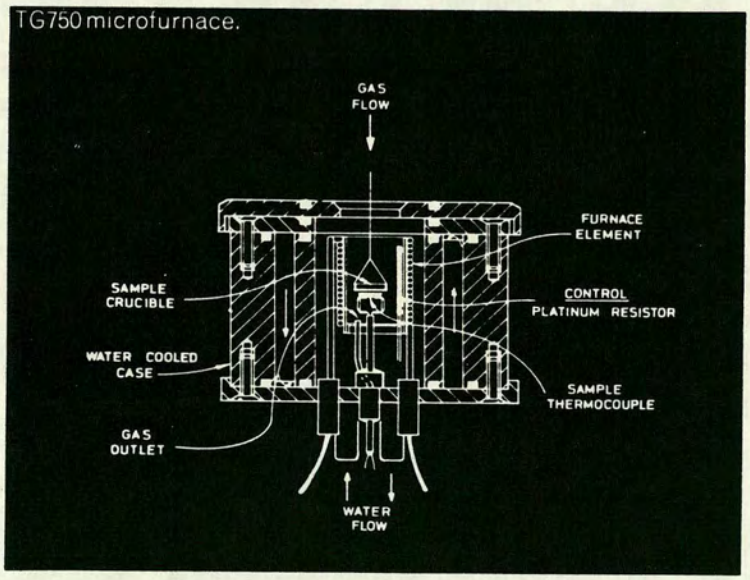

Fig. 3.10 Thermobalance and Microfurnace

In the TG curve, the weight axis may be scaled in one of several ways e.g.

(a) as a true weight scale

(b) as a percentage of the total weight

(c) as a percentage of the total weight loss or as a function of the total weight loss

(d) in terms of molecular weight units

(e) expressed in terms of fraction decomposed

The features of the TG curve may be identified as follows:

(i) horizontal portion i.e. plateau indicative of constant weight.

(ii) steepness of curve which is indicative of rate of weight loss. This passes through a maximum giving an inflexion with $\frac{dw}{dt}$ as a maximum.

(iii) An inflexion at which $\frac{dw}{dt}$ is a minimum, but not zero, may imply the formation of an intermediate compound. However, it may be due to disturbances in the heating rate or in thermocouple response.

The DTG curve has certain advantages over the TG curve in the matter of presentation, e.g. any change in rate of weight loss may be seen immediately as a trough indicative of two consecutive reactions, or as a shoulder to the peak which is indicative of two almost overlapping reactions, or as a tail to the peak indicative of strong adsorption of the volatile product on a new solid phase. DTG often shows considerable similarity to DTA curves and allows ready comparison to be made.

The use of TG results for evaluation of thermal stability has focused attention on the need for a workable definition of a suitable standard to describe decomposition. The temperature at which a reaction begins

in any particular thermobalance run is dependent on many variables of which heating rate is perhaps the most important. This temperature is neither a true decomposition temperature, below which the reaction rate is zero, nor is it a transition temperature. There is often little correlation between results from isothermal and non-isothermal runs. Knowledge of this temperature is useful and the term "procedural decomposition temperature" stresses the dependence of this temperature on the powerfully influential procedure details. A comparison of decomposition temperature has often led to controversy owing to lack of appreciation that the value is a function of method, apparatus and procedure. A clear statement of conditions should be made when decomposition temperatures are quoted.

3.5.2.3 Factors Affecting the Results Obtained

There are several factors which influence the shape of the TG curve, which must be accounted for in order to obtain meaningful and reproducible results, so that the TG data of different compounds may be confidently compared.

The heating rate for a single stage endothermic reaction, where Ti is the procedural decomposition temperature and Tf is the temperature at which the reaction is completed, shows that:

(i) $(Tf)_{\ell} > (Tf)_{s}$

(ii) $(Ti)_{\ell} > (Tf)_{s}$

(iii) $(Tf-Ti)_{\ell} > (Tf-Ti)_{s}$

where ℓ and s refer to fast and slow heating rate

At any given temperature, the extent of decomposition is greater at a slow rate of heating than for a similar sample heated at a faster rate. In an exothermic reaction, the sample temperature rises above the furnace temperature; this difference being greatest for the faster

heating rate when the reaction is occurring. In the case of successive reactions, the rate of heating may determine whether or not these reactions are separated. The appearance of a point of inflexion in the TG curve at a fast heating rate may resolve into a plateau at a slower heating rate. Hence heating rates are very important for the interpretation of results.

The sample weight can affect the TG curve in 3 ways:

(i) The extent to which endothermic or exothermic reaction of the sample will cause the sample temperature to deviate from a linear rise; in general all other factors being equal, it has been found that the greater the weight of the sample, the greater the deviation.

(ii) The degree of diffusion of the product gas through the void space around the solid particles; under static conditions the environmental atmosphere is governed by the bulk of the material in the crucible.

(iii) The possible uneveness of the temperature throughout the sample, particularly if it has a low thermal conductivity.

Thus, the use of as small a weight of sample as possible, within the limits of the sensitivity of the balance, is preferred.

The state of sub-division of the sample is important. The use of large crystals may result in spitting. The sample may foam and bubble. Most TG studies have been carried out on powders. The effect on particle size shows that the smaller the particle size, the greater the extent to which equilibrium is reached, and at any given temperature, the extent of decomposition is greater. The prehistory of the sample is also important.

The crucible geometry and composition may affect the TG curve. The best results are obtained with small dish crucibles [21] which permit homogeneous heating of the sample over a relatively large surface area. Consideration of the properties of substances investigated, such as decomposition or foaming leads to selection of suitable crucibles such as cylindrical, conical or closed. The composition of the crucible has been known to react with the sample e.g. in DTA work, catalytic oxidation of NH_3 by Pt crucible has been reported[25]; carbon attacks the Pt crucible. Also, the decomposition temperature of sodium carbonate is lower in a quartz or porcelain crucible than in a Pt one.

The effect of the atmosphere on the TG curve varies according to whether the atmosphere participates in the reaction. When the atmosphere does not participate, the role of the gas is to remove gaseous products from the vicinity of the sample, to ensure that the environmental atmosphere is kept as constant as possible throughout the experiment. Vacuum conditions have been employed to achieve the same results. Work may also be carried out such that the atmosphere used participates in the reaction, e.g. reducing atmospheres of hydrogen have been used. Some work has been carried out with atmospheres of humidified air and high pressure steam.

3.5.2.4 Conditions of Operation Selected in the Present Work

Trial TG runs with $CuSO_4 . 5H_2O$ were carried out to establish the optimum operating conditions. The results are shown in Table 3.5 and Fig. 3.11.

The optimum running conditions for this instrument were found to be: sample size of the order of 1 mg, heating rate 5°C min^{-1} with either 50 or 100% f.s.d. However, with sample size of 1 mg the balance is required to be set on range 3 and ratio 1; the ratio 1 setting is

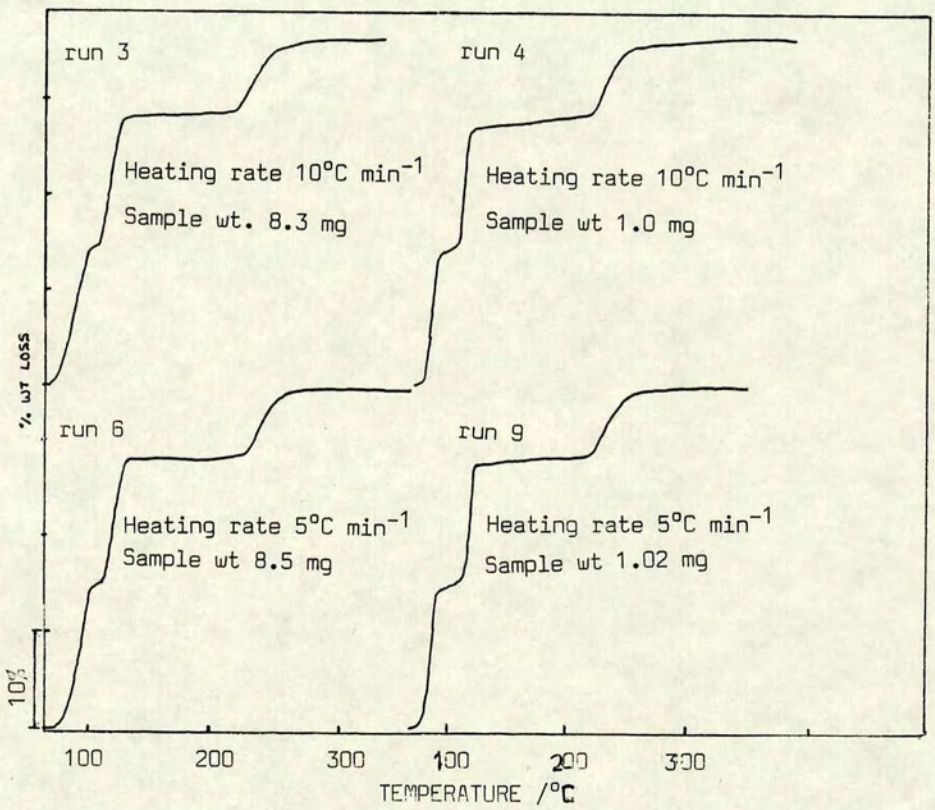

Fig. 3.11 Determination of optimum conditions of operation for TG Analysis

extremely sensitive to any movement in the room in which it is operated. At a heating rate of 5°C min^{-1} resolution of some of the weight losses in zeolite samples may be lost and only 2 runs per day could be achieved. Consideration of these factors led to the following conditions of operation: sample size 4-7 mg, ratio 2; heating rate 10°C min^{-1} (nominal), 8.5°C min^{-1} (actual); 50% f.s.d.; and temperature range, room temperature to 1000°C in most instances. The TG analysis was carried out in a dynamic atmosphere of dry air at 4.5 cm^3 min^{-1}.

Prior to subjecting the zeolite samples to thermal analysis the finely powdered samples were equilibrated with water vapour over saturated NaCl solution at 25°C for a minimum of 16 h.

Table 3.5

Effect of Sample Size and Heating Rate on TG Curve

SAMPLE: $CuSO_4$ $5H_2O$

RUN NO.	SAMPLE WT/mg	RATIO	HEATING RATE/°C min^{-1}	F.S.D./%	COMMENTS ON RESOLUTION OF TG CURVE
1	6.32	2	20	100	Poor
2	4.42	2	10	100	Fair
3	8.30	2	10	100	Good
4	1.0	1	10	100	Very good
5	1.36	1	10	50	Very good
6	8.5	2	5	100	Very good
7	6.13	2	5	50	Very good
8	1.08	1	5	50	Excellent
9	1.02	1	5	50	Excellent

3.5.3 Differential Thermal Analysis

3.5.3.1 Instrument Specification

Differential thermal analysis (DTA) was carried out on a Stanton Redcroft 673-4 differential thermal analyser. It is a sensitive apparatus for the ready evaluation of the thermal behaviour of a wide range of materials. The DTA curves are plots of Δ T v. temperature, where ΔT is the temperature between sample and reference alumina. The calibrated temperature range is 100°C to 1500°C. The DTA apparatus is composed of the following parts [26]:

(a) A dimpled Pt/Rh crucible for sample size of the order 0.1-200 mg;

(b) A head assembly module and furnace with programmed heating modes of heat, cool and isothermal. The head assembly and furnace comprise a base module complete with gas, cooling water and vacuum connections, a specimen holder assembly and an integral sheathed furnace. The head assembly consists of a DTA single stem assembly of earthed ceramic block with two 6 mm wells in which Pt/Rh thermocouples protrude and the Pt dimpled crucibles sit. Each assembly is individually aligned and standardised to give minimum drift with equal amounts of alumina reference material in both sample and reference well. The temperature programmer allows selection of heating mode. The unit is calibrated to work in the range of 100 to 1500°C and although the programme from room temperature to 100°C is not necessarily linear it is reproducible. Heating rates between 1.0 and 20°C may be selected.

(c) Amplifier with range selection of 20-1000 μv f.s.d. In normal operation 50 and 100 μv f.s.d are used, this corresponds to sensitivity reciprocal 0.25 and 0.5 μv min^{-1} respectively.

(d) A Kipp and Zonen BD9 two channel recorder of the same type as used for TG was connected to the DTA apparatus. Channel 1 records the temperature signal which reaches the recorder from the

reference thermocouple. The temperature of the reference material appears on the chart in °C as it is fitted with a digital temperature indicator. Channel 2 records ΔT, the differential temperature signal which reaches the recorder via the amplifier. A scale of 10 m V is selected for the amplified ΔT signal.

3.5.3.2 The DTA Curve

DTA, like TG, is a dynamic method and very much dependent on procedural details [22]. It does not necessarily follow that what is a good technique for TG is good for DTA. Much useful information can be obtained with equipment designed to carry out simultaneous DTA and TG on the same sample, but there are limitations. In DTA the sample is packed down in the crucible so that energy changes which occur in the course of the reaction produce a "good peak" and this requires the use of higher heating rates. In quantitative work for TG, however, both these operations would not be considered good practice. In DTA small quantities of a sample and reference material (alumina) are placed in a furnace where their temperatures are monitored by thermocouples. When the furnace temperature is raised steadily, the temperature of the sample differs from that of the reference by an amount which depends on the difference between their heat capacities and on the heating rate. The temperature difference ΔT is plotted as the ordinate on the X-Y recorder, and the furnace temperature T is plotted on the abscissa. Thus the temperature lag which results from the difference in heat capacities of the sample and reference is detected as a deflection from the chart base line. When an endothermic or exothermic process occurs a substantial deflection is superimposed on that which arises from differences in heat capacity. In a similar manner, any phase transition, such as fusion,

undergone by the sample is also observed. (The reference material must be carefully selected so as not to undergo any phase transition in the temperature range concerned.) During a phase transition, the sample temperature remains constant despite the fact that the temperature of the furnace and the reference continue to rise. When the sample has undergone the phase change, the sample temperature rises rapidly toward that of the furnace. Thus a phase change normally shows up as unsymmetric peaks on the recorder chart.

The DTA curve records all processes which produce changes in enthalpy (see Table 3.4), although it does not indicate the kind of change which occurs [21]. The nature and mechanism of the change can be analysed further by other methods such as XRD and TG.

3.5.3.3 Factors Affecting the DTA Curve

As with TG, sample preparation is one of the most important factors in obtaining good reliable DTA results. Reproducibility between successive experiments is obtained if precisely the same packing procedure is carried out each time [26]. As for TG, the samples in this work were finely ground powders, equilibrated with water vapour over saturated sodium chloride solution at 25°C for a minimum of 16 h. (The samples were not subject to excessive grinding, in order to avoid mechanical stresses which would induce transitions in the DTA curve.) The sample is firmly pressed down into the crucible to increase heat conductivity and to expel pockets of air which otherwise manifest themselves as jagged edged or drawn out peaks because of the larger temperature lag. The sample size in this work was of the order of 40-60 mg, ideally 50 mg, but in some cases this weight was insufficient to cover the dimple in the crucible and addition of more sample was necessary. The sample weight used was recorded for each run. It was found that

for some materials a large sample size produced split peaks and when this occurred the run was repeated with a smaller sample size. However, in some instances, the higher density of the sample would not allow reduced sample weight to be used as this would have led to the dimple being uncovered and given rise to further complications. In such instances, it was recognised that the split peak represented a single process. The peak area seems to decrease at high sample weight [23], the decrease in sensitivity is probably due to an increased heat flow between reference and sample caused by a larger temperature differential. The DTA was carried out in static air.

The heating rate was initially 10°C min^{-1} to enable comparison to be made with TG; however, it was found that the TG was in fact heating at ~8.5°C min^{-1} when set at 10°C min^{-1}. Consequently the temperature programme of the DTA was accordingly adjusted. (TG heating rates were fixed at 5, 10, 20°, whereas DTA could be set at any temperature.) It was observed that increased heating rates enhanced the sensitivity and shifted the peak to higher temperatures. This is because a large proportion of the reaction takes place in the same time interval and sets up steeper temperature gradients which in turn produce larger temperature differentials. However, the latter requires a wider temperature range in the DTA curve for their decay after endothermic or exothermic reactions in the sample, and this results in the loss of resolution. Peak temperature shifts due to the effect of heating rates may be eliminated [23] by direct contact of small sample weights with the thermocouple. For heating rates of up to 100°C min^{-1} a peak temperature shift of < 0.2°C for a sample weight of ~1 mg is observed by this method. However, if there is not sample contact with the thermocouple large lags develop.

In most runs the amplifier sensitivity was set to 100 μv and when dilution of organic samples was used 50 μv was employed in order to detect the peak.

The samples were heated to about 1000°C and only in a few instances was this temperature exceeded to observe exothermic effects which had commenced at around 960°C.

The overall DTA operating conditions employed throughout this work were: sample size 40-60 mg, heating rate ~ 8.5°C min^{-1}, sensitivity 100 μv or 50 μv, temperature range room temperature to 1000°C, chart recorder speed 2 mm min^{-1}. The DTA was carried out under static air conditions. The reference material was alumina; and Pt/Rh crucibles were used.

3.5.4 Quantitative Application of Thermal Analysis to Zeolites

Improved thermoanalytical instrumentation became widely available at about the same time as attention was directed to the industrial applications of zeolite properties [27] and consequently thermal analysis was applied to find ways to modify the zeolite properties. The quantitative use of the data allowed determination of: degree of ammonia removal by thermal treatment of NH_4-exchanged type Y via the exothermic intensity, calculation of heats of adsorption, thermal stability of the structure and related mechanistic behaviour.

The importance of thermal stability and the interest in high temperature properties of zeolites are largely related to their catalytic application, especially large scale use in the petroleum cracking reaction. This factor has led to emphasis on the study of materials most likely to be useful in such applications. The thermal behaviour of zeolites used primarily for adsorption has not been studied

extensively, but the thermal property relationships are quite important here. Adsorption and desorption of various gases as a function of temperature has been examined in great detail to allow design of a number of important adsorption processes. The change in thermal stability of the ion exchanged form of zeolite A has been extensively studied. The recrystallisation temperature at which a thermodynamically stable non-zeolite alkali aluminosilicate phase is formed may be obtained from DTA. This type of reaction is almost universal among zeolites, but is sometimes difficult to detect. It illustrates that under most sets of conditions zeolites exist as thermodynamically metastable species. Thermal stability data, represented by a measurement of the temperature at which structural collapse occurs may sometimes be misleading in that the degradation of the structure is a kinetic phenomena beyond some threshold temperature and is dependent on the time-temperature-atmosphere relationship and thermal history of the sample. Wide variations in results can easily be produced by changes in the conditions used or the technique employed. Various factors in preparation of the sample for testing also exert important effects.

Care must be taken in both the collection and interpretation of data. Relative comparisons can often be made if the relevant factors are recognised. Water vapour in the atmosphere, to which the zeolite is exposed, is often difficult to assess and frequently leads to disagreement between laboratory data and actual performance; e.g. thermal stability of K exchanged form of zeolite A is reduced, as determined by DTA, by addition of a small amount of water vapour. This illustrates that there is a difference between thermal stability and hydrothermal stability. However, in Edinburgh, this is overcome by equilibration of samples over NaCl at 25°C prior to analysis.

The thermal properties can be related to the other physicochemical properties of a zeolite and thus provide some predictive utility; e.g. DTA structural collapse temperature of stabilised zeolite Y is correlated to IR stretching frequencies. The collapse temperature is also correlated with unit cell parameters of the crystal. Decrease in aluminium content leads to decrease in some of the aluminosilicate framework bond lengths and thus a decrease in unit cell size. Decrease in the unit cell size implies an increase in framework SiO_2/Al_2O_3 ratio and correlates with increased thermal stability. Once the zeolite structural framework collapses, this explanation regarding the effects of changes in the SiO_2/Al_2O_3 ratio of the structure is not valid. The recrystallisation temperature of the amorphous collapsed structure to a stable high-temperature phase, increases with increasing unit cell size or decreasing SiO_2/Al_2O_3 ratio. A proposed explanation for this involves the nucleation inhibition effect and the presence of glass type phases formed after breakdown of the zeolite structure. The high temperature crystallisation phase for zeolite Y has been identified as mullite, which is also formed by several zeolites.

Thermal measurements of various kinds have been used to study various aspects of zeolites and their careful interpretation has contributed to an understanding of the material science and reaction mechanism relationships. Thermal methods are used in quality control of zeolite products and raw materials. Thermal analysis possesses the capacity for contribution to the many unanswered outstanding questions in the field of zeolites.

3.5.5 Applications of Thermal Analysis to the Present Work

In the present work thermal analysis (DTA, TG) is used in conjunction with XRD and pH measurements to monitor the crystallisation of zeolite Ω

from the optimum reaction composition determined by Lowe et al [30]. TG is shown to be capable of detection of microcrystalline structure which is amorphous to X-rays. A slight variation of the reaction composition in which the TMABr is partially replaced by the neutral molecule hexanediol, in an attempt to synthesise fault-free Ω , is made. Analysis by DTA would determine whether the hexanediol was incorporated into the main channel during synthesis.

Investigation of the effect of contact of water on zeolite Ω is examined by DTA/TG and XRD. The weight loss associated with each exotherm of the DTA established that redistribution of organic material occurs as a result of this treatment. Simple experiments analysed by DTA were devised to locate the decomposition temperature of organic material adsorbed by the external surface and main channel, in order to assist the understanding of the peak shift phenomena observed as a result of the washing process.

Sorption of molecules from the aqueous phase by organic free Ω and the as synthesised materials was analysed by DTA, TG, and XRD. Differentiation of adsorption by the external surface and main channel was achieved by DTA, and quantitatively measured from TG. The effect of sorbate occluded in the main channel on the TMA in the gmelinite cage is illustrated by DTA (Chapter 6).

3.5.6 Limitations of Thermal Analysis

Overall, thermal analysis applied to zeolite characterisation in this simple manner has provided an abundance of information. Much more could have been obtained from quantitative use of DTA/TG such as enthalpies and kinetics; however, this was not attempted as such measurements are inaccurate [28] from the dynamic temperature of DTA and enthalpies are best determined by Differential Scanning Calorimetry (DSC).

Although thermal analysis (DTA and TG) gives valuable information, on the properties of zeolites or zeolite catalysts, it does not provide a reproducible method for the measurement of thermal properties because too many factors associated with the particular instrument and conditions of the experiment influence the measured parameters. The technique is often useful for direct comparisons, although comparison of results from different authors is difficult.

3.6 pH Measurements

3.6.1 Introduction

A new technique which enables crystallisation of high silica and intermediate silica zeolite reactions to be monitored directly from the solid/solution phase makes use of pH measurements [4]. This technique, introduced by Lowe and Casci, is the first reliable, simple rapid procedure that allows quantitative measure of the progress of a crystallisation. Furthermore, after the pH of the gel has been measured, the solid may then be separated from the liquid phase and analysed by other techniques.

A rapid method to establish the end point of crystallisation of the desired phase is essential to prevent reaction over-run which is common in zeolite syntheses. pH measurements meet this criteria. They provide kinetic and mechanistic information and establish the end point of crystallisation. The results are comparable with those obtained from crystallinity measurements by X-ray diffraction.

Examples of reactions in which zeolite crystallisation can be studied by pH measurements are those in which quaternary ammonium cations or amines are used in the reaction composition. The highest pH increase during crystallisation is associated with the most stable zeolite. A succession of zeolite transformations producing successively

more stable products gives rise to a series of pH increases. The higher the pH for a given composition, the more stable the zeolite and less likely the reaction to over-run to other products. When the quaternary ammonium ion is occluded into the zeolite along with associated base (e.g. in silicalite formation) during the crystallisation process the pH measurement is less than expected and in some cases a decrease is observed. The percentage yield of zeolite is primarily dependent on the stoichiometry of the reaction mixture. Yields may be calculated for each pH value from the silica content and for a given composition it is possible to estimate the pH of the solution phase.

Incorporation of amine into the reaction system causes it to buffer, such that the change in pH is less than for the corresponding amine-free reaction and there is a significant increase in yield. Occlusion of substantial amounts of amine in the zeolite thus reduces the latter concentration in solution during crystallisation and so the pH is reduced. The equilibrium model is based on the theory which follows.

3.6.2 Theory of pH Measurements

3.6.2.1 Theory

Prior to 1983 [29] there was no quantitative basis for hydrothermal synthesis of zeolites. This process is basically the conversion of amorphous solid to crystalline solid in an alkaline medium. During the reaction to produce the high silica zeolites, the aluminium concentration is almost entirely in the solid phase, either in the gel or zeolite, and the negative charge is balanced by the cation.
It is assumed that aluminium is associated with the metal cation in the gel and zeolite. Both zeolite and solid gel dissolve to a limited extent in the absence of alkali and since they consist mainly of

silica an equilibrium between the solid phase and $Si(OH)_4$ in solution phase exists. The solubility of the gel must be greater than that of the zeolite for crystallisation to occur. The pH of the solution is independent of the amount of silica in the reaction mixture, provided some solid phase is present and is determined by the solubility of the most soluble solid. The pH of the reaction mixture remains constant until all the amorphous solid gel is converted to zeolite, therefore the rise in pH which accompanies crystallisation is unlikely to occur until a substantial amount of zeolite is produced and probably marks the final stage of the reaction - this is illustrated in the growth of EU-1 [4].

3.6.2.2 Limitations of the Theory

The theoretical equilibrium model assumes that the mother liquor is in equilibrium with the zeolite and is based on simple monomeric silicate species in solution with one negative charge per silicon; however, silicate oligomers may be present with less than this, and such anions allow retention of more silica in the solution phase. Thus, in circumstances when this conditon arises, pH and yields will be in poor agreement with the theory. Experimentally, contamination of zeolite product with small quantities of amorphous gel will cause reduction in pH of the mother liquor. The source of the amorphous material is precipitation consequent on samples of reaction mixture being cooled to room temperature. A further crop of crystals may result in some circumstances as the reaction mixture cools. The aluminosilicate species in the solution phase are most difficult to quantify as little information on their structures and stability is available, and the consequence of neglecting this is unknown.

3.6.3 Instrument Specification

The pH measurements in this work were made with two pH meters. The older model was a Philips PW 9409 digital pH meter used with EIL plastic bodied combination pH electrode type 180/200/UKP. The new model was Philips PW 9422 digital pH meter with automatic/manual calibration and automatic temperature compensation (Pt 100 resistance thermometer). It was used with a combination pH electrode, EIL type 180/200/BNC.

3.6.4 Experimental

3.6.4.1 Introduction

Crystallisation of zeolites with intermediate SiO_2/Al_2O_3 ratio may be studied by pH measurements. This technique was applied to Na-TMA-Ω crystallisation from the optimum composition [30]. Comparison of this data with that obtained when the temperature of mixing reactants was varied provided immediate information suggestive of a change in mechanism of the reaction. This was substantiated by the XRD results.

3.6.4.2 Procedure

The reaction mixture samples from a kinetic run were allowed to cool to room temperature in stoppered glass bottles. The pH electrode was regularly standardised in a reference buffer solution (pH = 9.2) and carefully washed with distilled water between measurements. The electrode was inserted into the sample bottle, allowed to stand for 10 minutes to attain equilibrium (slight drifting was observed when transferred to the alkaline medium) and a stable pH measurement recorded. The samples of each kinetic run were, as far as possible, analysed consecutively.

3.6.4.3 Accuracy

The absolute accuracy of measurements on solutions with pH values below 13 is believed to be < 0.1 unit. Differences of 0.03 or more between pH readings obtained at different times on different samples are considered significant. With the new model PW 9422 pH meter the accuracy of measurements was ± 0.004 units provided it was used with a perfect electrode with an ideal Nernst slope. The procedure is reliable and ideal for routine measurements.

3.7 Conclusion

Technological advances have produced rapid reliable techniques for zeolite characterisation compared with those available in the early days of the discovery of zeolites when time-consuming and poorly reliable techniques were employed. In time, these techniques classified as modern will no doubt be superceded by far more advanced computer aided scientific developments which will provide even more rapid recording and evaluation of data. Already computer linked SEM is available which gives quick prints of micrographs; EDXRF provides almost instantaneous compositional analysis from samples in any form [16]. Thermal analysis equipment linked to computer, XRD, mass spectrometers or microscopes are but a few of the more elaborate systems available [25, 28, 31-36]. Use of this type of apparatus would no doubt enable quicker compilation and evaluation of data such that much of the present work could be achieved far more rapidly.

Nonetheless, use of the instrumentation and application of the simple techniques discussed have provided an abundance of information which characterises the zeolites studied.

REFERENCES

1. J. M. Thomas, New Scientist, 1980, 21, 580.

2. S. Ramdas and J. M. Thomas, Chem. in Brit. 1985, Jan, p.49.

3. H. Lechert, NATO ASI Ser., Ser, E 1984, 80 (Zeolites:Sci-Technol.) 151.

4. J. L. Casci and B. M. Lowe, Zeolites, 1983, 3, 186.

5. H. P. Klugg and L. E. Alexander, "X-ray Diffraction Procedures for Polycrystalline and Amorphous Materials" 2nd Edition, Wiley-Interscience, New York, 1974.

6. J. Zussman, "Physical Methods in Determinative Mineralogy", (J. Zussman, ed.) Academic Press, London, 1977.

7. D. K. Smith and C. S. Barret, Adv. X-Ray Anal., 1979, 22, 1.

8. G. W. Brindley and G. Brown (Editors). Crystal Structure of Clay Minerals and their X-ray Identification. Min. Soc. Monograph 5, London Min. Soc. 1980.

9. S. T. Smith, R. L. Snyder and W. E. Brownell, Adv. X-Ray Anal. 1979, 22, 77.

10. E. M. Flanigen, Union Carbide, United States Patent 4 241 036, 1980.

11. H. S. Lipson and H. Steeple. "Interpretation of X-Ray Powder Diffraction Pattern" London, 1970.

12. A. R. West, "Solid State Chemistry and its Application", Wiley 1984.

13. R. M. Barrer, H. Villiger, J. Chem. Comm., 1969, 659.

14. P. Jacobs, E. G. Derouane and J. Weitkamp, J.C.S. Chem. Comm.,1981, 591

15. Z. Gabelica, J. B. Nagy and G. Debras, J.Cat. 1983, 84, 256.

16. M. Isherwood, Laboratory equipment digest, June 1985.

17. K. Norrish and B. W. Chappell, "Physical Methods in Determinative Mineralogy", (J. Zussman, ed.) Academic Press, London, 1977.

18. J. G. Fitton, D. E. James and M. F. Thirlwall, "A Users' Guide to X-Ray Fluorescence of Rock Samples", 2nd Edition, Edinburgh University, 1984.

19. W. W. Wendlandt and L. W. Collins (Editors), "Thermal Analysis", Halsted Press, Stroudsberg, 1976.

20. W. W. Wendlandt, "Thermal Methods of Analysis", 2nd Edition, Wiley-Interscience, New York, 1974.

21. A. Blazek, "Thermal Analysis", Van Nostrand Reinhold, London, 1973.

22. A. W. Coats and J. P. Redfern, The Analyst, 1963, 88, 906.

23. "Differential Thermal Analysis" Edited by R. C. Mackenzie, Vol. 2, Academic Press, London 1972.

24. Thermogravimetry, Stanton Redcroft literature.

25. C. B. Murphy, Analytical Chemistry, 1970, 42, No. 5, 268.

26. Differential Thermal Analysis, Stanton Redcroft literature.

27. W. H. Flank, Anal. Calorimetry, 1974, 3, 649.

28. C. B. Murphy, Analytical Chemistry, 1968, 40, No. 5, 380.

29. B. M. Lowe, Zeolites, 1983, 3, 301.

30. B. M. Lowe, A. Araya, T. J. Barber, D. S. Sinclair and A. Varma, 1984, 4, 263.

31. C. B. Murphy, Analytical Chemistry, 1964, 36, No. 5, 347.

32. C. B. Murphy, Analytical Chemistry, 1966, 38, No. 5, 443.

33. C. B. Murphy, Analytical Chemistry, 1972, 44, No. 5, 513.

34. C. B. Murphy, Analytical Chemistry, 1974, 46, No. 5, 451.

35. C. B. Murphy, Analytical Chemistry, 1978, 50, No. 5, 143.

36. C. B. Murphy, Analytical Chemistry, 1980, 52, No. 5, 106.

CHAPTER FOUR

The Crystallisation of Zeolite Ω

4.1 Introduction

The many routes used to synthesise zeolite Ω have been described in Chapter Two. The most recent work on the synthesis of Ω is that by Lowe et al [1], in which the optimum reaction composition for crystallisation at 95°C, in a stirred system was determined to be:

$$6\,Na_2O\ Al_2O_3\ 15\,SiO_2\ 300H_2O\ 3TMABr$$

In the present study the following additional variables were examined: the order in which the reactants are mixed, the partial replacement of TMABr by hexanediol, and the temperature at which the reactants are mixed.

The order of addition of TMABr to the reaction mixture was examined to determine any effects on the synthesis route to pure Ω and on the crystallisation rates. The partial replacement in the reaction composition of TMABr by the neutral molecule hexanediol was used to observe whether possible occlusion of this molecule in the main 12 ring channel occurs, and thus prevents the said structural stacking fault. The latter reduces the 7.5Å channel to ~ 4Å, and consequently the sorption capacity of what would otherwise be a good sorbent for large molecules. The effect on the crystallinity that results from the addition of hexanediol to the system is also examined. Since the reaction is carried out at 95°C, it was of interest to observe the effects on the course of crystallisation and the corresponding crystallinities from this optimum composition, when the reactant solutions are brought to a temperature of 95°C before being mixed and allowed to crystallise

under the usual conditions. Also the reaction in which partial substitution of TMABr by hexanediol was made, was similarly examined. A comparison was made with the normal procedure in which reactant solutions are mixed at approximately room temperature.

Several techniques may be used to monitor the crystallisation of a reaction; in this work X-ray powder diffraction (XRD), thermal analysis (TG and DTA) and pH measurements are used, with thermal analysis applied to the final products of all the reactions.

4.2 Experimental

4.2.1 Materials

The materials used were: fumed silica (Cab-O-Sil M5) and aluminium hydroxide obtained from BDH Chemicals; tetramethylammonium bromide (98% purity) and hexanediol (99% purity) from Aldrich Chemicals; AnalaR grade sodium hydroxide from Fisons; and glass distilled water was used for all the reaction mixtures.

4.2.2 Apparatus

The reaction vessels were wide necked one litre polypropylene bottles fitted with stainless steel stirrers. The reaction mixture could be sampled without stopping the stirrer by insertion of a modified pipette through a small hole drilled in the vessel lid. This hole was afterwards sealed with a rubber bung. All of the reactants were stirred at the same speed (150 rpm) and placed in the same thermostat bath at 95±1/°C.

Seeding effects from the reactors were prevented by the thorough cleaning of the polypropylene bottles, after each experiment, with 1M NaOH solution at 95°C for at least 24 h.

4.2.3 Preparation of Reaction Mixtures

The exact procedure used to prepare the gels from which zeolites crystallise can have an important effect on the length of the induction period, rate of crystallisation and products obtained. Hence in this work some of these variables are considered. For all the reactions, the amount of water required was weighed out in advance. Using this water the sodium hydroxide was dissolved to give a 50% (w/w) solution which with heating and stirring was used to completely dissolve the alumina trihydrate. A separate TMABr solution was prepared using a similar amount of water and similarly for the hexanediol solution when required. The Cab-O-Sil was weighed directly into the reactor. The variations in procedure, effect on the gel and ultimate product are recorded in Table 4.1. All the reaction mixtures were prepared by weight from the basic composition:

$$6Na_2O \quad Al_2O_3 \quad 15SiO_2 \quad 300H_2O \quad (3-x)TMABr \quad xHO(CH_2)_6OH$$

made up to 500 g, topped up with water which may have been lost due to evaporation from the sodium aluminate solutions. The reactors were mounted in a water bath, thermostated at 95°C, and stirred for varying periods of time.

4.2.4 Procedure

The reactions were sampled regularly during crystallisation by withdrawal of the gel (12 cm^3) from the reaction with the modified pipette. The samples were placed in small glass stoppered bottles and allowed to cool, at least overnight, before pH measurements were taken. The solid phase was filtered off, washed with distilled water, dried at 110°C and equilibrated with water vapour. The finely ground solid was subsequently examined by XRD and in some cases thermal analysis, DTA, and TG. The elemental analysis of most of the final products was

Table 4.1

Reaction Mixtures and Products

Optimum Composition: $6Na_2O$ Al_2O_3 $15SiO_2$ 3TMABr

Conditions: Agitated at 95°C for 144 h

REACTION	NO. OF MOLES HEXANEDIOL	NO. OF MOLES OF TMABr	VARIABLE	VARIATION IN REACTION MIXTURE PREPARATION AND CORRESPONDING EFFECT ON GEL	TIME /h	NATURE OF PRODUCTS
R1		3	Standard TMABr added before cold/warm base.	Water added to silica, stirred to viscous gel, TMABr (aq) stirred in - no change in gel texture. Warm $NaOH/Al(OH)_3$ (aq) solution added - viscous gel. On standing for 0.5 h, gel temperature increased and gel softened and became easier to stir.	100	Ω (73%)
R2	-	3	Order of mixing. TMABr added before base. Solutions at room temp.	Most of the water stirred in with the silica, followed by TMABr (aq) and finally $NaOH/Al(OH)_3$ (aq). A thick gel resulted.	212.5	Ω (83%)
R3	-	3	TMABr added after base. Solutions at room temp.	Water stirred in with the silica followed by $NaOH/Al(OH)_3$ (aq) and finally TMABr (aq). A thick gel resulted.	388	Ω (90%)
R4	-	3	Base added first. Solutions all at room temp.	$NaOH/Al(OH)_3$ (aq) solution added to silica, stirred to a thick gel with large proportion of unmixed silica. Water stirred in, produced thick stiff paste; TMABr (aq) stirred in and softened the gel.	145	Ω (86%)
R5	-	3	Solutions at 95°C. Base added first.	Hot $NaOH/Al(OH)_3$ (aq) solution added to the silica producing a soft easy to stir gel with some undissolved SiO_2. Addition of hot water produced a thin clear solution, followed by the addition of hot TMABr (aq) with stirring resulted in no noticeable change in the clear solution.	145	HS +Ω (17%)
R6	-	3	Alkali at 95°C. Water and TMABr (aq) at room temp.	Hot alkali stirred into the silica resulted in virtually complete dissolution of the silica. Addition of water and TMABr (aq) solutions at room temp, with stirring produced a thin gelatinous solution.	672	HS (59%) Ω (61%)
R7	1	2	Hexanediol and TMABr added before base. Solutions at room temp.	Addition of water to the silica, with stirring gave a powdery mixture. On addition of hexanediol (aq) soft stiff paste resulted; TMABr (aq) addition produced a sloppy gel which became viscous on addition of $NaOH/Al(OH)_3$ (aq).	576	Ω (100%)
R8	1	2	Hexanediol and TMABr added after base. Solutions at room temp.	Addition of water to the silica with stirring, followed by $NaOH/Al(OH)_3$ (aq) and then hexanediol (aq) and TMABr (aq) produced a viscous gel.	410	Ω (90%)
R9	1	2	TMABr (aq) added to silica.	Addition of TMABr (aq), with stirring, to the silica resulted in a thick gel, hexanediol (aq) stirred in and gave a thick gel. Water added and stirred, the gel remained viscous. Warm $NaOH/Al(OH)_3$ stirred into the gel with no change in viscosity. On standing for 0.5 h, gel was more easily stirred.	384	Ω (88%)
R10	2	1	Organic added before base.	Water stirred into the silica yielded a thick gel. Hexane-diol (aq) followed by TMABr (aq) were added with stirring and produced a very thick gel which was stirred with much difficulty. Finally warm $NaOH/Al(OH)_3$ (aq) added producing an extremely viscous gel.	72	Ω (77%)
R11	2	1	Organic added before base.	Water stirred in with silica resulted in a viscous gel with little change on addition of hexanediol (aq) and TMABr (aq). Addition of the alkali softened the gel slightly and it became easier to stir.	360	Ω (90%)
R12	2	1	Organic added after base.	Addition of water to the silica followed by alkali produced a stiff gel which softened on addition of hexanediol (aq) and TMABr (aq).	240	Ω (91%)
R13	1	2	Temperature. Solutions at 95°C. Alkali added first.	Hot alkali added to the silica and stirred until completely dissolved. Water, TMABr (aq) and hexanediol (aq) were stirred, in sequence, and gave a thin turbid solution.	288	HS (31%) + Ω (75%)
R14	2	1	Solutions at 95°C. Alkali added first.	Hot alkali added to the silica with stirring, followed by water, TMABr (aq) and hexanediol (aq). A thin paste resulted.	336	HS (100%) + Ω (44.5%)

The percentage crystallinity of Ω is based on X-ray powder diffraction peak heights for reaction R7 on the assumption that this is the highest value recorded and represents 100% crystallinity. The chosen peak was $2\theta = 23.4$, $d = 3.802$. Similarly for reactions R6, R13, R14, the most intense sodalite peak was assumed as representative of 100% crystalline sodalite. The chosen peak was $2\theta = 24.4$, $d = 3.648$. HS is probably a mixture of hydroxysodalite and TMA-sodalite, but is recorded simply as sodalite, HS.

carried out by XRF.

4.3 Results and Discussion

The products from these experiments are compared with three samples of zeolite Ω, DS2, DS3 and DS13 synthesised by Douglas Sinclair in Edinburgh.

4.3.1 Treatment of Results

The results are tabulated in Tables 4.2 to 4.10 and illustrated in Figs. 4.1 to 4.36.

The results are presented as follows:

(a) Order of mixing reactants as examined by XRD and pH

(b) Partial replacement of TMABr by hexanediol, examined by XRD and pH

  (i) Effect of concentration of hexanediol in the reaction mixture

  (ii) Effect of order of mixing of reactants

(c) Comparison of products and crystallinities from reactants mixed at 95°C and at room temperature, examined by XRD and pH

  (i) The standard method of preparation at room temperature compared with reactant solutions mixed at 95°C

  (ii) The reactants of the optimum composition, brought to temperature of 95°C and then mixed is compared with a reaction in which 2TMABr is substituted by hexanediol and solutions brought to temperature of 95°C and then mixed

(d) Examination of the crystallisation of selected reactions by XRD, pH, TG and DTA

  (i) Standard composition: $6Na_2O$ Al_2O_3 $15SiO_2$ $300H_2O$ 3TMABr

  (ii) Replacement of one mole of TMABr by hexanediol, i.e. 2TMABr $1HO(CH_2)_6OH$

  (iii) Replacement of two moles of TMABr by hexanediol, i.e. TMABr $2HO(CH_2)_6OH$

(e) Thermal analysis and classification of the final products according to DTA type.

(f) Comparison of DTA types with chemical composition (XRF), degree of crystallinity and reaction time.

4.3.2 Identification of Products

The products obtained from the optimum reaction composition for Ω synthesis were identified by XRD as pure Ω , and Ω in admixture with sodalite. Only reactions in which the reactants were mixed at 95°C gave sodalite and Ω mixtures. All other reactions in which the order of mixing reactants and partial TMABr replacement by hexanediol were investigated produced pure Ω. Reaction R7, which contained one mole hexanediol produced the most crystalline sample of Ω . The XRD pattern of this sample is given in Fig. 4.1 Comparison of the XRD data for a sample of Ω , DS3, is made with the literature: mazzite, ZSM-4 and Ω [2-4] in Table 4.2. Comparison of the XRD pattern of the product from reaction R14 with that of a pure sample of Ω (R7) and a sample of pure sodalite (Fig. 4.2) clearly indicates the presence of both species in the product of R14. The species identified as sodalite is probably a mixture of hydroxysodalite and TMA-sodalite. In reaction R5, on the basis of DTA evidence, the sodalite is present as only hydroxysodalite. In reactions R6, R13 and R14, the DTA of some samples taken early in the course of crystallisation show no exothermic oxidative degradation of TMA from the sodalite cage and thus hydroxysodalite phase is present; however the DTA of the final products show an exotherm additional to those assigned to Ω and not typical of the latter and is therefore probably TMA-sodalite. Thus in reactions R6, R13 and R14 it is highly probable that both hydroxy-sodalite and TMA-sodalite are present in addition to Ω . Differentiation between the two sodalite species is difficult from XRD (although theoretically possible) and so, for simplicity, the crystallisation product is considered as sodalite, though it must be appreciated that the species termed sodalite is probably hydroxysodalite and TMA-sodalite.

Table 4.2

Comparison of the XRD Data of Mazzite, ZSM-4, Omega and DS3

MAZZITE [2]		ZSM-4 [3]		Ω [4]		DS3	
d_{obs}/Å	I/I_o	d_{obs}/Å	I/I_o	d_{obs}/Å	I/I_o	d_{obs}/Å	I/I_o
		17.5	2				
15.93	35	16.0	17	15.84	ms	15.838	10
9.20	60	9.18	100	9.07	vvs	9.099	83
7.96	35	7.96	21	7.86	m	7.886	21
6.89	25	6.94	12	6.86	ms	7.070	27
6.02	53	6.01	34	5.94	s	5.961	40
5.53	12	5.53	4	5.47	w	5.485	7
5.31	17	5.29	8	5.23	mw	5.249	9
4.729	50	4.73	30	4.67	s	4.700	48
4.423	12	4.41	4	4.36	vw	4.370	4
		4.12	5				
3.986	20	3.97	13	3.92	mw	3.939	18
3.824	95	3.82	67	3.78	vs	3.806	100
3.717	25	3.74	11	3.69	m	3.715	39
3.655	47	3.64	31	3.60	m	3.616	39
3.531	90	3.54	30	3.50	s	3.524	79
3.474	12	3.46	7	3.423	mw	3.435	22
3.452	10						
		3.28	4	3.255	w	3.268	8
3.185	100	3.17	73	3.144	s	3.158	74
3.102	30	3.10	12	3.075	m	3.083	35
3.065	38	3.05	25	3.021	m	3.036	36
3.010	40	2.99	14	2.969	mw	2.977	23
2.941	100	2.93	43			2.915	74
				2.906	s		
2.865	10						
		2.83	4	2.823	w	2.834	8
		2.775	1	2.765	vw	2.770	3
2.681	12	2.67	3	2.731	vw	2.729	2
2.643	16	2.65	6	2.645	mw	2.654	12
		2.63	5	2.616	mw	2.625	11
2.552	20	2.56	1				
2.511	5	2.52	6	2.516	w	2.520	10
2.446	1	2.49	4	2.475	w	2.479	6
2.422	9	2.43	1			2.434	2
2.393	1	2.40	3				
		2.38	5	2.369	w	2.376	9
2.302	22	2.34	1			2.346	3
2.298	22	2.28	7	2.268	w	2.276	10
2.210	9						
		2.19	2			2.185	2
		2.17	1				
2.147	10	2.14	3	2.134	w	2.138	6
2.123	17	2.10	4			2.100	6
		2.09	2	2.094	vw		
				2.072	vw	2.079	4
2.037	10	2.04	1	2.03	w	2.032	7
2.006	7	2.02	3				
1.991	10	1.99	6	1.974	mw	1.983	11
1.9708	3					1.952	6
1.9100	18			1.902	mw	1.910	16
1.8860	1						
						1.869	3

X-Ray Diffraction Pattern of Pure Ω (R7)

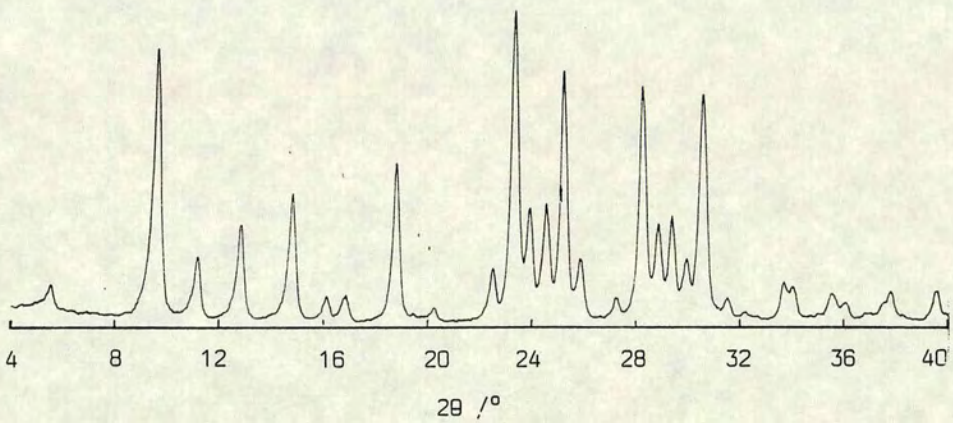

Fig. 4.1

Comparison of Ω in admixture with Sodalite, R14, (b) with the Pure Species (a) Ω and (c) Sodalite

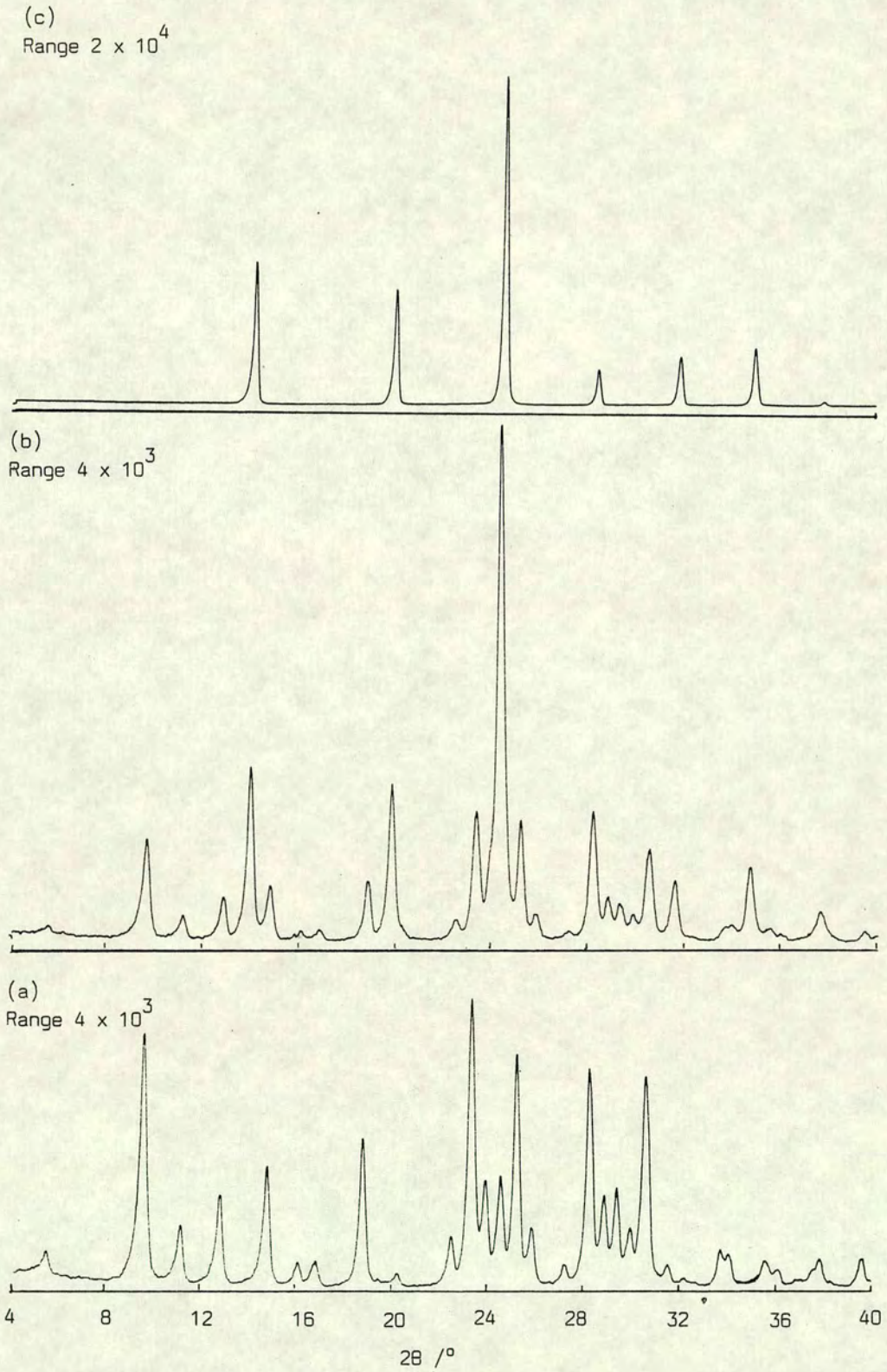

Fig. 4.2

4.3.3 Order of Mixing Reactants

In order to observe any effects due to the order in which the reactants are mixed, the standard preparation i.e. reaction R1 in which water is added to the silica followed by TMABr (aq) and finally the warm $NaOH/Al(OH)_3$ (aq) was compared with: R2, in which the order of addition is unchanged but the alkali is added at room temperature; R3, in which the TMABr (aq) is added after the base; and R4, in which the base is added to the silica.

Reactions R1, R2, and R3 produced viscous gels; however, by mixing the alkali, water and then TMABr (aq) in order with the silica, the gel is softened (R4).

The initial pH of the gels (see Fig. 4.3) showed that the standard preparation, R1, had a much lower pH than R2, the only difference being the addition of warm base in R1. Thus the temperature lowers the pH of the reaction.

Addition of TMABr after the base, R3, resulted in the pH reading being significantly lowered compared with that obtained when TMABr was added before the base, R2. Similarly addition of the base directly to the dry silica, R4, produced a gel with pH very close to that of TMABr added after the base, R3.

The order in which the reactants were mixed had a significant effect on the crystallisation rate as monitored by pH. Reaction R2 resulted in the fastest crystallisation rate with R1 the slowest, the only difference being the addition of warm base to the latter. Reaction R3, showed a sharp initial increase in pH and after 24 h ~ 50% crystalline material resulted with a much slower pH rise. In reaction R4, the pH increased slowly and steadily, tailing off after about 72 h.

Effect of Order of Mixing Reactants

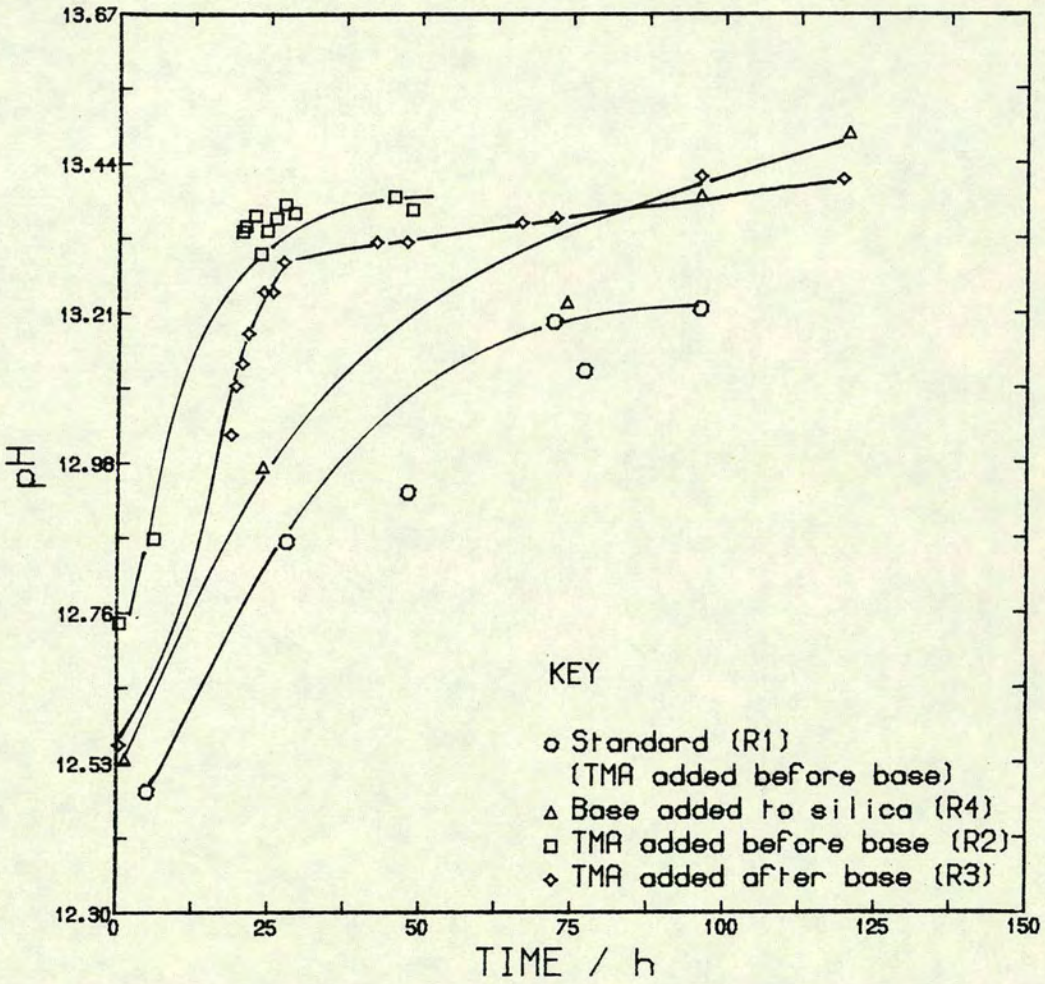

FIG. 4.3

Effect of Order of Mixing Reactants

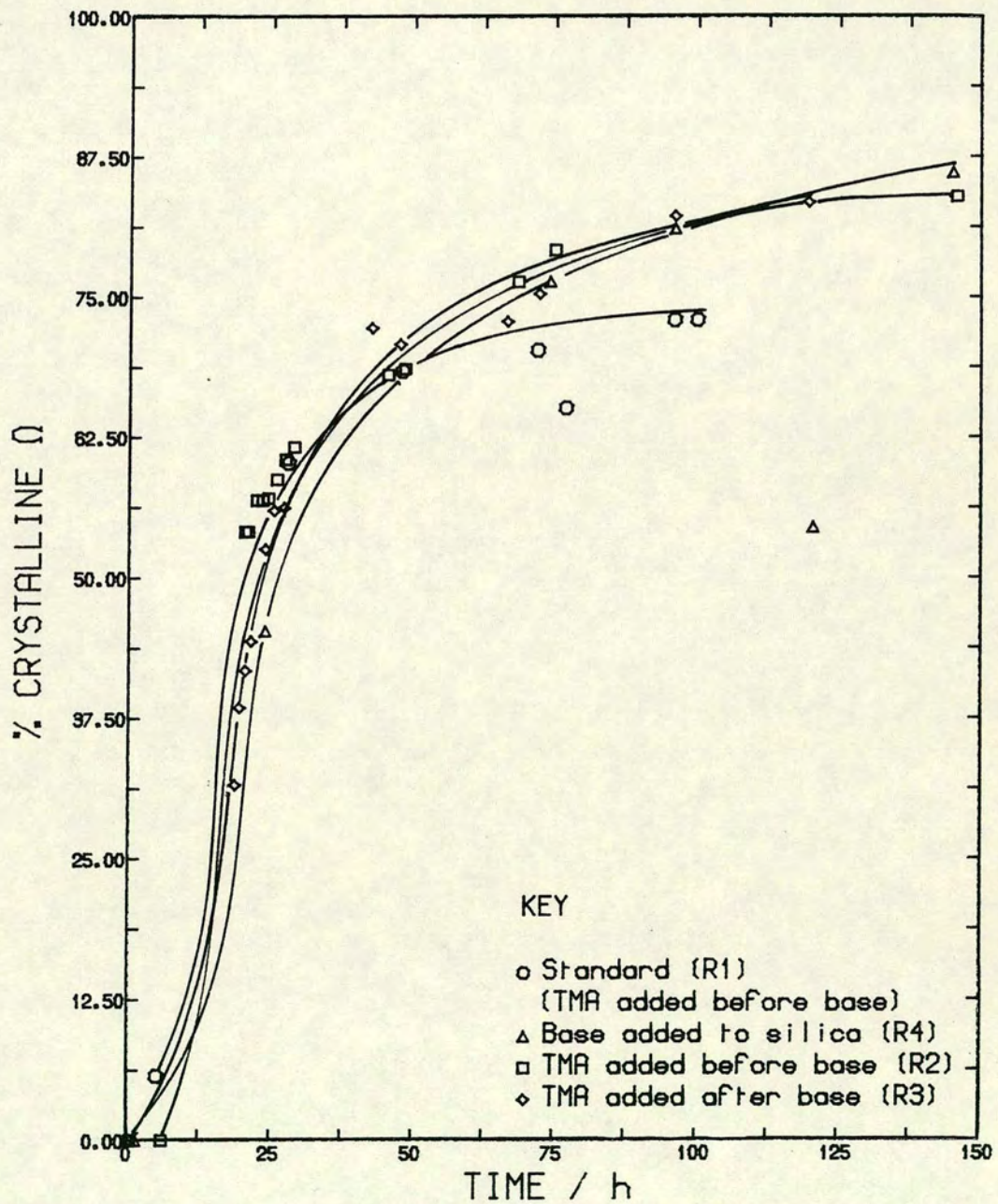

Fig. 4.4

In all the reactions the pH rose to >13.4 except in reaction R1 which rose to 13.2.

Similar trends are observed in the crystallisation curves obtained by XRD (Fig. 4.4). There is insufficient data at the onset of crystallisation to comment critically on changes in the induction periods brought about by the order in which the reactants are mixed. It can be seen that there is little difference in the crystallisation rates although addition of the base to the silica, R4, retards the initial rate, but later the crystallisation occurs at much the same rate and to the same degree of crystallinity as observed in reactions R2 and R3. It is remarkable that the addition of the warm base, in R1, increased the initial rate of crystallisation, but after 48 h growth virtually ceased, whereas in reactions R2, R3 and R4 a steady increase in crystallinity of Ω is observed.

The first 48 h of crystallisation was monitored closely for reactions R2 and R3. Comparison of the pH and crystallisation curves of these two reactions is illustrated in Figs. 4.5 and 4.6. They clearly illustrate that addition of TMABr before the base (R2) results in a higher pH of the reaction, and virtually more rapid crystallisation throughout the course of the reaction than when TMABr is added after the base (R3). Although the pH reading at 48 h is lower in R3 than in R2, the % crystallinity of R3 overtakes R2, but only slightly.

Thus, the pH rise and degree of crystallinity in decreasing order are:

pH	XRD	Order of Mixing Reactants
R2	R2	TMABr added before the base
~R3	~R3	TMABr added after the base
R4	~R4	Base added to silica
R1	R1	TMABr added before warm base

Effect of Order of Addition of TMA

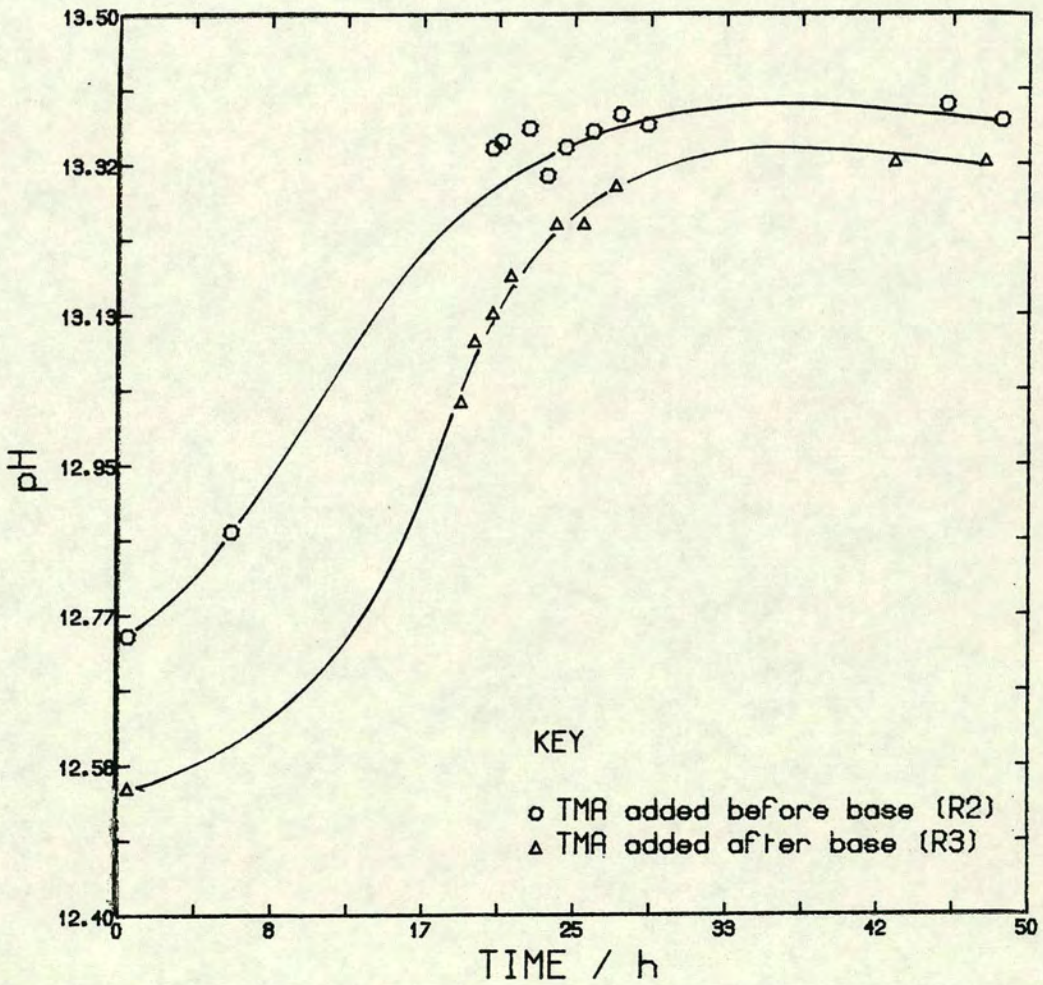

Fig. 4.5

Effect of Order of Addition of TMA

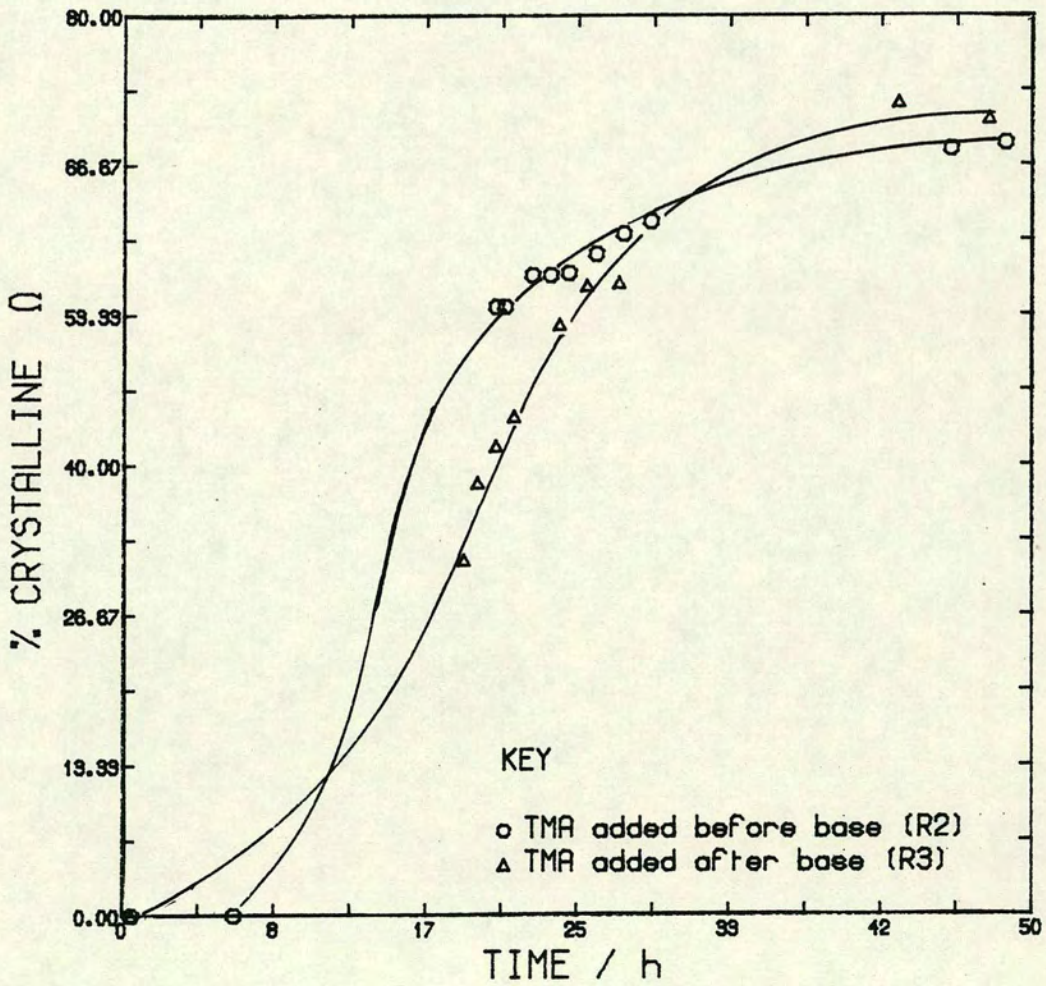

Fig. 4.6

According to the theory [5] used to describe the crystallisation of high silica zeolites, the pH of the reaction mixture remains constant until all the amorphous solid gel is converted to zeolite and so a rise in pH which accompanies crystallisation is unlikely to occur until a substantial amount of zeolite is produced and this probably marks the final stage of the reaction. However, with zeolite Ω , an 'intermediate' silica zeolite, the pH of the reaction mixture rises steadily as the amorphous solid is converted to product. Figs. 4.5 and 4.6 illustrate that in reaction R3 at 18.8 h, the solid is 31.5% crystalline Ω , the gel pH is 13.03 and that at 24 h the crystallinity has risen to 52.53% and pH is 13.25. The pH of the gel continues to rise with an increase in the % crystalline Ω . Reactions R1, R2, and R4 behave similarly; the effects are illustrated in Figs. 4.3 and 4.4.

4.3.4 Partial Replacement of TMABr by Hexanediol

The partial substitution of TMABr by hexanediol had little effect on the nature of the gel. When one mole of TMABr was replaced by one mole of hexanediol, in reactions R7, R8 and R9, a viscous gel resulted. When two moles of TMABr were replaced by two moles of hexanediol in R10, an extremely viscous gel resulted, however in reactions R11 and R12, the presence of hexanediol in the reaction mixture gave a softer gel which was more easily stirred.

4.3.4.1 Comparison of TMABr and Hexanediol Reactions with TMABr Reactions

The effects on pH and crystallinity produced by partial replacement of TMABr by hexanediol are compared with reactions R2 and R3 (Figs. 4.7, 4.8 and 4.9).

The initial pH of reaction R7, R11 and R12 are very close to, but slightly higher than that of reaction R3 in which TMABr was added after the base. The initial crystallisation rates as drawn are between those of reaction R2 and R3, but this is not truly representative of the onset of crystallisation and frequent sampling between 8 and 15 h would be required to obtain information on the induction period/initial crystallisation. Hexanediol addition to the reaction mixture before the base, R7, gave pH readings between those of reactions R2 and R3. Reactions R11 and R12 gave pH readings below those of R2 and R3 with reaction R11 (organic added before the base) giving much lower readings. This trend is continued up to at least 170 h (Fig. 4.8). The crystallinities show slightly different trends to pH readings. Reaction R11 with the lowest pH reading moves up above Reaction R2 in the crystallinity order. The crystallisation curve for reaction R8 (pH data not recorded) is very similar to reaction R11, but R8 leads to a slightly more crystalline product. The lowest crystallinity is that recorded for R12. Thus the degree of crystallinity (up to 60 h) in increasing order is:

$$R12 < R3 \lesssim R2 \lesssim R7 < R11 < R8$$

The crystallisation growth of R7 overtakes R8 and R11 at ~90 h and ultimately produces the most crystalline product at 576 h. Fig. 4.10 shows a comparison of the degree of crystallinities followed for longer periods. Growth of reactions R11 and R8 continue to produce highly crystalline materials at ~220 h and ~300 h respectively.

The overall crystallinity and pH rise recorded, in decreasing order, are:

pH	XRD	Order of Mixing Reactants
R7	R7	1Diol 2TMA added before base
	~R8	1Diol 2TMA added after base
	R11	2Diol 1TMA added before base
R2	R2	3TMA added before base
R3	~R3	3TMA added after base
R12	R12	2Diol 1TMA added after base
R11		2Diol 1TMA added before base

Effect of Partial Replacement of TMABr by Hexanediol

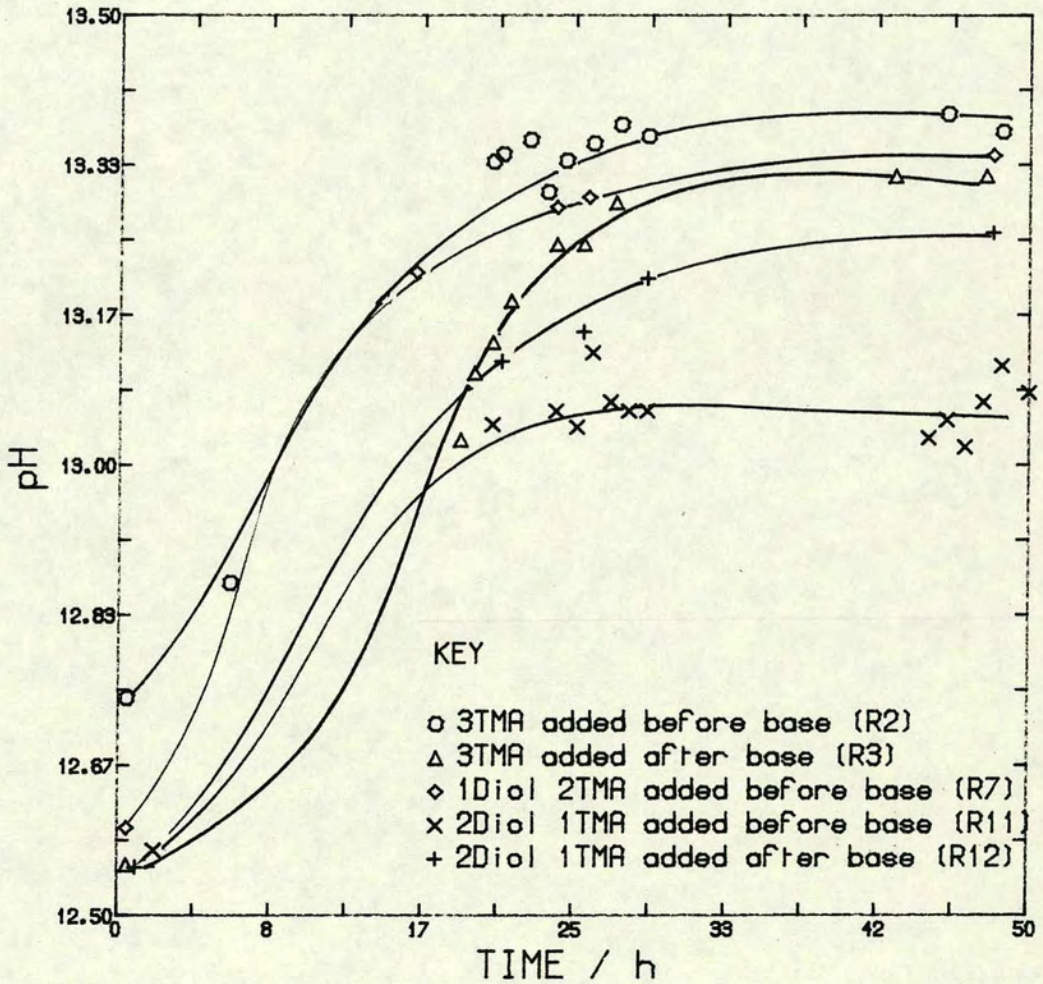

Fig. 4.7

Effect of Partial Replacement of TMABr by Hexanediol

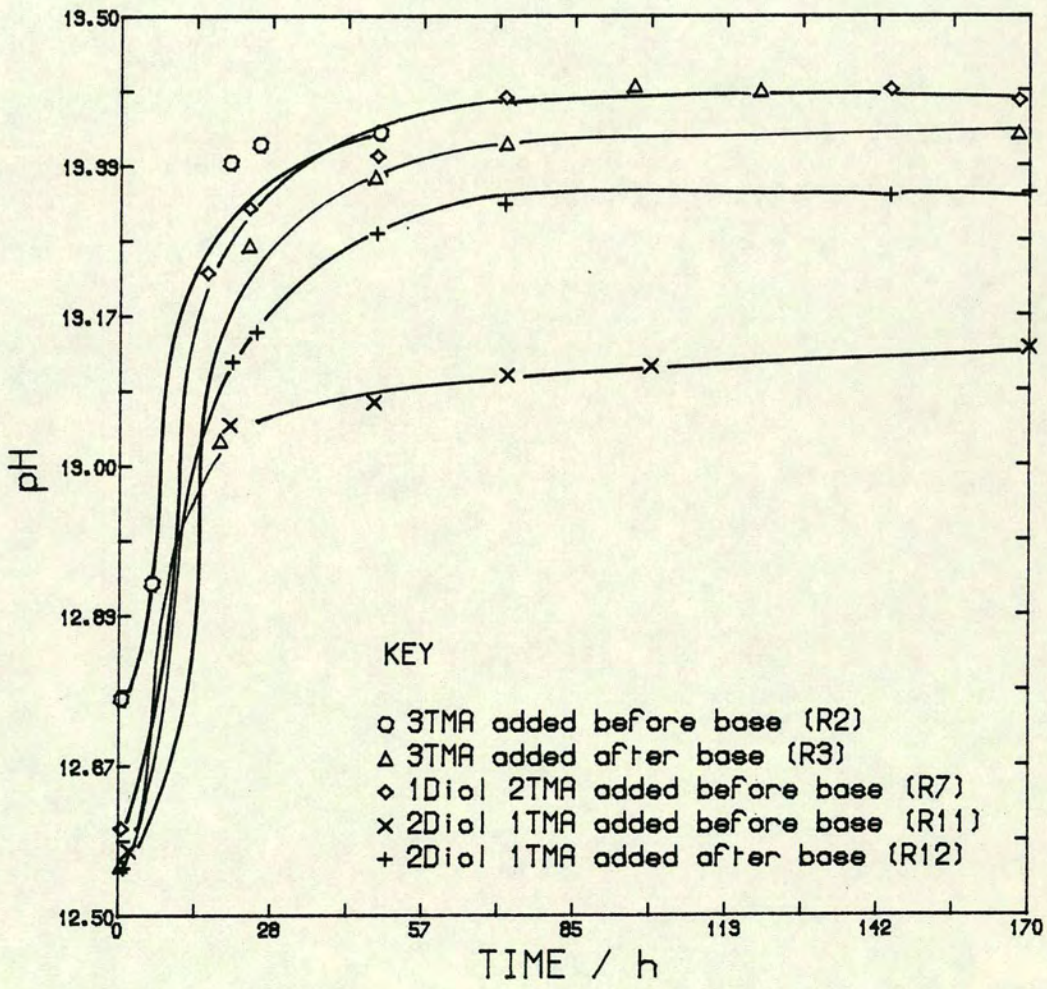

Fig. 4.8

Effect of Partial Replacement of TMABr by Hexanediol

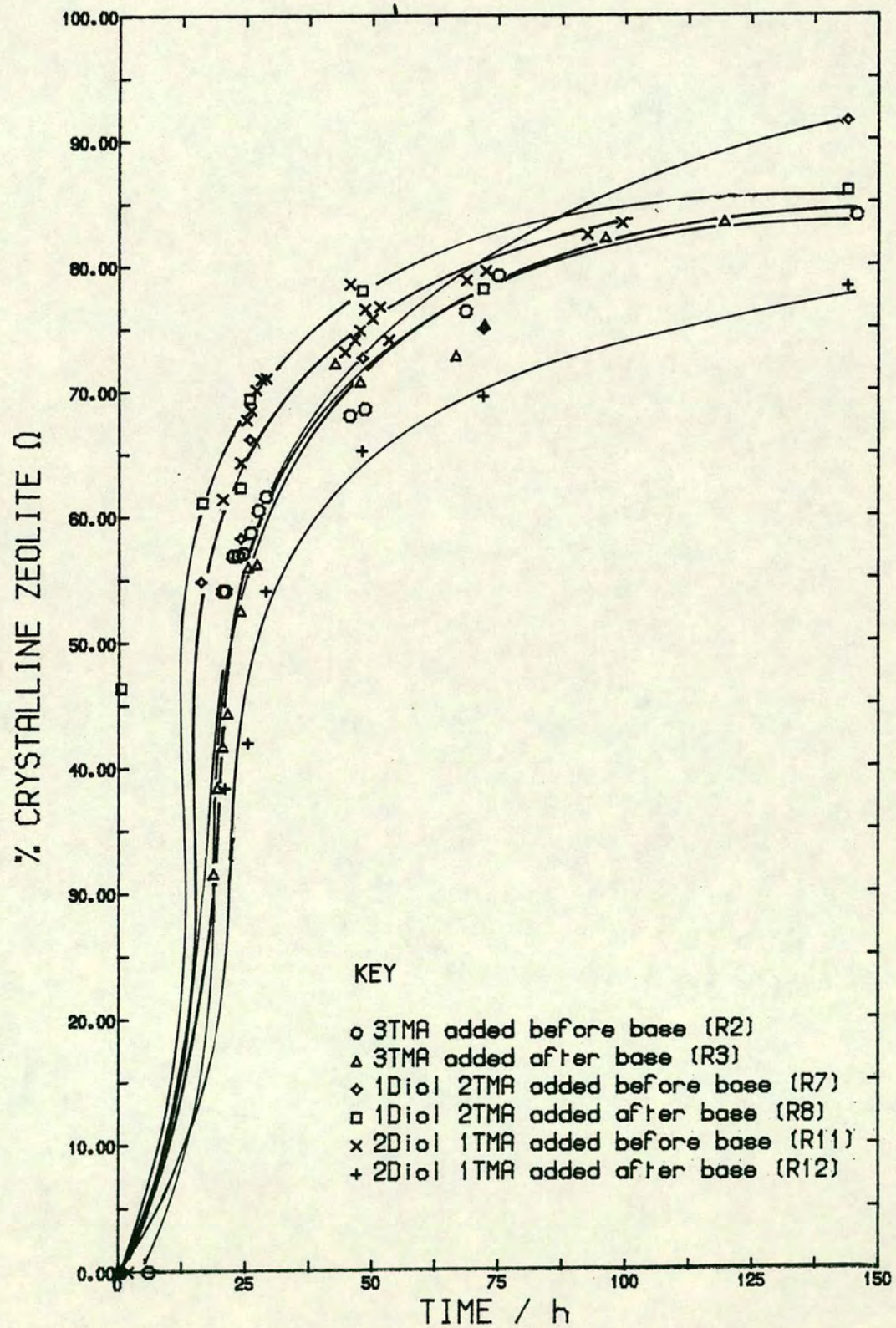

Fig. 4.9

Effect of Partial Replacement of TMABr by Hexanediol

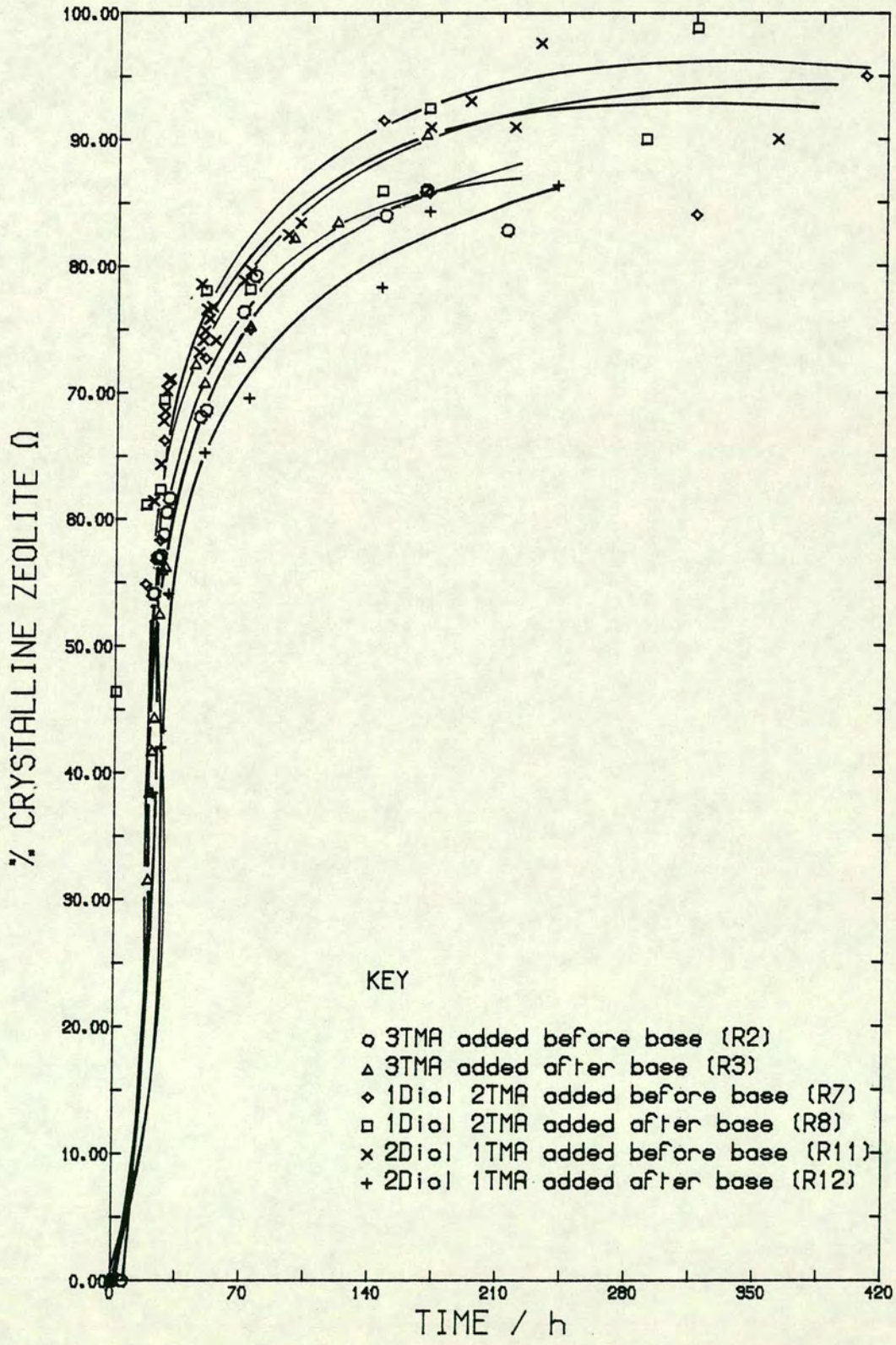

Fig. 4.10

Thus replacement of 1TMABr by hexanediol in this reaction composition produced a much improved crystalline sample of Ω under the normal crystallisation period of 144 h. Addition of the organic before the base gave the most crystalline product.

4.3.4.2 Effect of Hexanediol Concentration

Increase in the concentration of hexanediol in the reaction composition showed a substantial decrease in the gel pH_t throughout the crystallisation of the reaction (Fig. 4.11). The lowest pH readings were obtained with addition of 2 moles hexanediol before addition of the base. The pH rise recorded in decreasing order is:

R7 - 2TMA 1Diol added before base

R12 - 1TMA 2Diol added after base

R11 - 1TMA 2Diol added before base

The pH curves (Fig. 4.11) for reactions R7, R11 and R12 show that the gel pH is virtually constant after 72 h which is indicative of the completion of the reaction. However, the crystallisation curves (Fig. 4.12) show that the crystallinity continues to rise steadily but slowly after 72 h, by approximately 10%, except for reaction R8 which depicts an increase in the degree of crystallinity at a later time.

The crystallisation rates for reactions R7, R8 and R11 are virtually equal for the first 30 h with reaction R12 proceeding more slowly and producing a less crystalline material than the other reactions. After 30 h the crystallisation rates are much slower for all reactions.

Effect of Concentration of Hexanediol

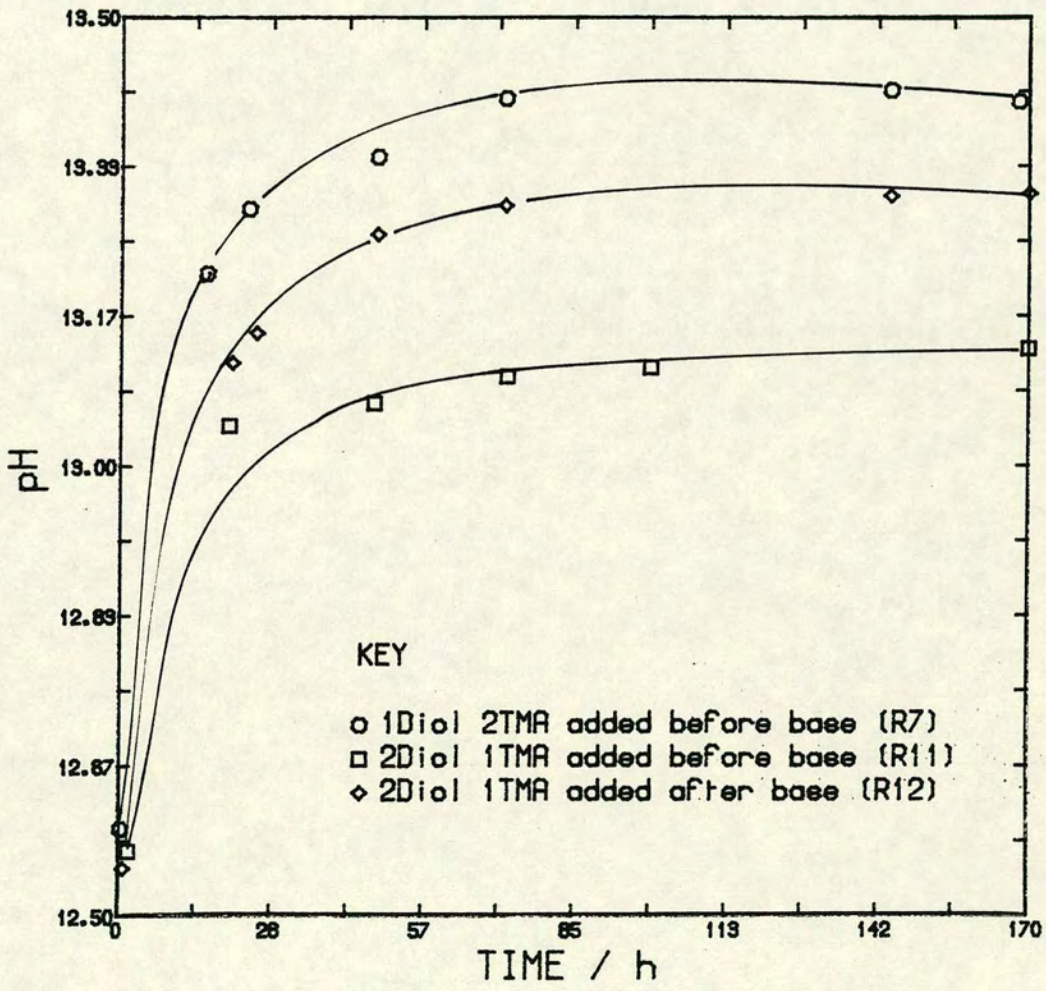

Fig. 4.11

Effect of Concentration of Hexanediol and Order of Mixing

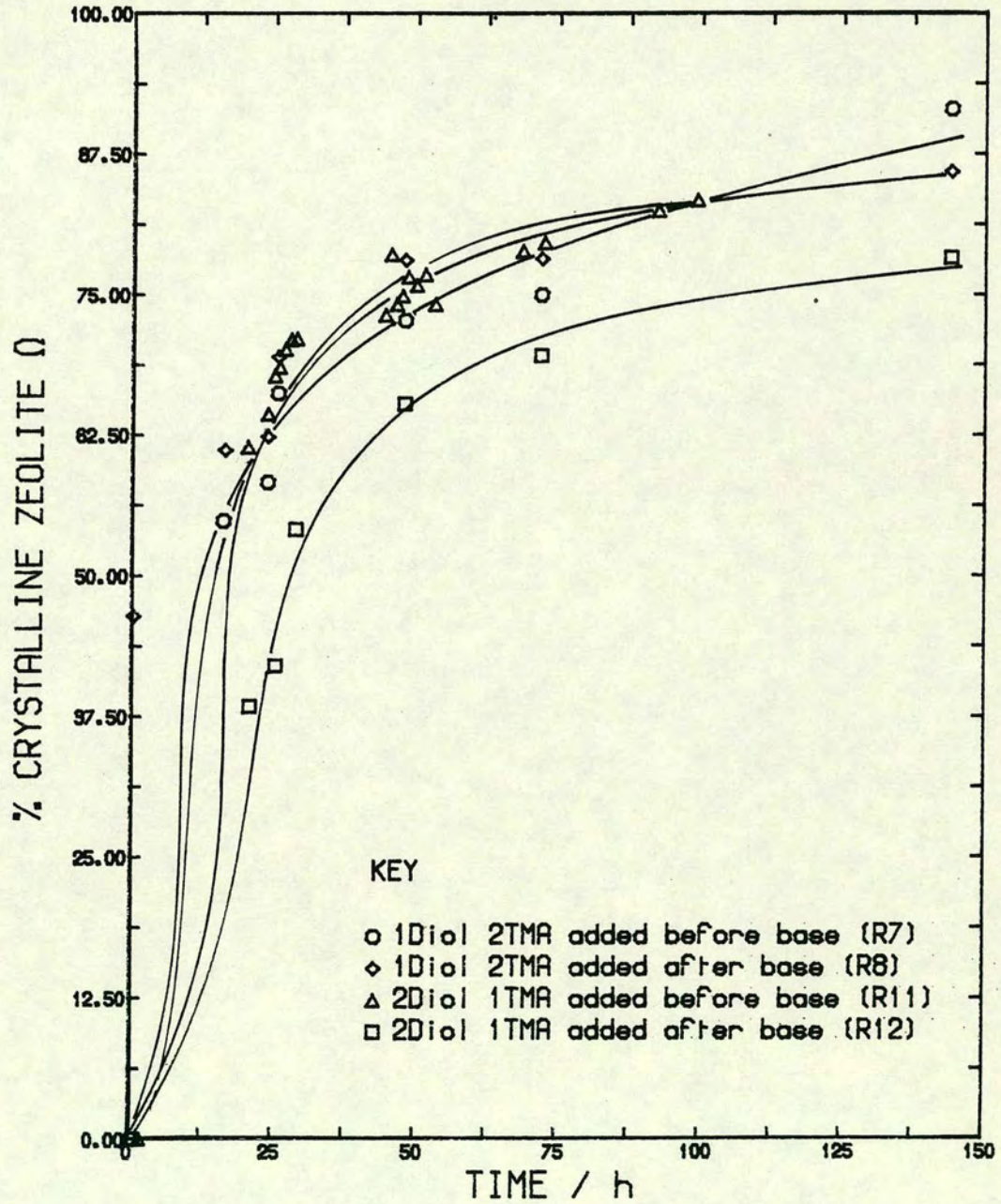

Fig. 4.12

The observed degree of crystallinity and pH rise, in decreasing order is:

R7 >R11 ~R8 >R12 % crystallinity

R7 >R12 >R11 pH measurements

i.e. the addition of 1 mole hexanediol to the system before the base increased the crystallinity of the zeolite, whereas 2 moles of hexanediol added to the system after the base significantly retarded the reaction and reduced the ultimate % crystallinity. The crystallinity observed by the addition of 1 mole hexanediol after the base is virtually equivalent to 2 moles added before the base.

4.3.5 Effect of Mixing Temperature

The standard method of preparation of the zeolite Ω reaction mixture is by mixing the reactants with the silica (Cab-O-Sil) in the following order:

water, TMABr (aq) and finally NaOH/$Al(OH)_3$ (aq)

The latter solution is prepared by dissolution of the alumina in hot sodium hydroxide solution; this solution requires considerable time to cool naturally to room temperature and so is usually added warm.

This procedure has been shown to lower the pH of the initial gel, the overall crystallisation rate, and the crystallinity of the product, compared with a preparation in which solutions are mixed at room temperature. The gel prepared from solutions mixed at room temperature is usually very viscous; much difficulty is experienced in the mixing of the final gel to a homogeneous paste before initiation of the reaction at 95°C. Samples from this reaction after 0.5 h at 95°C produced milky gels which when cooled form stiff solid gels.

Consequently, since the reaction is carried out at 95°C, it was considered that if the solutions were brought to the temperature of 95°C, quickly

mixed in the normal order, and rapidly mounted in the thermostated bath at 95°C, then the difficulty experienced in stirring the thick, stiff gel to homogenity would be overcome; a homogeneous gel would result and also perhaps a different type of product.

The standard composition for reaction R5 was prepared thus: the water, TMABr (aq) and $NaOH/Al(OH)_3$ (aq) were brought to the temperature of 95°C and mixed with the silica, in that order. A soft paste resulted when the alkali was mixed with the silica, which on addition of the water gave a thin clear solution with no change on addition of TMABr (aq). (This will be designated the hot reaction.) Comparison was made with reaction R4 (designated the cold reaction). The latter was prepared with solutions mixed at room temperature and produced the viscous gel.

4.3.5.1 Comparison of 'Hot' and 'Cold' Reactions

The pH of the samples from the hot reaction clearly indicated a change in the mechanism of the reaction. Fig. 4.13 shows the pH is considerably lowered in the hot reaction, to an initial pH of 12.11 and after 145 h is only 12.40; whereas the initial pH of the cold reaction, 12.48, is not even attained after 145 h. The pH readings of the hot reaction lie on a straight line unlike the typical s-shaped curve.

XRD analysis showed a consequence of the lower pH. The initial product was sodalite rather than zeolite Ω and only after 72 h was Ω formed in admixture with sodalite. The crystallisation of these two products, from the hot reaction, compared with that of the cold reaction, is illustrated in Fig. 4.14. Sodalite crystallisation occurs almost immediately and grows steadily with the s-shaped curve, whereas Ω growth does not commence until after 25 h; in the cold reaction 45% Ω is present at this time. At 74 h, 25% Ω has crystallised compared

Effect of Mixing Temperature

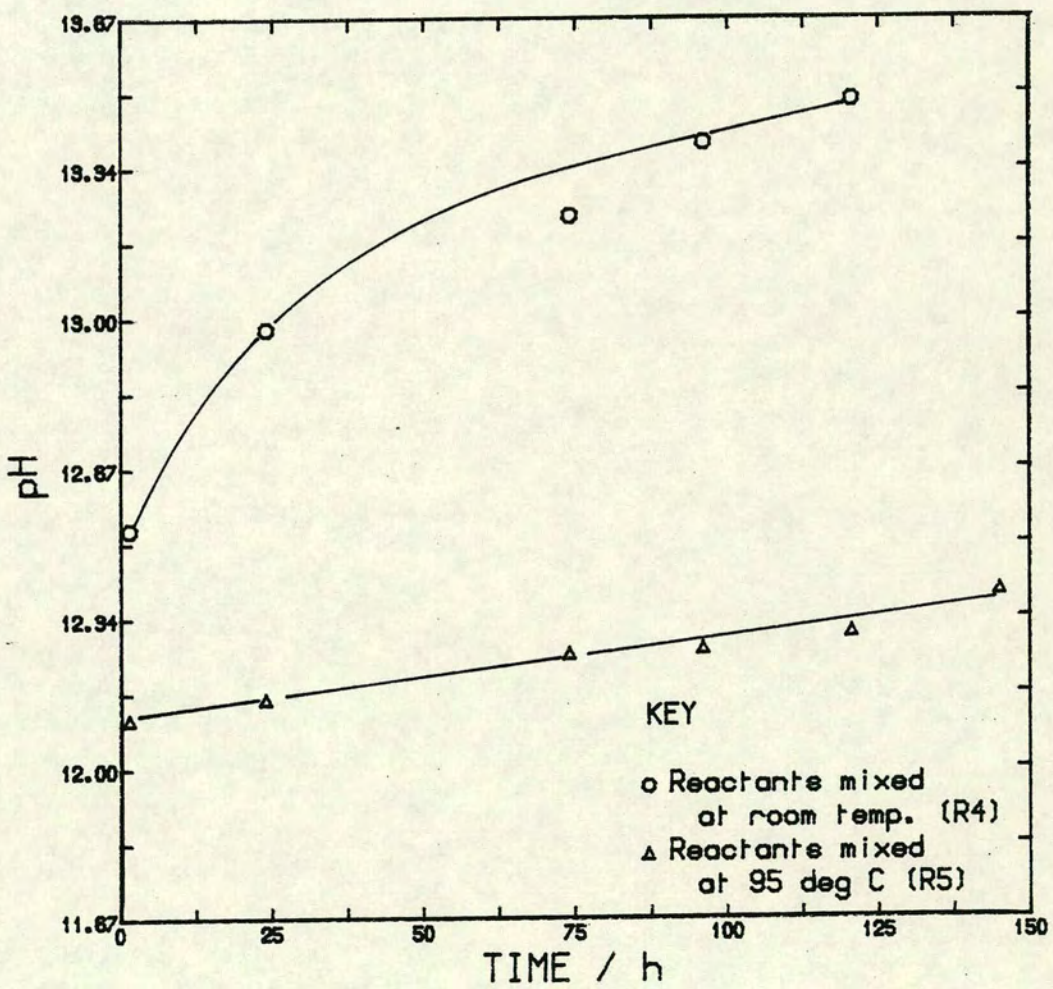

Fig.4.13

Effect of Mixing Temperature

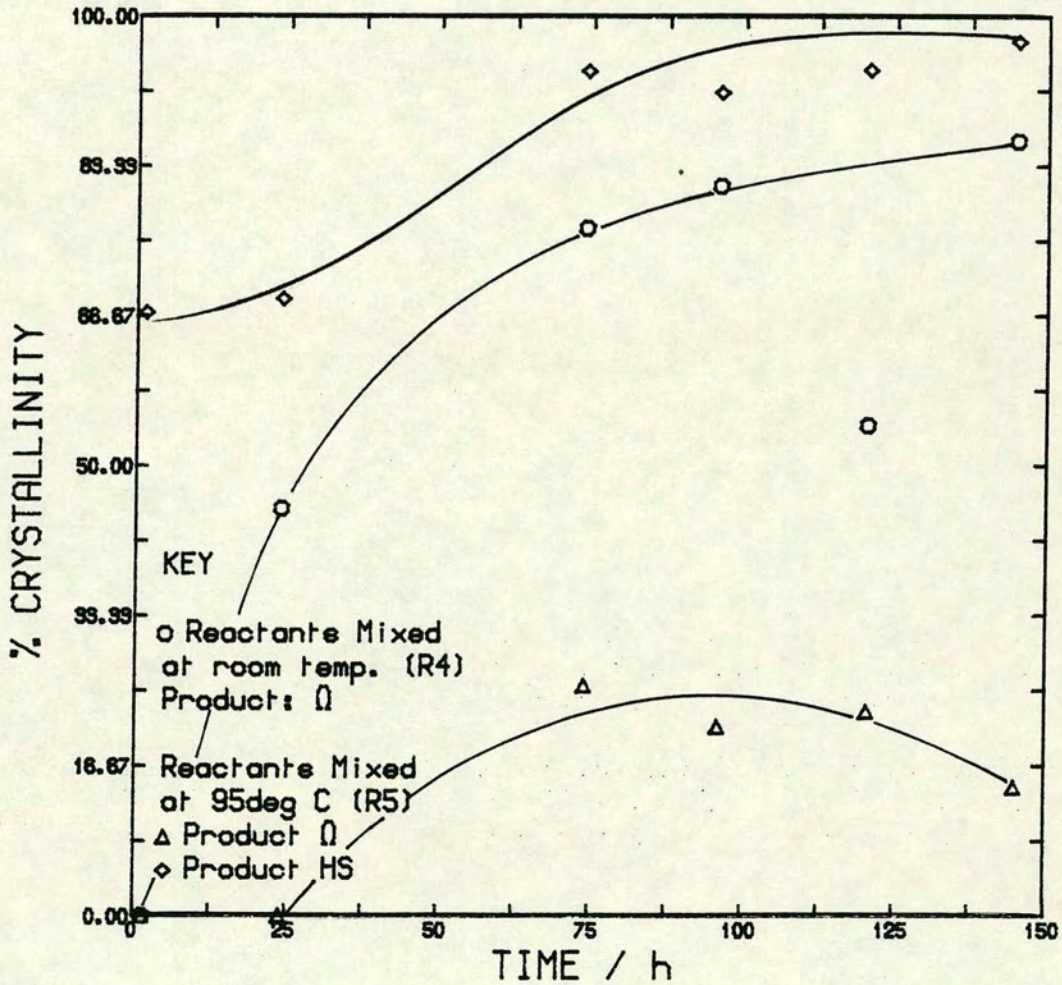

Fig. 4.14

with 76% in the cold reaction. However this 25% crystalline Ω is gradually diminished to 17% at 145 h as the sodalite growth is continued at the expense of the Ω .

4.3.5.2 Reactions R6, R13 and R14

Reaction R6 is a variation of the hot reaction in which the standard composition was mixed in the usual manner except that only the alkali was added at 95°C. Reactions in which 1 mole hexanediol and 2 moles hexanediol replaced the TMABr i.e. R13 and R14 were prepared by the mixing of all the solutions at 95°C with the silica. Reaction R6 gave a thin clear gelatinous solution, reaction R13 gave a thin turbid solution and reaction R14 produced a thin paste.

The crystallisation of reaction R6, monitored by XRD (Fig. 4.15) shows the steady growth of the sodalite phase which is less rapid after 100 h. The crystallisation of Ω suddenly appears between 24 h and 40 h, rises slightly, then falls as the sodalite continues to grow. Ω growth virtually ceases after 80 h. However the sodalite phase continues to rise appearing to inhibit further Ω crystallisation.

The crystallisation curves for reaction R14 are illustrated in Fig. 4.16. Sodalite growth commences almost immediately. The initial amount formed is greater than in R6 (19% c.f 10% in R6); however growth is somewhat inhibited for 80 h, then rises sharply to 26% at 88 h, 68% at 92 h and 93% at 96 h. Meanwhile Ω crystallisation commences simultaneously with the sudden surge of sodalite crystallisation. During the crystallisation a notable decrease in the amount of sodalite, up to 200 h, and then a sharp rapid rise is observed. Thus Ω once formed tries to grow at the expense of the sodalite, however little crystallises. The DTA of the final products in reactions R6, R13 and R14 are indicative of the presence of TMA-sodalite. Hydroxysodalite may also be present

"Hot" Reaction R6

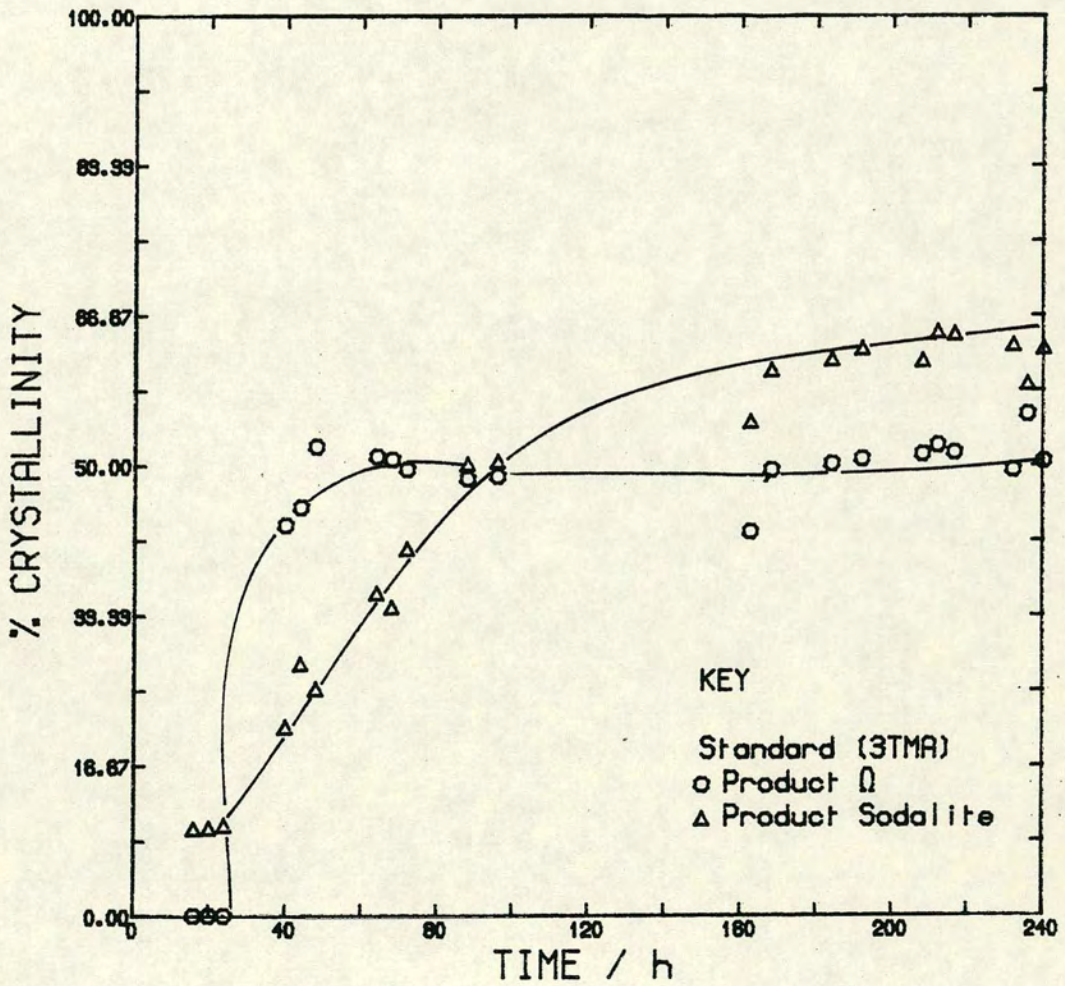

Fig. 4.15

"Hot" Reaction R14

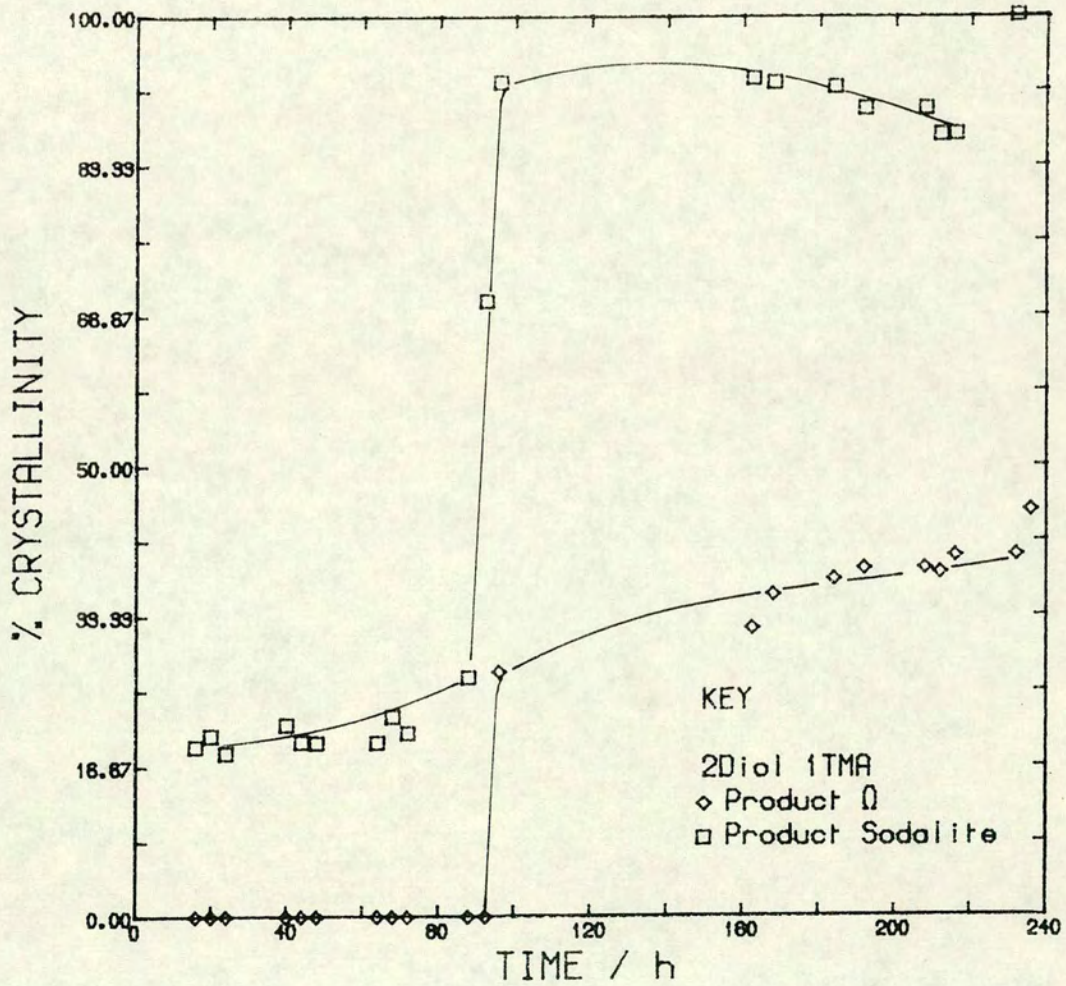

Fig.4.16

but from XRD it is difficult to distinguish between the two types and for simplicity it is all regarded as sodalite.

The crystallisation of reactions R6 and R14 monitored by pH measurements is shown in Fig. 4.17. It appears that some of the experimental points may be in error. The sudden appearance of Ω in R6 after 40 h (Fig. 4.18) corresponds to the enormous increase in pH; the presence of Ω, however, is not detected in R14 until 92 h and yet a similar pH increase at 40 h is observed. The rise in the latter could be due to formation of TMA-sodalite or an error in the experimental point. The pH increase at ~ 160 h for reaction R14 probably corresponds to the growth of Ω. However since the pH measurements are representative of the crystallisation of 3 phases, namely Ω, hydroxysodalite and TMA-sodalite, interpretation is somewhat limited as high pH readings may be due to Ω and TMA-sodalite.

Comparison of reaction R6 with R14 (Fig. 4.18) shows an increased induction period for the crystallisation of Ω in R14 (92 h) compared with R6 (between 24 h and 40 h). This could be due to three factors:

(a) The temperature of R6 is less than 95°C on mixing as the water and TMABr (aq) were added at room temperature and lower temperature of mixing favours growth of zeolite Ω.

(b) Less TMABr is present in R14 and so Ω crystallisation is more difficult as TMA is required as a template for growth.

(c) TMA may be used for TMA-sodalite growth and thus the reason for the low yield of Ω.

A surge in the percentage of sodalite in R14 which may be TMA-sodalite and hydroxysodalite, but is probably the latter, is accompanied by the sudden Ω growth. The Ω growth increases steadily at approximately the same rate as the corresponding decrease in sodalite phase.

Comparison of pH values of Reactions Mixed at 95deg C

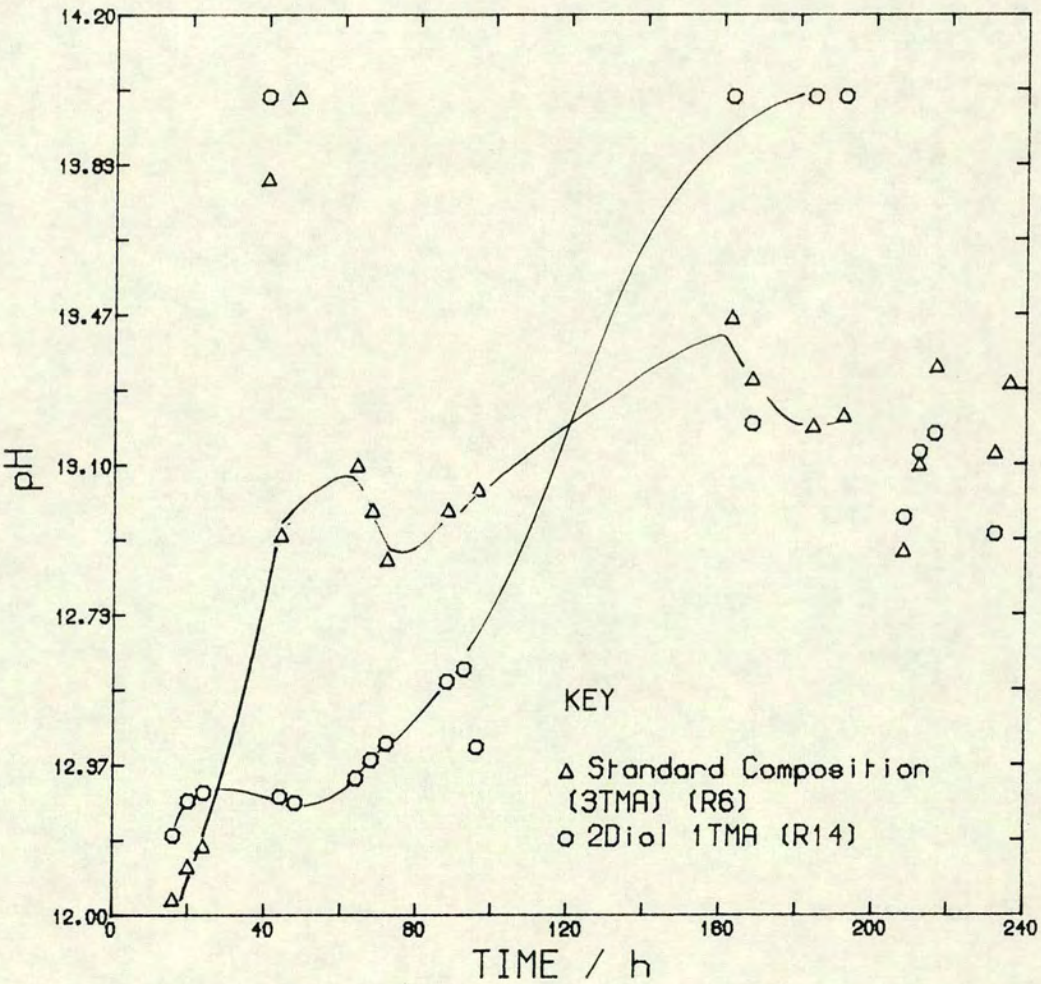

Fig. 4.17

Comparison of Crystallisation Curves of Products from Reactants Mixed at 95 deg C

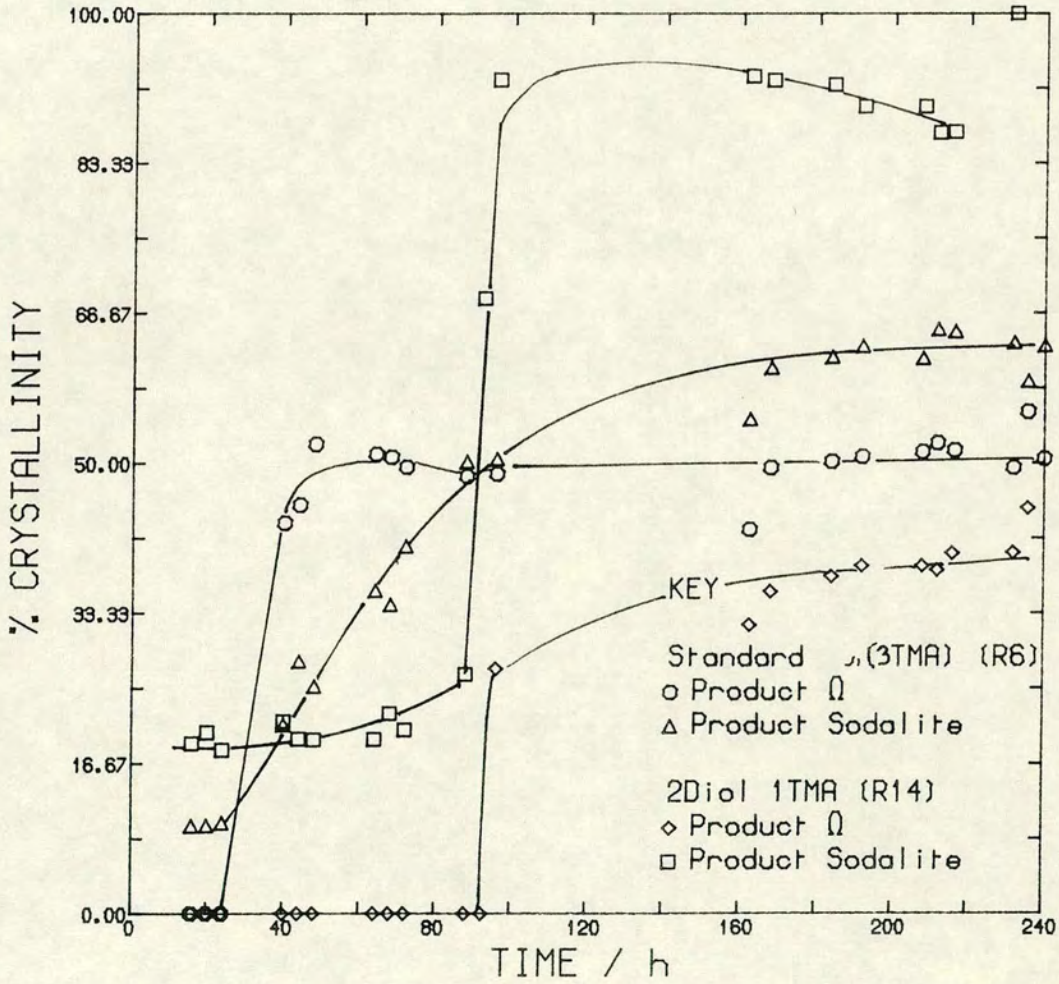

Fig 4.18

Perhaps the mechanism proceeds via the fragmentation of the TMA-sodalite to cage units which are converted to gmelinite cages by rotation of the middle through 60°. The gmelinite cages in which TMA is encapsulated provide the necessary building blocks for the Ω framework and thus the rate of disappearance of the sodalite phase corresponds to the rate of increase in the Ω phase. Alternatively a simple dissolution of the sodalite phase may occur and the Ω thus has further nutrient and grows at the rate of dissolution. Or perhaps the TMA-sodalite fragments to sodalite cage units which unite with the columns of gmelinite cages in the Ω framework and growth continues in this manner with the introduction of stacking faults into the Ω structure. According to Kokotailo et al [6] stacking faults may be introduced into the Ω framework by rotation of the middle of the gmelinite cage through 60° to produce a sodalite cage, and thus the 12 ring channel of Ω is blocked. Since TMA-sodalite is present in the reaction mixture, a dynamic equilibrium of TMA-sodalite formation and dissolution into its cages may be set up. At any particular time, the TMA-sodalite may fragment and the sodalite cage units can simply build onto the columns of gmelinite cages in the Ω framework and produce the faulted Ω structure. This may be the mechanism since reaction R6 continued to 672 h showed a gradual increase in the percentage of crystalline Ω with a corresponding gradual decrease in the amount of sodalite.

Thus, mixing of the reactant solutions at 95°C not only changes the gel to a liquid, but it also significantly changes the reaction mechanism such that it proceeds via sodalite/TMA-sodalite and initially inhibits Ω growth. Overall the sodalite phase is favoured under these conditions. This may be partly illustrative of Ostwald's law of successive transformations, however, whether sodalite is transformed to Ω or growth of the two species occurs simultaneously requires further investigation.

4.3.6 Proposed Explanation for the Synthesis of Faulted Ω

Irrespective of the reaction composition, the method of preparation and especially the temperature at which the reactants are mixed determines the product formed. Sodalite crystallisation is favoured from this 'Ω composition' when the reactants are mixed at higher temperatures. According to Kokotailo, sodalite cages, produced by the rotation of the gmelinite cages through 60°, in the Ω framework lead to stacking faults. This therefore suggests an alternative mechanism for the introduction of stacking faults.

Consider the reaction composition studied:

$$6Na_2O \quad Al_2O_3 \quad 15SiO_2 \quad 300H_2O \quad (3-x)TMABr \; xHO(CH_2)_6OH$$

at x = 0, when mixed at room temperature $\longrightarrow$ pure Ω

at x = 0, when mixed at 95°C $\longrightarrow$ HS + TMA-sodalite (?) + Ω

at x = 0, when alkali mixed at 95°C with water and TMABr (aq) at room temperature $\longrightarrow$ HS + TMA-sodalite (?) + Ω (more)

Thus between room temperature and 95°C there exists a temperature such that the TMA-sodalite crystallises first and Ω forms later, but because Ω is thermodynamically favoured, the sodalite framework must:

(1) dissolve into smaller units, i.e. sodalite cages and then 4 and 6 rings

(2) convert to gmelinite cages and stack onto the gmelinite columns of Ω

(3) dissolve into smaller units, i.e. sodalite cages and stack onto the gmelinite columns

Energy consideration would probably place them in order: (3), (2), and (1). From other experiments, it is known that sodalite may be converted to gmelinite, and gmelinite may be converted to TMA-sodalite [7]. If (3) is favoured, the sodalite framework would break down into sodalite

cages and then unite with the Ω framework. A few layers of sodalite cages would result in the faulted Ω structure as discussed in Chapter Two.

In Mobil's synthesis of Ω from TMA [8], a crystallisation directing agent (CDA) was employed in which the sodium aluminate, sodium silicate and water were mixed at 60°C and produced a clear solution. The reactants were heated at 100°C for 0.5 h before mixing with TMA. The exact details are given in Chapter Two. In the light of the present experiments, it seems highly probable that the CDA technique introduces the sodalite species during crystallisation. Furthermore by the mechanism proposed above it will give rise to stacking faults in Ω .

In Union Carbide's preparation of Ω [4], the more or less standard hydrogel technique, in which reactants are mixed at (presumably) room temperature, was employed. Thus Union Carbide's preparation may be fault free. Similarly, Ω synthesised from cold solutions, which eliminate the sodalite phases, may result in fault free Ω. Perhaps an improved route would be to mix the solutions at extremely low temperatures e.g. 5°C and thus certainly avoid the formation of a sodalite phase. Naturally sorption or transmission electron microscopy or HREM would be required to test the products.

4.3.7 The Gel, pH and Crystallisation Rates

These results suggest that the nature of the gel governs the pH, the mechanism, crystallisation products and rates for a given reaction composition. An increase in the temperature at which the reactants are mixed changes the gel from a thick paste to a clear thin liquid. The order of mixing of the reactants and partial substitution of TMABr for hexanediol alters the nature of the gel. From pH measurements alone,

it is difficult to determine the mechanism, but it is obvious that the species in the solid and solution phases are changed. The silica used, Cab-O-Sil M5, is a thickening agent and its surface chemistry [9] may assist in the development of a feasible explanation.

Cab-O-Sil consists of branched 3-dimensional chain like aggregates and during its preparation it acquires hydroxyl groups attached to some of the silicon atoms on the particle surface. This gives it hydrophilic and hydrogen bonding properties. In the presence of water hydrogen bonding occurs between Cab-O-Sil hydroxyls and the solvent molecules. This results in partial or total solvation of the Cab-O-Sil aggregates and so reduces or completely eliminates its chain formation.

Consider the hot reactions: R5, R6, R12 and R14. Addition of hot solutions to the silica gave clear solutions (R5) to thin pastes (R14). Initially substantial hydrogen bonding occurred with the surface hydroxyl groups of the Cab-O-Sil which probably resulted in complete solvation of the Cab-O-Sil aggregates. However the degree of dispersion was carried too far, causing a reduction in the final viscosity i.e. the Cab-O-Sil network was broken into extremely small pieces and widely scattered. The simplest units to form are 4 and 6 membered rings, these link together to produce sodalite cages which unite to form the sodalite framework. Since only the simplest ring structures are present in the 'gel', there are no competing species present and so crystallisation is rapid. During the course of the reaction, the TMA may adsorb on the surface of the sodalite cages and SiO_4 and AlO_4^- networks form around it giving rise to the TMA-sodalite and gmelinite cages necessary for Ω formation.

The order of mixing of the reactants is mainly important as regards the degree of hydrogen bond formation. Excessive hydrogen bonding causes breakdown of the silica network and the extent of this is reflected in

the initial pH values and rate of crystallisation.

There is no doubt that for a given composition the way in which the gel is prepared determines the course of the reaction and the products formed; it is thus critical to zeolite Ω synthesis in particular and indeed to zeolite synthesis in general.

4.3.8 The Crystallisation of Selected Reactions examined by XRD, pH and Thermal Analysis

The crystallisation of 3 reactions which gave pure Ω were monitored by XRD, pH and DTA. The chosen reactions were the standard preparation - reaction R1, a reaction in which one mole of TMABr was replaced by hexanediol - reaction R9, and a reaction in which 2 moles of TMABr were replaced by hexanediol - reaction R10.

4.3.8.1 The Standard Preparation - Reaction R1

The nature of the gel has already been discussed for this reaction. The crystallisation curves in Fig. 4.19 show a steady rise in pH which attains its maximum after 72 h, indicative of completion of the crystallisation. However the % crystallinity shows a slight increase after 72 h. The decrease in pH and % crystallinity at 77 h is reflected in a change in TG and DTA type.

The crystallisation of reaction R1 as monitored by DTA and TG (Figs. 4.20, 4.21 and Tables 4.3a, 4.3b, 4.3c) show some interesting changes. The crystallinity, as evidenced by XRD, of the first sample taken at 5.16 h is debatable. It is very slightly crystalline and the few peaks present in the XRD pattern were identified as Ω , but the pattern was incomplete. The DTA of this sample shows a double endotherm around 100°C, a broad endotherm from 154°C to 225°C and a very small exotherm centred at 347°C. According to Cole and Kouwenhoven [10], the exotherm at this temperature

Comparison of pH values and Crystallinity for Reaction R1

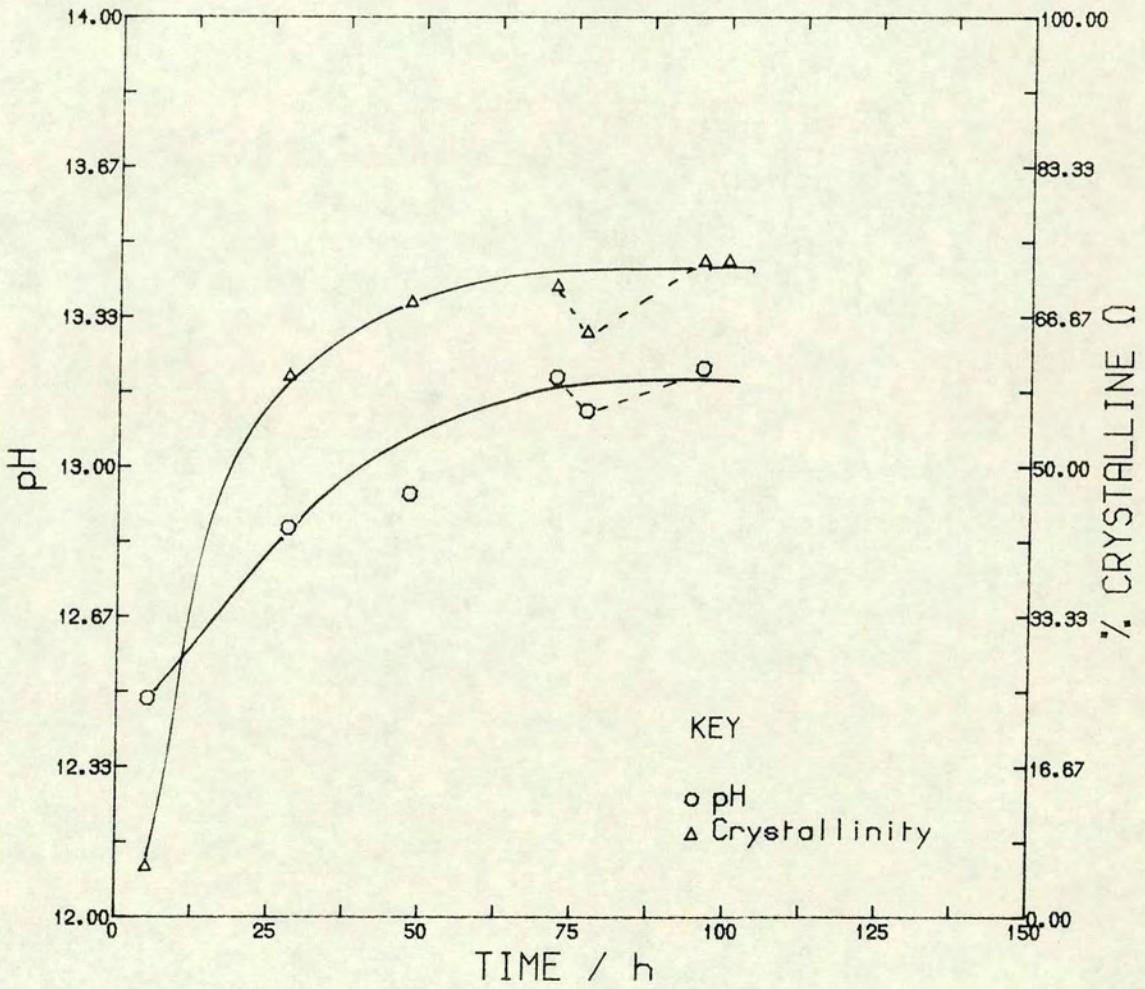

Fig. 4.19

Crystallisation of Reaction R1
monitored by DTA

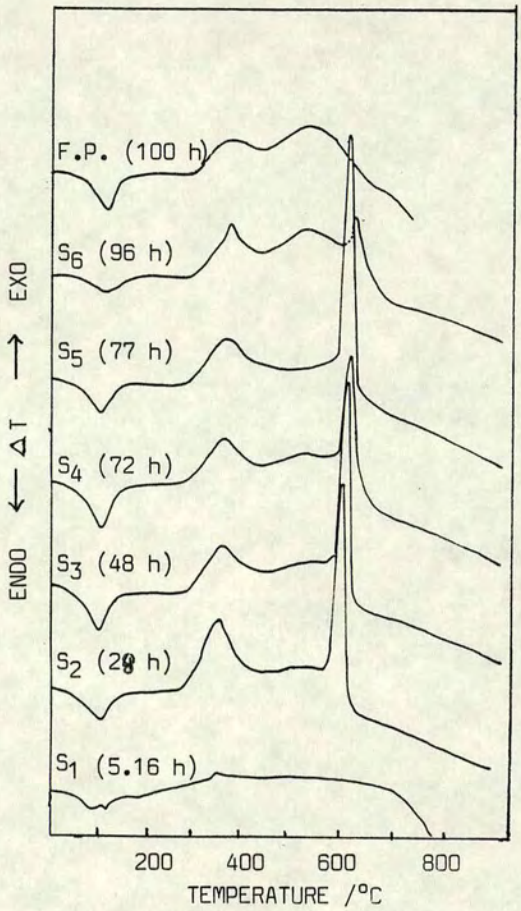

Fig. 4.20

Crystallisation of Reaction R1
monitored by TG

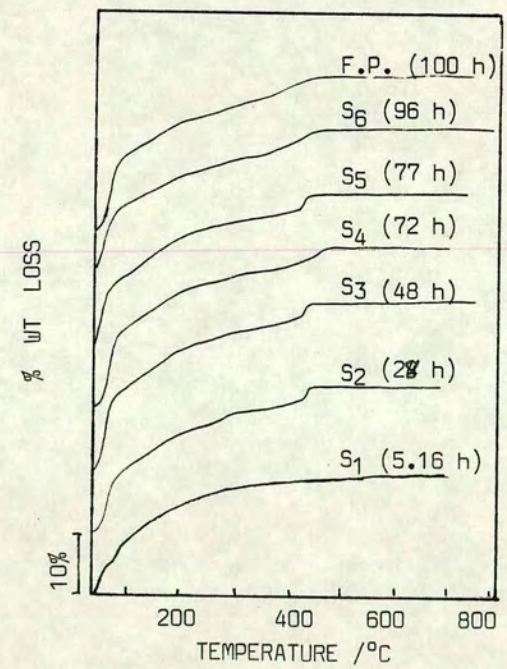

Fig. 4.21

is caused by the oxidative degradation of TMA in the 12 ring channel of Ω. (However, in the next chapter, it is identified as TMA adsorbed on the external surface of Ω and the site which corresponds to TMA in the main channel occurs at higher temperature.) The TG curve of sample S_1 shows two types of weight loss which correspond to the double endotherm at ~100°C. This is due to evolution of water from the main channel and loosely bound water adsorbed on the external surface. The gradual weight loss (154°C to 225°C) which corresponds to the broad endotherm is due to water from the intracrystalline channels. From the DTA, the small sharp exotherm centred at 347°C, which extends from 225°C to 363°C shows a corresponding weight loss of 3.3% from the TG curve albeit very gradual. At 697°C, the TG detects a slight change in gradient. The weight loss between the end of the small exotherm and change in the TG gradient is 2.4%. Comparison with the other TG curves suggest that the increase in rate of weight loss at 697°C is associated with TMA burning out of the gmelinite cages from the micro-crystalline structure. After 697°C no further weight change is recorded, and the DTA shows endothermic collapse. Thus although the sample is just detectable as crystalline, though not completely discernible as Ω , the DTA and TG provide evidence for the initial structure formation which is typical of Ω .

At 28 h (S_2) a characteristic pattern of Ω which corresponds to 60% crystallinity is formed. The DTA shows a single sharp endotherm at 102°C and a broad endotherm from 154°C to 272°C, which are attributed to loss of water; a large broad exotherm from 272°C to 450°C centred at 353°C, a small broad exotherm centred at 532°C and then a sharp exotherm centred at 610°C. The TG curve depicts a sharp weight loss up to 154°C and then a change in the rate of weight loss is observed; a sudden increase at about 340°C which corresponds to the exotherm centred at 352°C and then a gradual weight loss up to about 600°C. Finally there

is a sharp weight loss due to TMA burning out of the gmelinite cages. After complete removal of the TMA, the DTA shows gradual endothermic collapse of the structure.

After 48 h (S_3) the DTA shows a larger endotherm centred at 97°C and a much smaller exotherm centred at 360°C. This corresponds to the weight losses recorded in TG analysis; it illustrates that the decrease in the TMA adsorbed on the external surface results in that area being used to adsorb water, thus giving rise to a higher water content. The DTA curve also shows a broad endotherm from 143°C to 277°C; the associated weight loss, 5.5% (Table 4.3b) shows an increase in intracrystalline water compared with 4.4% in S_2.

The DTA curves of S_4 and S_3 are similar, but the exotherm at 359°C is smaller in S_4 than in S_3 and correspondingly an increase in the loosely bound water endotherm at 98°C is observed (Table 4.3b).

At 77 h, S_5 shows a decrease in pH and XRD crystallinity curves (Fig. 4.19) and is associated with a change in thermal behaviour. The major difference is the absence of an exotherm around 520°C immediately before the sharp exotherm at 613°C. The 352°C exotherm has a slight shoulder at 448°C, which is comparable to the weight loss for the similar process in S_4. The endotherm at 93°C is smaller than that recorded for S_3 and S_4 with a corresponding decrease in the weight loss; the broad endotherm (132°C to 285°C) has an increased intracrystalline water content.

At 96 h, S_6, a remarkable change in the DTA curve is detected. The endotherm is significantly reduced (however an increase is suggested from the TG weight loss curve), a much sharper exotherm at 365°C is observed, suggestive of increased localisation of TMA, and the peak at 517°C is enhanced with an increased weight loss of 3.1% compared

Table 4.3a

Crystallisation of Reaction R1

Thermal Analysis, Crystallinity and pH Data

TIME/h	pH	CRYSTALLINITY /%	EXO PEAK TEMP/°C	EXO PEAK RANGE/°C	WT LOSS /%	EXO PEAK TEMP/°C	EXO PEAK RANGE/°C	WT LOSS /%	EXO PEAK TEMP/°C	EXO PEAK RANGE/°C	WT LOSS /%	ADDITIONAL WT LOSS BETWEEN EXOS
5.16	12.485	5.7*	347	225-363	3.3	Broad	363-697**	2.4	-	697***	0.6	
28.0	12.865	60.2	352	272-450	3.8	532	487-565	0.8	610	565-627	3.3	0.4
48.0	12.940	68.4	360	277-432	2.6	530	465-547	1.0	612	547-632	3.9	0.4
72.0	13.200	70.3	359	283-415	2.1	517	457-555	1.3	615	555-645	3.1	0.4
77.0	13.125	65.1	352	285-417	2.3	448 (S)	417-466	0.4	613	567-656	3.3	1.4
96.0	13.220	73.0	365	287-417	2.3	517	447-597	3.1	617	597-662	1.8	0.4
100	-	73.0	355	268-428	2.9	545	428-647	4.5	676	647-940	0.8	

(S) = Shoulder

* Very slight trace of crystallinity, but Ω pattern is incomplete

** TEMP from TG curve

*** TG Curve records weight loss at this temp.

Table 4.3b

Reaction R1 Endotherms

TIME/h	ENDO PEAK TEMP/°C	ENDO PEAK RANGE/°C FROM RT TO	WT LOSS /%	ENDO PEAK (BROAD) RANGE /°C	WT LOSS /%
5.16	92 + 105	154	10.3	154-225	2.9
28.0	102	154	12.1	154-272	4.4
48.0	97	143	15.3	143-277	5.5
72.0	98	147	15.6	147-283	4.9
77.0	93	132	13.0	132-285	6.3
96.0	100	135	14.8	135-287	4.7
100.0	106	142	13.9	142-288	4.5

Sample at 5.16 h although 'X-ray amorphous' thermal analysis data suggestive of micro-crystalities.

RT = Room temperature

Table 4.3c

Reaction R1 Weight Loss

TIME/h	TOTAL WT LOSS DUE TO EXO PROCESS /%	TOTAL WT LOSS DUE TO ENDO PROCESS /%	OVERALL WT LOSS/%
5.16	6.3	13.1	19.4
28.0	7.8	16.5	24.3
48.0	7.9	20.8	28.6
72.0	6.9	20.5	27.4
77.0	7.3	19.3	26.5
96.0	7.5	19.5	27.0
100.0	8.1	18.4	26.5

with S_2, S_3 and S_4 which show weight losses of 0.8% to 1.3% at this site. The final exothermic peak at 617°C is much smaller and has a reduced associated weight loss of 1.8% compared with S_2 to S_5 which have weight losses between 3% and 4%.

The final product, 4 h later, at 100 h illustrates an even more remarkable change in the DTA curve. The endotherm due to loosely bound water is larger than for S_3, S_4 and S_5, and the intracrystalline water is reduced in S_3, S_4, S_5 and S_6. The exothermic processes are more interesting. The peak at 355°C which corresponds to surface TMA is larger than for S_3 to S_6 which thus accounts for the reduction of the loosely bound water. Furthermore, there is a much increased broader exotherm from 428°C to 647°C, centred at 545°C with an associated weight loss of 4.5%; the sharp exotherm is absent, but replaced with a slight broad exotherm shifted to the higher temperature of 676°C with a weight loss of only 0.8%. The DTA and TG residues from this sample were dark grey even though they were heated to temperatures >1000°C, indicative of organic material having much difficulty in burning out from the structure. The TG curve shows a continuous weight change >1000°C. Calcination of the final product in the furnace, in preparation for XRF analysis showed that regardless of temperature and length of time employed, the TMA could not be removed. Consequently XRF analysis could not be carried out on this sample as the organic material would have attacked the Pt/Au crucibles used for this technique. The DTA residue was glassy. It was not X-rayed as the diffractometer requires quite large samples compared with that used for DTA.

Table 4.3a shows that the first exothermic peak temperature fluctuates from 347°C to 365°C and the associated weight loss varies from 2.1% to 3.4%. The second exotherm, absent at 77 h, appears in the region of 517°C to 545°C, and is associated with a variation in weight loss.

The final exotherm centred in the region of 610°C to 617°C, except in the final product where it appears as a small broad exotherm shifted to the higher temperature of 676°C. Fig. 4.20 clearly shows the changes which occur during crystallisation. The initial surface TMA, in S_1, although recorded as 3.3% in the exothermic region of 225°C to 363°C only shows a very small peak, however it is broad, suggestive of wide distribution of TMA on the surface of the crystallites, although in some crystallites the TMA is bonded to the same degree and so a sharp peak at 347°C is observed. After 28 h, 60% crystalline Ω is formed with a large amount of surface TMA. This is perhaps suggestive of a mechanism which proceeds via the adsorption of TMA on the surface and acts as a template for the construction of the framework from SiO_4 and AlO_4^- units. It is noted that at 72 h the TMA at this site is reduced with a corresponding decrease in the crystallisation rate. At 100 h, the surface TMA is increased, but the crystallinity curve does not show a tendency towards increased crystallisation.

The second exotherm (~520°C) shows a gradual increase in size throughout crystallisation, except in S_5 from which it is absent and is associated with an increased TMA content from 0.8% at 24 h to 4.5% at 100 h.

The sharp exotherm at ~615°C shows a gradual decrease in the amount of TMA at this site, except for S_3 and S_5 in which it is somewhat enhanced. The decrease is from 3.3% at 28 h to 1.8% at 96 h and at 100 h is 0.8%. In the latter case the peak is also shifted to the higher temperature of 676°C.

Table 4.3c shows that during crystallisation, the amounts of loosely bound and intracrystalline water fluctuates. The total weight loss due to water varies and similarly that due to the exothermic processes varies. The major cause of this fluctuation is the variation in the amount of TMA that adsorbs on the external surface of the crystals. This is most

probably related to the crystal size and shape. SEM facilities were not available, but on the basis of texture, the crystals are probably spherulitic. Naturally, during crystallisation the crystals will increase in number and in size and consequently in surface area. A corresponding increase in the molecules/ions that adsorb on the external surface, i.e. water and TMA, is to be expected.

Thus the thermal analysis data shows a redistribution of TMA during the course of crystallisation, with the onset of the major changes occurring between 72 h and 77 h.

4.3.8.2 Reaction R10

The gel was prepared by mixing the reactants with the silica in the following order: water, hexanediol (aq), TMABr (aq), and finally warm aqueous base. A viscous gel resulted. It was allowed to crystallise for 72 h and produced a more crystalline product than reaction R1 which crystallised over a period of 100 h. In this reaction no crystalline material was detected by XRD at 24 h. According to XRD, zeolite Ω crystallised between 24 h and 40 h (Fig. 4.22). The induction period was much longer than in R1. The pH of the gel rose sharply up to 40 h and then gradually to 72 h. The crystallinity curve showed a gradual rise once crystallisation had commenced.

The crystallisation of reaction R10 as monitored by pH, XRD, DTA and TG (Figs. 4.22, 4.23, 4.24 and Tables 4.4a, 4.4b, 4.4c) shows some interesting features, particularly associated with TG and XRD.

The TG and DTA curves of S_1 (16.5 h) show that the amorphous sample has a sharp endotherm (90°C) due to loosely bound water, a broad endotherm (115°C to 152°C) which probably corresponds to intracrystalline water and a small but broad exotherm centred at 324°C with an associated

Table 4.4a

Crystallisation of Reaction R10

Thermal Analysis, Crystallinity and pH Data

TIME/h	pH	CRYSTALLINITY /%	EXO PEAK TEMP/°C	EXO PEAK RANGE/°C	WT LOSS /%	EXO PEAK TEMP/°C	EXO PEAK RANGE/°C	WT LOSS /%	EXO PEAK TEMP/°C	EXO PEAK RANGE/°C	WT LOSS /%
16.5	12.49	Am	324	152-570	8.0	-	-	-	-	-	-
24.0	12.629	Am	300	230-597	5.3	-	597-702*	3.0	-	-	-
40.5	13.095	60.3	353	250-397	3.1	516	435-552	1.3	604	552-642	3.1
72.0	13.30	73.0	360	291-444	3.3	525	444-565	2.0	605	565-633	4.1
72.0 (FP)	-	76.8	360	280-440	2.8	515	446-558	1.4	605	558-640	3.3

FP = Final product

Am = Amorphous

* Exo + Endo; TG for S_2 indicative of TMA in gmelinite cage, thus although no exotherm seen in DTA it is probably simultaneous exothermic TMA degradation and endothermic structural collapse. Endothermic process > Exothermic ∴ appears as endotherm

Table 4.4b

Reaction R10 Endotherms

TIME/h	ENDO PEAK TEMP/°C	ENDOPEAK RANGE/°C FROM RT TO	WT LOSS /%	ENDO PEAK (BROAD) RANGE/°C	WT LOSS /%	ENDO PEAK	ENDO PEAK RANGE/°C	WT LOSS /%
16.5	90	115	10.8	115-152	1.8	875	570-875	0.8
24.0	91	120	14.4	120-230	6.0	846 922	597-922	3.5
40.5	102	142	12.3	142-250	4.4	-	-	-
72.0	97	142	11.6	142-291	7.1	-	-	-
72.0 (FP)	92	130	10.6	130-280	6.3	1190		0.0

RT = Room temperature

Table 4.4c

Reaction R10 Weight Loss

TIME/h	TOTAL WT LOSS DUE TO EXO PROCESS /%	TOTAL WT LOSS DUE TO ENDO PROCESS /% <300	>300	OVERALL WT LOSS
16.5	8.0	12.8	0.8	21.6
24.0	8.3	20.4		28.7
40.5	8.0	16.6		24.6
72.0	9.4	18.8		28.2
72.0(FP)	7.4	16.9		24.3

Comparison of pH values and Crystallinity for Reaction R10

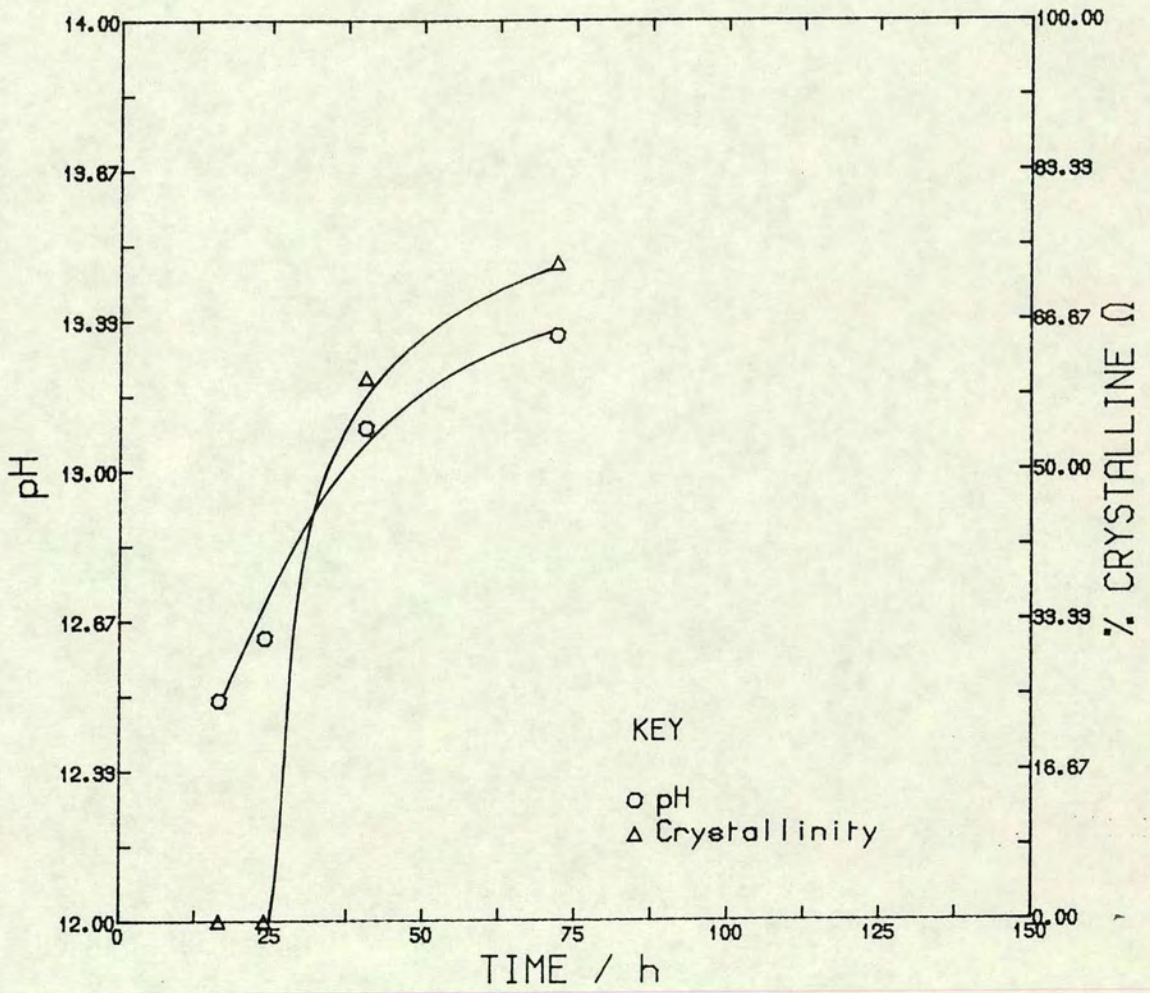

Fig. 4.22

Crystallisation of Reaction R10 monitored by DTA

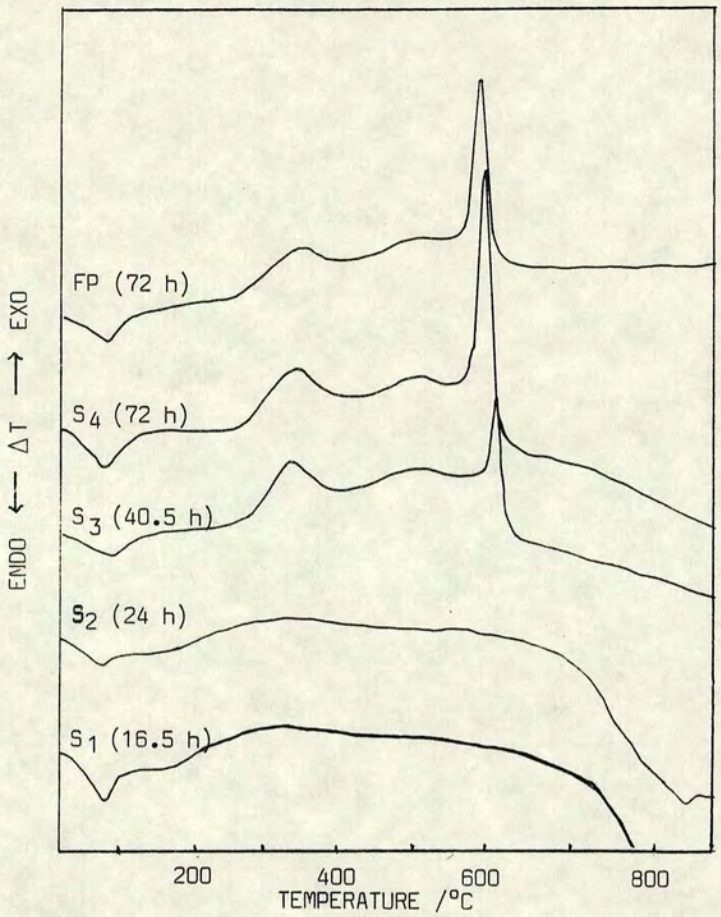

Fig. 4.23

Crystallisation of Reaction R10 monitored by TG

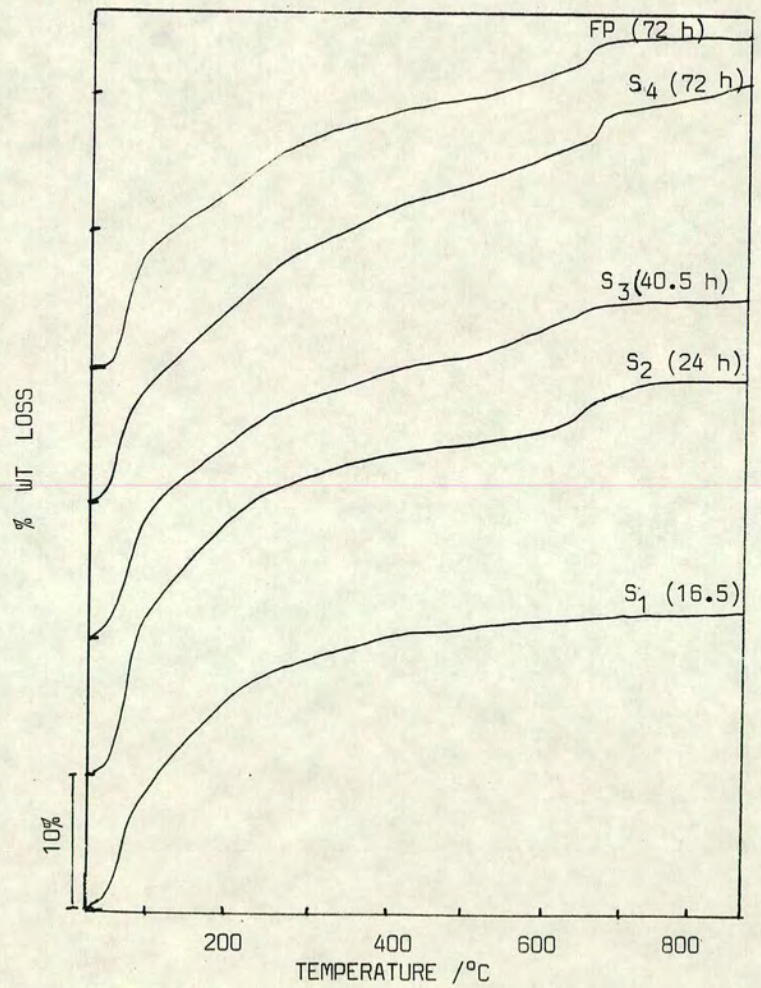

Fig. 4.24

weight loss of 8%.

At 24 h, S_2, the X-ray amorphous material showed a small but sharp endotherm (91°C), a broad endotherm (120°C to 230°C) and a broad exotherm (230°C to 597°C). The TG curve distinctly shows the loss of water in two stages, followed by the gradual loss of TMA up to 597°C and then a sharp weight loss of 3% at this temperature. The latter curve is typical of a crystalline sample of Ω. Thus, although X-ray amorphous, the TG curve provides evidence, as in reaction R1, for the presence of crystallites with Ω structure.

At 40.5 h, S_3, 60% crystalline Ω results. The DTA curve depicts a small broad endotherm, centred at 102°C, which is attributed to loosely bound water and a broad endotherm (142°C to 250°C) assigned to intra-crystalline water. The exothermic processes show a well defined peak (from 250°C to 397°C) centred at 353°C, due to TMA adsorbed on the external surface of the crystals; a small broad peak centred at 516°C with an associated weight loss of 1.3% and then a sharp peak at 604°C with an associated weight loss of 3.1%. The exotherms correspond to the calcination of the TMA.

At 72 h (S_4) the DTA curve is much the same as in S_3. The bulk final product showed a slightly different DTA curve. The resolution of the endotherms and low temperature exotherm is reduced. The total weight loss associated with the organic material in S_4 is greater than in the bulk product. This is probably due to a difference in weight loss for TMA adsorbed on the external surface, but it does not account for the total amount. The second exotherm centred at ~520°C in S_4 shows an increased amount of TMA at this site, 2.0% compared with 1.4% in the bulk product; also an increased amount of TMA associated with the peak at 605°C is observed (4.1% cf. 3.3% in the bulk). It follows that, either the TMA is capable of redistribution from site to site, or that

each crystal has a different amount of TMA at each site and thus the TG and DTA data provide an average of the distribution of TMA in the crystals.

Table 4.4a shows that during crystallisation, the exothermic peak at ~350°C shows a decrease in weight loss and the associated weight losses at ~520°C and ~605°C fluctuate. As in R1, the loosely bound water and intracrystalline water content varies (Table 4.4b). The total weight losses associated with the exothermic and endothermic processes fluctuate (Table 4.4c). They do not show any striking trends.

The DTA and TG curves for this reaction (R10) are similar to those for reaction R1 up to 72 h. Since the DTA curves are of the same type, it is apparent that hexanediol was not incorporated into the structure. Sorption measurements and/or TEM are thus required to determine whether or not the structure is faulted.

The most remarkable feature of this kinetic series is the thermal analysis of the X-ray amorphous samples. The TG and to a lesser extent DTA curves show the presence of zeolite structure in the X-ray amorphous material. Although the samples are not crystalline to X-rays, very small crystallites are present. Reports on X-ray amorphous samples of ZSM-5 with catalytic properties have been made and are referred to in Chapter Three. The present work adds to the zeolitic materials with crystalline structure undetected by X-rays.

4.3.8.3 Reaction R9

The gel for this reaction was prepared by mixing the reactants with the silica in the following order: TMABr (aq), hexanediol (aq), water and base. A viscous gel resulted. It was allowed to crystallise for 384 h and produced a good crystalline sample (88%) of Ω.

The crystallisation curves for the initial period (150 h) and the complete period (384 h) depict the typical s-shaped pH and crystallinity curves (Fig. 4.25 and 4.26). A sharp pH rise during the initial 50 h of crystallisation is observed, a gradual rise occurs up to 169 h and is then virtually constant up to 240 h (Table 4.5a). An increased induction period, as in R10, is observed, compared with reaction R1. This is not caused by the presence of hexanediol in the reaction mixture, as other reactions which contained the latter crystallised within 16 h, but is related to the way in which the gel was prepared. Crystallisation, as detected by XRD, occurred between 24 h and 48 h at which time 77% crystalline material resulted. The sudden decrease in crystallinity at 305 h and the lower crystallinity of the final product compared with the 240 h sample is reflected in the DTA and TG curves.

Thermal analysis of the X-ray amorphous samples (0.5 h and 24 h) of this series shows little structure formation (Figs. 4.27 and 4.28, Tables 4.5a, 4.5b, 4.5c, 4.5d), unlike reactions R1 and R10; however evidence for the two types of water is provided by the DTA curve (24 h).

The major thermal behavioural changes which take place during crystallisation are as follows:

At 48 h (S_3) 77% crystalline Ω is produced. The DTA curve exhibits the two characteristic endotherms, sharp at 107°C, and broad from 130°C to 297°C; and only two exothermic peaks centred at 357°C, and 602°C. The former exotherm corresponds to TMA adsorbed on the external surface, and the latter exotherm is attributed to TMA burning out of the gmelinite cages. Complete removal of the organic material results in gradual endothermic structural collapse. The latter behaviour is similar to that observed for S_5 of reaction R1.

Comparison of pH values and Crystallinity for Reaction R9

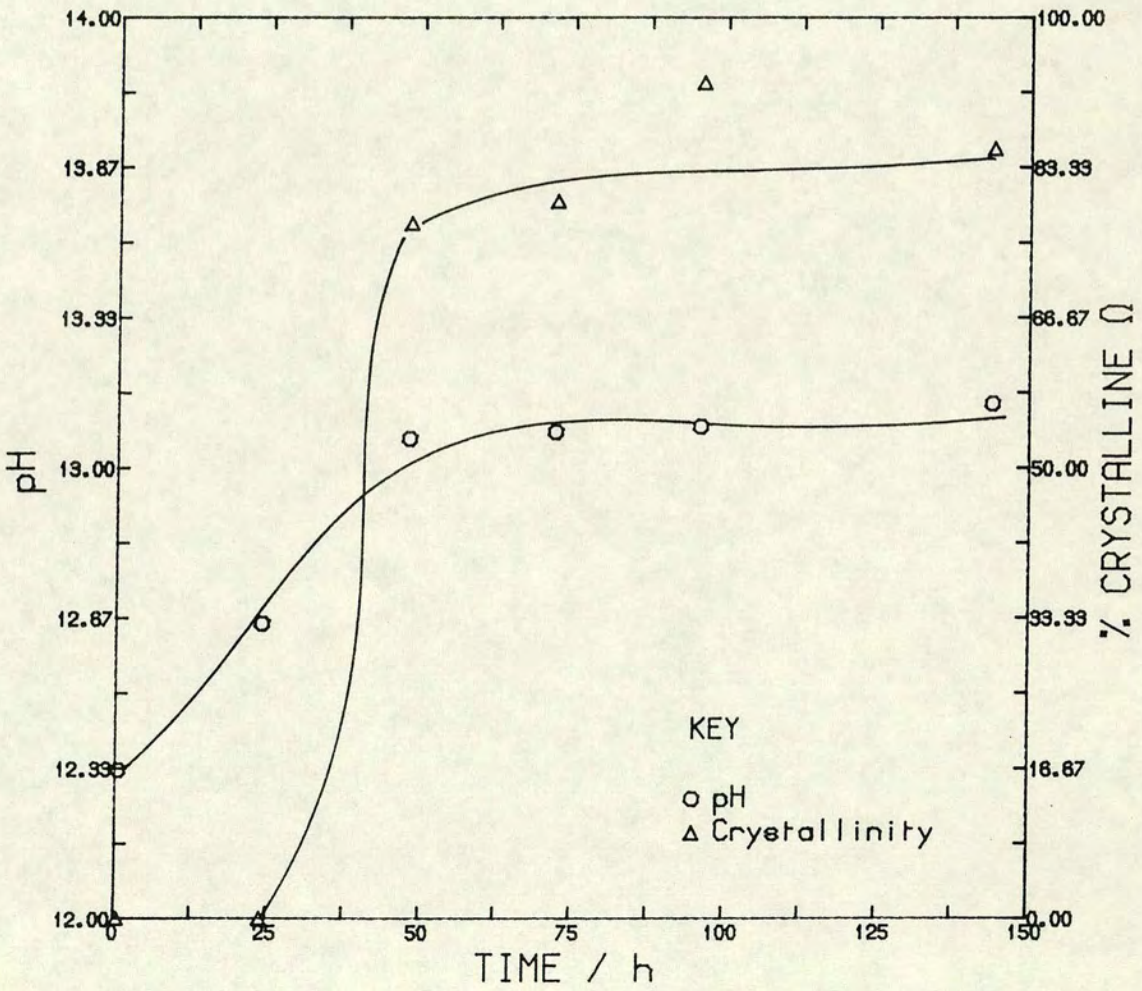

Fig. 4.25

Comparison of pH values and Crystallinity for Reaction R9

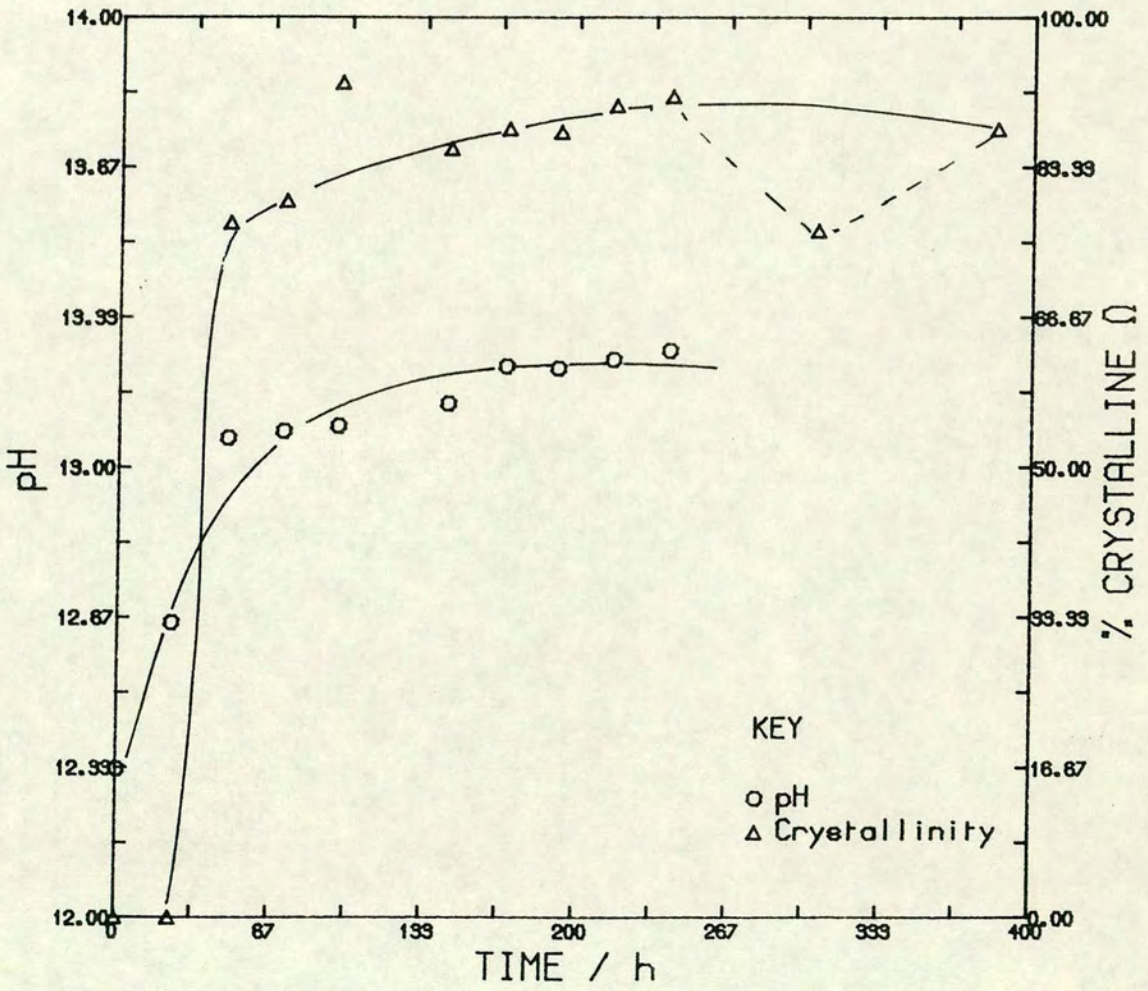

Fig. 4.26

Crystallisation of Reaction R9
monitored by TG

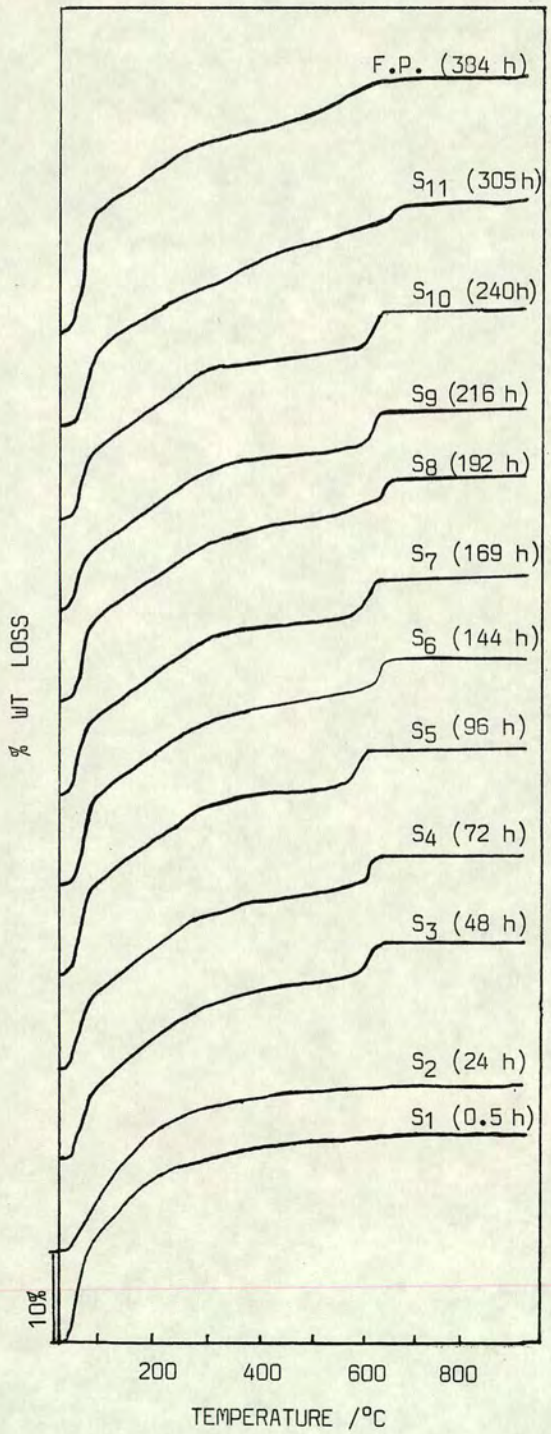

Fig. 4.28

Crystallisation of Reaction R9
monitored by DTA

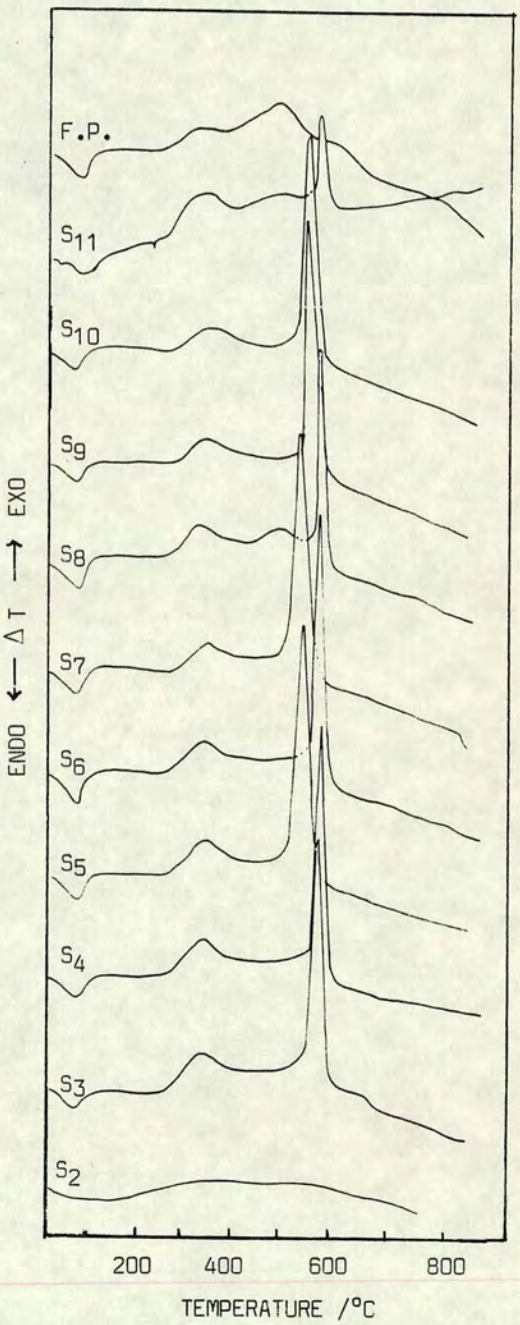

Fig. 4.27

F.P. = Final Product

Table 4.5a

Crystallisation of Reaction R9

Thermal Analysis, Crystallinity and pH Data

TIME /h	pH	CRYSTALLINITY /%	EXO PEAK TEMP /°C	EXO PEAK RANGE /°C	WT LOSS /%	EXO PEAK TEMP /°C	EXO PEAK RANGE /°C	WT LOSS /%	EXO PEAK TEMP /°C	EXO PEAK RANGE /°C	WT LOSS /%	EXO PEAK TEMP /°C	EXO PEAK RANGE /°C	WT LOSS /%	ADDITIONAL WT LOSS BETWEEN EXOS /%
0.5	12.330	Am	387*		1.5										
24.0	12.655	Am	405(b)	246-627	3.6										
48.0	13.065	77.2	357	297-415	1.9	602	552-620	4.0							1.3
72.3	13.080	79.6	359	287-408	2.0	607	567-625	3.5							1.5
96.0	13.092	92.8	363	292-417	1.8	567	519-598	4.5							0.6
144.0	13.142	85.4	362	287-504	2.5	600	567-622	3.9	527	504-567	0.8				-
169.0	13.225	87.6	372	300-412	1.3	562	515-595	4.9							0.5
192.2	13.220	87.2	355	283-397	2.1	602	555-622	3.9	515	452-555	1.0				0.5
216.3	13.240	90.2	365	290-422	1.4	587	556-615	4.6							0.9
240.8	13.26	91.2	367	297-412	1.1	580	532-605	4.5							0.8
305.4(S_{11})	-	76.3	355	285-410	3.5	603	580-732	2.5	505	442-580	2.6				0.3
384	-	87.6	345	275-395	1.8	615	573-675	2.0	513	395-573	3.8	1050		0.0	

(b) = broad

* Temp for TG curve

DTA and TG curves for S_{11} and Final product reproducible

Table 4.5b

Exotherms for S_{11} and Final Product

S_{11} EXO PEAK TEMP /%	WT LOSS /%	FINAL PRODUCT EXO PEAK TEMP	WT LOSS /%
355	3.5	345	1.8
505	2.6	513	3.8
603	2.5	615	2.0
772	0.3	1050	0.0
829	0.1		
923	0.9		
1130	0.0		
1190	0.0		

Table 4.5c

Reaction R9 Endotherms

TIME/h	ENDO PEAK TEMP /°C	ENDO PEAK RANGE /°C FROM RT TO	WT LOSS /%	ENDO PEAK (BROAD) RANGE /°C	WT LOSS /%	ENDO PEAK TEMP /°C	WT LOSS /%
0.5	90*	216	9.8				
24.0	134	246	14.5				
48.0	107	130	9.6	130-297	7.3		
72.3	93	127	9.9	127-287	6.6		
96.0	92	130	11.8	130-292	6.6		
144.0	97	130	11.4	130-287	6.5		
169.0	92	127	9.4	127-300	7.6		
192.2	98	132	11.1	132-283	5.9	940	0.0
216.3	90	125	8.3	125-290	7.0		
240.8	90	122	8.9	122-297	7.5	978	0.0
305.0	101	170	11.4	170-285	3.8	1028	0.0
384.0	105	142	15.5	142-275	5.0		

RT = Room Temperature

Table 4.5d

Reaction R9 Weight Losses

TIME/h	TOTAL WT LOSS DUE TO EXO PROCESS /%	TOTAL WT LOSS DUE TO ENDO PROCESS /%	OVERALL TOTAL WT LOSS /%
0.5	1.5	21.0	22.5
24.0	3.6	14.5	18.1
48.0	7.12	16.9	24.0
72.3	7.0	16.5	23.5
96.0	6.9	18.4	25.3
144.0	7.1	17.9	25.0
169.0	6.6	17.0	23.6
192.2	7.5	17.0	24.5
216.3	6.9	15.3	22.1
240.8	6.4	16.4	22.8
305.4	10.1	15.1	25.3
384.0	7.5	20.5	28.0

At 72 h (S_4) the appearance of a slight exothermic shoulder between 417°C and 519°C is detected. At 96 h (S_5) the sharp exotherm is shifted from 607°C to the lower temperature of 567°C, the site of the observed shoulder in S_4. At 144 h (S_6) the sharp exotherm is shifted back to the higher temperature (600°C) typical for Ω and the appearance of a slight shoulder at 527°C is detected. At 169 h (S_7) the sharp exotherm is again shifted to lowertemperature (562°C). At 192 h (S_8) the appearance of a small broad exotherm (452°C to 555°C) centred at 515°C is discerned, and the sharp exotherm is shifted to 602°C. At 216 h (S_9) the exotherm attributed to external surface TMA is seen to occur over a broader range (290°C to 422°C), the absence of the small exotherm centred at 515°C and the shift of the sharp exotherm to lower temperature (587°C) are observed. At 240 h (S_{10}) little change is detected except for the slight shift of the sharp exotherm to lower temperature (580°C).

At 305 h (S_{11}) dramatic changes are observed (Fig. 4.29, Table 4.5b) which are reflected by a decrease in crystallinity. The appearance of a sharp endotherm at 250°C corresponds to the boiling point of hexanediol. The intracrystalline water content is reduced from 7.5% in S_{10} to 3.8%. An increased amount of external surface TMA, >3 times that of the previous sample (1.1% to 3.5%), is detected. The reappearance of the exothermic peak at 505°C with an increased associated weight loss is observed, and the sharp exotherm at 603°C is diminished in size with an associated weight loss of 2.5% (4.5% in S_{10}). A series of exothermic peaks are detected at 772°C, 829°C and a comparatively large peak at 923°C (0.9%) is observed. The later exotherms are suggestive of a phase transition as simultaneous weight losses are not observed. These peaks occur at 1130°C and 1190°C. The final product (384 h) compared with S_{11} showed an increased intracrystalline water content (3.8% to 5.0%), a decreased amount of external surface TMA (3.5% to 1.8%), and

DTA and TG Curves for S_{11} of Reaction R9

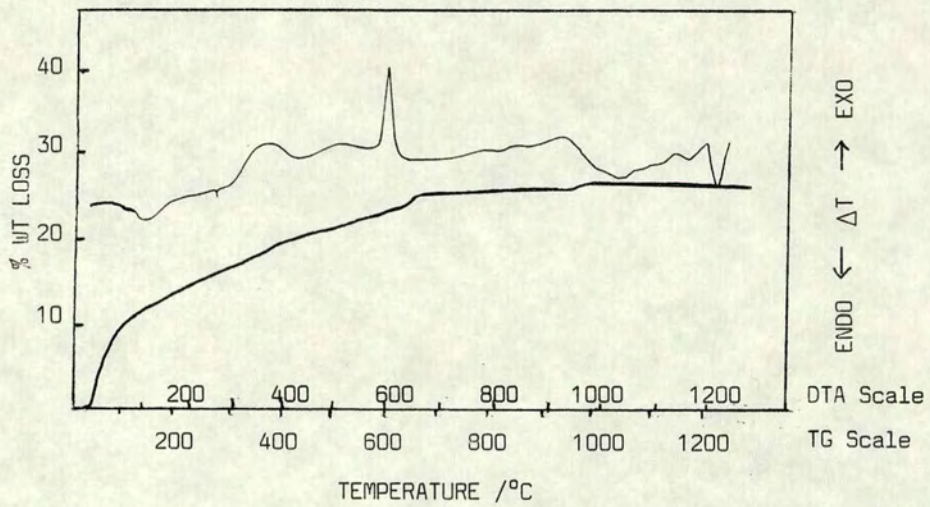

Fig. 4.29

DTA and TG curves for Final Product of Reaction R9

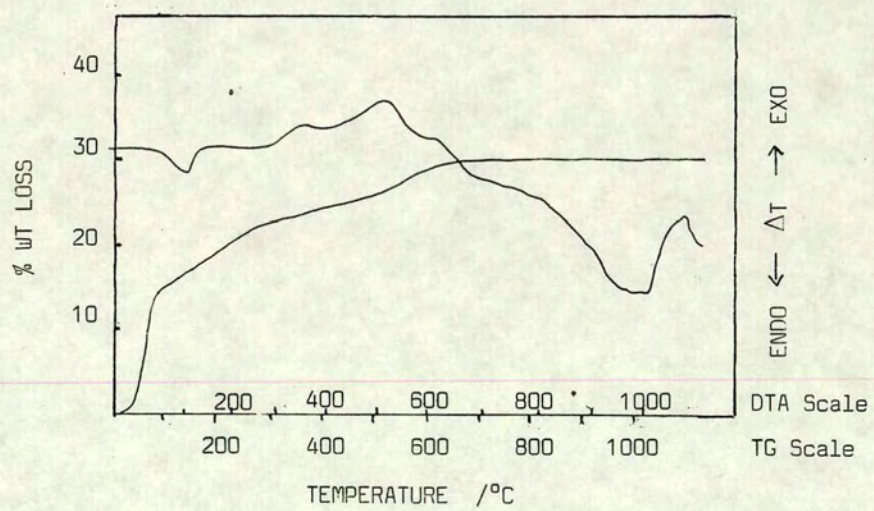

Fig. 4.30

an increased weight loss associated with the peak at 513°C (2.6% to 3.8%) which stretches from 395°C to 573°C. The sharp exotherm is replaced by a small broad peak at 615°C (2.0% weight loss). A large broad exotherm at 1050°C, with no corresponding weight loss is observed and thus indicative of a phase change (Fig. 4.30).

The glassy DTA residues from S_{11} and the final product were insufficient for X-ray powder diffraction analysis. The DTA residue of the final product viewed under the optical microscope showed it to be a glass.

During the crystallisation of this reaction (Tables 4.5a, 4.5c, 4.5d) fluctuation of the percentage of loosely bound water is observed. The intracrystalline water content is fairly constant up to 169 h, at which time an increase in the latter is observed. A reduced intracrystalline water content and decrease in crystallinity is seen for S_{11} and the final product. Fluctuation of the weight loss due to the external surface TMA is observed. The latter is probably related to the crystal size and shape. A large quantity of TMA on the external surface is exhibited by S_{11}. After 96 h, the temperature of the sharp exothermic peak is moved to lower temperature and a corresponding increase in weight loss is noted. Thus, it is apparent that the additional weight losses recorded between the exotherms are due to TMA in a site that loses organic material between ~400°C and 540°C. It is not readily detected by DTA in these instances. However, in some samples of Ω, there is sufficient TMA present to detect an exotherm around 515°C; in the final product, the majority of the TMA is located at this site. The total weight loss associated with the exothermic processes (Table 4.5c) for the crystalline materials varies from 6.3% to 7.5%, except in S_{11} which shows an exceptionally high value of 10.1%. The total water content of the crystalline materials varies from 16.4% to 17.9%, S_{11} exhibits a low value of 15.1%, but this is obviously compensated for

by the increase in organic content. The final product shows an extremely high weight loss for water (20.5%) but only a small organic weight loss (7.5%) of which 1.8% is associated with the external surface, giving 5% encapsulated in the structure. Thus the capacity of the final product is quite substantial.

The most outstanding feature of this crystallisation is the observed exotherms at ~1000°C at 305 h and 384 h which are extremely rare for zeolite Ω.

4.3.9 Classification of Products According to DTA Type

The products obtained from the crystallisation of the reactions studied (also R15* and 3 samples provided by D. Sinclair) may be classified according to their thermal behaviour. The classification, based on the exothermic processes only, as these show the distinctive changes, leads to five DTA types. Types I to IV (Figs. 4.31 to 4.34) are exhibited by pure Ω. The presence of hexanediol in the reaction composition and the order of mixing the reactants does not influence the DTA type as examples of each variation occur in the different categories. Thus hexanediol was not occluded by Ω during synthesis and hence sorption and/or TEM are required to determine whether a fault free Ω was achieved. Type V DTA (Fig. 4.35) is exhibited by Ω in admixture with TMA-sodalite and was produced by the 'hot' reactions.

The classification (Table 4.6) shows DTA Type I to be the most common. Type I depicts (Fig. 4.31, Table 4.7a) a small exothermic peak at ~350°C corresponding to surface TMA which varies from 1.5% to 2.8%; a small exotherm centred at ~520°C with associated weight loss of 0.8% to 1.9%; and a sharp exothermic peak at ~600°C which corresponds to TMA in the gmelinite cages with an associated weight loss of 3.3% to 4.1%.

* R15 prepared from the standard composition with solutions mixed at room temperature.

Thermal Analyses Curves for Pure Ω

Type I

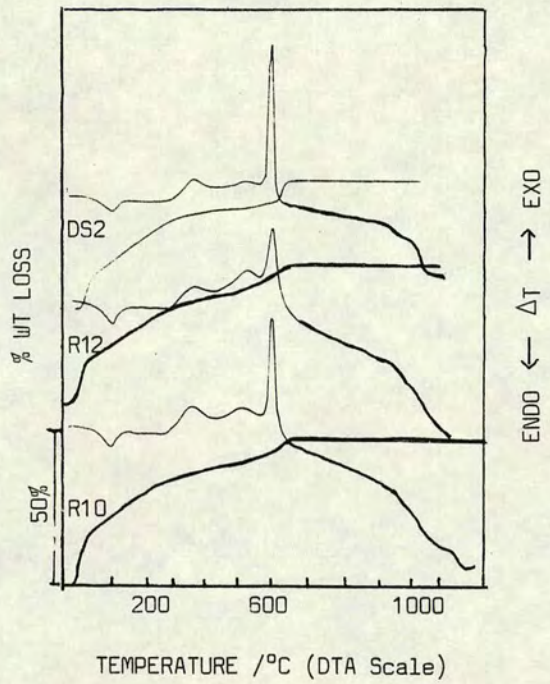

Fig. 4.31

Type III

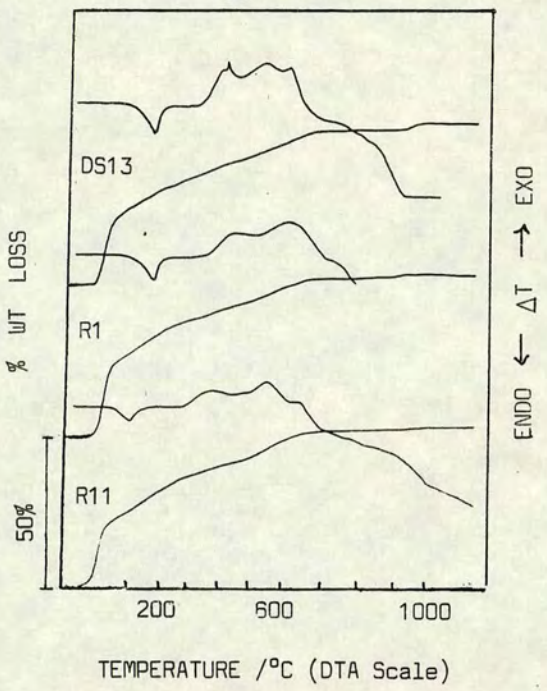

Fig. 4.33

Type II

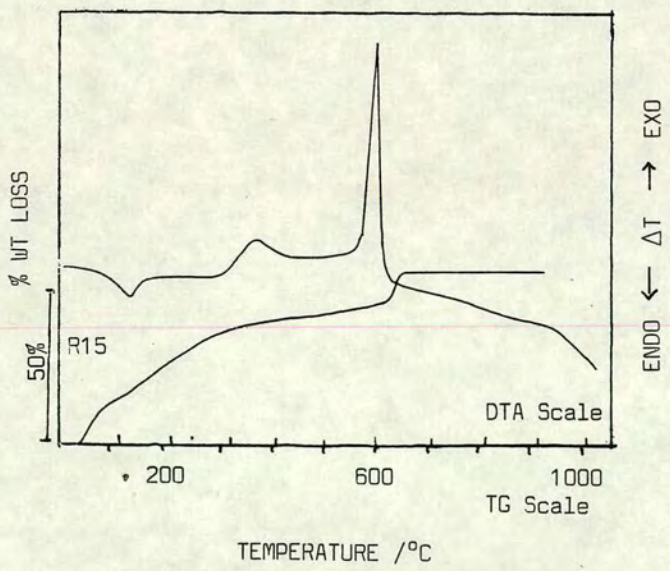

Fig. 4.32

Type IV

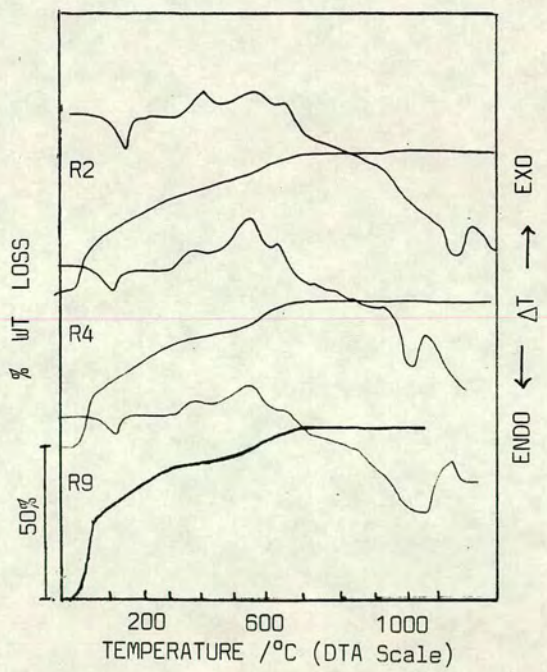

Fig. 4.34

Thermal Analyses Curves for Ω
in admixture with sodalite

Type V

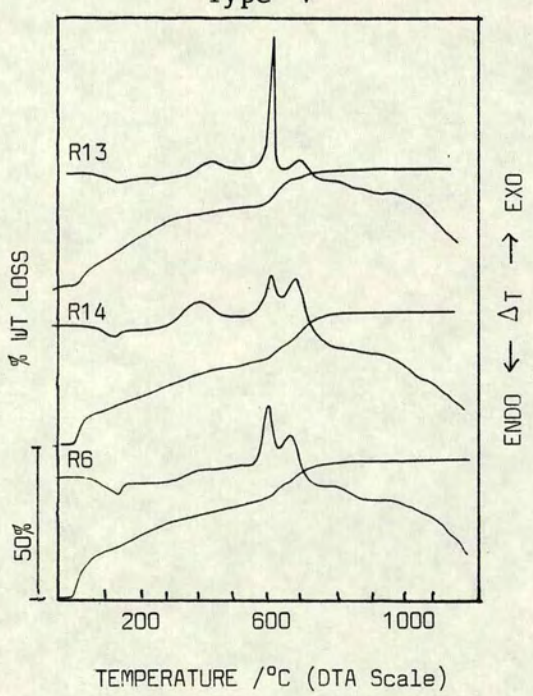

Fig. 4.35

Table 4.6

Classification of Products According to DTA Type

DTA TYPE I		DTA TYPE II		DTA TYPE III		DTA TYPE IV		DTA TYPE V		
REACTION	% Ω	REACTION	% Ω	REACTION	% Ω	REACTION	% Ω	REACTION	% Ω	% SODALITE
R[illegible]	90.4	R15	86.0	DS13	75.0	R4	86.0	R6	61.2	59
DS3	87.6			R1	73.0	R2	83.0	R13	75.3	31
DS2	73.8			R11	90.0	R9	87.5	R14	44.52	100
R7	100.0									
R8	90.0									
R12	91.0									
R10	76.8									

Table 4.10

Comparison of DTA Type with
Chemical Composition, Crystallinity and Reaction Time

REACTION	CRYSTALLINE Ω /%	DTA TYPE	XRF ANALYSIS/moles SiO_2/Al_2O_3	SiO_2/Na_2O	Na_2O/Al_2O_3	TIME/h
R7	100.0	I	6.30	7.08	0.89	576
R12	91.0	I	6.37	6.13	1.04	240
R3	90.4	I	6.55	6.68	0.98	388
R8	90.0	I	6.53	6.46	1.01	401
R11	90.0	III	6.50	6.25	1.04	360
R9	87.6	IV	6.42	5.84	1.10	384
DS3	87.6	I	6.59	7.49	0.88	144
R15	86.5	II				144
R4	86.1	IV	6.66	6.73	0.99	145
R2	82.8	IV	6.51	6.38	1.02	212.5
R10	76.8	I	6.81	7.32	0.93	72
R13	75.3	V	6.57	8.64	0.76	288
DS13	75.3	III	7.34	6.07	1.21	144
DS2	73.8	I	5.90	6.70	0.88	144
R1	73.0	III				100
* R6	61.2	V				672
* R14	44.5	V				240
* R5	17.2		3.13	2.95	1.06	144

* Sodalite present in final product

Table 4.7a

Comparison of Thermal Analysis Data for Pure Ω

Exothermic Processes

DTA TYPE	REACTION	EXO PEAK TEMP/°C	EXO PEAK RANGE/°C	WT LOSS /%	EXO PEAK TEMP/°C	EXO PEAK RANGE/°C	WT LOSS /%	EXO PEAK TEMP/°C	EXO PEAK RANGE/°C	WT LOSS /%	EXO PEAK TEMP/°C	EXO PEAK RANGE/°C	WT LOSS /%
I	OS2	358	304-405	1.5	526	465-560	0.8	607	560-623	4.1			
	R10	360	280-440	2.8	515	440-558	1.4	605	558-640	3.3			
	R12	342	299-407	1.8	503	407-538	1.9	580	538-620	3.6			
II	R15	362	303-450	1.8				597	450-622	5.4			
III	R1	355	268-428	2.9	545	428-647	4.5	676	647-940	0.8			
	OS13	372	284-420	3.0	517	420-572	3.1	597	572-670	1.9	770	670-880	0.75
	R11	347	270-413	3.0	524	413-583	4.3	612	583-677	1.3			
IV	R9	345	275-395	1.8	513	395-573	3.8	615	573-675	2.0	1050		0.0
	R2	356	283-397	2.1	509	397-569	3.8	604	569-656	2.4	1075		0.0
	R4	337	275-387	2.0	507	387-562	3.6	589	562-637	2.1	940		0.0

Table 4.7b

Comparison of Thermal Analysis Data for Pure Ω

Endothermic Processes

DTA TYPE	REACTION	ENDO PEAK TEMP/°C	ENDO PEAK RANGE/°C RT to	WT LOSS /%	ENDO PEAK (BROAD) RANGE/°C	WT LOSS /%	ENDO PEAK TEMP/°C	WT LOSS /%
I	OS2	96	130	7.6	130-304	7.3		
	R10	92	130	10.6	130-280	6.3		
	R12	92	130	8.4	130-299	6.7		
II	R15	92	130	5.5	130-303	6.9		
III	R1	106	142	13.9	142-268	4.5		
	OS13	112	153	13.1	153-284	3.9		
	R11	98	137	12.3	137-270	5.0		
IV	R9	105	142	15.5	142-275	5.0	1028	0.0
	R2	112	142	10.5	142-283	5.3		
	R4	105	140	11.0	142-275	5.1		

RT = Room Temperature

Type II DTA was observed for only reaction R15 (Fig. 4.32). However, this type has been observed during the crystallisation of reaction R9 (S_5 and S_7) and R1 (S_5). It is composed of two exotherms: a small broad exotherm (303°C to 450°C) centred at 362°C with an associated weight loss of 1.8% and a sharp exothermic peak at 597°C, associated with a weight loss of 5.4%.

Type III is characterised by small broad exothermic peaks (Fig. 4.33) which occur at temperatures of: ~360°C (weight loss 3.0%), ~525°C (weight loss 3.1% to 4.5%) and ~600°C (weight loss 0.8% to 1.9%).

The main features which characterise type IV (Fig. 4.34) are the exotherm at ~1050°C, which is not associated with a weight loss and thus indicative of a phase change, and 3 broad exotherms which occur at ~350°C with a weight loss of 1.8% to 2.0%, ~510°C with a weight loss of 3.6% to 3.8%, and ~600°C with a weight loss of 2.0% to 2.4%.

Type V, due to Ω in admixture with sodalite, is distinguished from types I to IV by the appearance of an additional exotherm, not typical for Ω, and probably associated with TMA-sodalite (Fig. 4.35 and Table 4.8a). The DTA curve is characterised by a small broad exotherm centred at ~360°C (associated weight loss 1.3% to 4.3%), a sharp exothermic peak at ~580°C (associated weight loss 2.1% to 3.4%) and the additional exotherm which may be due to TMA-sodalite at ~660°C (associated weight loss 1.8% to 3.5%).

Comparison of the endothermic behaviour for pure Ω (Table 4.7b) shows that the loosely bound water is least for type II (5.5%) and greater for type I (7.6% to 10.6%), type III (12.3% to 13.9%) and type IV (10.5% to 15.5%). A high value for loosely bound water is associated with a low value for intracrystalline water, except for R9 with type IV behaviour which shows the greatest loosely bound water content with

intracrystalline water (5.0%) of the same range for that group. R15 (type II) shows the second greatest value for intracrystalline water (6.9%) with DS2 (type I) showing the highest value (7.3%). Lowe et al [1] have reported that low loosely bound water content with high intracrystalline water is associated with fibrous Ω. Thus R15 is probably composed of fibrous crystals. Bulk density measurements for DS2 gave a value (0.6 gcm^{-3}) in between that for spherulitic and fibrous types, hence this sample is probably a mixture of the two morphologies and would therefore account for the high intracrystalline water content and low loosely bound water for type I. SEM is a necessary requirement to test these morphological deductions, however such facilities were not available.

Comparison of the exothermic behaviour for types I to V (Fig. 4.36, Tables 4.7a, 4.8a) show that exotherms centred in the region of 350°C and 600°C are present in all samples. The former is attributed to TMA adsorbed on the external surface and the latter to TMA encapsulated in the gmelinite cages. Types I, III and IV also show an exotherm around 520°C.

Types I and III show similar peak positions; the difference arises in the overall appearance of the DTA curve and the distribution of the organic material at these sites. The surface exotherm of type I has less associated weight loss (1.5% to 2.8%) than that of type III (~3.0%). At 520°C a much lower TMA content (0.8% to 1.9%) associated with this exotherm is observed for type I than for type III (3.1% to 4.5%). The 600°C exotherm of type I is very sharp with a much greater associated weight loss (3.3% to 4.1%) than the small broad exotherm of type III (0.8% to 1.9%). An extremely small broad exotherm in the region of 770°C (0.75% weight loss) is also discerned in type III.

Comparison of the Five DTA Types

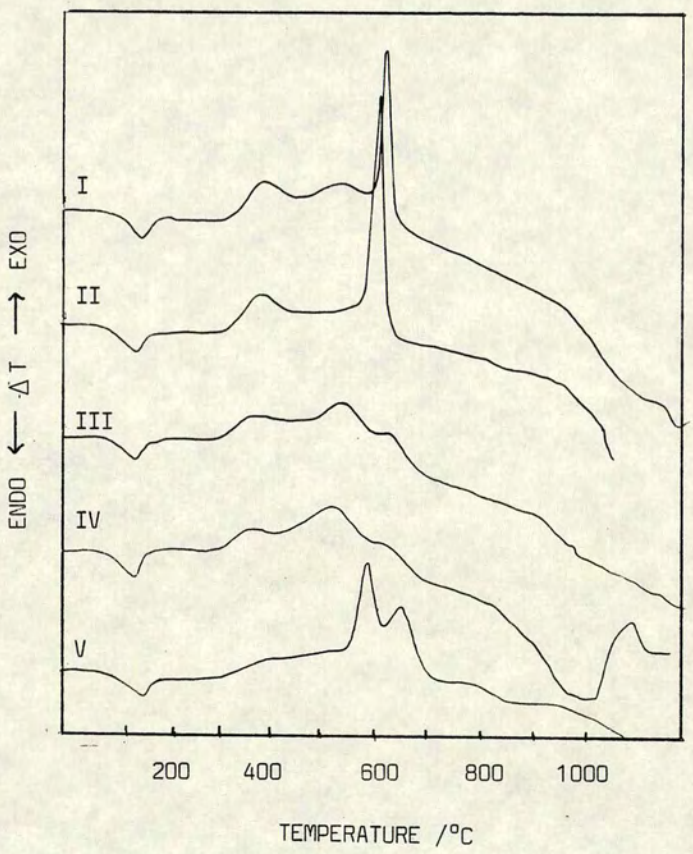

Fig. 4.36

Types III and IV exhibit similar behaviour up to ~ 950°C. Type III shows a larger weight loss associated with surface TMA (~ 3.0%) than type IV (~ 2.0%). The second exotherm occurs at a slightly lower temperature in type IV, 510°C, with less associated weight loss (3.8%) than type III which occurs at 520°C with a greater weight loss (3.1% to 4.5%). The chief difference arises in the thermal behaviour after 950°C. Type III exhibits gradual endothermic collapse after removal of the TMA. However, type IV exhibits an exotherm at ~1000°C which is not associated with a weight loss and thus indicative of a phase change or exothermic collapse. This is extremely rare for zeolite Ω and only one report (by Penchev et al [11]) has been made of such an occurrence. The DTA curve given in this paper is not the same as type IV. None of the four DTA types described here are exactly the same as those reported by other workers. The DTA types reported in the literature have been discussed in Chapter Two.

Type V DTA may be considered to be composed of type II and an additional exotherm assigned to TMA-sodalite. Comparison (Table 4.8a) shows that type V exhibits the sharp exotherm at a lower temperature (567°C to 585°C) than that recorded for type II (597°C) and also shows less weight loss associated with this peak (2.1% to 3.4%) than type II (5.4%). The additional exotherm centred in the region of 645°C to 656°C is at a temperature 50°C higher than that observed for TMA-sodalite. Perhaps a mixture of the two species effects evolution of TMA at a higher temperature for one component and at a lower temperature for the other component, than that observed for the pure species. If this is the case, then in type V the exothermic peak for Ω is shifted to the lower temperature and that for TMA-sodalite to the higher temperature. (Alternatively, the peaks may be incorrectly assigned.) The endothermic behaviour for types II and V (Table 4.8b) are similar but the latter shows slightly reduced water content. The intracrystalline

Table 4.8a

Comparison of Thermal Analysis Data for the 'Hot' Reactions

with R15 and Pure TMA-Sodalite - Exothermic Processes

REACTION	CRYSTALLINITY		EXO PEAK TEMP/°C	EXO PEAK RANGE/°C	WT LOSS /%	EXO PEAK TEMP/°C	EXO PEAK RANGE/°C	WT LOSS /%	EXO PEAK TEMP/°C	EXO PEAK RANGE/°C	WT LOSS /%	EXO PEAK TEMP/°C
	% SODALITE	% Ω										
R6	58.7	61.2	363	307-545	3.5	585	545-612	2.1	645	612-703	3.3	777 (S)
R13	31.0	75.3	368	300-438	1.3	567	438-595	3.0	657	595-697	1.8	770 (S)
R14	100	44.5	352	242-438	4.3	578	438-608	3.4	656	608-725	3.5	
R15	-	86.5	362	303-405	1.8	597	450-622	5.4	-	-	-	
TMA-Sodalite	Very cryst alline sample	-	-	-	-	-	-	-	607	555-643	15.3	742 (S)

(S) = Shoulder

Table 4.8b

Comparison of Thermal Analysis Data for the 'Hot' Reactions

with R15 and Pure TMA-Sodalite - Endothermic Processes

REACTION	CRYSTALLINITY		ENDO PEAK TEMP/°C	ENDO PEAK RANGE/°C RT to	WT LOSS /%	ENDO PEAK (BROAD) RANGE/°C	WT LOSS /%
	% SODALITE	% Ω					
R6	58.7	61.2	100	125	7.4	125-307	6.4
R13	31.0	75.3	78	160	7.5	160-300	5.0
R14	100	44.5	80	128	6.0	128-242	2.6
R15	-	86.5	92	130	5.5	130-303	6.9
TMA-Sodalite	Very cryst -alline sample	-	broad	555	5.3	-	-

RT = Room Temperature

water for type V is less than that for type II; this is probably related to the presence of TMA-sodalite which in the pure species is exhibited as a small broad endotherm stretching up to 550°C i.e. prior to commencement of exothermic release of TMA.

On the assumption that the additional exotherm at ~650°C observed in type V DTA is due to TMA-sodalite, then comparison of the weight loss associated with this exotherm should show some relationship with the TMA-sodalite content of the sample. An estimation of the latter based on the assumption that the TMA content of the pure material is representative of the % crystallinity is given in Table 4.9.

Table 4.9

Comparison of the % Calculated TMA-sodalite with Total Sodalite Content

REACTION	NO. MOLES TMA IN RC	% SODALITE*	WT LOSS DUE TO TMA-SODA -LITE /%	TMA-SODALITE** /%	REACTION TIME /h
R13	2	31.0	1.8	11.5	288
R6	3	58.7	3.3	21.3	672
R14	1	100	3.5	23.0	336
TMA-sodalite	3	v. crystal-line sample	15.3	100	-

RC = Reaction Composition

* Based on most intense sodalite peak from R14

** Based on TMA content of pure TMA-sodalite

An increase in the % TMA due to TMA-sodalite corresponds to an increase in the % total sodalite. Neither the concentration of TMA in the reaction composition nor the reaction time show any correlation with the % sodalite.

The total sodalite content is probably a mixture of TMA-sodalite and hydroxysodalite. Reaction R14 is indicative of this as the latter, recorded as 100% sodalite, shows only 3.5% TMA whereas R6, 58% sodalite shows 3.25%. Thus based on this assumption, it is theoretically possible to calculate the % TMA sodalite in the mixture.

4.3.10 Comparison of DTA Type with Chemical Composition (XRF) Crystallinity and Reaction Time

Comparison of the DTA type with chemical composition (XRF), crystallinity, and reaction time is given in Table 4.10. XRF analysis was not carried out on all the products as in some instances complete removal of the TMA was not effected.

The most crystalline samples prepared from the composition studied:

$$6Na_2O \quad Al_2O_3 \quad 15SiO_2 \quad 300H_2O \quad (3-x)TMABr \quad xHO(CH_2)_6OH$$

show DTA type I curves. Reaction R10 exhibits DTA type I curve, but lower crystallinity than expected for this type as it was reacted for only 72 h - half the normal crystallisation period. DTA types II, III, and IV cannot be correlated with the degree of crystallinity. Reactions R3, R8 and R12 illustrate that prolonged reaction times do not influence the degree of crystallinity. It is apparent that the most crystalline sample, reaction R7, had the longest reaction time (576 h), but from the crystallisation curve, crystallisation was completed long before the reaction was terminated. The DTA type is independent of the reaction time. No direct relationship between DTA type and the chemical composition of the product represented by SiO_2/Al_2O_3 and SiO_2/Na_2O is observed. However, it is remarkable that the Na_2O/Al_2O_3 ratio is close to unity (1.10, 0.99 and 1.02) for DTA type IV, with the charge generated by the alumina balanced by the Na. DTA type I shows Na_2O/Al_2O_3 < 1, (0.88) in three instances, but the remaining products show that

the Al_2O_3 is balanced by the Na_2O. The two reactions (R7 and DS3) with DTA type I and Na_2O/Al_2O_3 = 0.88 also show higher SiO_2/Na_2O ratios. In the latter reactions the TMA must balance the remaining charge. Reactions R2, R3 and R4, in which the order of mixing was investigated, show that the addition of TMABr (aq) before the base lowers the SiO_2/Na_2O ratio of the product:

Reaction	SiO_2/Na_2O	Order of Mixing
R2	6.38	TMA added before base
R3	6.68	TMA added after base
R4	6.73	Base added to silica

Addition of the base to the silica gives the highest SiO_2/Na_2O ratio. This suggests that the reaction commences before the reaction temperature is reached. Reactions R10 and R11 were prepared in the same manner, however crystallisation of reaction R10 is incomplete and shows much higher SiO_2/Al_2O_3 and SiO_2/Na_2O ratios than R11:

Reaction	Time/h	SiO_2/Na_2O	SiO_2/Al_2O_3
R10	72	7.32	6.81
R11	360	6.25	6.50

The XRF results for reaction R7, R8, R9 and R10, R11, R12 illustrate that for the same reaction composition, the order of mixing significantly alters the framework composition of the product.

REACTION	SiO_2/Na_2O	SiO_2/Al_2O_3	Na_2O/Al_2O_3	ORDER OF MIXING
R7	7.08	6.30	0.89	1Diol 2TMA added before base
R8	6.46	6.53	1.01	1Diol 2TMA added after base
R9	5.84	6.42	1.10	1Diol 2TMA added to silica before base
R10	7.32	6.81	0.93	2Diol 1TMA added before base
R11	6.25	6.50	1.04	2Diol 1TMA added before base
R12	6.13	6.37	1.04	2Diol 1TMA added after base

4.3.11 Summary

Investigation of the crystallisation of zeolite Ω from the optimum reaction composition with regard to:

(a) Order of mixing the reactants

(b) Partial replacement of TMABr by hexanediol

(c) Temperature of mixing the reactants

was most enlightening. For (a) little effect on the crystallisation rate and degree of crystallinity was observed. However mixing the TMABr before the base produced a higher pH reading throughout the crystallisation than when TMABr was added after the base and when the base was added directly to the dry silica.

The partial replacement of TMABr by hexanediol and order of mixing had a significant effect on the crystallinity. Mixing TMABr and hexanediol before addition of the base increased the crystallinity, compared with that mixed after addition of the base. Mixing 2TMABr and 1 hexanediol before addition of the base gave the most crystalline product, and mixing 1TMABr and 2 hexanediol after addition of the base gave the least crystalline product. Hexanediol addition had a significant effect on the gel pH throughout the crystallisation. Mixing 1TMABr and 2 hexanediol lowered the pH below that of the standard reaction and the reactions with 2TMABr and 1 hexanediol; addition of the organic mineraliser before the base gave the lowest pH values.

Temperature at which the reactants were mixed had a significant effect on the mechanism and products of the reaction. Mixing at 95°C changed the mechanism such that it proceeded via sodalite instead of the usual pure Ω observed when mixed at warm/room temperature. Mixing this composition at low temperatures favours Ω crystallisation while at high temperatures sodalite crystallisation is favoured with a considerably

increased induction period for Ω . The sodalite produced is probably a mixture of TMA-sodalite and hydroxysodalite. A mechanism for the formation of faulted Ω , based on the presence of the sodalite species in the reaction mixture, is proposed.

The crystallisation of 3 reactions for pure Ω , monitored by XRD, pH and thermal analysis showed that crystalline structure detected by thermal analysis was amorphous to X-rays.

Thermal analysis of the final products obtained lead to five DTA types, four of which were due to pure Ω and type V probably due to a mixture of TMA-sodalite and Ω . The four DTA types for pure Ω exhibited a small exotherm centred at ~360°C due to surface adsorbed TMA and an exotherm centred at ~600°C. In types I and II this exotherm is sharp with an associated weight loss of approximately 3.0% to 5.0%. In types III and IV the exotherm is small and broad with a reduced associated weight loss. Types I, III and IV exhibit an additional exotherm at ~ 520°C which has a large associated weight loss for type IV. Type IV is distinguished from the DTA types by the presence of a large exotherm at ~1000°C with no associated weight loss.

No direct relationship between the DTA type, chemical composition, crystallinity and reaction time was found, although the order of mixing was observed to influence the framework composition.

Thus the gel preparation for this reaction composition, and zeolite synthesis in general, is the most crucial factor which governs the mechanism, crystallisation rate, crystallinity, framework composition and the product produced.

REFERENCES

1. B. M. Lowe, A. Araya, T. J. Barber, D. S. Sinclair, and A. Varma, Zeolites, 1984, 4, 263.

2. E. Galli, E. Passaglia, D. Pongiluppi and R. Rinaldi, Contr. Min. and Petrol., 1974, 45, 99.

3. Mobil, United States Patent 4 091 007, 1978.

4. Union Carbide, United States Patent 4 241 036, 1980.

5. B. M. Lowe and J. L. Casci, Zeolites, 1983, 3, 186.

6. G. T. Kokotailo, A. C. Rohrman and S. Sawruk, 5th International Conf. on Zeolites, Naples 1980, Recent Progress Reports and Discussion, 1981.

7. B. M. Lowe and A. Varma, Unpublished work.

8. Mobil, British Patent 1 117 568, 1968.

9. Cab-O-Sil - Manufacturers' literature.

10. J. F. Cole and H. W. Kouwenhoven, Adv. Chem. Series, 1973, 121, 583.

11. V. Penchev, Ch. Minchev, V. Kanazirev, O. Pencheva, N. Borisova, L. Kosova, H. Lechert and H. Kacirck, Zeolites, 1983, 3, 249.

CHAPTER FIVE

Thermal Properties of Zeolite Ω with particular reference to the Effect of Contact with Water

5.1 Introduction

The reactions examined in the previous chapter lead to the discovery of four DTA types for pure zeolite Ω. These are illustrated in Fig. 5.1. The exothermic peak centred around 600°C is attributed to oxidative degradation of TMA in the gmelinite cages [1-7]. Cole [3] identified the exotherm centred at ~350°C, which extends to ~ 480°C as TMAOH or silicate occluded in the main channel of Ω. However, DTA types I, III and IV obtained in this work have resolved the single peak into two exotherms. A possible cause of these exotherms (excluding exotherm (G))is the adsorption of contaminants from the reaction mixture on to the external surface of the crystals.

It was therefore decided to investigate the effect of calcination on these exotherms for a sample which exhibited type I DTA. The effect of contacting the as synthesised sample of DS3 with water at room temperature and 70°C was also investigated. The time of contact with water, volume of contact water and prolonged hydrothermal treatment were also studied.

The 'washing' process was extended to as synthesised samples of Ω which exhibited DTA types II, III and IV so as to ascertain whether the observed effects are characteristic of Ω or unique to individual samples.

The effects of calcination and the washing process were examined by DTA, TG and XRD.

The four DTA Types for Zeolite Ω

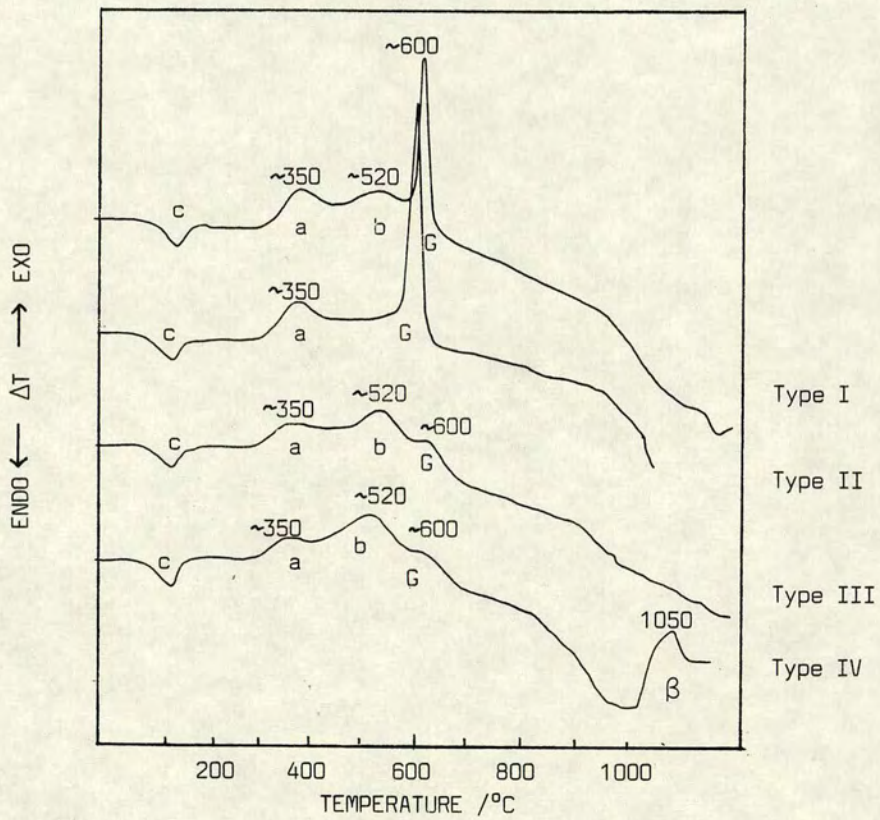

Fig. 5.1

Simple experiments to help elucidate the location of the organic species were devised in order to assist the interpretation of the DTA curves.

The understanding of the 'washing' process which may affect the properties of the zeolite, is an essential pre-requisite to studies of sorption by Ω from aqueous solution.

5.2 Experimental

5.2.1 Materials

The samples of Ω which exhibited DTA type I, II, III and IV behaviour were:

DS2, DS3 [8]	-	type I
R15	-	type II
R1, DS13 [8]	-	type III
R9	-	type IV

TMABr was obtained from Aldrich Chemical Company. Precipitated silica was from BDH Chemicals. Glass distilled water was used for all experiments.

5.2.2 Procedure

5.2.2.1 Calcination of Samples with Type I DTA

The removal of the exotherms exhibited in the DTA curves and the determination of the thermal stability was carried out as follows:

Samples of DS3 were placed in silica crucibles and calcined for 3 to 16 h at temperatures chosen by examination of the DTA and TG curves. The samples were equilibrated with water vapour in the usual manner, prior to analysis by DTA, TG and XRD.

5.2.2.2 Effect of Water on Zeolite Ω with Type I DTA

(a) Preliminary Water Contact Experiments

The effect of contact of the as synthesised material with water was carried out in the following manner:

Samples of DS3 (2 g) were contacted with water (100 cm^3) at room temperature for 2 h, at 70°C for 3 h, at 70°C for 24 h and also at 70°C for 7 days. The 70°C contact was carried out in a conical flask fitted with a condenser and stirred with a PTFE coated magnetic follower. The samples were filtered through a Büchner funnel, dried in an oven at 110°C, and equilibrated with water vapour, by the normal procedure, prior to analysis by the aforementioned techniques.

(b) Detailed Investigations

The effect of time of contact with water, volume of contact water and prolonged hydrothermal treatment were carried out as described below.

The as synthesised Ω, DS3 (0.25 g) was placed in a beaker to which water (100 cm^3) at room temperature (19°C) was added. The contents were left undisturbed for 3 minutes and then filtered through an ultra-filter. The procedure was repeated for various periods ranging from 5 to 60 minutes. The total time of contact with water was recorded as the sum of the time left stationary and that taken for completion of filtration.

Prolonged hydrothermal treatment was carried out by placing the as synthesised material (0.25 g) in a conical flask to which water (100 cm^3) was added; the apparatus was set up for reflux with stirring. Four more were set up in this manner and left for periods of 7, 11, 14, 21 and 28 days. Another reflux was set up with zeolite Ω (0.25 g) placed in the conical flask to which water (500 cm^3) was added and left

stirring for 11 days. This was to determine any effects arising from increased volume of contact water. The contents of the flask were filtered using the ultrafilter. The effect of pouring a known volume of water (500 cm^3) over DS3 (0.25 g) on the ultrafilter at room temperature was investigated to observe any difference in running water compared with stationary water.

All the samples were dried at 110°C, prepared and analysed in the usual manner.

(c) Effect of Water on DTA types I, II, III and IV

In order to determine whether the effects of contact with water exhibited by type I DTA were characteristic of zeolite Ω , samples of the four DTA types were contacted with water for various periods of time in the aforementioned manner.

(d) Investigation of "Spurious" Peaks in XRD Pattern

An investigation of the effect of carrying out the reaction in glass and plastic flasks, stirred with PTFE and plastic coated magnetic followers was carried out to assist the identification of the cause of an additional peak in the XRD pattern of DS3 effected by preliminary water contact at 70°C for 1 week.

A series of experiments in which a sample of Ω was refluxed with water in both pyrex glass and plastic flasks was set up. The mixture was stirred with plastic or PTFE coated magnetic followers, or left unstirred. In each case the procedure was carried out for 7 days. The samples were filtered through an ultrafilter and prepared for analysis.

A sample of Ω was placed in contact with PTFE tape in an oven at 95°C for 7 days, and subsequently subjected to analysis by XRD. Also a

sample of PTFE tape, which had been stretched to increase the ordered structure was X-rayed.

The aqueous solution which had been in contact with the zeolite was in some instances analysed for the presence of the anions: bromide, silicate and aluminate using silver nitrate solution, ammonium molybdate solution and aqueous ammonia solutions respectively. The alkalinity of the solutions were measured by pH or indicator paper and analysed for sodium ions by a simple flame test.

5.2.2.3 Location of Organic Species

Observation of the oxidative degradation of TMA in an environment similar to that of a zeolite, but in which the organic cation was not encapsulated in a cage (c.f Ω) was carried out by the following procedure. An 8% TMA/SiO_2 mixture (1 g) i.e. approximate organic content of zeolite Ω , was prepared by mixing precipitated silica (0.92 g) with TMAOH solution (0.4 g) to which a small amount of water was added to enable thorough mixing. This mixture was left to dry on top of the oven (110°C) and then subjected to DTA.

A sample of the as synthesised DS3 was calcined for 3 h at 625°C; analysis by DTA and TG showed it to be free from organic material, and XRD showed it to be crystalline. A sample of the calcined material (0.5 g) was soaked in IM TMABr solution at room temperature for 20 days. This species, labelled TMABr-cal- Ω was filtered and thoroughly washed with distilled water over a Büchner funnel until the washings were free of bromide. It was then dried in an oven at 110°C and prepared and analysed in the usual manner.

5.3 Results and Discussion

The results are tabulated in tables 5.1 to 5.26 and illustrated in Figs. 5.2 to 5.21.

5.3.1 Calcination of DS3-Type I DTA

A sample of Ω , DS3, which exhibited type I DTA was subjected to calcination in order to remove the exotherms. The presence of exotherm (a) was believed to be due to contaminants adsorbed on the crystal surface. The calcination temperatures employed and the corresponding effect on the XRD peak heights (2θ = 9.75° and 23.4°) are recorded in Table 5.1 and illustrated in Fig. 5.2. The changes in DTA and TG curves are shown in Fig. 5.3 and 5.4 and the corresponding data is recorded in Tables 5.2 and 5.3.

Complete removal of the organic material as evidenced by the disappearance of the exotherms, is achieved by 625°C (see Figs. 5.3 and 5.4). Evidence for the interpretation of the observed heat change in the DTA curve at ~ 316°C, as an endotherm is provided by this sample. Since total removal of the organic material is accomplished by 625°C, then the only practical interpretation of the weight loss which is associated with a heat change in the DTA is the evolution of water. Thus, this broad exotherm must be caused by the evolution of water from the small pores of the zeolite over a period of time. This water takes time to diffuse out and this process is probably not just a temperature controlled effect, but one which is also time dependent. The sharp endotherm centred at ~85°C, corresponds to the main water loss, and is associated with evolution of water from the main 12 ring channel. The initial rapid weight loss is probably due to loss of loosely bound water from the crystal surface.

Calcination at 550°C did not effect complete removal of the organic material. Although no exotherm is discernible in the DTA curve, the TG curve showed a small change in gradient from ~572°C to ~790°C with an associated weight loss of 1.5%. This suggests the presence of trace amounts of TMA in the gmelinite cage. Perhaps prolonged calcination at this temperature would have effected complete removal of the organic

Effect of Calcination Temperature on Crystallinity of Zeolite Ω

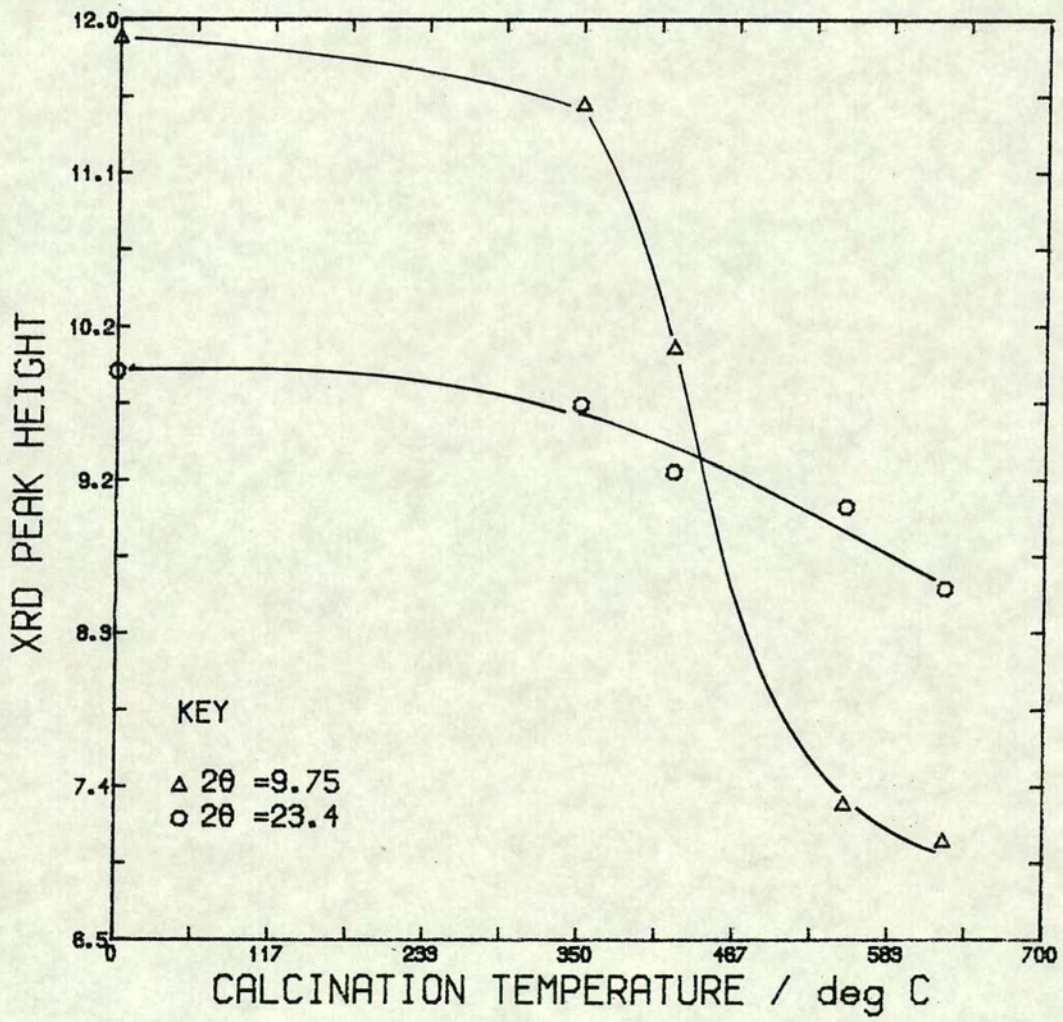

Fig. 5.2

Calcination of Type I DTA, Sample DS3
compared with the As Synthesised material

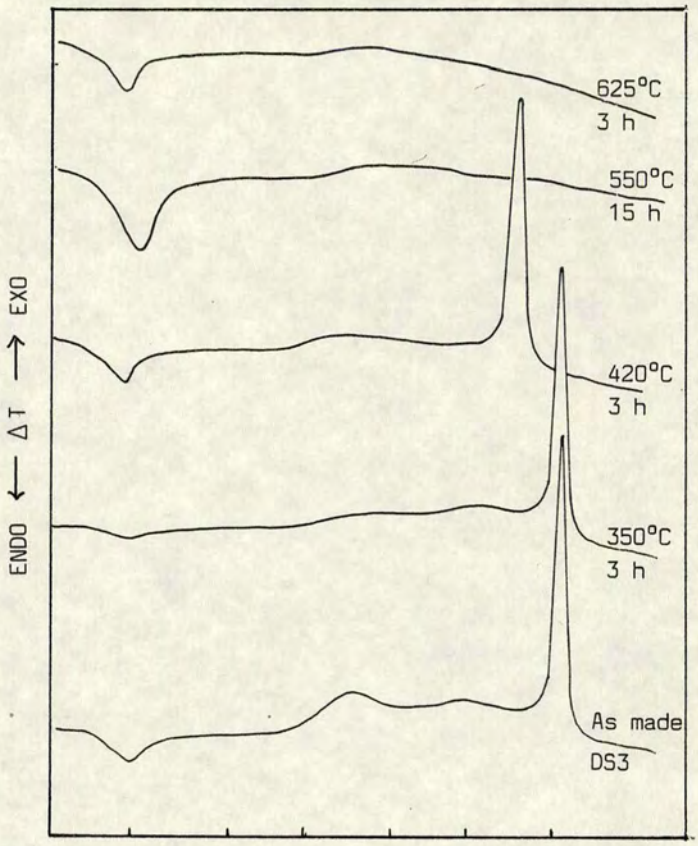

Heating rate 5°C min^{-1}

Fig. 5.3

TG Curves of Calcined DS3 compared with
As Synthesised material

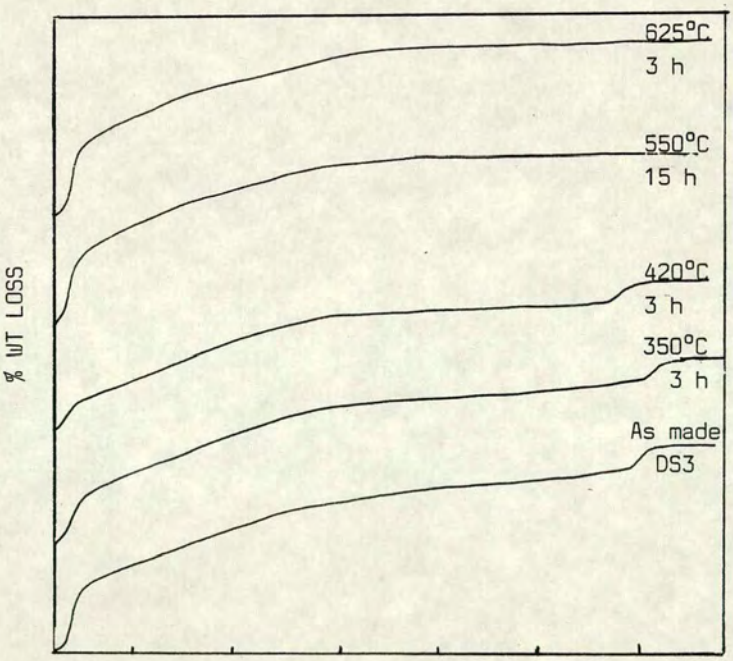

Heating rate 5°C min^{-1}

Fig. 5.4

Table 5.1

Effect of Calcination Temperature on DS3:XRD Pattern

CALCINATION TEMPERATURE /°C	DURATION OF CALCINATION /h	XRD PEAK HEIGHT /cm	
		2θ = 9.75	2θ = 23.4
As made	-	9.9	11.9
350	3	9.7	11.5
420	3	9.3	10.05
420	8	8.9	9.50
550	16	9.09	7.32
625	3	8.60	7.1

Table 5.2

Effect of Calcination Temperature on DS3:DTA Exotherms*

CALCINATION TEMP /°C	(a) EXO PEAK TEMP /°C	% WT LOSS EXO PEAK RANGE	(b) EXO PEAK TEMP /°C	% WT LOSS EXO PEAK RANGE	EXO PEAK TEMP /°C	% WT LOSS EXO PEAK RANGE	(G) EXO PEAK TEMP /°C	% WT LOSS EXO PEAK RANGE
As made	347	2.3	492	1.0			602	3.8
350	357	1.3	497	0.8			600	3.6
420 (3 h)	-	-			583			
420 (8 h)	372	1.5	-	-	592	4.0	-	-
550	-	-	-	-	-	-	-	-
625 (3 h)	-	-	-	-	-	-	-	-
625 (16 h)	-	-	-	-	-	-	-	-

*Heating rate 5°C min^{-1}

Table 5.3

Effect of Calcination Temperature on DS3:DTA Endotherms

CALCINATION TEMP	TEMP /°C ENDO OR EXO PEAK	TEMP /°C ENDO OR EXO PEAK	WT LOSS IF ENDO / %	WT LOSS IF EXO /%	ENDO PEAK TEMP /°C	WT LOSS OVER ENDO PEAK /%
As made	273		5.9	-	80	11.3
350	283		6.5	-	77	9.5
420 (3 h)	275		8.5	-	85	5.4
420 (8 h)	287	372	7.5	1.5	95	7.3
550	320	395	6.0	0.3	100	14.5
625 (3 h)	316	382	7.8	0.5	85	10.8
625 (16 h)	318	390	5.5	0.3	97	10.3

material.

Calcination at 420°C (3 h) caused a shift to lower temperature of exotherm (G) and probably removed exotherm (a). A similar result was obtained when this was repeated for a longer period (8 h). Comparison with the as synthesised material shows an overall decrease in organic content and thus partial TMA removal was achieved. It is noted that exotherm (a) recorded a 1.5% weight loss, a reduction of 0.8%, and exotherm (G) had a weight loss of 4.0%, an increase of 0.2%. It therefore appears that not only was TMA decomposed, but also redistributed.

Calcination at 350°C appeared to have removed exotherm (a) from the DTA curve, but a weight loss of 1.3% over the temperature range for this peak was observed. Comparison with the as synthesised material shows that only 1% of the organic material was decomposed. The decrease in the water content is unaccountable.

The effect of calcination on crystallinity (Fig. 5.2) shows that partial removal of the exotherm (a) occurs at the onset of structural changes in the framework. Complete removal of the organic material caused a significant decrease in the crystallinity. Total collapse of the structure, by calcination, has been recorded by Lowe et al [7].

5.3.2 Effect of Water on DS3 - Preliminary Studies

Removal of the surface contaminants was attempted by further washing with water. The effects were evaluated by DTA and TG and are illustrated in Figs. 5.5 and 5.6.

Contact with water at room temperature for only 2 h caused the shift of exotherm (G) from 602°C to the lower temperature of 550°C. Treatment with hot water at 70°C shifted the peak to the lower tempera-

Effect of Water on DS3: DTA Curves

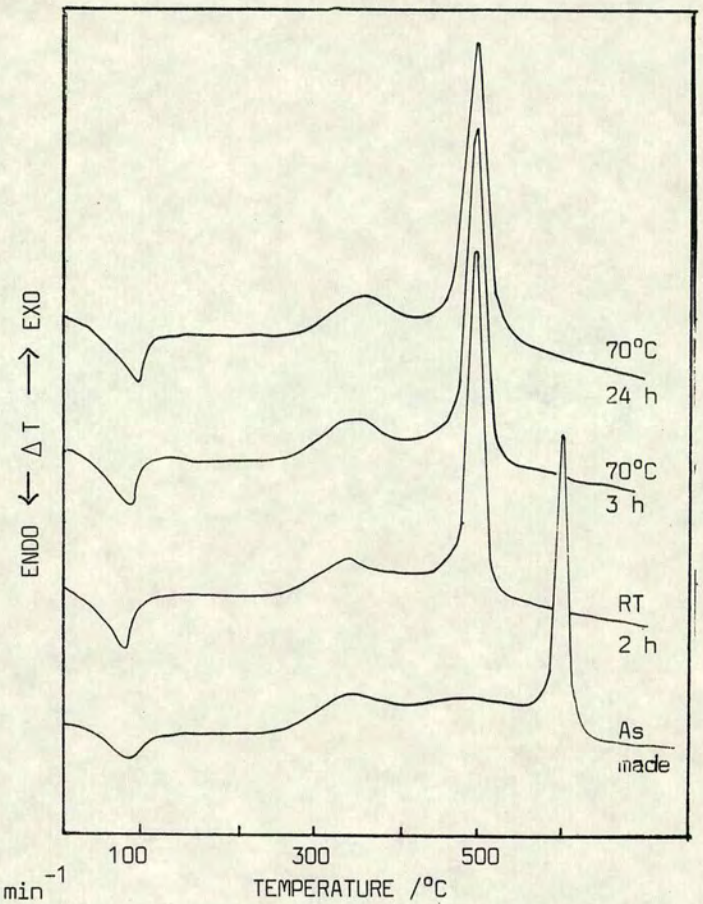

Heating rate 5°C min^{-1}

Fig. 5.5

Effect of Water on DS3 : TG Curves

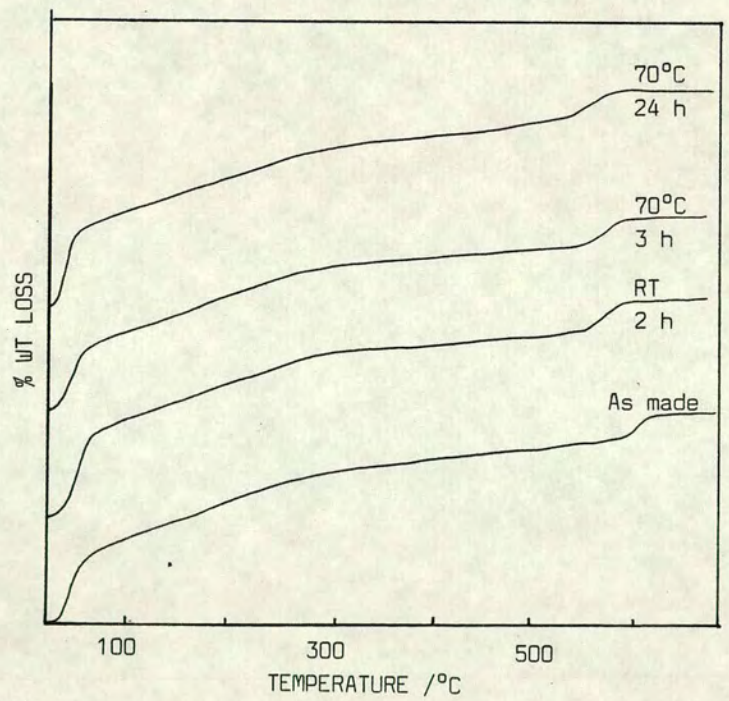

Heating rate 5°C min-1

Fig. 5.6

ture of 535°C after 24 h. Exotherm (a) is shifted/removed/replaced by a higher temperature exotherm centred at 372°C after treatment with cold water, and 389°C after treatment with hot water. The weight changes associated with the exothermic process (Table 5.4) compared with the as synthesised material show that exotherm (a) which, when shifted/removed to a new site shows a decrease in weight from 2.3% to 1.1%. The exotherm (G) when shifted to lower temperature shows an increase in weight loss from 3.8% to 5.0%. This weight is probably a combination of exotherm (G) and exotherm (b) and some from exotherm (a). Thus mere washing with water appears to have caused redistribution of TMA in the zeolite.

This washing process also affects the endothermic process. An increase in intracrystalline water (5.9% to 7.5%) in the small pores is observed, however the water attributed to the main channel and surface remains virtually constant (Table 5.5).

Although a dramatic change in the DTA curve is observed as a result of the washing process, there is little detectable change in the structure as evidenced from XRD (Table 5.6), however a sharper XRD pattern is obtained.

5.3.3 Detailed Investigation of the Effects of Water on DS3

A detailed investigation of the effect of water on DS3 was launched to ascertain whether or not the shift of exotherm (G) and removal/shift of exotherm (a) was time dependent and affected by the temperature and amount of water used.

In all the experiments on DS3, the volume of contact water was 100 cm^3 unless otherwise stated.

Table 5.4

Effect of Water on DS3: DTA Exotherms*

SAMPLE	(a) EXO PEAK TEMP /°C	% WT LOSS OVER PEAK RANGE	(b) EXO PEAK TEMP /°C	% WT LOSS OVER PEAK RANGE	EXO PEAK TEMP /°C	% WT LOSS OVER PEAK RANGE	(G) EXO PEAK TEMP /°C	% WT LOSS OVER PEAK RANGE
DS3	347	2.3	492	1.0	-	-	602	3.8
DS3 (19°C, 2 h)	372	1.2	-	-	550	5.0	-	-
DS3 (70°C, 3 h)	385	1.1	-	-	545	5.4	-	-
DS3 (70°C, 24 h)	389	1.4	-	-	535	5.0	-	-

* Heating rate = 5°C min^{-1}

Table 5.5

Effect of Water on DS3: DTA Endotherms

SAMPLE	ENDO PEAK TEMP /°C	% WT LOSS OVER PEAK RANGE	ENDO PEAK	% WT LOSS OVER PEAK RANGE	ENDO PROCESS TOTAL WT LOSS/%
DS3	80	11.3	broad	5.9	17.1
DS3 (19°C, 2 h)	87	12.1	broad	7.4	19.5
DS3 (70°C, 3 h)	95	10.5	broad	7.3	17.8
DS3 (70°C, 24 h)	102	11.3	broad	7.8	19.0

Table 5.6

Effect of Water on DS3: XRD Patterns

SAMPLE	TEMP OF WATER /°C	DURATION OF CONTACT /h	XRD PEAK HEIGHT /cm 2θ = 9.70°	2θ = 23.40°
As made	-	-	9.90	11.90
DS3 (19°C, 2 h)	19	2	10.08	12.30
DS3 (70°C, 3 h)	70	3	10.10	12.20
DS3 (70°C, 24 h)	70	24	10.29	12.30

5.3.3.1 Exothermic Peak Shift brought about by Treatment with Water at Room Temperature

When DS3 is contacted with water, exotherm (G) is shifted to lower temperatures. The as synthesised material is taken as zero water contact time. Contact of DS3 with water for only 3 minutes (total contact time 6 minutes i.e. including period for filtration) shifted exotherm (G) from 625°C to 583°C (Fig. 5.7), a position between that of the original exotherm (G) and exotherm (b). Also exotherm (a) at 369°C was shifted/removed with the advent of an exotherm centred at 405°C, this will be designated exotherm (M). Table 5.7 and Fig. 5.8 show that increase of time of contact with water results in a gradual shift of exotherm (G) to 570°C. After 45 minutes the exotherm has attained its minimum temperature as is indicated by constant peak temperature reading after 8 days. After 8 days, this peak is considerably broadened suggestive of reduced localisation of TMA in the gmelinite cage.

The removal/shift of exotherm (a) is effected within a maximum time of 6 minutes (see Table 5.8 and Fig. 5.7); and another exotherm appears at 405°C (M). This peak temperature is seen to fluctuate slightly between 405-398°C which is suggestive of movement and indicative of an equilibrium. The percentage weight loss due to each exotherm as determined by TG analysis is given in Table 5.9. (The additional weight loss in the final column is that which occurs between the completion of the exotherm (M) and commencement of exotherm (G)-temperatures according to DTA.) From Table 5.9, the as synthesised material (time of contact = 0) shows weight loss of 3.3% in exotherm (G) and weight loss of 1.5% in exotherm (b). All the other species show a weight loss of ~4.8% due to TMA in the gmelinite cage (exotherm (G)). Summation of the weight loss due to exotherm (G) and (b) in the as synthesised material gives 4.8% and hence it appears that the

Differential Thermal Analysis Curves
Illustrative of Peak Shift with
treatment in Water

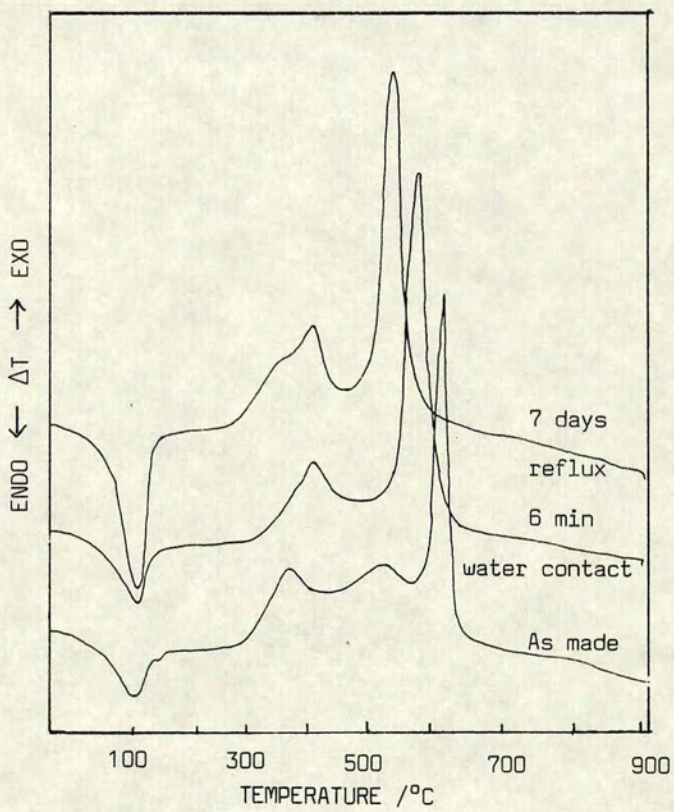

Fig. 5.7

Change in Temperature of
Exotherm (G) Peak
brought about by Contact with Water
at Room Temperature

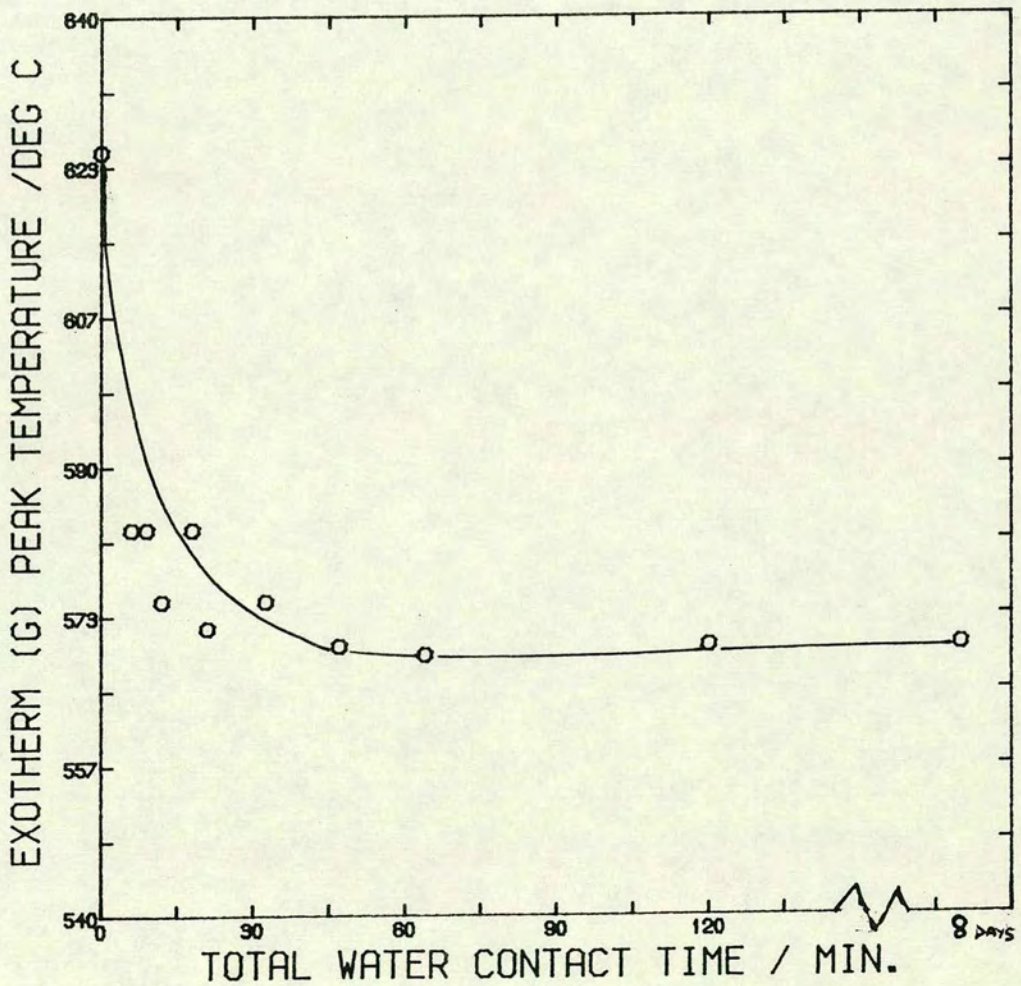

Fig. 5.8

additional weight loss added to the final column should have been included with exotherm (M) which then gives an approximately constant weight loss of 1.8%. (This becomes more obvious in the hydrothermal results.)

The weight loss due to the oxidative degradation of TMA in the gmelinite cage, in the as synthesised material is only 3.3%, whereas in the water contacted species it is 4.8%. This therefore suggests either TMA from another site is capable of entering the gmelinite cage or 2 types of organic nitrogen material are already present which are evolved at 528°C and 625°C, and contact with water converts it to the same material giving rise to only one broadened peak. The first suggestion is virtually impossible from the structural point of view, i.e. without causing damage to the framework. XRD does not indicate structural change and so if the latter does occur, structural damage remains undetected (Table 5.10) and thus unlikely. Hence if there is movement, it occurs without damage to the lattice - unless the lattice already contains imperfections additional to the stacking faults. This is a possibility since the degree of crystallinity of DS3 is less than some other samples of Ω. If imperfections are present in the lattice, they are such that the TMA has increased freedom of movement than would be possible in a framework free from additional defects. The second suggestion of the initial presence of two types of organic nitrogen species, which subsequently convert to the same species implies decay of TMA as a result of attack by water according to the equation:

$$(CH_3)_4N^+ + H_2O \longrightarrow (CH_3)_3N + CH_3OH + H^+$$

i.e. partial hydrolysis had already occurred and further hydrolysis of TMA is effected by contact with water. However, the literature cited on tetramethylammonium salts in aqueous solution [9] does not mention

Table 5.7

Variation of Exotherm (G) Peak Temperature with Time of Contact with Water at Room Temperature

TIME IN WATER /min	TOTAL WATER CONTACT TIME /min	EXO (G) PEAK TEMP/°C
0	0	625
3	6	583
5	9	583
7	12	575
10	21	572
15	18	583
30	32.5	575
45	47	570
60	64	569
120 (stirred)		570
8 days		570

Table 5.14b

Variation of Exotherm (G) Peak Temperature with Time of Contact under Reflux

DURATION OF REFLUX IN 100 cm^3 WATER /Days	EXO (G) PEAK TEMP/°C
0	625
1	562
7	537
11	539
14	530*
21	536
28	535

* F.S.D. on chart recorder set a T = 20 mV (all other readings T = 10 mV) hence error in temperature reading increased.

Table 5.8

Observed Exothermic Peak Temperatures
With Time of Contact With Water at Room Temperature

TOTAL TIME OF WATER CONTACT /min	TEMPERATURE OF OBSERVED EXOTHERM /°C (G) 1st	(G) 2nd	(G) 3rd
0	369	528	625
6	405	583	
9	400	583	
12	402	575	
21	397	572	
18	397	583	
32.5	395	575	
47	392	570	
64	392	569	
120	403	570	
8 days	398(b)	570	

Table 5.14a

Observed Exothermic Peak Temperatures
With Time of Contact Under Reflux

DURATION OF REFLUX IN 100 cm^3 H_2O /Days	TEMPERATURE OF OBSERVED EXOTHERM /°C (a)	(M)	(G)
0	369	528	625
1		402	562
7	362 (S)	410	537
11	357	435 (vb)	539
14	365 (S)	390	530
21	-	432	536
28	357 (S)	418	535

(S) = Shoulder (b) = broad (vb) = very broad

Table 5.9

Time of Water Contact at Room Temperature and Weight Loss due to each Exotherm

WATER CONTACT TIME/min	EXO TEMP RANGE /°C	WEIGHT LOSS/%	EXO (b) EXO TEMP RANGE /°C	EXO (b) WEIGHT LOSS/%	EXO (G) EXO TEMP RANGE /°C	EXO (G) WEIGHT LOSS/%
0	290-415	1.8	448-569	1.5	569-652	3.3
6	308-445	1.3			485-635	4.9 + 0.3
9	312-430	1.0			495-635	4.6 + 0.4
12	300-460	1.4			487-635	4.8 + 0.4
21	303-455	1.4			490-623	4.8 + 0.3
18	305-455	1.6			502-630	4.6 + 0.3
32.5	292-445	1.5			490-617	4.5 + 0.3
47	295-447	1.4			480-620	4.8 + 0.3
64	302-445	1.5			480-612	4.8 + 0.3
120	303-485	1.9			485-625	5.0
8 days	282-448	1.7			482-615	4.6 + 0.3

Additional weight loss (~0.3%) is that incurred between completion of first exotherm and commencement of next exo as determined by DTA.

Table 5.11

Total Weight Loss with Time of Water Contact at Room Temperature

WATER CONTACT TIME/min	TOTAL WEIGHT LOSS DUE TO EXOTHERMIC PROCESS /%
0	6.5
6	6.4
9	6.0
12	6.4
21	6.3
18	6.5
32.5	6.3
47	6.3
64	6.4
120	6.9
8 days	6.5

the decomposition of TMA to trimethylamine. It may be that some of the trapped TMA is present as TMAOH, and it is perhaps possible that the reaction below occurs:

$$(CH_3)_4N^+ + OH^- \longrightarrow (CH_3)_3N + CH_3OH$$

and that this is catalysed by the zeolite, and assisted by the presence of water.

The total organic content in the sample used appears to vary (Table 5.11) although Table 5.9 indicates that the organic content of the gmelinite cage is virtually constant. The variation of the total organic content may be attributed to the sample being non uniformly washed.

The effect of 'washing' the zeolite over the filter funnel with a fixed volume of cold water (500 cm^3) was also investigated. The DTA showed exotherm (G) at 570°C with an associated weight loss of 5.0% and exotherm (M) at 415°C (1.5%). The filtration time required was > 1 h and so exotherm (G) had attained its minimum temperature under these conditions (see Table 5.12, Fig. 5.9, and 5.10).

Shift of exotherm (G) showed virtually no effect on the structure as evidenced by XRD (Tables 5.13 and 5.10). However a slight increase in the observed intensity at $2\theta = 23.46°$ and slight variation in peak angle is noted, but this may be due to the packing of the zeolite in the XRD holder. Overall, any effect on XRD may be considered absent.

5.3.3.2 Hydrothermal Effect

The effect on the DTA curve as a result of refluxing DS3 in water for 7 days compared with the as synthesised material is illustrated in Fig. 5.7. It shows that exotherm (G) is shifted to the lower temperature of 537°C which is virtually coincident with exotherm (b) in the

Effect of Temperature and Volume of contact water on Exothermic Peak Position

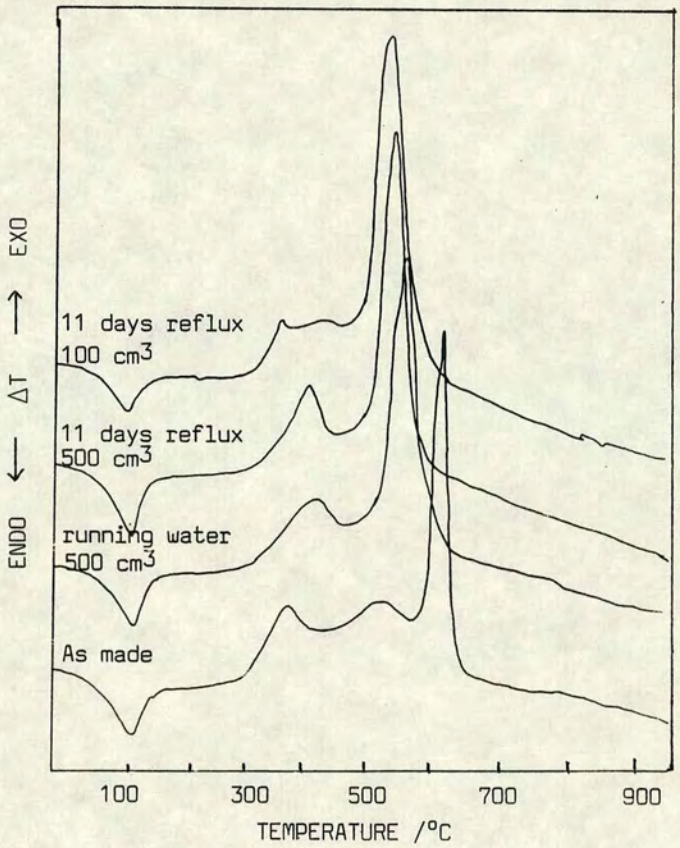

Heating rate
10°C min-1

Fig. 5.9

Effect of Temperature and Volume of contact water on Weight Loss Curves

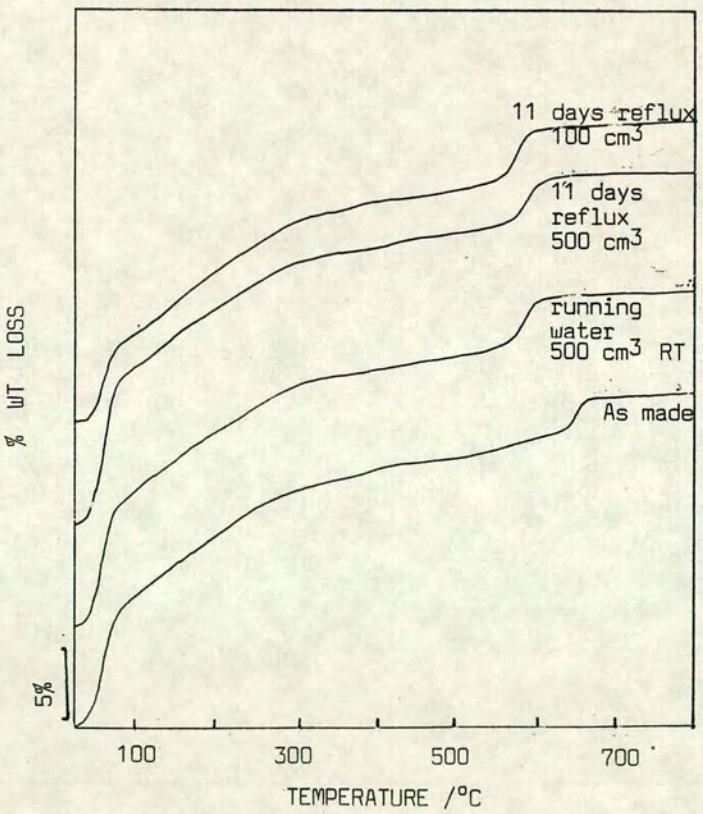

Heating rate
10°C min-1

Fig. 5.10

Table 5.10

Effect of Water Contact Time on XRD Pattern

WATER CONTACT TIME /MIN	XRD			
	2θ /°	ABSOLUTE INTENSITY /cm	2θ /°	ABSOLUTE INTENSITY /cm
0	9.75	9.46	23.46	10.90
6	9.80	9.90	23.56	11.59
9	9.76	9.00	23.46	11.30
12	9.69	9.45	23.39	11.12
21	9.77	9.90	23.49	11.70
8 days	9.72	9.22	23.42	11.10

Table 5.17

Effect of Duration of Reflux on XRD Pattern

DURATION OF REFLUX IN 100 cm^3 WATER /DAYS	XRD			
	2θ /°	ABSOLUTE INTENSITY /cm	2θ /°	ABSOLUTE INTENSITY /cm
0	9.75	9.46	23.46	10.90
7	9.87	9.40	23.52	11.50
11	9.69	9.40	23.42	11.08
14	9.72	9.50	23.42	11.40
21	9.77	9.26	23.51	11.71
28	9.67	9.20	23.37	11.29

Table 5.12

Effect of Volume of Contact Water on Exotherm Temperatures

VOLUME OF WATER /cm^3	EXO TEMP RANGE /°C	WEIGHT LOSS /%	EXO TEMP RANGE /°C	WEIGHT LOSS /%	EXO TEMP RANGE /°C	WEIGHT LOSS /%
11 days, 100	317-370	0.8	370-458	0.8	458-608	5.0
11 days, 500	305-437	1.5			467-587	4.8 + 0.3
Running Water, 500 at Room Temp	303-445	1.5			482-635	5.0

Table 5.13

Effect of Volume of Contact Water at Reflux Temperatures on XRD Pattern

DURATION OF REFLUX IN WATER /DAYS	XRD			
	2θ /°	ABSOLUTE INTENSITY /cm	2θ /°	ABSOLUTE INTENSITY /cm
0	9.75	9.46	23.46	10.90
11 (100 cm^3)	9.69	9.40	23.42	11.08
11 (500 cm^3)	9.67	8.61	23.42	10.47

as made material. (A better illustration is given in Fig. 5.14.) Reference to Table 5.14b and Figs. 5.12 shows that heating at 70°C for 1 day does not effect complete shift of exotherm (G). After 7 days it is shifted to its ultimate position (at reflux temperature) which is retained for 21 days. The base of exotherm (G) is much broader than is observed in both the as synthesised and 6 minutes water contact species. It is considerably further broadened as a result of prolonged reflux for 28 days. The weight loss associated with exotherm (G) under reflux conditions (Table 5.15) appears to fluctuate from 4.8% to 5.5%. The value of 5.5% is that obtained after 14 days, all other values do not exceed 5.1%. The TG curves for 14 days reflux (Fig. 5.13) show that the TMA is evolved in 3 distinct stages with an increase in the amount in exotherm (M) compared with other time periods. The results are again suggestive of movement of the organic material into the gmelinite cage and other sites, namely the 12 ring channel. This is further supported from the appearance of the DTA curves in Fig. 5.11 and peak temperatures in Table 5.14a. The result of 11 days reflux shows almost total loss of resolution of exotherm (M) and occurs at a higher temperature of 435°C compared with the others; the 21 days reflux shows exotherm (M) at 432°C and is almost blended in with exotherm (G).

After 7 days reflux, exotherm (M) is well resolved and occurs at 410°C (Fig. 5.11). A variable shift in this peak temperature and variable degree of resolution with duration of reflux is apparent. Thus it appears that movement of the organic material occurs and perhaps an equilibrium is set up. Consequently the associated weight loss due to the said exotherm is variable (Table 5.15).

A distinct shoulder is discernible after 7 days which occurs at 362°C, after 14 days it occurs at 365°C and after 28 days at 357°C. These

Effect of Duration of Reflux in Water
on DTA curves of DS3

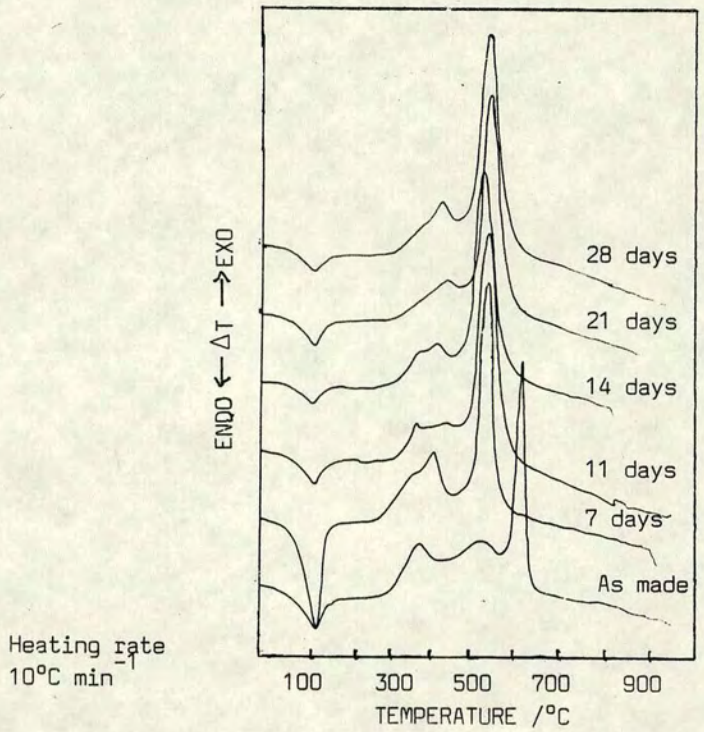

Fig. 5.11

Effect of Duration of Reflux in Water
on TG Curves

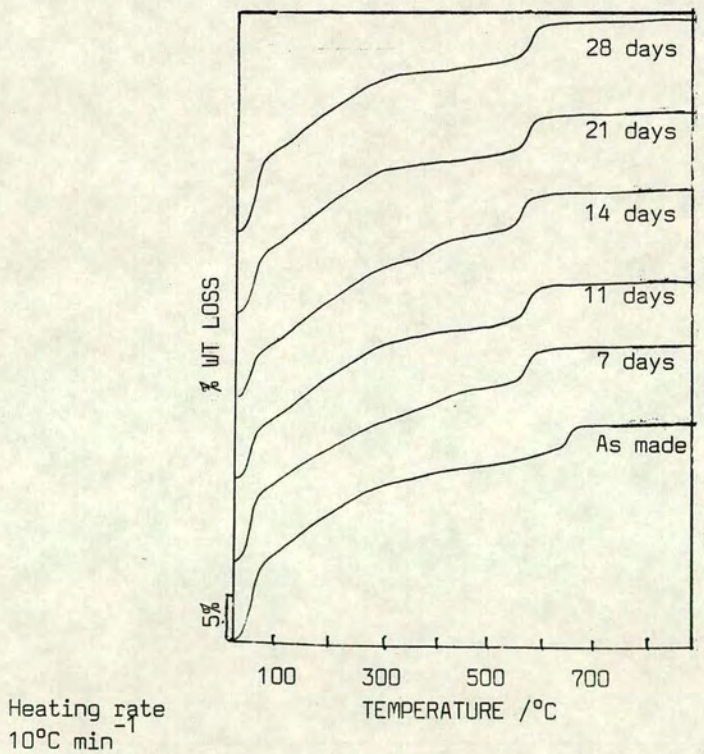

Fig. 5.13

Change in Temperature of
Exotherm (G) Peak
brought about by treatment
under Reflux Conditions

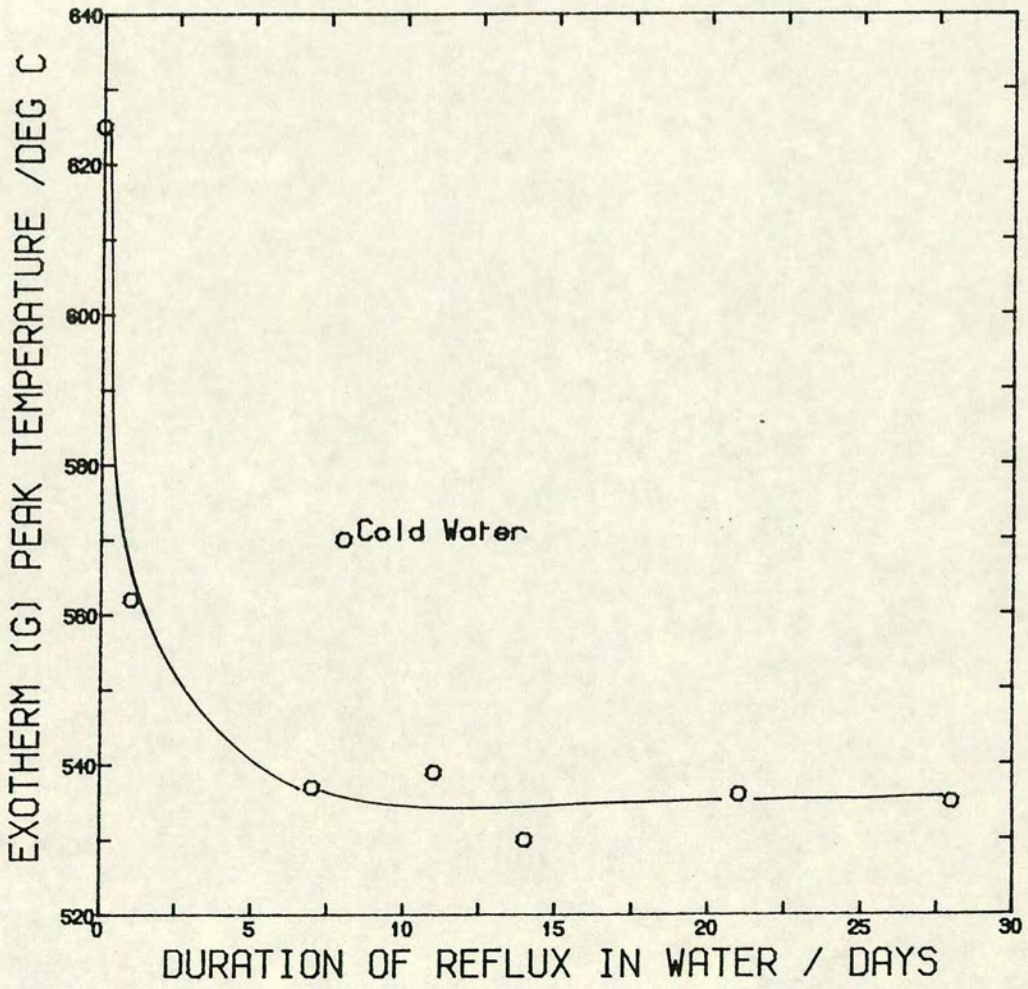

Fig. 5.12

temperatures are coincident with exotherm (a) of the as made material at 369°C. The sample after 1 and 21 days displayed no shoulder, however, the exotherm (M) peak is very broad (Figs. 5.11 and 5.5). After 11 days a sharp exotherm is observed to occur at 357°C as opposed to a shoulder which is attributed to the same cause (as yet not accounted for) as in the as synthesised material. The weight loss due to each exotherm with duration of reflux is given in Table 5.15, this shows variable weight loss with fluctuation in the exotherm range. The total weight loss for the exothermic process (Table 5.16) is virtually constant except for 7 and 14 days reflux which show 8.5% to 8.8% compared with 6.5% for the other species.

The volume of contact water used under reflux conditions produced a marked difference in the DTA curve after 11 days (Table 5.12, Fig. 5.9). Exotherm (M) at 405°C is very well resolved in 500 cm^3 water whereas a broad stretch is observed in 100 cm^3 water. There appears to be little difference between the exotherm (M) resulting from contact with running cold water (500 cm^3) over the filter funnel and 11 days at reflux temperature, albeit exotherm (G) shift is greater under reflux than in running cold water. These results are suggestive of a more dramatic effect as a result of a decrease in the volume of contact water.

XRD on all the samples, in an attempt to observe any structural damage showed only slight variation in intensity (increase in peak height $2\theta = 23.46°$) - Tables 5.17 and 5.10. Hence there is no observed structural damage as indicated by XRD. DTA is suggestive of movement of the organic material to another lower temperature site. The peak broadening feature implies that the TMA is no longer in a fixed site and the fact that it broadens significantly after 28 days suggests it may be possible to further lower the temperature of the exotherm and thus observe what would be, in effect, peak overlap i.e. shift of

Table 5.15

Weight Loss due to each Exotherm with Duration of Reflux in Water

DURATION OF REFLUX IN 100 cm^3 H_2O /DAYS		EXO TEMP RANGE/°C	WEIGHT LOSS/%	EXO TEMP RANGE/°C	WEIGHT LOSS/%	EXO TEMP RANGE/°C	WEIGHT LOSS/%
0		290-415	1.8	448-569	1.5	569-652	3.3
1		310-472	1.6			472-625	5.1
7	(S)	270-378	1.7	378-437	1.3	467-603	4.8 + 0.5
* 11		317-370	0.8	370-458	0.8	458-608	5.0
14	(S)	298-385	2.4**	385-434	0.6	434-605	5.5
21		293-453	1.4			478-600	4.9 + 0.3
28	(S)	300-383	0.7	383-445	0.6	460-605	5.0 + 0.3

(S) = Shoulder

* resolved into 3 exothermic peaks

** checked

Table 5.16

Total Weight Loss for Exothermic Process in each treated Specimen of Zeolite Ω

DURATION OF REFLUX IN 100 cm^3 H_2O /DAYS	TOTAL % WEIGHT LOSS DUE TO EXOTHERMIC PROCESS
0	6.5
1	6.7
7	8.8
11	6.5
14	8.5**
21	6.5
28	6.6

organic in the gmelinite cage to the even lower temperature exotherm site of ~400°C - exotherm (M).

These results further support the concept of the presence of additional faults in the structure which are undetected by XRD.

5.3.3.3 Comparison of Hydrothermal and Room Temperature Effects

Under reflux conditions exotherm (G) is shifted to the much lower temperature of 536°C compared with 570°C attained by treatment at room temperature. The exotherm (M) at ~400°C showed only slight variation in position with virtually constant weight loss when contacted with water at room temperature. However reflux conditions appear to cause significant movement of the organic from one site to the other. The effect of heat obviously increases thermal motion of TMA. In the cold water experiments, bromide ion was detected in the filtrate after 8 days, a few of the other solutions showed traces of bromide and this suggests that some organic material is adsorbed onto the surface of the zeolite. No bromide was detected in the solution that underwent reflux. Both hot and cold water treatment gave rise to alkaline solutions (pH ~8). This may be suggestive of aluminate ions being leached out of the lattice, but as there is no X-ray detectable damage to the structure, this is unlikely. The presence of silicate was confirmed by ammonium molybdate test. Ion exchange of Na^+ with H^+ from the water may occur. This would account for the slightly alkaline solution and no effect on structure. The extent of ion exchange is small as the solution is only just alkaline. A flame test for sodium ions in the filtrate solution proved to be positive.

5.3.4 Assignment of the Exotherms Observed in DTA Curves

The preparation of 8% TMAOH/SiO_2 mixture provided a material with

Assignment of Environment of Exothermic Peaks in Zeolite Ω

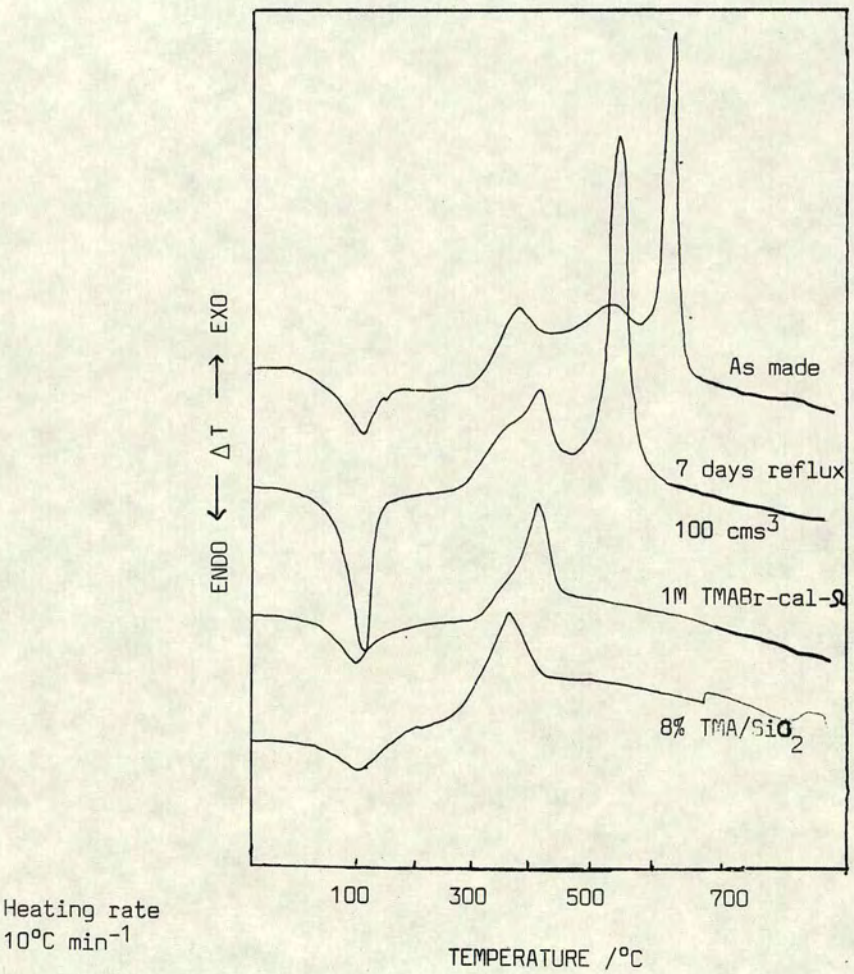

Heating rate
10°C min^{-1}

Fig. 5.14

similar organic content to that of zeolite Ω in an environment analogous to that of a zeolite. It was effectively an amorphous TMA silicate (Table 5.18). This therefore provides a substance in which TMA is loosely bound to SiO_2 and hence the DTA of this sample should show an exotherm similar to that which would be observed if TMA adsorbed onto the external zeolite surface. Fig. 5.14 shows that the TMA exotherm, in a free environment, occurs at ~350°C.

The 1M TMABr-calcined Ω gave an exothermic peak at ~415°C. The XRD pattern showed it to be crystalline Ω with no extra lines associated with TMA occluded in the zeolite. Cole and Kouwenhoven have reported TMAOH imbibed in the main channel during synthesis [3].

Sorption of TMA by the as synthesised material has been investigated and shows an exotherm at this temperature (next chapter). Hence the position of TMA was determined.

From these results it is clear that the exotherm (a) at ~360°C in the as made material is due to a surface coating of ~1.8% TMA and hence the shoulders which appeared under reflux conditions may also be attributed to TMA adsorbed on the external surface (Table 5.19). The percentage of organic material lost from the surface is variable. The samples contacted with water at room temperature showed no exothermic peak around ~350°C and hence adsorption of TMA on the surface does not occur under these conditions. The exotherm (M) in the room temperature contacted species is due to TMA imbibed in the 12 ring channel. The percentage weight loss at site (M) is equivalent to that previously coating the zeolite, site (a). Hence the surface TMA is dissolved in water, the silicate blocking the main channel is gradually released into solution and then TMA enters the framework where it is occluded. The variation in the exotherm temperature and broadness of the peak suggests that there is considerable movement of TMA. In the reflux experiments, exotherm (M) is due to imbibed TMA in the 12 ring channel

Table 5.18

Analysis of the under-noted Species by XRD

TREATMENT	XRD PATTERN
8% $TMAOH/SiO_2$	Amorphous
TMAOH	Crystalline
As synthesised	Crystalline
Ω calcined 625°C 3 h	Decrease in crystallinity
TMABr-CAL- Ω-625	Decrease in crystallinity

Table 5.19

Assignment of Environment of Exothermic Peaks in DTA

TREATMENT	EXO (a)				EXO (G)	
	TEMP RANGE /°C	PEAK TEMP /°C	TEMP RANGE /°C	PEAK TEMP /°C	TEMP RANGE /°C	PEAK TEMP /°C
As synthesised	290-415	369	448-569	528	569-652	625
Reflux in 100 cm^3 H_2O for 7 days	270-378	362	378-437	410	467-603	537
TMABr-Calcined Ω (S)	308-378	-	378-447	415	-	-
8% $TMAOH/SiO_2$	232-403	350	-	-	-	-

(S) = Shoulder

Schematic Representation of
Exothermic Peak Positions

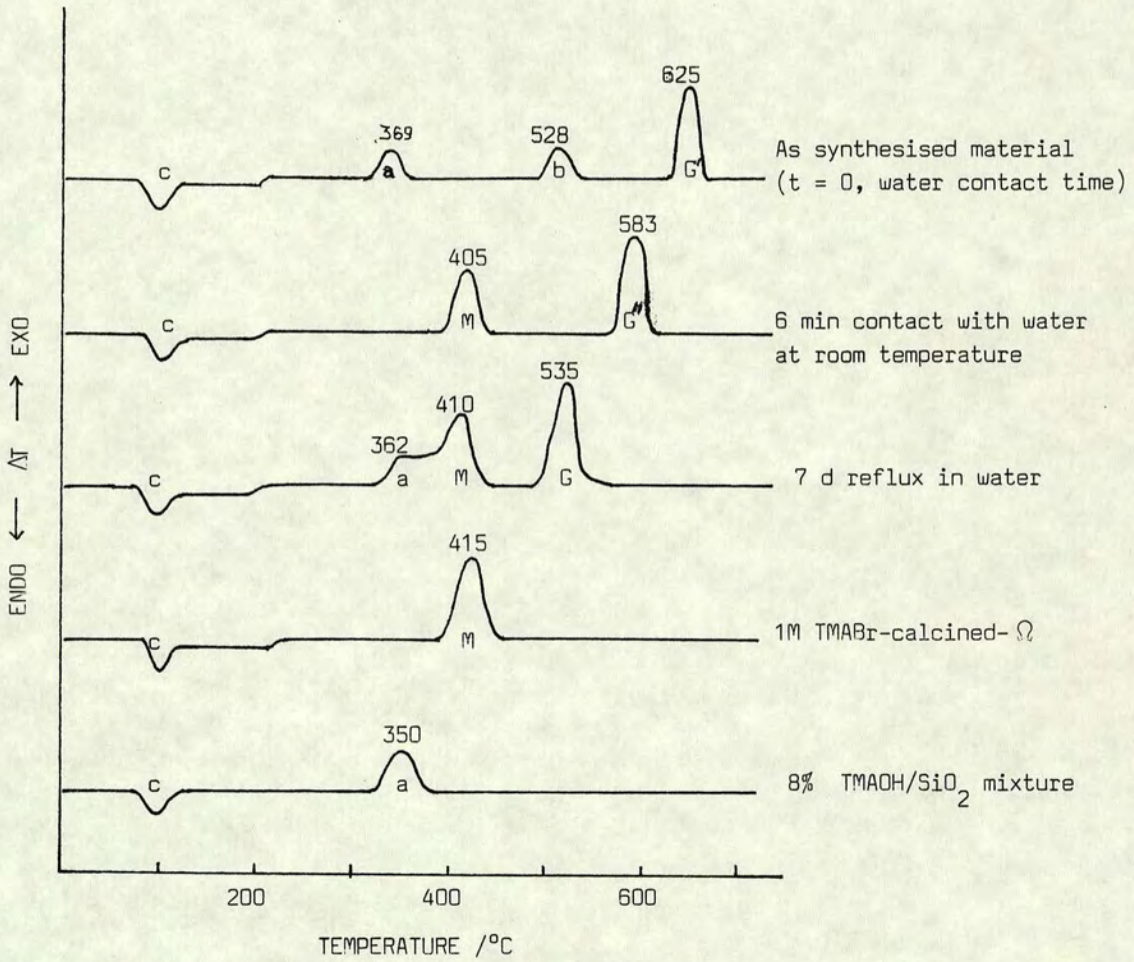

Fig. 5.15

c = endotherm due to water
a = TMA adsorbed on surface
M = TMA occluded in 12 ring channel
G = probably TMA in gmelinite cage
G′ = probably TMA in gemlinite cage
G″ = probably TMA in gmelinite cage

and because of the variation in the weight loss and appearance/ disappearance of shoulders this suggests rapid oscillation of TMA between the channel and surface. The final site occupied by exotherm (G) after 7 days reflux is coincident with exotherm (b) of the as synthesised material showing that this is the lowest energy site occupied by TMA in the gmelinite cage. A representation of the exothermic peak positions is shown in Fig. 5.15.

The sample of Ω used had ~1.8% TMA adsorbed on the surface - this amount is by no means constant as is observed from the total weight loss in Tables 5.16 and 5.11. The variation may be attributed to previously non-uniformly washed sample - the TMA source being the unreacted material from the reaction mixture. No TMA is observed in the 12 ring channel in the as synthesised material. Thus, this coating is so thick and strongly bound that only when in a large excess of water is it removed from the surface by dissolution in water. The silicate species trapped in the 12 ring channel is then able to diffuse out and the TMA penetrates the lattice and remains in the main channel. This may be represented diagrammatically as shown in Fig. 5.16.

5.3.5 Explanation of Results

The results obtained obviously require some explanation. The alkaline solution which resulted from contact of Ω with water is probably due to exchange of the H^+ ions from water with Na^+ ions in the small channels of the structure. The presence of the sodium ions in solution was confirmed by a positive flame test. The solutions were only slightly alkaline around pH 8-8.5 indicative of ion exchange on a small scale.

The filtrate was analysed for silicate and aluminate ions, the ammonium

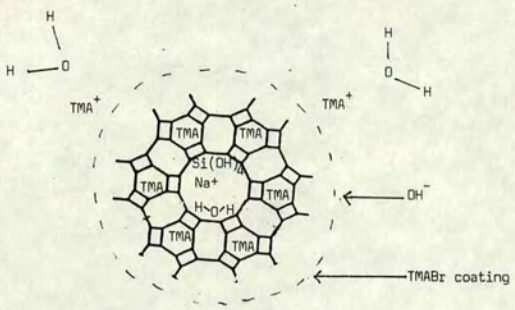

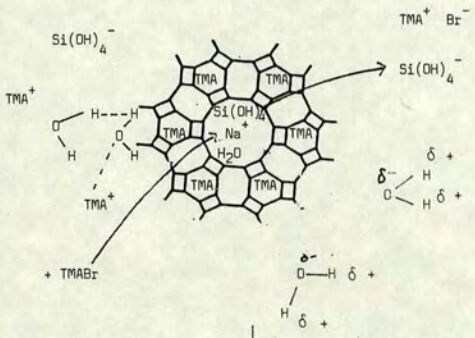

(1) Entry of TMA into main channel

(2) Gradual removal of silicate from main channel

cold water [DS3 only]

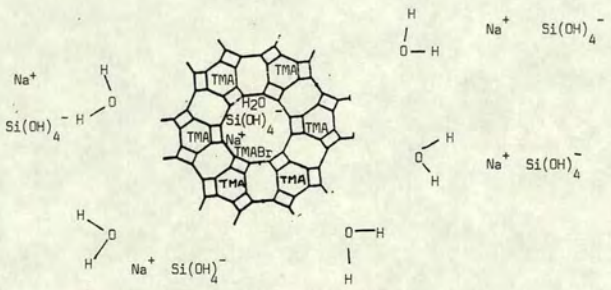

Reflux or cold water

Types I, III, IV

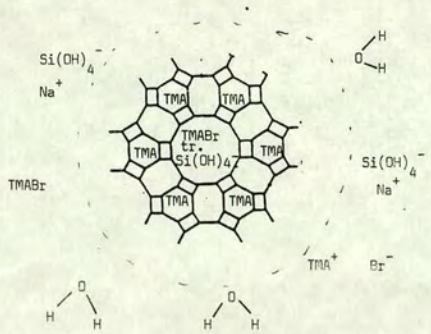

TMABr in channel ⇨
channel not completely blocked

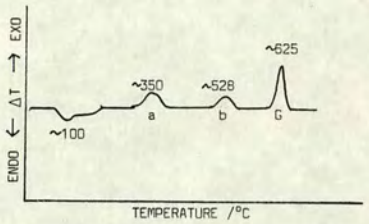

a = surface TMA
b = TMA in gmelinite cage and exit channel not blocked by silicate
G = TMA in gmelinite cage. Exit channel blocked by silicate.

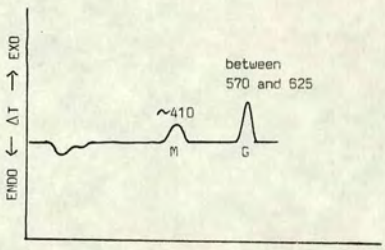

M = TMA in main channel
G = TMA in gmelinite cage. Exit channel partially unblocked.

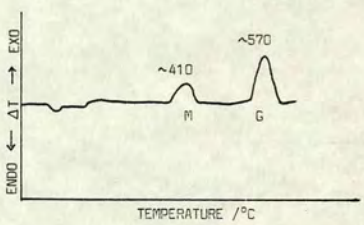

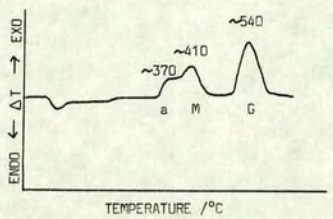

a = surface TMA
M = TMA in main channel
G = TMA in gmelinite cage. Exit channel significantly freed of silicate.

Fig. 5.16

molybdate test for silicate was positive, but the aluminate test was negative. Thus another source of Na^+ could be from the sodium silicate.

Any explanation that accounts for the shift of exotherm (G), which occurs at 625°C in the as synthesised material, to 570°C when 'washed' with cold water, and to 536°C when treated with hot water must also be applicable to the shift to 583°C observed in the sample which was calcined at 420°C for 3 h and 8 h.

5.3.5.1 Decay of TMA to $(CH_3)_3N$

Consider the case of:

$$(CH_3)_4N^+ + OH^- \longrightarrow (CH_3)_3N + CH_3OH$$

The as synthesised material shows two exothermic peaks at high temperature i.e. exotherm (G) at 625°C and exotherm (b) at 528°C. Exotherm (b) is perhaps due to $(CH_3)_3N$ formed by partial hydrolysis of TMA during the synthesis and which like the TMA could act as a template in the formation of Ω . Hence two different species may be incorporated in the gmelinite cage and this would explain exotherm (G) and exotherm (b) in the DTA. Contact with cold water would dissolve the TMA coating and open the framework surface to penetration by any ions/salts in solution. However, little occlusion would occur if the channel were filled with silicate species. Water molecules could penetrate the main channel and cause partial dissolution and removal of the silicate ions. Probably, at the same time entry of TMA into the main channel is favoured on the basis of charge and size. A positive charge results and thus for electrical neutrality uptake of a negative ion must occur. Since the final solution is alkaline, and only in the case of the 8 days reaction was Br^- detected, there must be some salt adsorbed

on the surface, and uptake of mainly bromide occurs, but OH^- could equally accompany the TMA. Thus the predominant species imbibed in the main channel is TMABr. Water is now able to penetrate the structure via the surface and also from the main channel, and so hydrolysis of the TMA in the gmelinite cage occurs resulting in the formation of $(CH_3)_3N$, which is evolved at lower temperature. Under reflux conditions the same reaction will occur. The silicate species will be further dissolved in hot water. If $(CH_3)_3N$ is evolved from the gmelinite cages then it should occur at the same temperature as in the cold water experiments. In cold water, exotherm (G) occurs at 570°C, in hot water it occurs at 536°C. Within the limits of experimental error in reading the temperature of the exotherms from the DTA curve, they are considerably different. Calcination of the sample at 420°C resulted in peak shift to 583°C which is not even as low as the temperature obtained in cold water. This case would imply evolution of $(CH_3)_3N$ at 3 different temperatures and is thus somewhat doubtful. C/N analysis was not sufficiently accurate to differentiate between $(CH_3)_3N$ and TMA.

5.3.5.2 Opening of the Main Channel by Removal of Trapped Silicate Species

Consider the as synthesised material DS3. The DTA curve exhibits 3 exotherms, exotherm (G), (b) and (a). Exotherm (a) has been assigned to TMA adsorbed on the external surface. Exotherm (G) - the major peak - occurs at 625°C and exotherm (b) - the small peak occurs at 528°C. Therefore the TMA is present in two different environments. The structure of the zeolite is such that water molecules line the main channel. These water molecules will be able to penetrate the gmelinite cages and thus interact with TMA ions. However the main channel is perhaps partially blocked with silicate ions and so only

the parts of the channel which are not totally blocked by the silicate allows free movement of water molecules and interaction with TMA in the gmelinite cage. Thus the TMA is evolved at a lower temperature than the remainder TMA. (Also the amount of water present is limited to that in the main channel.)

Once the zeolite is immersed in water, the surface adsorbed TMA is dissolved in water, the surface framework is now open. In cold water some of the silicate species diffuses out of the main channel and the TMABr is occluded in the main channel. TMA may displace the silicate as exotherm (M) position is taken up virtually immediately, whereas the shift of exotherm (G) is gradual. Thus removal of the silicate from the channel allows TMA to exit from the gmelinite cages at a lower temperature. The displacement of silicate by the interaction of water molecules and TMA, is gradual and thus accounts for the slow shift of exotherm (G). In cold water, molecules have less energy than in hot water and so they are unable to completely interact with the silicate and displace it, consequently the peak shift is only to 570°C. However under reflux conditions, the water molecules and TMA ions have increased energy, the silicate solubility is increased and so further silicate is displaced from the main channel. Thus TMA from the gmelinite cage may exit via the main channel at the lower temperature of 537°C.

Under reflux conditions a dynamic equilibrium is set up between the TMA in the main channel and TMA in solution which results in surface TMA. At room temperature the equilibrium appears to lie over to TMA in the main channel:

$$\text{TMA (surface)} \underset{\text{hot}}{\overset{\text{cold}}{\rightleftharpoons}} \text{TMA (main channel)}$$

The sample calcined at 420°C for a duration of 3 h and 8 h showed at least partial removal of surface TMA i.e. exotherm (a). This sample was equilibrated over saturated sodium chloride solution at 25°C for at least 16 h before analysis by DTA. Thus the water molecules were able to penetrate the framework and interact/displace some of the silicate from the main channel. Since the sample was equilibrated over sodium chloride solution, there is a limited amount of water vapour and so only slight interaction of water molecules with the silicate occurred and peak shift to 583°C was observed. This is the same temperature as that attained after 6 minutes water contact. The advantage of washing the sample is that no structural damage occurs, whereas calcination results in some damage.

Displacement of the silicate species from the main channel seems to be a favourable explanation - though there may be some flaws in it which as yet are not apparent.

Many of the observed effects may also be due to hydrolysis:

$$(Na^{+}Z^{-})_z + H_2O \longrightarrow (H^{+}Z^{-})_z + Na^{+}OH^{-}\ (aq)$$

5.3.6 Effect of Water on Zeolite Ω with DTA Type I, III and IV

In order to ascertain whether the observed effects of contact with water on DS3, which exhibited type I behaviour, are typical of Ω further samples which displayed type I, III and IV DTA were investigated. These investigations were carried out at room temperature.

5.3.6.1 DTA Type I, Sample DS2

Another sample of Ω which exhibited type I DTA is DS2. This sample was subjected to water contact at room temperature in the usual manner for duration of 3.5 h and 24 h. The zeolite/volume of water ratio

was varied. The results are shown in Fig. 5.17 and tabulated in Table 5.20. The shift phenomena is again observed. Exotherm (G) is virtually shifted to exotherm (b) position of 545°C. In n2, zeolite/volume of water ratio of 1.5 g/150 g, the base of the peak is broadened after 3.5 h contact with water. This is suggestive of reduced localisation of TMA in the gmelinite cage. Exotherm (G) peak is split. It has been previously mentioned in Chapter Three that this is probably the result of a large sample weight, however in this instance the TG curve is resolved into 2 stages of weight loss in the corresponding temperature region. It is probably indicative of incomplete washing of the sample and so the exotherm (G) is observed at two temperatures. Exotherm (a) is shifted to the higher temperature of 376°C, is much broader and extends from 297°C to 440°C. This perhaps suggests that the TMA has entered the main channel, and partial adsorption on the surface has occurred. The sharp endotherm (c) is reduced, and thus a substantial amount of TMA is probably adsorbed on the surface.

In n3, the zeolite/water ratio was 0.5 g/150 g. Exotherm (G) was not split after 24 h contact with water, suggestive of complete uniform washing. Exotherm (a) peak is shifted to a higher temperature of 385°C, extending from 292°C to 438°C, again indicative of TMA partially adsorbed on the external surface of the crystals and partly imbibed in the channel. There is less TMA at this site (Table 5.20) and a corresponding increase in the endotherm is observed - evidence for replacement of TMA by loosely bound water.

Increase of the zeolite/water ratio to 10 g/500 g for 24 h contact with water, n4, prevents complete washing to take place and exotherm (G) is shifted to only 555°C (Table 5.20). An increase in the TMA adsorbed on the surface/main channel is observed.

Effect of Water Contact on DTA Type I
Sample DS2

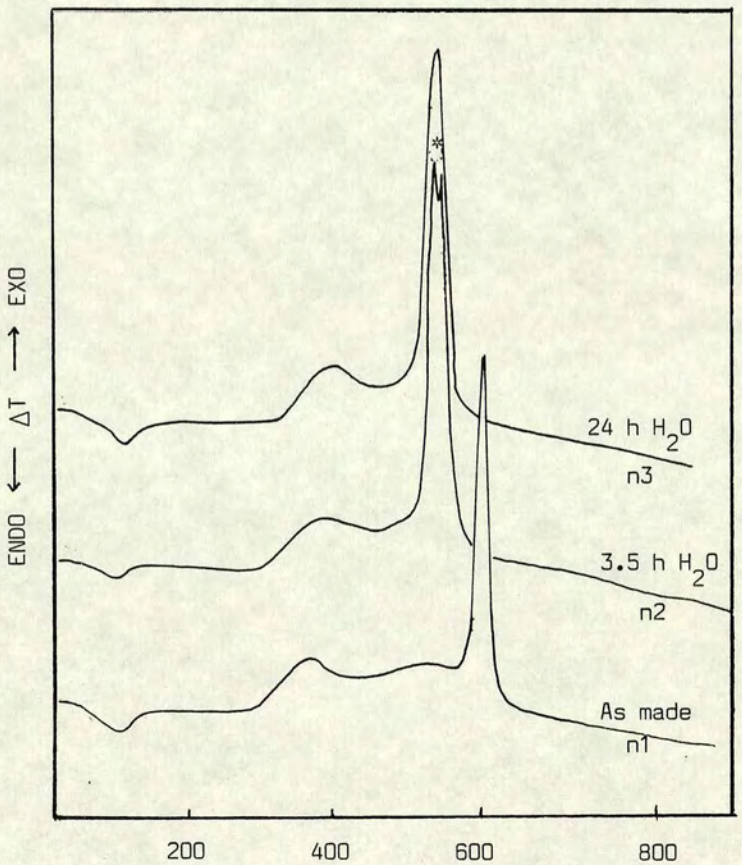

Heating rate
8.5°C min^{-1}

Fig. 5.17

*TG similarly resolved into two weight losses at this temperature region.

The bulk density of DS2 was determined to be 0.6 g cm^{-3}. This is an intermediate value for spherulitic habit (0.9 g cm^{-3}) and fibrous habit (0.3 g cm^{-3}) and indicative of a mixture of morphological types. This could account for the reduced weight loss at exotherm site (a) (excluding n4) since fibrous crystals will have a smaller surface area. In n4, there is probably more spherulitic crystals present which would account for the increase in surface TMA. The origin of the fluctuation of the weight loss from the gmelinite cage is unknown.

Thus DS2 behaves similarly to DS3 when contacted with water.

5.3.6.2 DTA Type II, R15

R15 provided a sample of type II DTA. This was contacted with water and exotherm (G) was shifted to lower temperature. Further details are not available.

5.3.6.3 DTA Type III, DS13 and R1

Two samples of DTA type III were investigated: R1 and DS13. The dramatic change of DTA type for DS13 is illustrated in Fig. 5.18 and the associated data in Table 5.21. The pointed exotherm in the as synthesised material which occurs at 372°C is rather low for it to be assigned to TMA in the main channel, but the sharpness suggests localisation; the overall peak extends from 284°C to 420°C with an associated weight loss of 3%. This weight loss must, in part, be due to TMA imbibed in the channel, and partly TMA adsorbed on the surface. This would therefore account for the large sharp endotherm.

After only 8 minutes contact with water a significant change in appearance of the DTA curve is observed. Fig. 5.18 illustrates a reduction in size of the sharp endotherm, an increase in the surface TMA and occlusion

Effect of Water Contact on DTA Type III, DS13

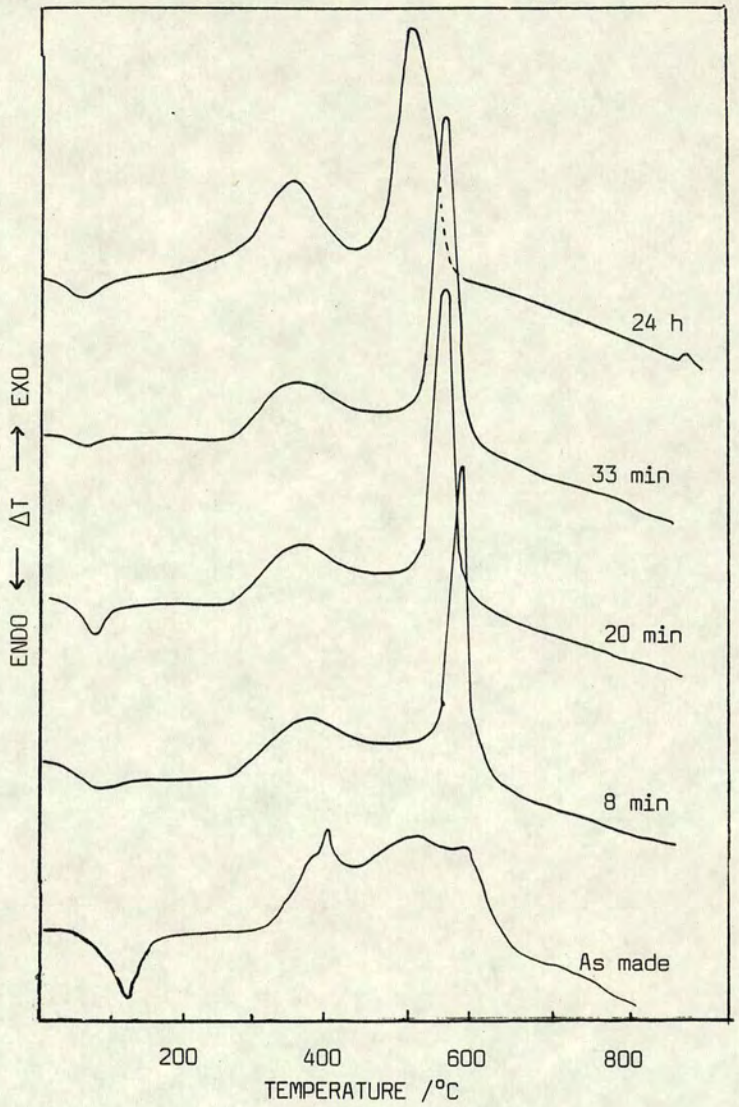

Fig. 5.18

Effect of Water Contact for 24 h on DTA Type III, R1

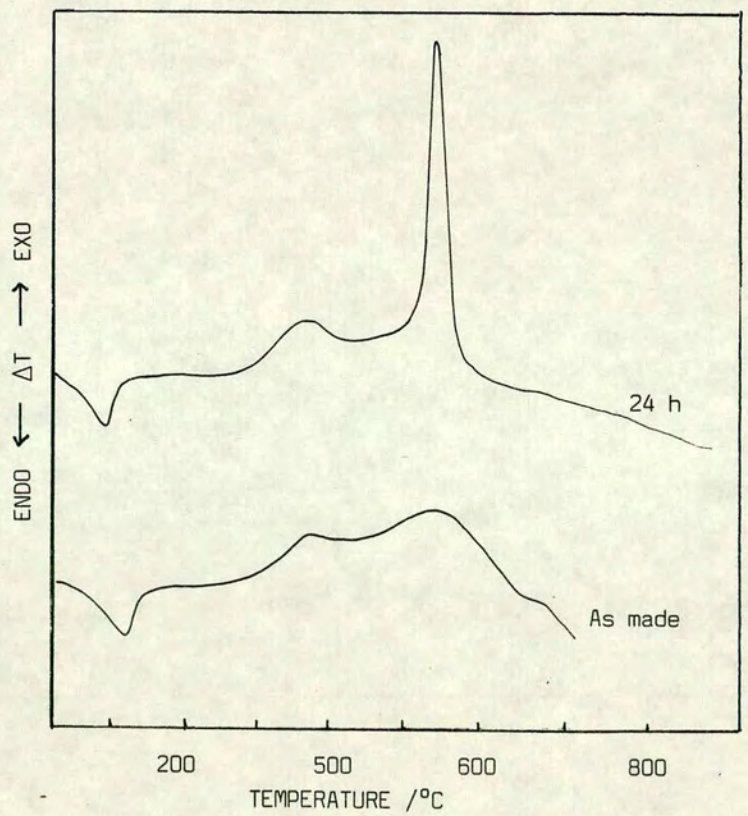

Fig. 5.19

Table 5.20

Gradual Shift of Exotherms* in DTA Type I
as a Result of Contact with Water

REACTION DS2

NO.	WATER CONTACT TIME/h	(a) EXO PEAK TEMP/°C	PEAK RANGE /°C	WT LOSS /%	(b) EXO PEAK TEMP/°C	PEAK RANGE /°C	WT LOSS /%	EXO PEAK TEMP /°C	PEAK RANGE /°C	WT LOSS /%
n1	0	358	304-405	1.5	526	465-560	1.5	607	560	4.1
n2	3.5	376	297-440	1.6	*545	440-590	5.9			
n3	24	385	292-438	1.0	535	438-587	5.1			
n4	24	392	287-438	2.1	555	438-590	5.3			

* TG curve resolves weight loss from gmelinite cage into 2 stages
n2 zeolite/water ratio = 1.5 g/150g
n3 zeolite/water ratio = 0.5g/100 g, therefore the lower the ratio the further the shift of exotherm to lower temperature
n4 zeolite/water ratio = 10 g/500 g

Table 5.21

Gradual Shift of Exotherms* in DTA Type III
as a Result of Contact with Water

REACTION DS13

WATER CONTACT TIME/min	EXO TEMP/°C	EXO PEAK RANGE/°C	WT LOSS /%	EXO PEAK TEMP/°C	EXO PEAK RANGE/°C	WT LOSS /%	EXO PEAK TEMP/°C	EXO PEAK RANGE/°C	WT LOSS /%	EXO PEAK TEMP/°C	EXO PEAK RANGE/°C	WT LOSS /%
0	372	284-420	3.0	517	420-572	3.1	597	572-670	1.9	770	670-880	1.1
8	365	308-438	2.0				597	490	5.1			
20	363	275-417	n.r.				587	447-614	n.r.			
25	380	282-453	n.r.				583	453-617	n.r.			
33	370	285-492	2.8				580	492	5.8			
24	374	247-437	4.6				540	402-596	5.6			

n.r. = not recorded

Table 5.22

Gradual Shift of Exotherms* in DTA Type IV
as a Result of Contact with Water

REACTION R9

TIME OF WATER CONTACT/min	EXO PEAK TEMP/°C	EXO PEAK RANGE/°C	EXO PEAK TEMP/°C	EXO PEAK RANGE/°C	EXO PEAK TEMP/°C	EXO PEAK RANGE/°C	EXO PEAK TEMP/°C	EXO PEAK RANGE/°C	EXO PEAK TEMP/°C	EXO PEAK RANGE/°C
0	345	275-395	513	395-573	-	-	615	573-675	1050	1005-1060
5	368	283-432			555	515-567			1125	1060-1150
20	370	300-430			550	504-587				
60	378	295-428			547	498-570				

* Heating rate 8.5°C min^{-1}

of TMA in the channel as indicated by the temperature range of the peak (308°C to 438°C). The appearance of exotherm (G) is dramatically changed. Increased duration of contact with water shifts exotherm (G) to 540°C and broadens (247°C to 437°C) the exotherm centred at 374°C.

Type III DTA may contain TMA imbibed in the main channel. A sample from Reaction R1 which depicted type III behaviour is illustrated in Fig. 5.19. After 24 h in water, the change in DTA is equivalent to that of 33 minutes of water contact time with DS13. This may be due to a substantially larger quantity of the silicate species blocking the channel and thus longer time is required for its removal. Table 5.23 shows that DS13 and R1 both have much higher weight losses than the other samples prior to washing. It is interesting to note that an increase in weight loss after washing is observed for DS13 and a decrease is observed for R1. This is probably indicative of a considerable variation in crystal size of the zeolite and so each sample taken has a variable amount of TMA adsorbed/occluded in the main channel (DS13). Conversion of DTA type III is slower in R1 and is probably related to the inability to effect complete removal of TMA from the sample in preparation for XRF analysis. This provides evidence that the TMA is perhaps trapped between layers of amorphous silicate such that alternating layers of silicate and TMA may occur in the main channel, and so type III *may* be fault free.

5.3.6.4 DTA Type IV, Reaction R9

This sample is a relatively rare form of Ω as it exhibits an exotherm at 1050°C with no corresponding weight loss (Table 5.22) and is thus suggestive of a phase transition. When contacted with water amazing changes occur. These are illustrated in Fig. 5.20. Complete removal of the exotherm at 1050°C is accomplished after contact with water for

Effect of Water on DTA Type IV
Reaction R9

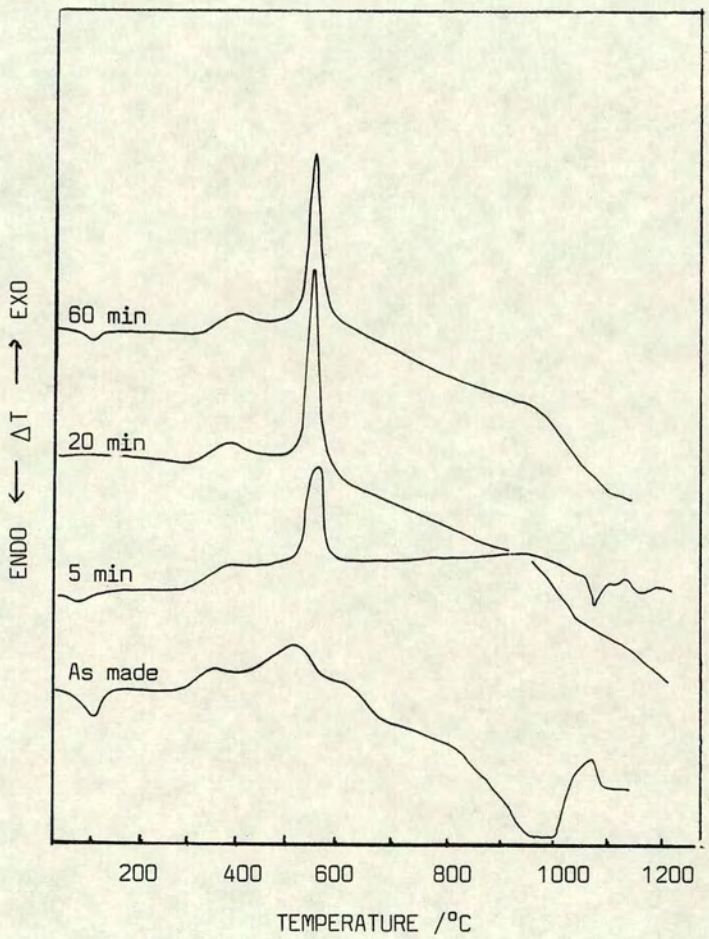

Fig. 5.20

only 5 minutes, although a small exotherm at 1125°C is discernible. This may have been present in the as synthesised sample, but the DTA was not run to that temperature. A shift of the 615°C exotherm, i.e. exotherm (G), and redistribution of the organic material to the site of the 555°C exotherm, with increased localisation is observed. Exotherm (a) centred at 345°C is shifted to 368°C, but the commencement of this peak is only 10°C higher and it is very broad. This broad distribution of organic material is attributed to TMA adsorbed on the external surface and also imbibed in the main channel. After 20 minutes contact with water, complete removal of the high temperature exotherm around 1050°C is effected, and exotherm (b) is considerably sharpened but the base is broader. Increase in the size of the exotherm (M) which extends from 300°C to 420°C occurs and suggests redistribution of the TMA. A remarkable feature is the absence of the endotherm. After 1 h contact with water, the endotherm reappears and exotherm (G) is shifted to its lowest temperature (547°C). The small exotherm centred at 378°C which extends from 295°C to 428°C is probably due to TMA occluded in the main channel and adsorbed on the surface.

Type IV DTA illustrates the most dramatic change of all the DTA curves as a result of further washing. Complete removal of the exotherm at 1050°C provides further evidence for layers of TMA and silicate in the main channel; and only by thorough washing with a large quantity of water is the silicate removed from the channel and thus allows the TMA to exit.

5.3.6.5 Comparison of DTA Types I, III and IV

The data for samples with DTA types I, III and IV before and after contact with water are given in Tables 5.23, 5.24, 5.25 and 5.26. Part of

Table 5.23

Thermal Analysis of the As Synthesised Material
in relation to the Exothermic Processes

SAMPLE	EXO PEAK TEMP /°C	EXO PEAK RANGE/°C	WT LOSS /%	EXO PEAK TEMP/°C	EXO PEAK RANGE/°C	WT LOSS /%	EXO PEAK TEMP/°C	EXO PEAK RANGE/°C	WT LOSS /%	EXO PEAK TEMP/°C	EXO PEAK RANGE/°C	WT LOSS /%	EXO PEAK TEMP/°C	WT LOSS /%
OS3	389	290-415	1.8				528	448-569	1.5	625	569-652	3.3		
OS2	358	304-405	1.5				526	465-560	0.8	607	560-623	4.1		
OS13	363(S)	284-420	3.0	372	284-420	3.0	517	420-572	3.1	592	572-670	1.9	770	1.1
R1	355	268-428	2.9				545	428-647	4.5	676	647-940	0.8		
R9	345	275-395	1.8				513	395-573	3.8	619	573-675	2.0	1050	0.0

(S) = Shoulder

Table 5.25

Thermal Analysis of As Synthesised Material Following Contact with Water
Exothermic Processes

SAMPLE	TIME OF CONTACT /h	EXO PEAK TEMP /°C	EXO RANGE /°C	WT LOSS /%	EXO PEAK TEMP /°C	EXO RANGE /°C	WT LOSS /%
OS3	2	403	303-485	1.9	570	485	5.0
OS2	24	385	322-438	1.0	535	438-587	5.12
OS13	24	374	247-437	4.6	540	462-590	5.6
R1	24	375	294-427	1.5	560	427-600	5.0
R9	1	378	295-428	n.r.	547	428-570	n.r.

n.r. = not recorded

N.B. OS3 run at heating rate of 10°C min^{-1} and so probably accounts for the slightly higher recorded temperatures than the other samples - heating rate 8.5°C min^{-1}

Table 5.24

Thermal Analysis of the As Synthesised Material
in relation to the Endothermic Processes

SAMPLE	ENDO PEAK TEMP /°C	ENDO RANGE /°C	WT LOSS /%	ENDO PEAK	ENDO RANGE /°C	WT LOSS /%
DS3	103	RT-145	12.0	broad	145-290	5.0
DS2	96	RT-130	7.6	broad	130-304	7.0
DS13	112	RT-153	13.1	broad	153-284	3.9
R1	106	RT-142	13.9	broad	142-268	4.5
R9	105	RT-142	15.5	broad	142-275	5.0

RT = Room Temperature

Table 5.26

Thermal Analysis of As Synthesised Material following Contact with Water
Endothermic Process

SAMPLE	ENDO PEAK TEMP /°C	ENDO RANGE /°C	WT LOSS /%	ENDO PEAK	ENDO RANGE /°C	WT LOSS /%
DS3	103	RT-129	9.3	broad	129-303	6.8
DS2	85	RT-117	6.9	broad	117-322	8.3
DS13	85	RT-205	9.1	broad	205-247*	1.2
R1	97	RT-125	11.6	broad	125-294	6.9

RT = Room Temperature

* Could be exo but on the basis of other samples assigned as endo

Tables 5.23 and 5.24 have been given in Chapter Four. Comparison of the exothermic behaviour after contact with water shows that only DS3 has an exotherm centred at 403°C. All the other samples have exotherms centred at ~375°C. The peak range for the latter is varied. The exotherms occur between the positions of exotherm (a) and exotherm (M). In R1 and R9, the peak range is the same, 295°C to 428°C. In DS2 and DS13 the exothermic peak ends at 438°C. It is only for DS3 that the exotherm extends to 485°C. Thus the exotherm at this site is probably due to surface and main channel TMA. Exotherm (G) occurs at 570°C in DS3, at 560°C in R1, but is shifted to ~540°C in DS2, DS13, and R9 i.e. the temperature acquired by DS3 after reflux for 7 days. The weight loss associated with exotherm (G), i.e. from the gmelinite cage, is ~ 5%, with a significantly higher value of 5.6 % for DS13. The weight loss associated with endotherm (c) fluctuates from ~7 to 11%. DS13 shows very little intracrystalline water, but has a much increased surface/main channel content.

Examination of the XRD patterns, after thorough washing, showed little change in the observed peak intensities; the slight variations observed are probably due to variations in the packing of the sample holder.

Thus thorough washing of zeolite Ω at room temperature converts the four DTA types to one pattern.

5.3.6.6 Spurious Peak in XRD Pattern

An additional peak was observed in the XRD pattern of DS3, at $2\theta = 18.2°$, after the zeolite had been stirred with a PTFE magnetic follower for 1 week with water at 70°C. It was found that prolonged stirring caused the grinding of the PTFE follower and was consequently mixed in with the sample. The XRD pattern of a sample of PTFE tape exhibited an extremely intense peak at $2\theta = 18.2°$ which was off scale when X-rayed

in the usual range for zeolites. This was caused by the stretching of the PTFE tape which thus increased the degree of order and hence crystalline nature of the polymer. Thus the additional peak was identified as PTFE.

5.3.7 Comparison with the Literature

A schematic representation of the ultimate DTA curves for zeolite Ω is shown below in Fig. 5.21:

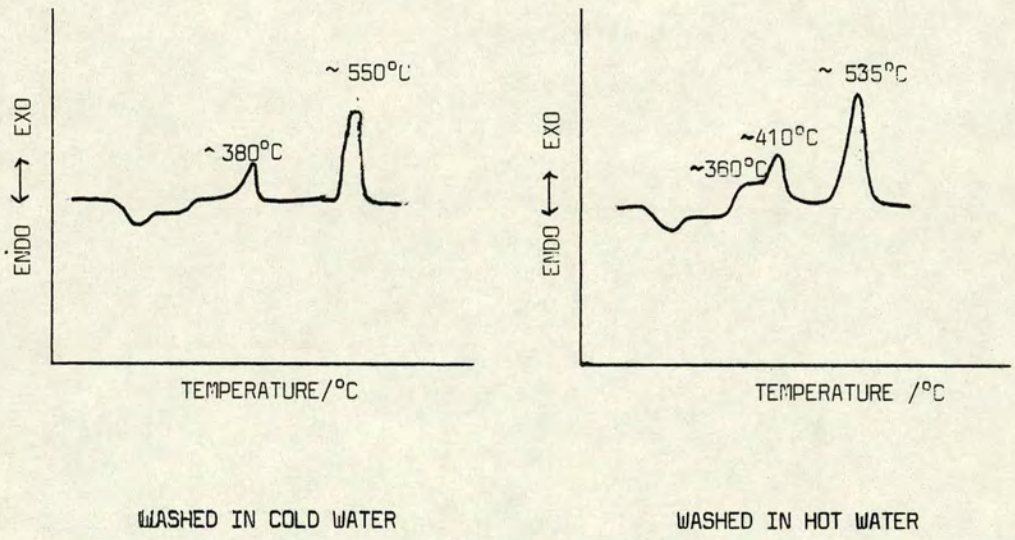

Fig. 5.21

Comparison of the ultimate DTA curve observed after prolonged washing with water with those in the literature shows close correlation with only that published by Lowe et al [7]. Their samples were washed with a large excess of hot water, thus the silicate from the channel was displaced and exotherm (G) occurred at 515°C, with exotherm (M), assigned to TMA in the main channel, located at 450°C.

The DTA obtained by Penchev et al [6] (previously mentioned in Chapter Two) shows sharp exotherms at ~375°C, 460°C, 525°C and 960°C. The observation of an exotherm at 960°C is indeed rare for zeolite Ω. It may be related to the exotherm observed at 1050°C in type IV DTA. However it has been shown that thorough washing removes this exotherm and thus one may only speculate on the consequences of further washing of the sample synthesised by Penchev et al. This exotherm is not associated with a weight change and so it is indicative of a phase transition. This was also the case in type IV DTA of R9, but contact with excess water gradually removed the trapped silicate and also the exotherm. The exotherm at 375°C may be attributed to TMA adsorbed on the external surface of the crystals, the 460°C exotherm may be assigned to TMA in the main channel, and the 525°C exotherm to TMA in the gmelinite cage. If Penchev's material behaved like the samples investigated in this work, then thorough washing would remove the 375°C exotherm and increase the size of that at 460°C and completely remove the 960°C 'phase transition'.

The DTA curve obtained by Qinhua et al [5], after adjustment of the base line (as already discussed in Chapter Two) shows a shoulder on the 480°C exotherm and a 720°C exotherm. The 720°C exotherm is not as they suggest due to collapse of the structure, but it is more likely that it is due to oxidative degradation of TMA in the gmelinite cage. The 480°C peak can be assigned to TMA in the main channel and the shoulder attributed to TMA adsorbed on the surface. The exotherm at 720°C, if it is due to TMA in the gmelinite cage is at an extremely high temperature and may be due to inadequate washing. The presence of the 480°C peak suggests that it has been washed sufficiently to effect uptake of TMA in the main channel, but not completely to lower exotherm (G).

Cole's DTG [3] illustrated a large broad peak centred at 350°C which has been assigned to decomposition of TMAOH and silicate occluded in the main channel, and a sharp intense peak between 500°C and 600°C due to TMA decomposition in the gmelinite cage. According to the results obtained from the present investigation, the broad DTG peak centred at 350°C, which extends from ~200°C to ~480°C is probably due to an excessive amount of TMA adsorbed on the external surface and TMA occluded in the main channel. The crystals from Cole's work were said to be extremely small and thus the overall surface area of the crystals will be large and so a substantial amount of TMA is adsorbed on the external surface with the result that the surface TMA and main channel TMA positions overlap.

Barrer and Aiello [2] only observed one sharp exotherm at ~580°C which they attributed to TMA burning out of the gmelinite cage. No surface or occluded TMA was observed. Thus Barrer's sample must have been thoroughly washed. The temperature of the exotherm corresponds roughly to that obtained by washing DS3 with cold water.

Consideration of the channel size of Ω (7.4Å reduced to ~4.5Å with stacking faults) and the size of the TMA ion (~6.6Å) suggests that occlusion of TMA in the main channel may only occur in a fault free, unblocked channel or a sample in which the main channel pores are open to the surface. On this basis, Barrer's sample must be faulted, the main pores end with a layer of sodalite cages and thus block the channel. The samples of Penchev et al, Qinhua et al, Lowe et al, and present work may have:

(1) freedom from stacking faults

(2) main channel windows opening onto the surface

(3) a mixture of faulted and 'unfaulted' Ω

Perhaps in the present work the samples contain a mixture of faulted and perfect material. Blockage of the main channel by silicate as opposed to stacking faults may be the cause of the reduced sorption capacity for Ω .

Only type III DTA provides evidence for the possible occlusion of TMA during synthesis, although even in this case the TMA may be adsorbed on the external surface. Thus silicate is preferentially occluded to TMA in the main channel. The explanation proposed earlier for the effect of water on DS3 type I may account for the behaviour of DTA type III in water.

Since exotherm (G) is shifted to a significantly lower temperature by simple washing with excess water, then complete removal of the organic material by calcination may be achieved at a lower temperature with reduced structural damage to the framework.

The removal of silicate and the pore opening of Ω , by washing with excess water, is analogous to the conversion of small port mordenite to large port mordenite [10] by removal of the silicate from the main channel by heat treatment.

5.3.8 Summary

A poorly washed sample of zeolite Ω may exhibit four types of DTA curves. In type I, 3 exotherms are depicted and 2 endotherms. The sharp endotherm is due to removal of water from the main channel and surface, and the broad endotherm is caused by removal of water from the small pores. The exotherms are due to TMA decomposition from different sites. The exothermic peaks occurred at:

exotherm (a) 369°C due to TMA adsorbed on the outer surface

exotherm (b) 528°C)
exotherm (G) 625°C) due to TMA in the gmelinite cage

Immersion in water results in virtually immediate removal of the surface TMA coating at room temperature, and uptake of TMA into the 12 ring channel. Thoroughly washed samples exhibit only 2 exotherms in the DTA curve:

exotherm (M) at ~400°C ≡ TMA in main channel

exotherm (G) at ~570°C ≡ TMA in gmelinite cage

A time factor is involved in the shift of exotherm (G) to 570°C; this is achieved within at least 45 minutes and this corresponds to the time required for removal of the silicate from the main channel.

The DTA curve for samples contacted with hot water show 2 exotherms and one shoulder. The shoulder at ~360°C is attributed to TMA surface coating. The exotherm at ~415°C is attributed to TMA in the 12 ring channel and exotherm at 536°C is attributed to TMA in the gmelinite cages. Under reflux conditions a dynamic equilibrium is set up between TMA in the main channel and TMA in solution which gives rise to the outer surface TMA. At room temperature the equilibrium appears to lie over to TMA in the main channel:

$$TMA_{(surface)} \underset{hot}{\overset{cold}{\rightleftharpoons}} TMA_{(main\ channel)}$$

However in DTA types III and IV the equilibrium at room temperature is equivalent to that of DTA type I under reflux conditions.

Washing with water under both hot and cold conditions results in a shift and broadening of the exotherm (G). Both features are more pronounced after treatment in hot water. The peak broadening effect suggests reduced localisation of TMA in the gmelinite cages. This and the peak shifts are *thought* to occur as a result of removal of silicate from the main channel and the interaction of water molecules with TMA in the gmelinite cages.

Types II, III and IV behave similarly in water.

Thus zeolite Ω, synthesised in these reactions has a characteristic DTA curve. One may only speculate on the effects of thorough washing of the samples for which DTA curves have been reported in the literature.

REFERENCES

1. Union Carbide, British Patent 1 178 186, 1970.

2. R. M. Barrer and R. Aiello, J. Chem. Soc (A), 1970, 1470.

3. J. F. Cole and H. W. Kouwenhoven, Adv. Chem. Series, 1973, 121, 583

4. Sh. J. Sidamondize, G. V. Tsitsishvili, D. M. Shavladze, I. I. Iashvili, M. N. Gvilano, Soobstrich Akad. Nauk Gruz, SSR, 1978, 90 3, 597.

5. X. Qinhua, Zhang Huizhu, Dong Jialu and Wang Rui, Kexue Tongbao, 1980, 25, (10), 833.

6. V. Penchev, Ch. Minchev, K. Kanazirev, O. Pencheva, N. Borisova, L. Kosova, H. Lechert and H. Kacirek, Zeolites, 1983, 3, 249.

7. B. M. Lowe, A. Araya, D. S. Sinclair, T. J. Barber, A. Varma, Zeolites, 1984, 4, 263.

8. D. S. Sinclair, Unpublished work.

9. Wen-Yang Wen, "Water and Aqueous Solutions", edited by R. A. Horne, Wiley-Inter-Science, USA, 1972, p.163.

10. E. F. Christian Marcilly and F. Raatz, J. Chem. Soc., Chem. Commun., 1982. 309.

CHAPTER SIX

Sorption of TMA from Aqueous Solution by Zeolite Ω

6.1 Introduction

There have been several studies on the sorption of gases by zeolite Ω (see Chapter Two), but sorption from aqueous solution has not been reported. Likewise there have been no studies on salt occlusion (or imbibition) by zeolite Ω . In view of the manner in which zeolite Ω is formed by templating about the TMA cation, it seemed likely that it might sorb other molecules from aqueous solution. Only preliminary experiments designed to establish whether this does indeed occur were carried out.

The present work investigates room temperature (~ 16°C) sorption of TMA from aqueous TMABr solution by:

(a) organic free Ω i.e. (Na, H)- Ω

(b) as synthesised Ω (DTA type I) i.e. (Na, TMA)- Ω

(c) as synthesised Ω which exhibits DTA types I, II and III

In the latter case, a comparison of sorption for the three materials at 95°C is made. Also a room temperature isotherm for the uptake of TMA from aqueous solution by (Na, TMA)- Ω is attempted.

Although these experiments are discussed in terms of the sorption of TMA (with appropriate anion) it is recognised that in practice both ion exchange and sorption may occur.

The main principles of sorption have been mentioned in Chapter One. Several methods for measurement of salt occlusion/sorption exist. They are predominantly techniques which involve weighing of the samples.

The present work employs TG and DTA - the latter distinguishes between the sorption sites. The technique may be universally applied to all zeolites and silicalites.

6.2 Experimental

6.2.1 Materials

TMA free Ω (prepared as described in Chapter Five); 8% TMA/SiO_2 (prepared as described in Chapter Five); samples of Ω:
DS3, DS2 - DTA type I, DS13- DTA type III, R15 - DTA type II .
TMABr from Aldrich Chemical Company. Glass distilled water.

6.2.2 Procedure

Sorption of TMA from aqueous solution was carried out as follows: Solutions of TMABr (1M) were prepared. The TMA free Ω i.e. calcined Ω (0.5g) was soaked in TMABr solution (100 cm^3) in a stoppered conical flask and left undisturbed at room temperature for 14 days. The as synthesised samples DS3, DS2, DS13 and R15 (0.5g) were similarly soaked in 1M TMABr solutions (100 cm^3) in stoppered conical flasks and left static at room temperature for 8 days. Comparison of sorption at 95°C was carried out by the same procedure, but the samples were maintained at 95°C for 24 h.

The room temperature sorption isotherm was obtained by soaking samples of DS3 (0.25g) in TMABr solution (50 cm^3) of concentrations 0.0M (i.e. pure water) to 3.0M in stoppered conical flasks for 8 days. Agitation was not employed.

After the time period specified, the samples were filtered over a Büchner funnel and washed with water until the washings were free from detectable bromide. In this way all loosely bound TMABr is removed

The zeolite samples were dried in an oven at 110°C, equilibrated in the aforementioned manner and subjected to analysis by DTA, TG and XRD.

6.3 Results and Discussion

The results are presented in Tables 6.1 to 6.4 and illustrated in Figs. 6.1 to 6.4.

6.3.1 Uptake of TMA by Zeolite Ω

The reaction composition from which zeolite Ω is synthesised contains an excess of TMABr. Structural studies show that the TMA is encapsulated in the gmelinite cages of the structure of Ω. The 12 ring channel has a diameter of ~7.4Å; however, the presence of stacking faults reduce it to ~4Å. In view of these facts it was of interest to determine whether a large organic molecule TMABr (~6.6Å) could be sorbed and the site it would occupy.

It was speculated that if TMA or TMABr were sorbed by calcined Ω i.e. (Na, H)-Ω, it could occupy two sites:

(a) the external surface of the crystals

(b) the main 12 ring channel

If it were to occupy the external surface, then the DTA would give an exotherm at ~350°C i.e. the temperature of the exotherm obtained for a TMABr/SiO_2 mixture. If it were to occupy the main channel, then the observed TMA decomposition temperature from DTA would be higher as it would be in an 'enclosed' system. If it were to enter the main channel, then structural considerations would imply:

(1) The channel is not blocked by so called stacking faults

(2) The stacking faults (which are reported to extend over 25Å and recur every 300Å) are present, but a significant portion of channels are open to the surface.

(3) A mixture of faulted and perfect material is present.

The thermal removal of TMA causes structural damage (observed in Chapter Five), and also a decrease in the sorption capacity [1]. Thus it was speculated, that if sorption of TMA or TMABr by calcined Ω were to occur and if it occupied the main channel, then the (Na, TMA)- Ω i.e. the as synthesised material should also be capable of sorbing TMABr. If sorption of large molecules was to be examined, the only possible sorption sites would be the external surface and the main channel. Thus it is unnecessary to calcine the zeolite since the TMA is encapsulated in the gmelinite cages and this would not interfere with sorption. The advantage of using (Na, TMA)-Ω is that no structural damage is incurred and so a true sorption capacity for the site(s) is determined.

6.3.2 Sorption of TMABr by (Na, H)-Ω and (Na, TMA)-Ω

The results of sorption from aqueous solution of TMABr by (Na, H)-Ω, (Na, TMA)- Ω and SiO_2 as analysed by DTA are illustrated in Fig. 6.1 and thermal analysis data are given in Table 6.1. They clearly show that the main TMA/TMABr sorption site for (Na, H)- Ω is at the higher temperature of 412°C compared with 350°C for sorption on silica, and so must be in the main channel. The presence of a shoulder at 378°C and the extent of the exotherm from 308 to 378°C implies that minor sorption of TMA onto the surface occurs. The major sorption site is in the main channel. Similarly, the (Na, TMA)-Ω shows a large exotherm centred at 417°C with broad base from 360 to 460°C with a

DTA Curves Illustrating Sorption of TMABr

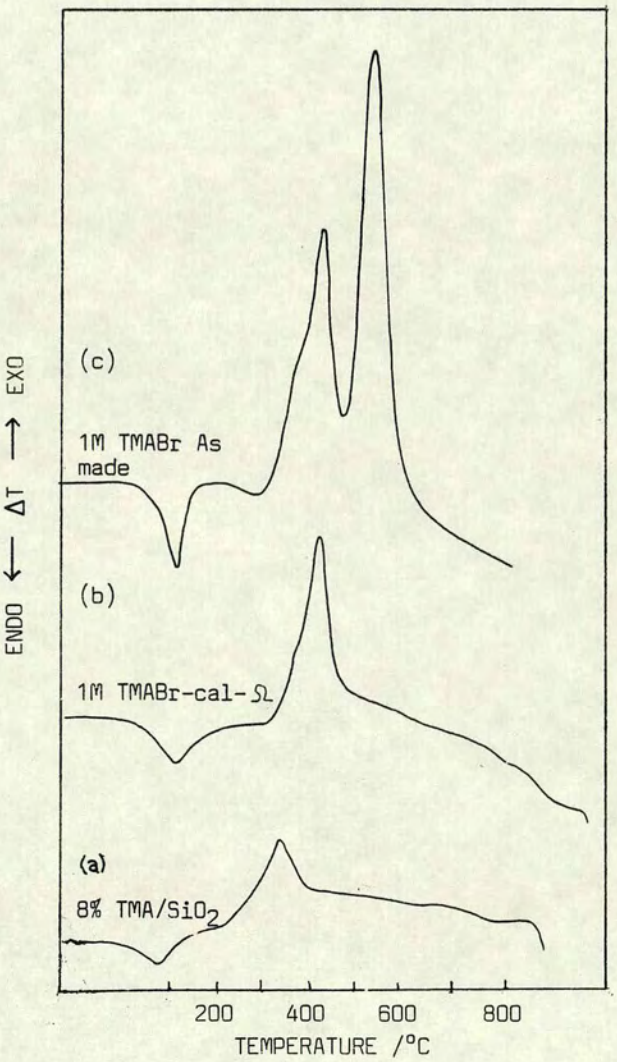

Heating rate
10°C min^{-1}

Fig. 6.1

Table 6.1

Thermal Analysis Data for Sorption of TMABr from Aqueous Solution by Zeolite Ω

SAMPLE: DS3 (Room Temp)

	EXO PEAK TEMP /°C (a)	PEAK RANGE /°C	EXO PEAK TEMP /°C (M)	PEAK RANGE /°C	EXO PEAK TEMP /°C (G)	PEAK RANGE /°C
SiO_2	350	232-403				
Cal-Ω	378 (S)	308-378	412	378-447		
As Syn	360(S)	282-360	417	360-460	527	460-600
'washed' As syn			398	282-482	570	482-600

(S) = Shoulder

Heating rate 10°C min^{-1}

As Syn = As synthesised

Table 6.2

Thermal Analysis Data for Sorption of TMABr from Aqueous Solution by (Na, TMA)- Ω

(IM TMABr @ RT)

SAMPLE	DTA TYPE	EXO PEAK TEMP (a) /°C	PEAK RANGE /°C	WT LOSS /%	EXO PEAK TEMP (M) /°C	PEAK RANGE /°C	WT LOSS /%	EXO PEAK TEMP (G) /°C	PEAK RANGE /°C	WT LOSS /%
DS3	I	360(S)	282-360	1.3	417	360-460	2.4	527	460-600	5.3
DS2	I	365(S)	297-365	1.0	402	365-435	1.6	492	435-522	5.0
DS13	III	357	305-378	2.3	407	378-442	1.5	505	442-550	5.3
R15	II	350(S)	283-389	1.5	414	389-455	1.4	525	455-560	4.9

(S) = Shoulder

Heating rate 8.5°C min^{-1}

Table 6.3

Thermal Analysis Data for Sorption of TMABr from Aqueous Solution by (Na, TMA)- Ω

(IM TMABr @ 95°C)

SAMPLE	DTA TYPE	EXO PEAK TEMP (a) /°C	PEAK RANGE /°C	WT LOSS /%	EXO PEAK TEMP (M) /°C	PEAK RANGE /°C	WT LOSS /%	EXO PEAK TEMP (G) /°C	PEAK RANGE /°C	WT LOSS /%
DS2	I	362(S)	297-362	1.3	402	362-435	2.0	492	435-525	4.8
DS13	III	335(S)	282-355	1.1	403	355-432	1.9	490	432-540	5.5
R15	II	345(S)	292-345	0.5	402	345-440	2.4	504	440-577	4.9

(S) = Shoulder

Heating rate 8.5°C min^{-1}

Tables 6.2 c.f 6.3, at 95°C more organic in main channel and correspondingly less adsorbed on surface cf. RT

Two reasons:

(a) Increased thermal vibrations of framework windows and TMABr at 95°C so more adsorbed by channel
(b) More silicate displaced from main channel by TMABr (aq) in hot solutions so increased space for organic

Evidence for (b) supported by further lowering of exotherm (G) by TMABr in both hot and cold solution c.f water

shoulder at 360°C. Thus (Na, TMA)- Ω sorbs TMA from aqueous solution and it predominantly occupies the main channel with minor sorption on the external surface. Comparison of this DTA curve with that obtained for the same as synthesised material after it had been washed in pure water (see Chapter Five) shows that treatment with aqueous TMABr shifts the exotherm (G) from 570°C to 527°C. Thus it appears that further silicate, if it is the cause of the exotherm shift, is displaced from the main channel by TMA/TMABr and thus facilitates the exit of TMA molecules from the gmelinite cages.

A most remarkable feature of this DTA curve (Fig. 6.1 curve (c)) is the enhancement of the intracrystalline water endotherm. It is now distinctly visible. The change could be brought about by the removal of silicate which thus enables more water to be readily evolved at the same temperature and not gradually.

6.3.3 Comparison of Sorption of TMABr by As Synthesised Zeolite Ω with DTA type I, II and III

The work with (Na, TMA)-Ω , DS3, with type I DTA demonstrated that TMA is occluded in the main channel and treatment with aqueous TMABr lowers the temperature of exotherm (G). Thus it was deemed necessary to investigate other samples of Ω and determine if this is characteristic behaviour for Ω .

The room temperature sorption of TMABr from aqueous solution by (Na, TMA) - Ω , which exhibited DTA types I, II and III, is demonstrated by the DTA curves shown in Fig. 6.2. The corresponding thermal analysis data is given in Table 6.2.

All DTA types exhibit an exotherm centred at ~ 410°C due to the decomposition of TMA in the main channel. DS2, DS13 and R15 show that

Room Temperature Sorption of TMABr by
Zeolite Ω of DTA Types I, II and III

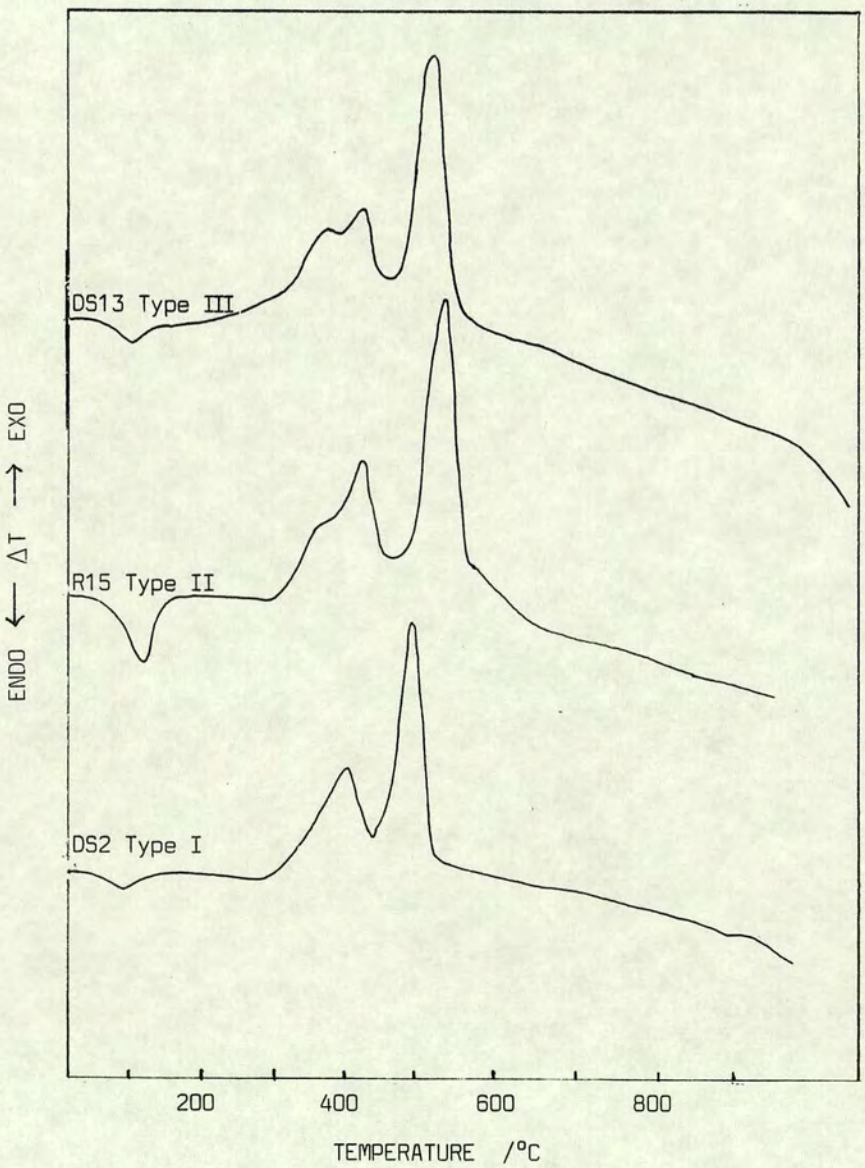

Fig. 6.2

sorption of TMA/TMABr is typical behaviour for Ω. The change in the general features of the DTA curve is not entirely due to sorption of salt; Chapter Five has shown that this change is effected by simple thorough washing. The shift to the lower temperature of exotherm (G) must be attributed to TMA/TMABr displacing further silicate from the main channel, which thus facilitates exit of TMA ions from the gmelinite cages.

For materials with type I DTA, i.e. DS2 and DS3, the shoulder associated with external surface TMA is not resolved into a peak as it is for those of type II (R15) and type III (DS13). For R15 and DS13, the weight loss associated with exotherm (a) is greater than that of DS2 and DS3, with DS13 exhibiting the largest weight loss.

The percentage sorption of TMA/TMABr by the main channel fluctuates. DS3 shows the largest value of 2.4% with the others in the range of 1.4 to 1.6%.

6.3.4 Comparison of Room Temperature and 95°C Sorption of TMABr by (Na, TMA)- Ω

A comparison of the sorption of TMABr from aqueous solution by (Na, TMA) - Ω at room temperature (RT) and 95°C was carried out and analysed by DTA (Fig. 6.3). The change in the DTA curve is typical for the samples of Ω examined. The main changes which occur at 95°C are the loss of resolution of the shoulder i.e. surface TMA, increase in size of exotherm (M) i.e. amount of TMA in the main channel, and shift of exotherm (G) to lower temperature with considerable increase in the width of the base of the exotherm. The latter is suggestive of decreased localisation of TMA in the gmelinite cages. Table 6.3 shows there is a decrease in the surface TMA content (except for DS2), and a considerable increase in sorption by the main channel. This

Comparison of TMABr Sorption by (Na, TMA)- Ω
at 95°C and Room Temperature

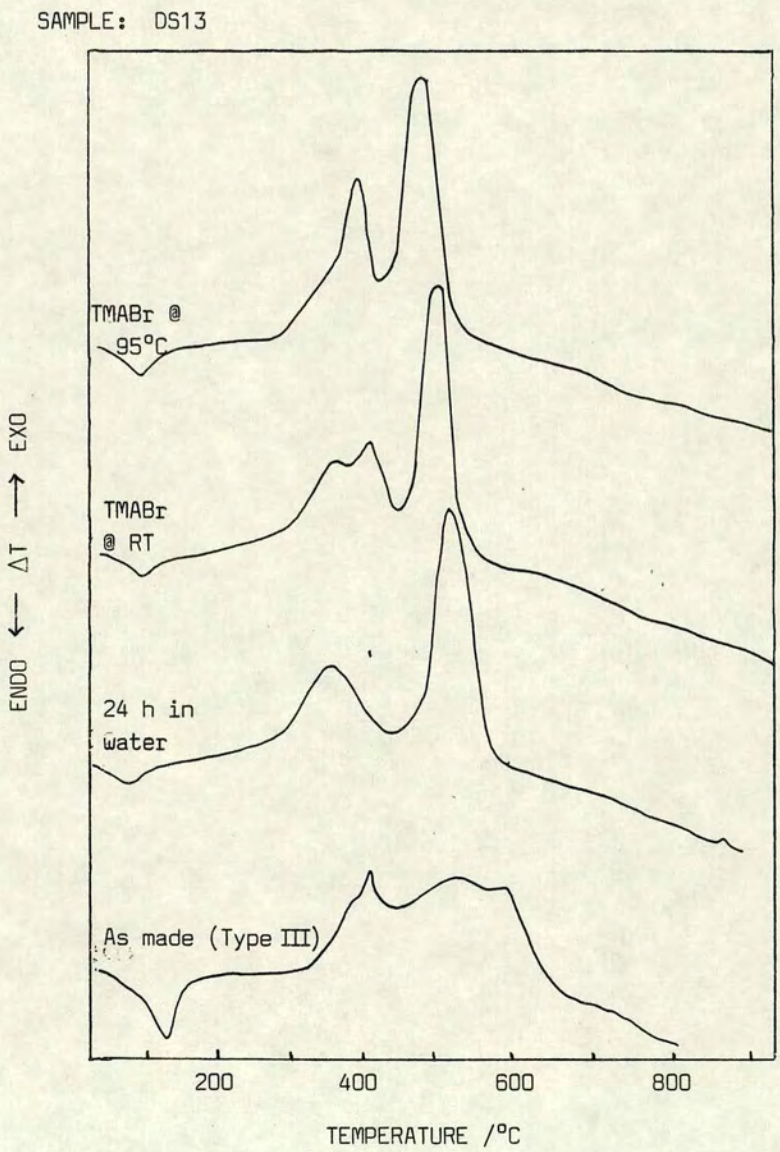

Fig. 6.3

may be attributed to two factors:

(a) Further displacement/dissolution of silicate, and thus increased space for sorption of TMA/TMABr. Evidence which supports this is the further lowering of the temperature of exotherm (G) by aqueous TMABr solution at 95°C, beyond that obtained by treatment with either hot or cold water.

(b) Increased thermal vibration of the framework windows at 95°C which therefore allows an increased number of molecules and also molecules of dimensions larger than the windows at RT to enter the main channel. This is partially in accordance with Barrer's results of sorption at high temperatures [2]. However, Barrer states that at higher temperatures, reduced sorption occurs in the channels because the volume of sorbed molecules tends to increase with temperature as in bulk liquid or solid.

6.3.5 Room Temperature Isotherm for Sorption of TMABr from Aqueous Solution by (Na, TMA)- Ω

An isotherm for the uptake of TMABr from aqueous solution by (Na, TMA)- Ω (DS3) was attempted, using measurements made by TG and DTA. The (Na, TMA)- Ω was chosen as opposed to (Na, H)- Ω because the latter undergoes structural damage and suffers a reduction in sorption capacity as a result of thermal TMA removal [1]. Analysis of the data obtained by TG and DTA provides 3 sorption isotherms. These correspond to:

(a) Total sorption capacity of the main channel and external crystal surface, i.e. that which is usually recorded.

(b) Sorption capacity of the external surface - according to the literature this is ~ 1%.

(c) Sorption capacity of the main channel - this has not been previously reported.

Table 6.4

Thermal Analysis Data for RT Isotherm for Sorption of TMABr from Aqueous Solution by (Na, TMA)- Ω

SAMPLE: As Synthesised OS3
1 g /100 cm^3 solution

Static, 8 days

[TMABr] /M	EXO PEAK TEMP /°C	PEAK RANGE /°C	(a) WT LOSS /%	EXO PEAK TEMP /°C	PEAK RANGE /°C	(M) WT LOSS /%	EXO PEAK TEMP /°C	PEAK RANGE /°C	WT LOSS /%	(a) + (M) TOTAL WT LOSS /%
0.0				398	282-482	1.9	570	482-600	4.9	1.9
0.2	365(S)	282-365	1.1	425	365-465	1.9	537	465-600	4.9	3.0
0.4	363(S)	297-363	0.9	422	363-465	2.0	535	465-600	4.9	2.9
0.6	354(S)	307-354	0.8	426	354-465	2.1	532	465-600	5.3	2.9
0.8	364(S)	292-364	1.3	428	364-463	2.3	532	463-600	5.0	3.6
1.0	360(S)	282-360	1.3	417	360-460	2.4	527	460-600	5.3	3.7
1.5	355(S)	295-355	0.9	418	355-455	2.6	522	455-600	5.3	3.5
2.0	367(S)	275-367	1.8	423	367-463	2.4	530	463-600	5.3	4.2
2.5	362(S)	282-362	1.4	425	362-462	2.3	530	462-600	5.3	3.7
3.0	348(S)	277-348	1.3	418	348-460	2.3	538	460-600	5.3	3.6

(S) = SHOULDER

Heating rate 10°C min^{-1}

This technique allows the sorption sites to be distinguished but the accuracy of the measurements is dependent on the thermobalance.

The 3 isotherms obtained are illustrated in Fig. 6.4 (data in Table 6.4).

According to the DTA curve for DS3 and the assignment of TMA sites as external surface or main channel, as identified in this work, the as made material did not show any detectable TMA in the main channel (see Chapter Five for details). Therefore sorption from 0.0M TMABr i.e. pure water should theoretically be zero. However, since the as synthesised material had adsorbed TMA on the external surface, in aqueous solution it is dissolved, enters the main channel and probably assists in silicate displacement. The amount sorbed by the main channel corresponds to 1.9% TMA i.e. that previously adsorbed by the surface.

Although the TMABr soaked samples were washed until free of bromide, the isotherm for sorption by the external surface shows an initial decrease in uptake and then fluctuates. This has a corresponding effect on the total sorption isotherm. Thus inconsistencies in washing affect the external surface sorption and the overall isotherm.

Sorption by the main channel showed a steady slow rise in the uptake of TMA/TMABr (with concentration) which attained its maximum capacity at 1.5M. After treatment with 1.5M TMABr, exotherm (G) for DS3 is shifted to its lowest temperature, 522°C. At higher concentrations the weight loss due to exotherm (M) decreased from 2.6 to 2.3% and correspondingly exotherm (G) was shifted to higher temperature. This shift suggests the channel is again partially blocked by silicate. This is confirmed by the reduction of the TMA/TMABr content at site (M). This situation is difficult to explain; the following are offered as tentative explanations:

Room Temperature Isotherm for Sorption of TMABr from Aqueous Solution by Zeolite Ω

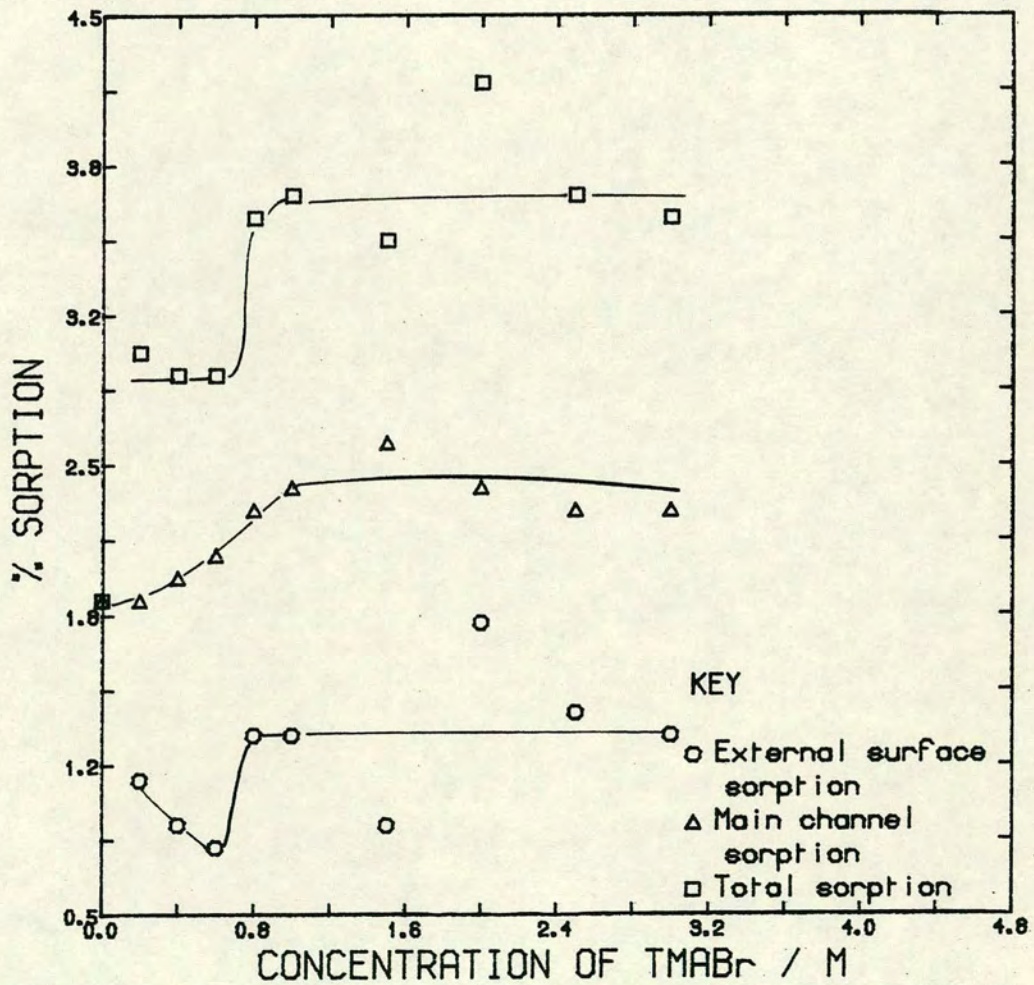

Fig. 6.4

(a) The increase in the concentration of TMA/TMABr molecules in aqueous solution sets up a "molecular traffic jam" and prevents the exit of silicate ions into the surrounding solution. This would reduce the rate of equilibration, but should not perturb the equilibrium sorption capacities.

(b) The water molecules of the TMABr solution are mainly used to solvate the TMABr, leaving fewer free water molecules to interact with the silicate ions and effect dissolution, i.e. silicate anions are expected to be less soluble in TMABr solutions than in pure water.

If (b) is true, then the shift of exotherm (G) is only due to water dissolving the silicate and TMA does not assist in the displacement.

These reasons may account for the absence of TMA in the main channels of Ω during synthesis.

From the room temperature isotherm, the sorption capacity of the main channel under these conditions is 2.6%. Perhaps prior thorough washing of the zeolite followed by sorption in this manner would lead to an increased TMA/TMABr uptake.

The XRD patterns of these samples generally had sharper peaks than the untreated material. No superimposed structure due to TMA/TMABr in the main channel was observed.

Throughout this chapter, the species sorbed is referred to as TMABr or TMA. Analysis of the 0.0M contact solution i.e. pure water showed it to be alkaline (pH ~ 8.5). This suggests that OH^- ions are not sorbed into the main channel, and that in the presence of bromide, TMABr is the sorbed species. However, this need not be the case. In more concentrated solutions it is difficult to know whether Br^-,

OH^-, both or just TMA is sorbed. The latter would imply ion exchange with say Na ions rather than salt occlusion. Although the account given in this chapter is written in terms of sorption, it seems likely that what has been observed is a mixture of sorption (especially on the external surface) and ion exchange with sodium ions (in the main channels). Many of the observed effects may be due to hydrolysis:

$$(Na^+Z^-)_z + H_2O \rightleftharpoons (H^+Z^-)_z + Na^+ (aq) + OH^- (aq)$$

6.4 Implications of the Shift of Exotherm (G)

An important implication of the shift of exotherm (G) to lower temperature is that complete removal of TMA from the gmelinite cage may be effected at considerably lower temperatures with reduced structural damage. Preliminary calcination experiments showed that thoroughly washed samples, and those treated with aqueous TMABr, could be freed of organic at ~450°C. (This is much lower than might be expected from thermal analysis results.)

Ion exchange with IM NH_4Cl at RT and 95°C, further lowered the exotherm (G) temperature to ~480°C. Thus ideally if complete sorption capacity for Ω is required, ion exchange with NH_4Cl using a large volume/solid ratio or several ion exchange cycles is required. This will lower the calcination temperature and minimise structural damage.

Treatment with aqueous TMABr may well act in a similar manner, the TMA replacing sodium ions which in the as synthesised zeolite Ω block the egress of the TMA from the gmelinite cages.

6.5 Advantages of this Technique

The prime advantage of sorption from aqueous solution by (Na, H)- Ω and (Na, TMA)- Ω , as has been shown, is that simultaneous dissolution of silicate from the channels and uptake of organic molecules occurs. If these samples were used for gas phase sorption it is expected that they would show poor sorption capacities. The (Na, H)- Ω obtained by calcination at 625°C for 3 h with consequent structural damage, contained silicate in the main channel. Contact with aqueous salt solution dissolved the silicate and thus increased the capacity for TMA.

This technique of mixing sorbate with SiO_2 and subjecting it to analysis by DTA provides a unique method for determination of adsorption sites due to the external surface. Similarly, the DTA of calcined Ω which had been soaked in TMABr solution provides the alternative sorption sites namely, in this instance, the main channel. Measurement of the amount of sorbate by TG in conjunction with DTA provides a good method for determination of the uptake due solely to the main channel.

REFERENCES:

1. J. F. Cole and H. W. Kouwenhoven, Adv. Chem. Series, 1973, 3, 283

2. R. M. Barrer, J. of Inclusion Phenomena, 1983, 1, 105.

Concluding Remarks

This investigation has led to the discovery of new information on three aspects of the chemistry of zeolite Ω: the consequences of using hot reagents in the preparation of the synthesis gel; the effect on its thermal properties produced by prolonged contact with water; and some of the sorption/ion exchange properties observed by thermal analysis. However much remains to be done. Further work on the relationship between the temperature at which the reactants are mixed and the product formed would be of interest and in particular the transition temperature at which a sodalite phase is crystallised in preference to Ω should be determined. If the proposed mechanism for faulted Ω synthesis is correct, then it is anticipated that pure Ω samples produced from mixtures prepared at high temperatures would have a higher degree of faulting than Ω obtained by mixing at low temperatures. The latter may be fault free. Verification of this hypothesis by sorption from aqueous solution studied by the thermal analysis method described in Chapter Six should be carried out. This method would provide the true sorption capacity for each zeolitic site. Comparison of the sorption capacity of the thoroughly washed as synthesised sample with that of the calcined organic free material should provide valuable information on the reduction in sorption capacity caused by thermal removal of TMA. Prior to sorption work, the effect of treatment with water requires further investigation to determine whether the TMA exchanged/sorbed in the main channel may be removed by exhaustive 'washing'.

These proposals, although made for the development of work on zeolite Ω, may equally be applied to all molecular sieves. The temperature of mixing may be the key factor which determines the reproducibility of zeolite crystallisation from a given reaction composition and thus other

systems require investigation. Amorphous silicate in the channels of any zeolite will reduce sorption capacity and thus the washing process should be applied to other zeolites. Thermal analysis provides a unique technique for the determination of the true sorption /ion exchange capacity of different zeolitic sites and deserves application to other molecular sieves.

Hence, much scope exists for future developments in this area of zeolite chemistry.